Publ. Astron. Soc. Japan (2014) 66 (2), 30 (1–83)
doi: 10.1093/pasj/psu014

Survey of period variations of superhumps in SU UMa-type dwarf novae. V. The fifth year (2012–2013)

Taichi Kato,[1,*] Franz-Josef Hambsch,[2,3,4] Hiroyuki Maehara,[5,6] Gianluca Masi,[7] Francesca Nocentini,[7] Pavol A. Dubovsky,[8] Igor Kudzej,[8] Kazuyoshi Imamura,[9] Minako Ogi,[9] Kenji Tanabe,[9] Hidehiko Akazawa,[9] Thomas Krajci,[10] Ian Miller,[11] Enrique de Miguel,[12] Arne Henden,[14] Ryo Noguchi,[15] Takehiro Ishibashi,[15] Rikako Ono,[15] Miho Kawabata,[15] Hiroshi Kobayashi,[15] Daisuke Sakai,[15] Hirochika Nishino,[15] Hisami Furukawa,[15] Kazunari Masumoto,[15] Katsura Matsumoto,[15] Colin Littlefield,[16] Tomohito Ohshima,[1] Chikako Nakata,[1] Satoshi Honda,[17,18] Kenzo Kinugasa,[17,19] Osamu Hashimoto,[17] William Stein,[20] Roger D. Pickard,[21,22] Seiichiro Kiyota,[23] Elena P. Pavlenko,[24] Oksana I. Antonyuk,[24] Aleksei V. Baklanov,[24] Kirill Antonyuk,[24] Denis Samsonov,[24] Nikolaj Pit,[24] Aleksei Sosnovskij,[24] Arto Oksanen,[25] Caisey Harlingten,[26] Jenni Tyyskä,[27] Berto Monard,[28,29] Sergey Yu. Shugarov,[30,31] Drahomir Chochol,[31] Kiyoshi Kasai,[32] Yutaka Maeda,[33] Kenji Hirosawa,[34] Hiroshi Itoh,[35] Richard Sabo,[36] Joseph Ulowetz,[37] Etienne Morelle,[38] Raúl Michel,[39] Genaro Suárez,[39] Nick James,[40] Shawn Dvorak,[41] Irina B. Voloshina,[30] Michael Richmond,[42] Bart Staels,[14,43] David Boyd,[44] Maksim V. Andreev,[45,46] Nikolai Parakhin,[45] Natalia Katysheva,[30] Atsushi Miyashita,[47] Kazuhiro Nakajima,[48] Greg Bolt,[49] Stefano Padovan,[14] Peter Nelson,[50] Donn R. Starkey,[51] Denis Buczynski,[52] Peter Starr,[53] William N. Goff,[54] Denis Denisenko,[55] Christopher S. Kochanek,[56] Benjamin Shappee,[56] Krzysztof Z. Stanek,[56] José L. Prieto,[57] Koh-ichi Itagaki,[58] Shizuo Kaneko,[59] Rod Stubbings,[60] Eddy Muyllaert,[61] Jeremy Shears,[62] Patrick Schmeer,[63] Gary Poyner,[64] and Miguel Rodríguez-Marco[65]

[1]Department of Astronomy, Kyoto University, Kitashirakawa-Oiwake-cho, Sakyo-ku, Kyoto 606-8502
[2]Groupe Européen d'Observations Stellaires (GEOS), 23 Parc de Levesville, 28300 Bailleau l'Evêque, France
[3]Bundesdeutsche Arbeitsgemeinschaft für Veränderliche Sterne (BAV), Munsterdamm 90, 12169 Berlin, Germany
[4]Vereniging Voor Sterrenkunde (VVS), Oude Bleken 12, 2400 Mol, Belgium
[5]Kiso Observatory, Institute of Astronomy, School of Science, The University of Tokyo, 10762-30 Mitake, Kiso-machi, Kiso-gun, Nagano 397-0101
[6]Kwasan and Hida Observatories, Kyoto University, Kitakazan-Ohmine-cho, Yamashina-ku, Kyoto 607-8471
[7]The Virtual Telescope Project, Via Madonna del Loco 47, 03023 Ceccano (FR), Italy

[8]Vihorlat Observatory, Mierova 4, Humenne, Slovakia
[9]Department of Biosphere-Geosphere System Science, Faculty of Informatics, Okayama University of Science, 1-1 Ridai-cho, Okayama, Okayama 700-0005
[10]Astrokolkhoz Observatory, Center for Backyard Astrophysics New Mexico, PO Box 1351 Cloudcroft, NM 83117, USA
[11]Furzehill House, Ilston, Swansea, SA2 7LE, UK
[12]Departamento de Física Aplicada, Facultad de Ciencias Experimentales, Universidad de Huelva, 21071 Huelva, Spain
[13]Center for Backyard Astrophysics, Observatorio del CIECEM, Parque Dunar, Matalascañas, 21760 Almonte, Huelva, Spain
[14]American Association of Variable Star Observers (AAVSO), 49 Bay State Rd., Cambridge, MA 02138, USA
[15]Osaka Kyoiku University, 4-698-1 Asahigaoka, Kashiwara, Osaka 582-8582
[16]Department of Physics, University of Notre Dame, Notre Dame, IN 46556, USA
[17]Gunma Astronomical Observatory, 6860-86 Nakayama, Takayama, Agatsuma, Gunma 377-0702
[18]Center for Astronomy, University of Hyogo, 407-2 Nishigaichi, Sayo-cho, Sayo, Hyogo 679-5313
[19]Nobeyama Radio Observatory, NAOJ, 462-2 Nobeyama, Minamimaki, Minamisaku, Nagano 384-1305
[20]6025 Calle Paraiso, Las Cruces, NM 88012, USA
[21]The British Astronomical Association, Variable Star Section (BAA VSS), Burlington House, Piccadilly, London, W1J 0DU, UK
[22]3 The Birches, Shobdon, Leominster, Herefordshire, HR6 9NG, UK
[23]Variable Star Observers League in Japan (VSOLJ), 7-1 Kitahatsutomi, Kamagaya, Chiba 273-0126
[24]Crimean Astrophysical Observatory, Kyiv Shevchenko National University, 98409, Nauchny, Crimea, Ukraine
[25]Hankasalmi Observatory, Jyvaskylan Sirius ry, Vertaalantie 419, FI-40270 Palokka, Finland
[26]Searchlight Observatory Network, The Grange, Erpingham, Norfolk, NR11 7QX, UK
[27]Jyväskylän Lyseo Upper Secondary School, IB Section, Yliopistonkatu 13, FI-40101 Jyväskylä, Finland
[28]Bronberg Observatory, Center for Backyard Astronomy Pretoria, PO Box 11426, Tiegerpoort 0056, South Africa
[29]Kleinkaroo Observatory, Center for Backyard Astronomy Kleinkaroo, Sint Helena 1B, PO Box 281, Calitzdorp 6660, South Africa
[30]Sternberg Astronomical Institute, Lomonosov Moscow University, Universitetsky Ave., 13, Moscow 119992, Russia
[31]Astronomical Institute of the Slovak Academy of Sciences, 05960, Tatranska Lomnica, The Slovak Republic
[32]Baselstrasse 133D, CH-4132 Muttenz, Switzerland
[33]12-14 Kaminishiyama-machi, Nagasaki, Nagasaki 850-0006
[34]216-4 Maeda, Inazawa-cho, Inazawa, Aichi 492-8217
[35]VSOLJ, 1001-105 Nishiterakata-machi, Hachioji, Tokyo 192-0153
[36]2336 Trailcrest Dr., Bozeman, MT 59718, USA
[37]Center for Backyard Astrophysics Illinois, Northbrook Meadow Observatory, 855 Fair Ln, Northbrook, IL 60062, USA
[38]9 rue Vasco de GAMA, 59553 Lauwin Planque, France
[39]Instituto de Astronomía UNAM, Apartado Postal 877, 22800 Ensenada B.C., México
[40]11 Tavistock Road, Chelmsford, Essex, CM1 6JL, UK
[41]Rolling Hills Observatory, 1643 Nightfall Drive, Clermont, FL 34711, USA
[42]Physics Department, Rochester Institute of Technology, Rochester, NY 14623, USA
[43]Center for Backyard Astrophysics (Flanders), American Association of Variable Star Observers (AAVSO), Alan Guth Observatory, Koningshofbaan 51, Hofstade, Aalst, Belgium
[44]Silver Lane, West Challow, Wantage, OX12 9TX, UK
[45]Institute of Astronomy, Russian Academy of Sciences, 361605 Peak Terskol, Kabardino-Balkaria, Russia

[46]International Center for Astronomical, Medical and Ecological Research of NASU, Ukraine 27 Akademika Zabolotnoho Str. 03680 Kyiv, Ukraine
[47]Seikei Meteorological Observatory, Seikei High School, 3-3-1 Kichijoji-Kita-machi, Musashino, Tokyo 180-8633
[48]Variable Star Observers League in Japan (VSOLJ), 124 Teradani, Isato-cho, Kumano, Mie 519-4673
[49]Camberwarra Drive, Craigie, Western Australia 6025, Australia
[50]1105 Hazeldean Rd, Ellinbank 3820, Australia
[51]DeKalb Observatory, H63, 2507 County Road 60, Auburn, IN 46706, USA
[52]Conder Brow Observatory, Fell Acre, Conder Brow, Little Fell Lane, Scotforth, Lancashire, LA2 0RQ, UK
[53]Warrumbungle Observatory, Tenby, 841 Timor Rd, Coonabarabran NSW 2357, Australia
[54]13508 Monitor Ln., Sutter Creek, CA 95685, USA
[55]Space Research Institute (IKI), Russian Academy of Sciences, Moscow, Russia
[56]Department of Astronomy, The Ohio State University, Columbia, OH 43210, USA
[57]Department of Astrophysical Sciences, Princeton University, NJ 08544, USA
[58]Itagaki Astronomical Observatory, Teppo-cho, Yamagata, Yamagata 990-2492
[59]14-7 Kami-Yashiki, Kakegawa, Shizuoka 436-0049
[60]Tetoora Observatory, Tetoora Road, Victoria, Australia
[61]Vereniging Voor Sterrenkunde (VVS), Moffelstraat 13, 3370 Boutersem, Belgium
[62]"Pemberton", School Lane, Bunbury, Tarporley, Cheshire, CW6 9NR, UK
[63]Bischmisheim, Am Probstbaum 10, 66132 Saarbrücken, Germany
[64]BAA Variable Star Section, 67 Ellerton Road, Kingstanding, Birmingham, B44 0QE, UK
[65]Alberdi, 42, 2F 28029 Madrid, Spain

*E-mail: tkato@kusastro.kyoto-u.ac.jp

Received 2013 August 6; Accepted 2013 October 26

Abstract

Continuing the project described in Kato et al. (2009, PASJ, 61, S395), we collected times of superhump maxima for SU UMa-type dwarf novae mainly observed during the 2012–2013 season. We found three objects (V444 Peg, CSS J203937, and MASTER J212624) having strongly positive period derivatives despite the long orbital period ($P_{\rm orb}$). By using the period of growing stage (stage A) superhumps, we obtained mass ratios for six objects. We characterized nine new WZ Sge-type dwarf novae. We made a pilot survey of the decline rate in the slowly fading parts of SU UMa-type and WZ Sge-type outbursts. The decline time scale was found to generally follow an expected $P_{\rm orb}^{1/4}$ dependence, and WZ Sge-type outbursts also generally follow this trend. There are some objects which show slower decline rates, and we consider these objects good candidates for period bouncers. We also studied unusual behavior in some objects, including BK Lyn which made a transition from an ER UMa-type state to a novalike (standstill) state in 2013, and unusually frequent occurrences of superoutbursts in NY Ser and CR Boo. We applied the least absolute shrinkage and selection operator (Lasso) power spectral analysis, which has been proven to be very effective in analyzing the Kepler data, to the ground-based photometry of BK Lyn, and detected a dramatic disappearance of the signal of negative superhumps in 2013. We suggested that the mass-transfer rates did not strongly vary between the ER UMa-type state and novalike state in BK Lyn, and this transition was less likely caused by a systematic variation of the mass-transfer rate.

Key words: accretion, accretion disks — novae, cataclysmic variables — stars: dwarf novae

1 Introduction

Cataclysmic variables (CVs) are close binary systems transferring matter from a low-mass dwarf secondary to a white dwarf. The transferred matter forms an accretion disk. In dwarf novae (DNe) being of a class of CVs, the instability in the accretion disk produces outbursts. SU UMa-type dwarf novae, a class of DNe, show superhumps during their long outbursts (superoutbursts), whose period is generally a few percent longer than the orbital period. It is generally considered that the tidal instability in the accretion disk caused by the 3:1 resonance (Whitehurst 1988) is responsible for the superhump and superoutburst phenomenon (Osaki 1989, 1996). For general information on CVs, DNe, SU UMa-type dwarf novae, and their superhumps, see, e.g., Warner (1995a).

In a series of papers (Kato et al. 2009a, 2010, 2012a, 2013a) we systematically surveyed SU UMa-type dwarf novae, laying particular emphasis on period variations of superhumps (positive superhumps; namely, superhumps having periods longer than the orbital period), which have been the main theme since Kato et al. (2009a). The change in the superhump period reflects the precession angular velocity of the eccentric (or flexing) disk, and would be an excellent probe for studying the structure of the accretion disk during dwarf nova outbursts. In addition to the systematic survey of period variations of superhumps, we have studied properties of newly discovered WZ Sge-type dwarf novae. For WZ Sge-type dwarf novae, see, e.g., Bailey (1979), Downes (1990), Kato et al. (2001b).

In the meantime, epoch-making progress has been made in understanding the SU UMa-type phenomenon and interpreting the superhump period, and we briefly review the history.

An anticipation of this new progress started from the analysis of Kepler data of V344 Lyr (Still et al. 2010), which detected likely persistent negative superhumps in quiescence. Cannizzo et al. (2010) studied the systematics of outbursts in V344 Lyr. Wood et al. (2011) analyzed the positive and negative superhumps in the same object.

In Kato et al. (2012a), we analyzed the Kepler data of V344 Lyr and V1504 Cyg in the same way we have adopted, and compared them with other SU UMa-type dwarf novae. This work led to two works (Osaki & Kato 2013a, 2013b) in which the thermal-tidal instability (TTI) model (Osaki 1989) has been proven to be the best explanation of the Kepler observation. In particular, Osaki and Kato (2013a) used the frequency of negative superhumps (superhumps having periods shorter than the orbital period) which are believed to arise from a tilted accretion disk (e.g., Harvey et al. 1995; Patterson et al. 1997a; Wood & Burke 2007) to derive the variation of the disk radius, and directly confirmed the prediction of the TTI model. Osaki and Kato (2013b) further analyzed the frequency variation of the coexisting negative and positive superhumps, and confirmed that the variation of the disk radius predicted by the TTI model gives a consistent explanation of the variation of the negative and positive superhumps.

Osaki and Kato (2013b) also introduced the pressure effect in interpreting the period of positive superhumps. Although the pressure effect has been long known (Lubow 1992; Hirose & Osaki 1993; Murray 1998; Montgomery 2001; Pearson 2006), there have been no direct applications to an interpretation of the period variation of (positive) superhumps during the superoutburst. The treatment of the pressure effect is difficult, and Osaki and Kato (2013b) partly succeeded in interpreting the variation of the superhump period during the initial growing stage (stage A) and the fully developed stage (early stage B)—see Kato et al. (2009a) for the notation of stages A–B–C of superhumps. This interpretation led to an important consequence: the precession frequency of the superhumps during the growing stage (stage A) corresponds to the dynamical precession rate at the radius of the 3:1 resonance. This interpretation enabled us to dynamically determine the binary's mass ratios ($q = M_2/M_1$) only from superhump observations and the orbital period. This method has indeed been shown to be effective in comparison with q values from eclipse observations or radial-velocity studies (Kato & Osaki 2013b), and has been successfully used for characterizing the WZ Sge-type dwarf nova with multiple rebrightenings (Nakata et al. 2013) and identifying the elusive period bouncers[1] (Kato et al. 2013b). We should also note that our initial approximation in Kato et al. (2009a) did not include the pressure effect, and the disk radius was normalized to the radius of 3:1 resonance for the early phase of the stage B superhump, and the resultant radii were systematically estimated to be larger in Kato et al. (2009a). Since qualitative estimation of the pressure effect during the superoutburst is still a difficult task, we leave the understanding of the period variation of superhumps to future work.

In Kato et al. (2012a), we also made a pilot survey of variation of superhump amplitudes and indicated that the amplitudes of superhumps are strongly correlated with orbital periods, and the dependence on the inclination is weak in systems with an inclination smaller than 80°. In Kato et al. (2013a), we systematically studied ER UMa-type dwarf novae (see, e.g., Kato & Kunjaya 1995; Robertson et al. 1995), which have recently become a hot topic in the field of cataclysmic variables since the discovery of negative superhumps even during the superoutburst (Ohshima et al. 2012) and the possible identification of BK Lyn—an object having recently changed from

[1] CVs evolved beyond the minimum orbital period during their secular evolution; for a recent review of CV evolution, see, e.g., Knigge, Baraffe, and Patterson (2011).

a novalike variable to an ER UMa-type dwarf nova—with an ancient classical nova (Patterson et al. 2013), shedding light on the evidence of the long-sought transition from classical novae to dwarf novae (the hibernation model; see, e.g., Livio & Shara 1987).

Cannizzo et al. (2012), Barclay et al. (2012), and Ramsay et al. (2012b) also studied Kepler data for four dwarf novae, V344 Lyr, V1504 Cyg, the background dwarf nova of KIC 4378554, and V447 Lyr. The work by Cannizzo et al. (2012) tried to reproduce the outburst morphology by the pure thermal instability model—see Osaki and Kato (2014) for a discussion on the difficulty of this model. Ramsay et al. (2012b) and Cannizzo (2012) indicated the presence of a "shoulder" in long outbursts of an SS Cyg-type dwarf nova, which Ramsay et al. (2012b) and Cannizzo (2012) considered to be analogous to the precursor outburst in SU UMa-type dwarf novae. Rapid progress was also made in the interpretation and numerical simulation of negative and positive superhumps, part of which is associated with Kepler observations (Montgomery & Bisikalo 2010; Montgomery & Martin 2010; Montgomery 2012a, 2012b).

Keeping the brand-new progress in dwarf novae in mind, we proceed to the new observations.

This paper is structured as follows: section 2 describes the observation and analysis technique; section 3 deals with individual objects we observed; section 4 discusses the general properties following Kato et al. (2009a, 2012a); section 5 provides a new pilot survey of the decline rate during the superoutburst, which has led to a new promising method for identifying period bouncers; section 6 examines the recently reported new OGLE dwarf novae; section 7 presents topics on some objects which show new types of behavior in dwarf novae; section 8 provides a summary.

2 Observation and analysis

The data were obtained under campaigns led by the VSNET Collaboration (Kato et al. 2004b). In some objects, we used the public data from the American Association of Variable Star Observers (AAVSO) International Database.[2]

The majority of the data were acquired by time-resolved CCD photometry with telescopes in the 30 cm class, whose observational details will be presented in future papers dealing with analysis and discussion on individual objects of interest. The list of outbursts and observers is summarized in table 1. The data analysis was performed in the same way as described in Kato et al. (2009a, 2012a). The time of all observations is expressed in Barycentric Julian Date (BJD).

We also used the same abbreviations: $P_{\rm orb}$ for the orbital period and $\varepsilon \equiv (P_{\rm SH}/P_{\rm orb}) - 1$ for the fractional superhump excess. After Osaki and Kato (2013a), the alternative fractional superhump excess in the frequency unit, $\varepsilon^* \equiv 1 - (P_{\rm orb}/P_{\rm SH}) = \varepsilon/(1+\varepsilon)$, has been introduced since this fractional superhump excess can be directly compared to the precession rate. We therefore used ε^* when referring to the precession rate.

We used phase dispersion minimization (PDM: Stellingwerf 1978) for period analysis, and 1σ errors for the PDM analysis were estimated by the methods of Fernie (1989) and Kato et al. (2010). In Kato et al. (2013a), we introduced the least absolute shrinkage and selection operator (Lasso) method (Tibshirani 1996; Kato & Uemura 2012), which has been proven to be very effective in separating narrowly spaced periods. We have further extended the application of this Lasso analysis to two-dimensional power spectra (Kato & Maehara 2013; Osaki & Kato 2013b; Kato & Osaki 2013a). These two-dimensional Lasso power spectra have sometimes been helpful in detecting negative superhumps (cf. Osaki & Kato 2013b) as well as superhumps with varying frequencies (cf. Kato & Maehara 2013).

The derived $P_{\rm SH}$, $P_{\rm dot}$, and other parameters are listed in table 2 in the same format as in Kato et al. (2009a). The definitions of parameters P_1, P_2, E_1, E_2, and $P_{\rm dot}$ are the same as in Kato et al. (2009a). We also present comparisons of different superoutbursts in the $O-C$ diagrams since this was one of the motivations of these surveys (cf. Uemura et al. 2005).

We used the terminology of superhumps summarized in Kato et al. (2012a). We especially call the reader's attention to the term "late superhump." We only used "traditional" late superhumps when an ~ 0.5 phase shift is confirmed.[3] Early superhumps are double-wave humps seen during the early stages of WZ Sge-type dwarf novae, and have a period close to the orbital period (Kato et al. 1996; Kato 2002a; Osaki & Meyer 2002). We used the period of early superhumps as an approximate orbital period, since their periods differ only by less than 0.1% (Ishioka et al. 2002; Kato 2002a).

The same as in Kato et al. (2009a), we have used coordinate-based optical transient (OT) designations for some objects, such as Catalina Real-time Transient Survey (CRTS: Drake et al. 2009)[4] transients, and listed the original identifiers in table 1. The CRTS team has recently provided a public data release[5] and provided the International

[2] ⟨http://www.aavso.org/data-download⟩.

[3] See also table 1 in Kato et al. (2012a) for various types of superhumps; the lack of an ~ 0.5 phase shift in V585 Lyr in the Kepler data has been also confirmed (Kato & Osaki 2013a).

[4] ⟨http://nesssi.cacr.caltech.edu/catalina/⟩. For the information on the individual Catalina CVs, see ⟨http://nesssi.cacr.caltech.edu/catalina/AllCV.html⟩.

[5] ⟨http://nesssi.cacr.caltech.edu/DataRelease/⟩.

Table 1. List of superoutbursts.

Subsection	Object	Year	Observers or references*	ID†
3.1	KX Aql	2012	Ioh, KU, SRI, AAVSO, Hsk	
3.2	NN Cam	2012	OUS	
3.3	V485 Cen	2013	OkC, HaC	
3.4	Z Cha	2013	SPE	
3.5	YZ Cnc	2011	SWI, HMB, DKS, MEV, Boy, BSt, UJH, Nyr, AAVSO	
3.6	GZ Cnc	2013	Kis, Hsk	
3.7	V503 Cyg	2012	SWI, MEV, AAVSO, Boy	
		2012b	RPc, IMi	
3.8	OV Dra	2013	LCO	
3.9	AQ Eri	2012	OUS, Kis, Aka, Hsk	
3.10	V660 Her	2012	IMi	
		2013	DPV, NDJ	
3.11	V1227 Her	2012a	IMi, RPc, Mhh, OKU, deM	
		2012b	SRI, IMi, CRI	
		2013	RPc	
3.12	MM Hya	2013	IMi, Mdy	
3.13	AB Nor	2013	MLF, HaC	
3.14	DT Oct	2013	OkC	
3.15	GR Ori	2013	AKz, Ioh, MLF, SWI, Mdy, Aka, Nel, deM, AAVSO, KU, RPc, DKS, DRS, SAc, DPV, HaC, PSD, SRI, Buc	
3.16	V444 Peg	2012	Mhh, HaC, Hsk, IMi, AAVSO	
3.17	V521 Peg	2012	Hsk	
3.18	V368 Per	2012	AAVSO, IMi	
3.19	TY PsA	2012	HaC, OUS, Kis, Aka	
3.20	QW Ser	2009	Ioh, Njh	
		2013	HaC, Aka	
3.21	V493 Ser	2013	Aka, Mic, HaC	
3.22	AW Sge	2012	Kai, BSt, HMB, Mas, DPV, Mhh, OUS, IMi, AAVSO	
3.23	V1212 Tau	2013	RPc	
3.24	BZ UMa	2012	Aka	
3.25	CI UMa	2013	CRI	
3.26	CY UMa	2013	DPV	
3.27	MR UMa	2013	DPV, AAVSO	
3.28	ASAS SN-13ao	2013	KU, DPV	
3.29	ASAS SN-13as	2013	DPV	
3.30	ASAS SN-13ax	2013	deM, DPV, IMi, Shu, NKa	
3.31	ASAS SN-13bj	2013	LCO	
3.32	ASAS SN-13bm	2013	Kai, NDJ	
3.33	ASAS SN-13bp	2013	NDJ, Mdy	
3.34	ASAS SN-13br	2013	DPV, Kai, Shu, Mic	
3.35	CSS J015051	2012	KU, Mhh, LCO	CSS 111006:015052+332622
3.36	CSS J015321	2012	AKz, Mas	CSS 081026:015321+340857
3.37	CSS J102842	2013	MLF, deM	CSS 090331:102843−081927
3.38	CSS J105835	2012	Kis, HaC, OKU, Nyr	CSS 081025:105835+054706
3.39	CSS J150904	2013	AKz	CSS 130324:150904+465057
—	CSS J174033	2013	T. Ohshima et al. in preparation	CSS 130418:174033+414756
3.40	CSS J203937	2012	MLF, deM, RIT, HaC, LCO, Mas, UJH, AAVSO	CSS 120813:203938−042908
3.41	CSS J214934	2012	Mas	CSS 120922:214934−121908
3.42	DDE 26	2012	LCO, CRI	
3.43	MASTER J000820	2012	Mas	MASTER OT J000820.50+773119.1
3.44	MASTER J001952	2012	OKU, Mas	MASTER OT J001952.31+464933.0

Table 1. (Continued)

Subsection	Object	Year	Observers or references*	ID†
3.45	MASTER J030128	2012	deM, Mas, RPc, Kra	MASTER OT J030128.77+401104.9
3.46	MASTER J042609	2012	AKz, deM, MEV, Mhh, HaC, OKU, LCO, SWI, Vol	MASTER OT J042609.34+354144.8
3.47	MASTER J054317	2012	Mhh, HaC, OKU, AKz, Mas	MASTER OT J054317.95+093114.8
3.48	MASTER J064725	2013	SWI, Nyr, LCO, OKU, DPV	MASTER OT J064725.70+491543.9
3.49	MASTER J073418	2013	IMi, RIT	MASTER OT J073418.66+271310.5
3.50	MASTER J081110	2012	AKz, Mas, Mhh	MASTER OT J081110.46+660008.5
3.51	MASTER J094759	2013	OKU, CRI, KU, HaC, deM, Mdy	MASTER OT J094759.83+061044.4
3.52	MASTER J105025	2012	Kra, Mas	MASTER OT J105025.99+332811.4
3.53	MASTER J111759	2013	deM, DPV	MASTER OT J111759.87+765131.6
3.54	MASTER J165236	2013	KU, Kra, DPV, AKz	MASTER OT J165236.22+460513.2
3.55	MASTER J174902	2013	DPV	MASTER OT J174902.10+191331.2
3.56	MASTER J181953	2013	OKU, Kai, KU, Mic, CRI, Mdy	MASTER OT J181953.76+361356.5
—	MASTER J203749	2012	Nakata et al. (2013)	MASTER OT J203749.39+552210.3
—	MASTER J211258	2013	Nakata et al. (2013)	MASTER OT J211258.65+242145.4
3.57	MASTER J212624	2013	Shu, DPV, Kai	MASTER OT J212624.16+253827.2
3.58	OT J112619	2013	SWI, UJH, deM, GFB, Mas, DKS, SRI, IMi	CSS 130106:112619+084651
3.59	OT J191443	2012	Mas	Itagaki (Yamaoka et al. 2008)
3.60	OT J205146	2012	Mhh, Vol, Shu	CSS 121004:205146−035827
3.61	OT J220641	2012	Kra, Mas	CSS 110921:220641+301436
3.62	OT J232727	2012	Mhh, LCO, CRI, MEV, Mas, Ter, OKU, Kis, Shu, RPc	Itagaki et al. (2012)
3.63	PNV J062703	2013	Nyr, deM, Ioh, DPV, Aka, OUS, AAVSO	PNV J06270375+3952504 (Kaneko)
3.64	SDSS J075107	2013	IMi	SDSS J075107.50+300628.4
3.65	SDSS J080033	2012	Mas	SDSS J080033.86+192416.5
3.66	SDSS J162520	2010	Kato et al. (2010)	SDSS J162520.29+120308.7 (Wils)
3.67	SSS J122221	2013	Kato et al. (2013b)	SSS J122221.7−311523
3.68	SSS J224739	2012	HaC, GBo	SSS J224739.7−362253
3.69	TCP J153756	2013	MLF, Kis, SWI, HaC, UJH	TCP J15375685−2440136 (Itagaki)
3.70	TCP J175219	2012	Mas	TCP J17521907+5001155 (Mikuz)

*Key to observers: Aka (H. Akazawa, OUS), AKz (Astrokolkhoz Obs.), BSt (B. Staels), Boy‡(D. Boyd), Buc (D. Buczynski), CRI (Crimean Astrophys. Obs.), deM (E. de Miguel), DKS‡(S. Dvorak), DPV (P. Dubovsky), DRS‡(D. R. Starkey), GBo (G. Bolt), GFB‡(W. N. Goff), HaC (F.-J. Hambsch, remote obs. in Chile), HMB (F.-J. Hambsch), Hsk (K. Hirosawa), IMi‡(I. Miller), Ioh (H. Itoh), Kai (K. Kasai), Kis (S. Kiyota), Kra (T. Krajci), KU (Kyoto Univ., campus obs.), LCO‡(C. Littlefield), MEV‡(E. Morelle), MLF (B. Monard), Mas (G. Masi), Mdy (Y. Maeda), Mhh (H. Maehara), Mic (R. Michel-Murillo), NDJ‡(N. James), Nel‡(P. Nelson), Njh (K. Nakajima), NKa (N. Katysheva), Nyr‡(Nyrola and Hankasalmi Obs.), OkC‡(A. Oksanen, remote obs. in Chile), OKU (Osaka Kyoiku Univ.), OUS (Okayama Univ. of Science), PSD‡(S. Padovan), RIT (M. Richmond), RPc‡(R. D. Pickard), SAc (Seikei High School), Shu (S. Yu. Shugarov), SPE‡(P. Starr), SRI‡(R. Sabo), SWI‡(W. Stein), Ter (Terskol Obs.), UJH‡(J. Ulowetz), Vol (I. B. Voloshina), and AAVSO (AAVSO database).
†Original identifications, discoverers or data source.
‡Inclusive of the AAVSO database.

Astronomical Union (IAU) designations for the cataloged objects. We used these IAU designations whenever available, beginning with the present paper.

3 Individual objects

3.1 KX Aquilae

KX Aql had been long known as a dwarf nova with very low outburst frequency (cf. Garbusov 1979). Based on the long bright outburst in 1980, this object was suspected to be an SU UMa-type dwarf nova—see Kato et al. (2010) for more history. Tappert and Mennickent (2001) first presented a spectrum of this object, clearly showing the low mass-transfer rate. The long-awaited superoutburst finally occurred in 2010 and superhumps were detected (Kato et al. 2010).

Although the 2012 outburst was not a superoutburst, we report on it here because it showed an interesting phenomenon. The outburst was reported on 2012 August 22.907 UT at an unfiltered CCD magnitude of 16.0 (BAAVSS alert 2997). The object further brightened

Table 2. Superhump periods and period derivatives.

Object	Year	P_1 (d)*	Error*	E_1*		P_{dot}†	Error†	P_2 (d)*	Error*	E_2*		P_{orb} (d)‡	Q§
NN Cam	2012	0.074140	0.000057	0	41	—	—	—	—	—	—	0.0717	C
V485 Cen	2013	0.042136	0.000013	0	95	4.2	1.5	—	—	—	—	0.040995	C
YZ Cnc	2011	0.090648	0.000096	18	34	—	—	0.090379	0.000036	40	130	0.0868	B
GZ Cnc	2013	0.092842	0.000084	0	76	—	—	—	—	—	—	0.08825	C2
V503 Cyg	2012	0.081446	0.000096	21	51	—	—	0.081121	0.000026	49	123	0.077759	CM
V503 Cyg	2012b	0.081232	0.000165	0	24	—	—	—	—	—	—	0.077759	CG
AQ Eri	2012	0.062398	0.000097	0	63	29.5	13.4	—	—	—	—	0.06094	C
V660 Her	2012	0.080891	0.000164	0	26	—	—	—	—	—	—	—	CG
V660 Her	2013	0.081081	0.000040	0	50	—	—	0.080568	0.000128	99	126	—	C
V1227 Her	2012a	0.065032	0.000083	0	29	—	—	0.064839	0.000136	92	123	—	CP
V1227 Her	2012b	0.065150	0.000027	0	122	7.5	2.2	—	—	—	—	—	BP
V1227 Her	2013	0.065083	0.000046	0	19	—	—	—	—	—	—	—	CP
MM Hya	2013	—	—	—	—	—	—	0.058633	0.000103	0	29	0.057590	C
AB Nor	2013	0.079756	0.000027	0	30	—	—	0.079413	0.000032	28	105	—	C
GR Ori	2013	0.058333	0.000021	11	142	6.4	1.5	—	—	—	—	—	B
V444 Peg	2012	0.097645	0.000052	10	61	14.5	6.2	—	—	—	—	—	B
V521 Peg	2012	0.0603	0.0002	0	3	—	—	—	—	—	—	—	C
V368 Per	2012	—	—	—	—	—	—	0.078946	0.000050	0	27	—	C
TY PsA	2012	0.087809	0.000019	19	91	− 1.2	2.6	0.087655	0.000032	98	179	0.08423	A
QW Ser	2009	0.076858	0.000014	0	132	− 2.0	1.3	—	—	—	—	0.074572	CG
QW Ser	2013	0.077088	0.000051	0	34	—	—	0.076496	0.000016	46	86	0.074572	C
V493 Ser	2013	0.082917	0.000062	0	54	—	—	0.082618	0.000030	53	132	0.08001	C
AW Sge	2012	0.074733	0.000030	16	59	− 3.1	7.5	0.074312	0.000064	57	97	—	B
CI UMa	2013	0.062381	0.000084	0	32	—	—	—	—	—	—	—	C
MR UMa	2013	0.065336	0.000069	0	34	—	—	0.064615	0.000035	47	110	—	C
ASAS SN-13as	2013	0.072522	0.000095	0	42	—	—	—	—	—	—	—	CG2
ASAS SN-13ax	2013	0.056155	0.000010	52	177	4.5	0.6	—	—	—	—	—	A
ASAS SN-13bm	2013	0.069015	0.000026	0	61	—	—	—	—	—	—	—	C
ASAS SN-13bp	2013	0.06828	0.00016	0	5	—	—	—	—	—	—	—	C
ASAS SN-13br	2013	0.065337	0.000020	0	79	9.6	1.6	0.065008	0.000029	76	125	—	B
DDE 26	2012	0.089320	0.000063	0	31	− 27.4	10.6	—	—	—	—	—	CG
CSS J015051	2012	0.072706	0.000032	0	74	1.9	5.9	0.072293	—	74	116	—	C
CSS J015321	2012	0.096658	0.000096	0	23	74.0	27.0	—	—	—	—	—	C
CSS J102842	2013	0.038197	0.000006	154	315	2.6	0.5	—	—	—	—	—	C
CSS J105835	2012	0.057882	0.000025	33	117	6.5	3.0	—	—	—	—	—	C
CSS J150904	2013	0.069860	0.000043	0	18	—	—	—	—	—	—	0.06844	C
CSS J174033	2013	0.045548	0.000003	60	385	1.6	0.1	—	—	—	—	0.045048	AE

Table 2. (Continued)

Object	Year	P_1 (d)*	Error*	E_1*		P_{dot}†	Error†	P_2 (d)*	Error*	E_2*		P_{orb} (d)‡	Q§
CSS J203937	2012	0.111210	0.000042	18	98	9.0	3.3	—	—	—	—	0.10572	B
MASTER J000820	2012	0.082697	0.000087	0	13	—	—	—	—	—	—	—	C
MASTER J001952	2012	0.060955	0.000035	15	113	10.4	2.7	—	—	—	—	—	C
MASTER J030128	2012	0.062831	0.000166	96	114	—	—	—	—	—	—	—	C2
MASTER J042609	2012	0.067557	0.000029	0	40	—	—	0.066904	0.000052	81	158	0.065502	C
MASTER J054317	2012	0.075949	0.000029	39	131	6.5	3.4	0.075608	0.000044	123	211	—	B
MASTER J064725	2013	0.067774	0.000041	0	82	—	—	0.067337	0.000031	82	157	—	C
MASTER J073418	2013	—	—	—	—	—	—	0.061999	0.000055	0	36	—	C
MASTER J081110	2012	0.058137	0.000011	40	246	4.0	0.3	—	—	—	—	—	B
MASTER J094759	2013	0.056121	0.000020	45	214	3.0	1.1	—	—	—	—	0.05588	BE
MASTER J111759	2013	—	—	—	—	—	—	0.069721	0.000029	100	172	—	C
MASTER J165236	2013	0.084732	0.000085	11	32	—	—	—	—	—	—	—	C
MASTER J174902	2013	0.101908	0.000040	0	40	—	—	—	—	—	—	—	C
MASTER J181953	2013	0.057519	0.000010	35	157	2.6	1.1	—	—	—	—	0.05684	BE
MASTER J203749	2012	0.061307	0.000009	36	157	2.9	1.0	—	—	—	—	0.06062	CE
MASTER J211258	2012	0.060227	0.000008	50	155	0.8	1.0	—	—	—	—	0.059732	BE
MASTER J212624	2013	0.091281	0.000073	9	65	28.6	4.3	—	—	—	—	—	C
OT J112619	2013	0.054886	0.000010	55	260	3.6	0.4	—	—	—	—	0.05423	BE
OT J191443	2012	0.071331	0.000033	0	13	—	—	—	—	—	—	—	C
OT J205146	2012	0.057245	0.000035	0	93	12.3	2.5	0.056799	0.000057	92	216	—	C
OT J220641	2012	0.071152	0.000106	0	9	—	—	—	—	—	—	—	C
OT J232727	2012	0.053438	0.000012	41	217	4.0	1.1	—	—	—	—	0.05277	BE
PNV J062703	2013	0.059026	0.000026	0	108	6.3	1.3	—	—	—	—	0.05787	CE
SDSS J075107	2013	0.057980	0.000016	0	51	−2.9	4.1	—	—	—	—	—	C2
SDSS J080033	2012	0.080421	0.000034	0	26	—	—	—	—	—	—	—	C
SSS J122221	2013	0.076486	0.000013	203	362	−1.1	0.7	—	—	—	—	—	B
TCP J153756	2013	0.061899	0.000023	—	—	—	—	—	—	—	—	0.06101	CE
TCP J175219	2012	0.066925	0.000091	0	13	—	—	—	—	—	—	—	C

*P_1: superhump period during stage B, Error: 1 σ error, E: interval used for calculating the period (corresponding to E in section 3), P_2: superhump period during stage C.

†In units of 10^{-5}.

‡References: NN Cam (Denisenko, D. 2007, vsnet-alert 9557); V485 Cen (Augusteijn et al. 1996); YZ Cnc (Shafter & Hessman 1988); GZ Cnc (Sheets et al. 2007); V503 Cyg (this work); AQ Eri (Thorstensen et al. 1996); MM Hya (Patterson et al. 2003); TY PsA, QW Ser (this work); V493 Ser (Kato et al. 2009a); CSS J150904 (this work); CSS J174033 (T. Ohshima et al. in preparation); CSS J203937, MASTER J042609, MASTER J094759, MASTER J181953 (this work); MASTER J203749, MASTER J211258 (Nakata et al. 2013); OT J112619, OT J232727, PNV J062703, TCP J153756 (this work).

§Data quality and comments: A, excellent; B, partial coverage or slightly low quality; C, insufficient coverage or observations with large scatter; G, P_{dot} denotes global P_{dot}; M, observational gap in middle stage; 2, late-stage coverage, the listed period may refer to P_2; E, P_{orb} refers to the period of early superhumps; P, P_{orb} refers to a shorter stable periodicity recorded in outburst.

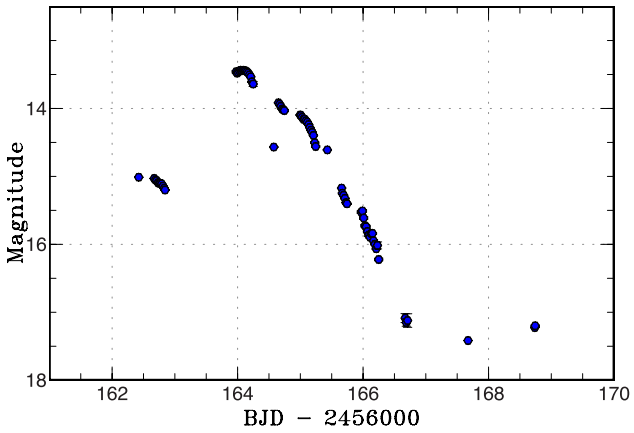

Fig. 1. Light curve of KX Aql (2012). The data were binned to 0.02 d.

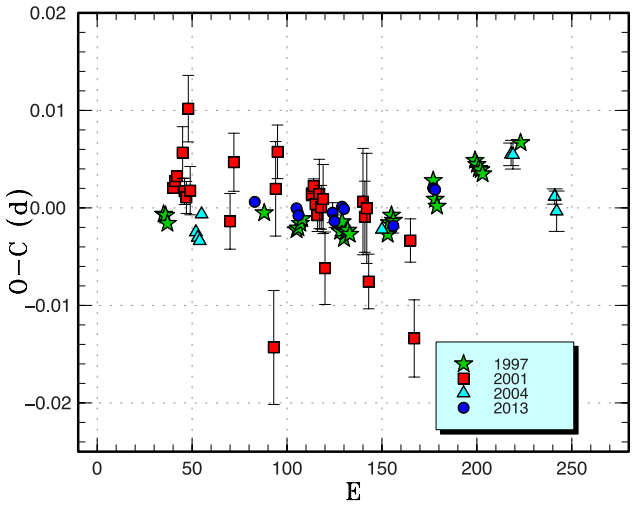

Fig. 2. Comparison of different superoutbursts of V485 Cen in the $O - C$ diagrams. A period of 0.04212 d was used to draw this figure. Approximate cycle counts (E) after the start of the superoutburst were used. Since the start of the 2013 superoutburst was not well constrained, we shifted the $O - C$ diagram to best fit the others.

relatively slowly for an SU UMa-type dwarf nova. Furthermore, there was a precursor-like fading during the rising stage of the outburst (figure 1). Such a precursor-like phenomenon in a normal outburst has been seen in frequently outbursting objects such as V1504 Cyg (Kato et al. 2012a) or V516 Lyr (Kato & Osaki 2013a). In V1504 Cyg, negative superhumps[6] appeared. In V516 Lyr, an inside-out outburst may by responsible for the double precursor event (Kato & Osaki 2013a). In the case of KX Aql, the slow rise may be interpreted as the signature of an inside-out outburst, and such a case is rare in low mass-transfer systems. In the present data, we could not detect either positive or negative superhumps during the fading stage of the outburst.

[6] Likely an "impulsive negative superhump" (Osaki & Kato 2013b).

Table 3. Superhump maxima of NN Cam (2012).

E	Max*	Error	$O - C^{\dagger}$	$N^{\ddagger}$
0	56241.1152	0.0005	−0.0012	63
1	56241.1915	0.0007	0.0011	58
39	56244.0111	0.0078	0.0032	40
40	56244.0803	0.0013	−0.0016	74
41	56244.1546	0.0013	−0.0015	71

*BJD−2400000.
†Against max = 2456241.1163 + 0.074140 E.
‡Number of points used to determine the maximum.

3.2 NN Camelopardalis

NN Cam (= NSV 1485) is a recently recognized dwarf nova (cf. Khruslov 2005), The first-ever-recorded superoutburst, preceded by a distinct precursor, was observed in 2007 (Kato et al. 2009a). We reported on two more superoutbursts in 2009 (Kato et al. 2010) and 2011 (Kato et al. 2013a). We observed another superoutburst in 2012. The times of superhump maxima are listed in table 3. The resultant period suggests that the observation revealed stage B superhumps.

3.3 V485 Centauri

V485 Cen is one of the prototypes of a small group of dwarf novae having an orbital period below the period minimum while displaying hydrogen-rich spectra (Augusteijn et al. 1993, 1996; see also T. Ohshima in preparation for the discussion of this group of objects). Olech (1997) reported on a positive period derivative. We reported the reanalysis of Olech (1997) and two additional superoutbursts in 2001 and 2004 in Kato et al. (2009a).

We observed the 2013 April superoutburst of this ultra-compact binary. The times of superhump maxima are listed in table 4. The resultant $P_{\rm dot}$ was similar to those obtained in the past observations (Olech 1997; see also Kato et al.

Table 4. Superhump maxima of V485 Cen (2013).

E	Max*	Error	$O - C^{\dagger}$	$N^{\ddagger}$
0	56399.8162	0.0003	0.0014	42
22	56400.7422	0.0002	0.0004	42
23	56400.7836	0.0002	−0.0004	38
41	56401.5421	0.0010	−0.0004	14
42	56401.5833	0.0006	−0.0013	15
46	56401.7533	0.0003	0.0002	41
47	56401.7951	0.0004	−0.0001	41
73	56402.8885	0.0007	−0.0022	33
94	56403.7769	0.0004	0.0013	41
95	56403.8189	0.0004	0.0011	31

*BJD−2400000.
†Against max = 2456399.8149 + 0.042136 E.
‡Number of points used to determine the maximum.

2009a for the correction of Olech 1997). The $O - C$ diagram also exhibited behavior similar to that in the past superoutbursts.

3.4 Z Chamaeleontis

Only single-night observations for the 2013 February superoutburst of this well-known dwarf nova were available. Two superhump maxima were recorded: BJD 2456341.1272(10) ($N = 46$) and 2456341.2042(5) ($N = 46$).

3.5 YZ Cancri

This is also a well-known SU UMa-type dwarf nova (cf. the light curve in Szkody & Mattei 1984). The reported superhump period (Patterson 1979) long remained incorrect until a new measurement became available (Kato et al. 2009a).

A superoutburst in 2011 March was observed. This outburst showed a precursor 4 d ahead of its maximum, and a rising stage to the maximum and growing superhumps were partly observed (figure 3). There was a deep dip following the precursor, as shown in the superoutburst of V344 Lyr around BJD 2456190 in the Kepler data (Osaki & Kato 2014). Unlike the Kepler data, our observations were unable to detect superhumps evolving during the dip phase. The times of superhump maxima are listed in table 5. The maxima after $E = 131$ were traditional late superhumps with an ~ 0.5-phase jump. This transition to traditional late superhumps occurred ~ 4 d ahead of the rapid decline from the superoutburst plateau. These late superhumps persisted during the post-superoutburst stage and survived during the next normal outburst.

This observation showed the first detection of stage A superhumps in YZ Cnc. Since YZ Cnc is known as one of the most frequently outbursting SU UMa-type dwarf novae, this detection confirmed the wide existence of stage A superhumps in SU UMa-type dwarf novae. The nominal q value from this measured period of stage A superhumps was 0.17, which appears to be a little too small. This was probably due to the rapid growth of the pressure effect in high-q systems, resulting in slowing the precession rate even in the latter part of stage A. If we had recorded a growing superhump during the dip following the precursor, we would have obtained a better q estimate, which was able to become a target for the next observation.

The rapid growth of the superhump amplitude when the object was rising to the maximum (figure 3) agrees well with the consequence of the TTI model (Osaki & Kato 2013a, 2013b).

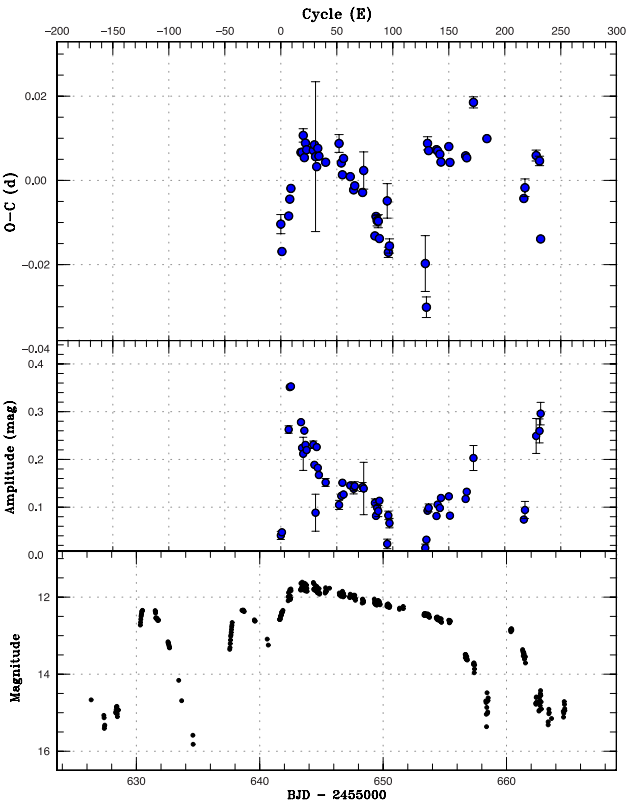

Fig. 3. $O - C$ diagram of superhumps in YZ Cnc (2011). Above: $O - C$ diagram. The maxima after $E = 131$ were traditional late superhumps with an ~0.5-phase jump. We used a period of 0.090768 d for calculating the $O - C$ residuals. Center: Amplitudes of superhumps. The growing superhumps during stage A were clearly detected. Below: Light curve. The superoutburst had a precursor outburst and a dip following it.

3.6 GZ Cancri

GZ Cnc is a variable star discovered by K. Takamizawa (TmzV34), which later turned out to be a dwarf nova (Kato et al. 2001d). Kato et al. (2002a) reported on a high number of short outbursts in this system. Tappert and Bianchini (2003) finally clarified that this is an object near the lower edge of the period gap. Although the orbital period of 0.08825(28) d would suggest an SU UMa-type dwarf nova, no secure superoutburst had been recorded until 2010 (there was a long outburst in 2007, which was only recognized retrospectively).

In 2010, the long-awaited superoutburst of this object was recorded (Kato et al. 2010). There was another superoutburst in 2013 February, and we observed it. The AAVSO data indicate that this outburst started with a precursor outburst. The times of superhump maxima are listed in table 6. Although our observations covered only the late stage of the superoutburst, the resultant period was close to that of stage B superhumps in Kato et al. (2010). A PDM analysis also yielded a period of 0.09291(2) d. This period

Table 5. Superhump maxima of YZ Cnc (2011).

E	Max*	Error	$O-C^{\dagger}$	$N^{\ddagger}$	E	Max*	Error	$O-C^{\dagger}$	$N^{\ddagger}$
0	55641.6988	0.0023	−0.0104	42	84	55649.3205	0.0007	−0.0132	72
1	55641.7831	0.0008	−0.0169	112	85	55649.4159	0.0008	−0.0086	94
7	55642.3361	0.0003	−0.0085	191	86	55649.5057	0.0012	−0.0096	93
8	55642.4309	0.0002	−0.0045	193	87	55649.5963	0.0016	−0.0097	69
9	55642.5242	0.0003	−0.0019	66	88	55649.6830	0.0005	−0.0139	249
18	55643.3497	0.0003	0.0066	95	95	55650.3273	0.0041	−0.0049	81
19	55643.4405	0.0003	0.0066	95	96	55650.4059	0.0012	−0.0171	86
20	55643.5352	0.0016	0.0107	21	97	55650.4981	0.0017	−0.0156	92
21	55643.6207	0.0003	0.0054	136	129	55653.3985	0.0066	−0.0198	101
22	55643.7150	0.0002	0.0088	239	130	55653.4789	0.0024	−0.0302	95
23	55643.8041	0.0002	0.0073	239	131	55653.6086	0.0016	0.0087	80
29	55644.3486	0.0005	0.0071	46	132	55653.6976	0.0008	0.0070	77
30	55644.4407	0.0004	0.0084	94	139	55654.3332	0.0006	0.0072	98
31	55644.5286	0.0178	0.0056	16	140	55654.4237	0.0005	0.0069	105
32	55644.6170	0.0005	0.0032	135	142	55654.6045	0.0006	0.0061	98
33	55644.7122	0.0003	0.0076	245	143	55654.6934	0.0005	0.0043	123
34	55644.8011	0.0003	0.0057	245	150	55655.3324	0.0009	0.0079	124
40	55645.3442	0.0006	0.0043	91	151	55655.4194	0.0004	0.0042	151
52	55646.4379	0.0021	0.0087	33	165	55656.6917	0.0004	0.0057	240
54	55646.6148	0.0006	0.0041	89	166	55656.7820	0.0004	0.0053	243
55	55646.7028	0.0005	0.0013	270	172	55657.3398	0.0013	0.0184	103
56	55646.7974	0.0004	0.0052	300	184	55658.4204	0.0004	0.0098	178
62	55647.3377	0.0004	0.0008	96	217	55661.4016	0.0009	−0.0044	181
65	55647.6069	0.0008	−0.0023	53	218	55661.4949	0.0021	−0.0019	99
66	55647.6986	0.0008	−0.0013	74	228	55662.4102	0.0013	0.0058	85
73	55648.3324	0.0006	−0.0029	81	231	55662.6812	0.0011	0.0045	95
74	55648.4284	0.0044	0.0023	18	232	55662.7535	0.0008	−0.0140	95

*BJD−2400000.
†Against max = 2455641.7092 + 0.090768 E.
‡Number of points used to determine the maximum.

Table 6. Superhump maxima of GZ Cnc (2013).

E	Max*	Error	$O-C^{\dagger}$	$N^{\ddagger}$
0	56329.9777	0.0009	0.0045	55
1	56330.0602	0.0028	−0.0058	36
21	56331.9304	0.0016	0.0075	96
22	56332.0144	0.0004	−0.0014	166
44	56334.0521	0.0008	−0.0062	84
54	56334.9844	0.0008	−0.0023	158
76	56337.0328	0.0012	0.0036	105

*BJD−2400000.
†Against max = 2456329.9732 + 0.092842 E.
‡Number of points used to determine the maximum.

appears to be incompatible with the assumption of a large change of period in Kato et al. (2010). We could not, however, find a solution to smoothly express both 2010 and 2013 observations mainly due to the limited coverage in both data sets. It looks as though a phase jump occurred in the 2010 superoutburst, while it did not occur in the 2013 one (figure 4). Future observations are absolutely needed to solve this issue. According to the AAVSO data, the outburst immediately preceding this superoutburst was longer duration (3–4 d), and this outburst may have been a failed superoutburst similar to those seen in the Kepler data of V1504 Cyg (Kato et al. 2012a) and in NY Ser (subsection 7.3).

3.7 V503 Cygni

V503 Cyg is one of the representative dwarf novae which exhibited negative superhumps (Harvey et al. 1995). Kato, Ishioka, and Uemura (2002b) noticed a dramatic variation of the number of normal outbursts and suggested that normal outbursts may be suppressed under certain conditions. Osaki and Kato (2013a) proposed that the disk tilt, which is supposed to cause negative superhumps, is responsible for the suppression of normal outbursts. In recent years, V503 Cyg has not shown distinct negative superhumps (Kato et al. 2013a; Pavlenko et al. 2012).

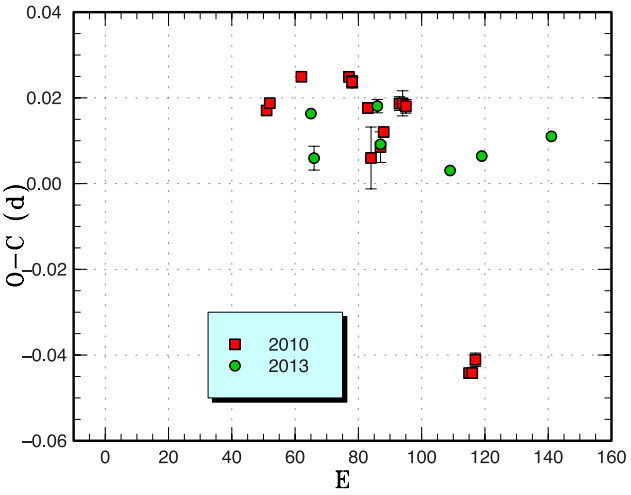

Fig. 4. Comparison of different superoutbursts of GZ Cnc in the $O-C$ diagrams. A period of 0.09290 d was used to draw this figure. Approximate cycle counts (E) after the start of the superoutburst were used.

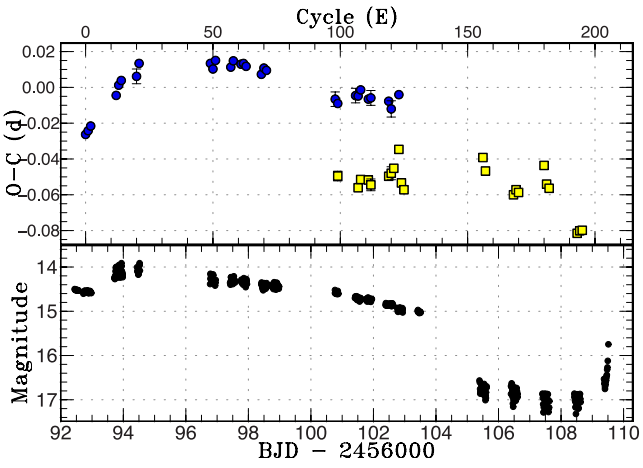

Fig. 5. $O-C$ diagram of superhumps in V503 Cyg (2012). Upper: $O-C$ diagram. The filled circles represent primary maxima of superhumps. The filled squares represent secondary maxima of superhumps and persisting superhumps. A period of 0.08146 d was used to draw this figure. Lower: Light curve. The observations were binned to 0.008 d.

Table 7. Superhump maxima of V503 Cyg (2012).

E	Max*	Error	$O-C$†	N‡
0	56092.7677	0.0012	−0.0267	76
1	56092.8513	0.0008	−0.0246	77
2	56092.9353	0.0010	−0.0220	75
12	56093.7670	0.0003	−0.0049	141
13	56093.8542	0.0003	0.0008	234
14	56093.9383	0.0003	0.0035	178
20	56094.4293	0.0041	0.0057	15
21	56094.5180	0.0004	0.0130	37
49	56096.7989	0.0006	0.0129	124
50	56096.8773	0.0003	0.0098	159
51	56096.9635	0.0013	0.0145	50
57	56097.4485	0.0005	0.0108	109
58	56097.5335	0.0005	0.0143	57
61	56097.7760	0.0014	0.0124	108
62	56097.8579	0.0006	0.0128	159
63	56097.9377	0.0003	0.0112	115
69	56098.4220	0.0008	0.0067	57
70	56098.5070	0.0003	0.0102	126
71	56098.5872	0.0015	0.0089	18
98	56100.7705	0.0041	−0.0072	52
99	56100.8495	0.0011	−0.0097	76
106	56101.4242	0.0041	−0.0053	68
107	56101.5054	0.0014	−0.0055	69
108	56101.5903	0.0012	−0.0021	81
111	56101.8295	0.0014	−0.0072	85
112	56101.9116	0.0041	−0.0066	86
119	56102.4800	0.0017	−0.0084	90
120	56102.5572	0.0045	−0.0127	87
123	56102.8095	0.0013	−0.0048	155

*BJD−2400000.
†Against max = 2456092.7944 + 0.081463 E.
‡Number of points used to determine the maximum.

We observed the 2012 June superoutburst, including the quiescent segments before and after this superoutburst. We also partly observed the 2012 September superoutburst. The times of superhump maxima in the 2012 June superoutburst are listed in table 7. After BJD 2456101 ($106 \leq E$), the profile became double waves, and in this table we listed one of the peaks which are on the smooth extension from the earlier epochs of superhump maxima. The other peak became stronger than the former peak in the latter part of the superoutburst. This behavior is very similar to V344 Lyr (Wood et al. 2011; Kato et al. 2012a) and ER UMa (Kato et al. 2009a); see figure 5 for the $O-C$ behavior. The times of the secondary maxima (during the late plateau phase) and times of the post-superoutburst superhumps are listed in table 8. The exact identification of the post-superoutburst superhumps is not perfectly clear; on the first three nights (BJD 2456105–2456107), the period was close to the superhump period before this phase, while the period was much shorter [0.0795(1) d] on the last two nights (BJD 2456107–2456109). The nature of the superhump may have changed during this period.

We can see a very clear stage A–B transition in the early part of this superoutburst. This part followed a precursor outburst. Stage A superhumps were for the first time detected in V503 Cyg. The ε^* value of stage A superhumps was 6.88(12)%, which corresponds to $q = 0.218(5)$.

The times of superhump maxima during the 2012 September superoutburst are listed in table 9.

A comparison of different superoutbursts in the $O-C$ diagrams is shown in figure 6.

We also analyzed quiescent segments after removing the first quiescent interval following the superoutburst, when

Table 8. Superhump maxima (secondary and post-superoutburst maximum) of V503 Cyg (2012).

E	Max*	Error	$O-C$†	N‡
0	56100.8090	0.0027	−0.0043	86
8	56101.4542	0.0019	−0.0092	86
9	56101.5402	0.0015	−0.0043	70
12	56101.7843	0.0015	−0.0040	66
13	56101.8631	0.0033	−0.0065	85
20	56102.4381	0.0020	−0.0003	80
21	56102.5212	0.0036	0.0016	84
22	56102.6055	0.0006	0.0046	62
24	56102.7789	0.0005	0.0156	103
25	56102.8417	0.0005	−0.0030	159
26	56102.9193	0.0012	−0.0066	112
57	56105.4626	0.0010	0.0178	65
58	56105.5365	0.0007	0.0104	72
69	56106.4193	0.0009	−0.0006	60
70	56106.5036	0.0009	0.0025	73
71	56106.5835	0.0008	0.0011	73
81	56107.4132	0.0008	0.0183	40
82	56107.4842	0.0008	0.0080	68
83	56107.5633	0.0009	0.0059	67
94	56108.4343	0.0009	−0.0170	48
95	56108.5171	0.0009	−0.0153	68
96	56108.5989	0.0015	−0.0149	59

*BJD−2400000.
†Against max = 2456100.8133 + 0.081255 E.
‡Number of points used to determine the maximum.

Table 9. Superhump maxima of V503 Cyg (2012b).

E	Max*	Error	$O-C$†	N‡
0	56177.6011	0.0005	−0.0018	85
11	56178.4989	0.0007	0.0024	88
12	56178.5793	0.0006	0.0016	90
22	56179.3844	0.0040	−0.0056	27
23	56179.4733	0.0005	0.0021	90
24	56179.5536	0.0005	0.0012	90

*BJD−2400000.
†Against max = 2456177.6029 + 0.081232 E.
‡Number of points used to determine the maximum.

the superhump still persisted. The four quiescent segments in 2012 showed no signs of negative superhumps, and this behavior was similar to the 2011 one (Kato et al. 2013a). The orbital period derived from the 2012 quiescent data was 0.077755(1) d. Similarly, the 2011 quiescent data (Kato et al. 2013a) yielded 0.077766(5) d. A combined analysis of the 2011 and 2012 data yielded 0.0777591(2) d, which we adopted as a refined orbital period. This period is in agreement with 0.077760(3) d reported in Pavlenko et al. (2012).

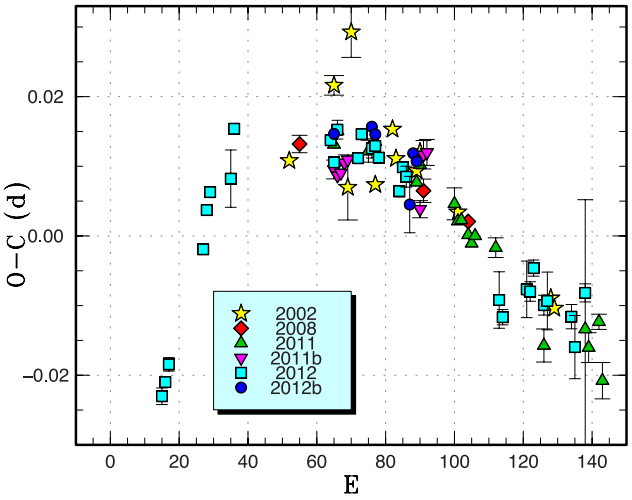

Fig. 6. Comparison of different superoutbursts of V503 Cyg in the $O-C$ diagrams. A period of 0.08152 d was used to draw this figure. Approximate cycle counts (E) after the start of the superoutburst were used. Since the starts of the superoutbursts other than the 2012 one were not well constrained, we shifted the $O-C$ diagrams to best fit the best-recorded 2012 one.

3.8 OV Draconis

This object (= SDSS J125023.85+665525.5) is a CV selected during the course of the Sloan Digital Sky Survey (SDSS: Szkody et al. 2003). Dillon et al. (2008) confirmed that this is a deeply eclipsing CV. The 2008 and 2009 superoutbursts were reported in Kato et al. (2010) and another in 2011 was reported in Kato et al. (2012a).

Only single-night observations for the 2013 February superoutburst of this eclipsing dwarf nova were available. Three superhump maxima were recorded: BJD 2456341.7864(12) ($N = 56$), 2456341.8432(10) ($N = 34$), and 2456341.9070(11) ($N = 60$). The epoch of the eclipse minimum (average of four eclipse observations) was BJD 2456341.8182(1) determined by the Markov-chain Monte Carlo (MCMC) analysis introduced in Kato et al. (2013a). We also updated the eclipse ephemeris using our 2008–2013 observations:

$$\mathrm{Min(BJD)} = 2453407.5600(1) + 0.058735677(4)E. \quad (1)$$

3.9 AQ Eridani

AQ Eri is a well-known dwarf nova whose SU UMa-type nature was first clarified by Kato, Fujino, and Iida (1989). Kato (1991, 2001) reported on observations of superhumps with limited coverage, and Kato and Matsumoto (1999a) reported a photometric study of a normal outburst. The spectroscopic study and the measurement of the orbital period were performed by Mennicken and Vogt (1993). The first well-observed superoutburst occurred in 2008

Table 10. Superhump maxima of AQ Eri (2012).

E	Max*	Error	$O-C^{\dagger}$	$N^{\ddagger}$
0	56213.2582	0.0011	0.0035	25
1	56213.3172	0.0006	0.0001	58
32	56215.2486	0.0005	−0.0018	264
33	56215.3094	0.0003	−0.0035	319
48	56216.2379	0.0026	−0.0105	67
49	56216.3117	0.0017	0.0010	68
62	56217.1310	0.0012	0.0095	111
63	56217.1878	0.0008	0.0040	111
96	56219.2375	0.0021	−0.0045	46
97	56219.3065	0.0004	0.0022	123

*BJD−2400000.
†Against max = 2456213.2548 + 0.062366 E.
‡Number of points used to determine the maximum.

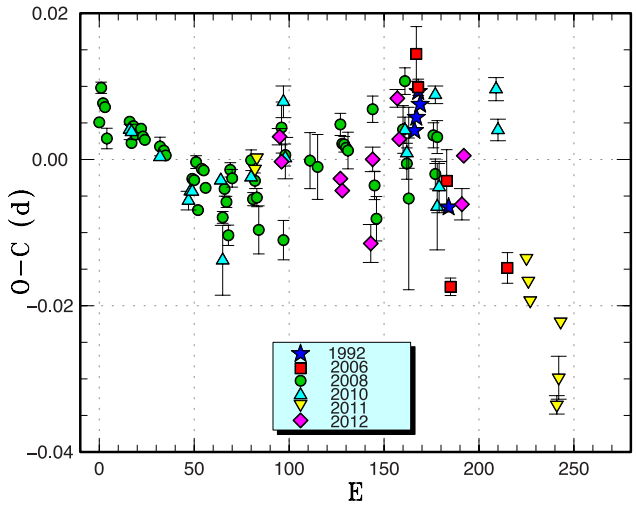

Fig. 7. Comparison of different superoutbursts of AQ Eri in the $O-C$ diagrams. A period of 0.06238 d was used to draw this figure. Approximate cycle counts (E) after the start of the superoutburst were used. Since the start of the 2012 superoutburst was not well constrained, we shifted the $O-C$ diagram to best fit the best-recorded 2008 one.

(Kato et al. 2009a). Two more superoutbursts in 2010 and 2011 were also reported in Kato et al. (2010) and Kato et al. (2013a), respectively.

We observed the 2012 superoutburst during its (presumably) latter part. The times of superhump maxima are listed in table 10. Stages B and C can be recognized. A comparison of $O-C$ diagrams of AQ Eri between different superoutbursts is shown in figure 7. The object shows a long-lasting stage C such as was observed in QZ Vir (Kato et al. 2009a; Ohshima et al. 2011).

3.10 V660 Herculis

V660 Her was discovered to be a dwarf nova by Shugarov (1975). Spogli, Fiorucci, and Tosti (1998) reported on color variations during an outburst. Liu et al. (1999) reported a spectrum confirming its dwarf-nova-type nature, and suggested that the object has a low mass-transfer rate and a short orbital period. Thorstensen and Fenton (2003) conducted a radial-velocity study and confirmed a short [0.07826(8) d] orbital period. Olech et al. (2005) confirmed the SU UMa-type nature during the 2004 superoutburst. We also reported the 2009 superoutburst in Kato et al. (2010).

The 2012 superoutburst was detected by G. Poyner visually. The times of superhump maxima are listed in table 11. The result for the 2013 superoutburst, which was detected by M. Rodríguez and contained a precursor (vsnet-alert 15930, 15945), is shown in table 12. The data showed both stage B and stage C superhumps. A comparison in the $O-C$ diagrams (figure 8) suggests that the 2012 observation recorded early stage C. The initial part of the

Table 11. Superhump maxima of V660 Her (2012).

E	Max*	Error	$O-C^{\dagger}$	$N^{\ddagger}$
0	56177.3446	0.0032	−0.0051	30
1	56177.4355	0.0006	0.0049	86
13	56178.4019	0.0006	0.0007	77
25	56179.3717	0.0005	−0.0002	84
26	56179.4525	0.0008	−0.0004	77

*BJD−2400000.
†Against max = 2456177.3496 + 0.080891 E.
‡Number of points used to determine the maximum.

Table 12. Superhump maxima of V660 Her (2013).

E	Max*	Error	$O-C^{\dagger}$	$N^{\ddagger}$
0	56482.3481	0.0006	−0.0073	34
1	56482.4323	0.0002	−0.0039	84
2	56482.5134	0.0002	−0.0036	81
12	56483.3257	0.0011	0.0005	23
13	56483.4065	0.0004	0.0005	79
14	56483.4868	0.0003	−0.0000	169
25	56484.3814	0.0006	0.0055	54
26	56484.4598	0.0004	0.0030	83
27	56484.5402	0.0007	0.0027	45
50	56486.4033	0.0004	0.0069	82
99	56490.3584	0.0006	0.0017	36
112	56491.4088	0.0013	0.0014	29
113	56491.4936	0.0012	0.0055	87
114	56491.5669	0.0020	−0.0021	44
124	56492.3735	0.0008	−0.0036	41
125	56492.4526	0.0008	−0.0054	43
126	56492.5370	0.0012	−0.0018	34

*BJD−2400000.
†Against max = 2456482.3554 + 0.080821 E.
‡Number of points used to determine the maximum.

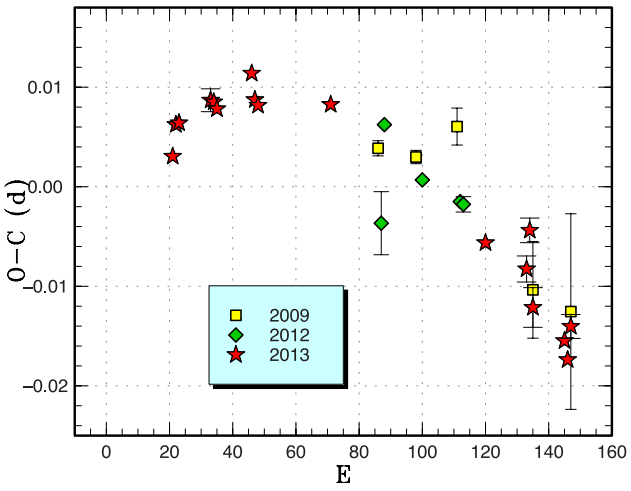

Fig. 8. Comparison of different superoutbursts of V660 Her in the $O - C$ diagrams. A period of 0.08100 d was used to draw this figure. Approximate cycle counts (E) after the start of the superoutburst were used. Since the start of the 2012 superoutburst was not well constrained, we shifted the $O - C$ diagram to best fit the rest.

2013 observation may have recorded the terminal part of stage A.

3.11 V1227 Herculis

This object (= SDSS J165359.06+201010.4) was selected as a CV during the course of the SDSS (Szkody et al. 2006, who detected superhumps with a period of 1.58 h during one of its superoutbursts). Two superoutbursts have been observed in detail in 2010 (Kato et al. 2010) and in 2012 May (Kato et al. 2013a; Shears et al. 2013).

The object again underwent two superoutbursts in 2012 September (detected by R. Sabo and relayed by J. Shears, BAAVSS alert 3017) and 2013 May (detected by J. Shears, BAAVSS alert 3288). Since new data became available after the publication of Kato et al. (2013a), we have updated the table of superhump maxima in the 2012 May superoutburst (table 13) and listed the revised periods in table 2. The times of superhump maxima for the new superoutbursts are listed in tables 14 and 15. Although $E = 168$ in the 2012 September observation likely corresponds to a stage C superhump, we could not determine the period of stage C superhumps. We have been able to determine $P_{\rm dot}$ of stage B superhumps for the first time. In figure 9, we show a comparison of different superoutbursts of V1227 Her in the $O - C$ diagrams. In figure 51 of Kato et al. (2013a), we assumed that the 2010 observation started soon after the start of the outburst. This appears less likely because its rapid fading started 9 d after the detection, and because the $O - C$ diagram does not match the present observation. We therefore shifted the 2010 one from $E = 0$ to 65 to best match the present observation.

Table 13. Superhump maxima of V1227 Her (2012 May).

E	Max*	Error	$O - C^{\dagger}$	$N^{\ddagger}$
0	56062.5237	0.0071	−0.0020	8
1	56062.5904	0.0004	−0.0004	67
2	56062.6574	0.0004	0.0015	52
14	56063.4328	0.0004	−0.0039	105
15	56063.4999	0.0004	−0.0018	116
23	56064.0246	0.0062	0.0023	19
24	56064.0890	0.0009	0.0016	70
25	56064.1506	0.0011	−0.0019	52
29	56064.4077	0.0008	−0.0050	47
30	56064.4857	0.0120	0.0080	21
92	56068.5138	0.0007	0.0019	64
93	56068.5818	0.0034	0.0048	15
106	56069.4275	0.0093	0.0046	26
107	56069.4898	0.0009	0.0019	57
108	56069.5504	0.0007	−0.0026	55
116	56070.0722	0.0022	−0.0013	132
117	56070.1372	0.0023	−0.0014	82
122	56070.4682	0.0016	0.0042	119
123	56070.5185	0.0020	−0.0105	80

*BJD−2400000.
†Against max = 2456062.5237 + 0.065067 E.
‡Number of points used to determine the maximum.

Table 14. Superhump maxima of V1227 Her (2012 September).

E	Max*	Error	$O - C^{\dagger}$	$N^{\ddagger}$
0	56182.6775	0.0003	0.0036	56
1	56182.7404	0.0003	0.0014	57
10	56183.3260	0.0009	0.0007	33
11	56183.3940	0.0003	0.0036	67
15	56183.6539	0.0003	0.0029	54
16	56183.7179	0.0003	0.0019	56
31	56184.6919	0.0006	−0.0013	56
32	56184.7547	0.0007	−0.0035	51
39	56185.2065	0.0015	−0.0077	32
40	56185.2750	0.0009	−0.0043	47
41	56185.3413	0.0008	−0.0032	69
42	56185.4086	0.0007	−0.0010	51
77	56187.6913	0.0010	0.0019	56
78	56187.7537	0.0011	−0.0009	56
91	56188.5928	0.0032	−0.0085	19
92	56188.6709	0.0005	0.0044	56
93	56188.7357	0.0012	0.0040	34
107	56189.6442	0.0005	0.0006	55
108	56189.7057	0.0008	−0.0029	54
122	56190.6322	0.0010	0.0116	31
168	56193.6135	0.0052	−0.0034	23

*BJD−2400000.
†Against max = 2456182.6739 + 0.065137 E.
‡Number of points used to determine the maximum.

Table 15. Superhump maxima of V1227 Her (2013).

E	Max*	Error	$O-C^{\dagger}$	$N^{\ddagger}$
0	56418.4412	0.0022	−0.0012	30
1	56418.5091	0.0002	0.0016	72
2	56418.5730	0.0001	0.0003	72
3	56418.6370	0.0002	−0.0007	72
16	56419.4838	0.0003	−0.0005	71
17	56419.5497	0.0002	0.0003	72
18	56419.6148	0.0002	0.0003	72
19	56419.6794	0.0008	−0.0002	37

*BJD−2400000.
†Against max = 2456418.4424 + 0.065115 E.
‡Number of points used to determine the maximum.

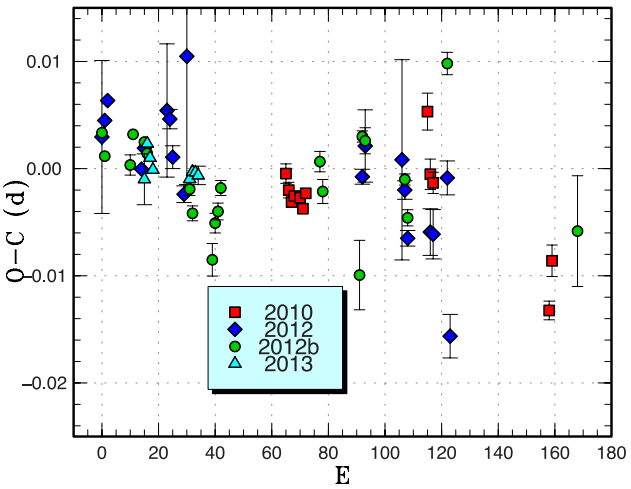

Fig. 9. Comparison of different superoutbursts of V1227 Her in the $O-C$ diagrams. A period of 0.06520 d was used to draw this figure. Approximate cycle counts (E) after the start of the superoutburst were used. Since the starts of the 2010 and 2013 superoutbursts were not well constrained, we shifted the $O-C$ diagrams to best fit the best-recorded 2012b one.

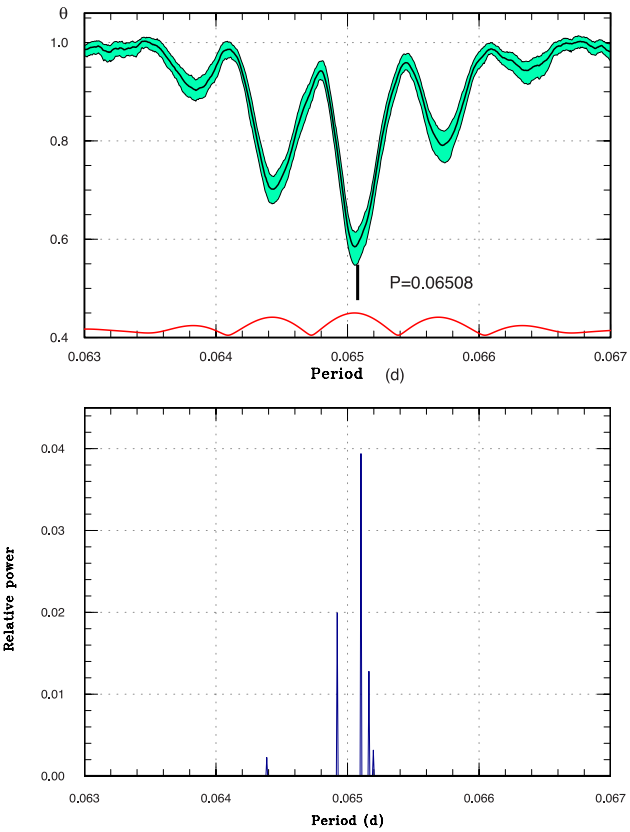

Fig. 10. Period analysis in V1227 Her (2012 May). Upper: PDM analysis. The curve at the bottom refers to the window function. Lower: Lasso analysis ($\log\lambda = -2.11$). The main signal of the superhump is split due to the variation in the period.

The 2012 May and September superoutbursts were also studied by Shears et al. (2013) using data partly overlapping with the present data. Shears et al. (2013) reported the analysis of superhumps and also suggested a possible orbital period. The orbital period in Shears et al. (2013) was suggested by the possible presence of eclipse-like phenomena. Since this period is close to the side lobe of the main superhump signal (e.g., see the window function in figure 10), we undertook both PDM and Lasso analyses (figures 10 and 11). It appears that a signal around 0.0644 d is commonly present in these data. By combining these data, a PDM analysis yielded a period of 0.0644246(5) d (figure 12; the selection of the period was made by comparing the periods obtained from individual superoutbursts). Following Shears et al. (2013), we chose this period as the candidate orbital period. The profile is, however, not eclipse-like as reported in Shears et al. (2013). As described in Shears et al. (2013), this $P_{\rm orb}$ gives a relatively small ε. The identity of the period needs to be confirmed by further observations.

3.12 MM Hydrae

MM Hya was originally selected as a CV by the Palomar–Green survey (Green et al. 1982). Misselt and Shafter (1995) suggested that it may be a WZ Sge-type dwarf nova based on the short orbital period. Patterson et al. (2003) reported a mean $P_{\rm SH}$ of 0.05868 d during the 1998 superoutburst. Not much details were known about this object except for a mean supercycle of ∼380 d, which does not answer the expectation of Misselt and Shafter (1995). In 2011, the first well-observed superoutburst occurred and we reported on it in Kato et al. (2012a). Information on other (rather poorly studied) superoutbursts was also reported in Kato et al. (2009a, 2012a, 2013a).

We observed the late plateau phase and the declining phase of the 2013 superoutburst. The times of maxima

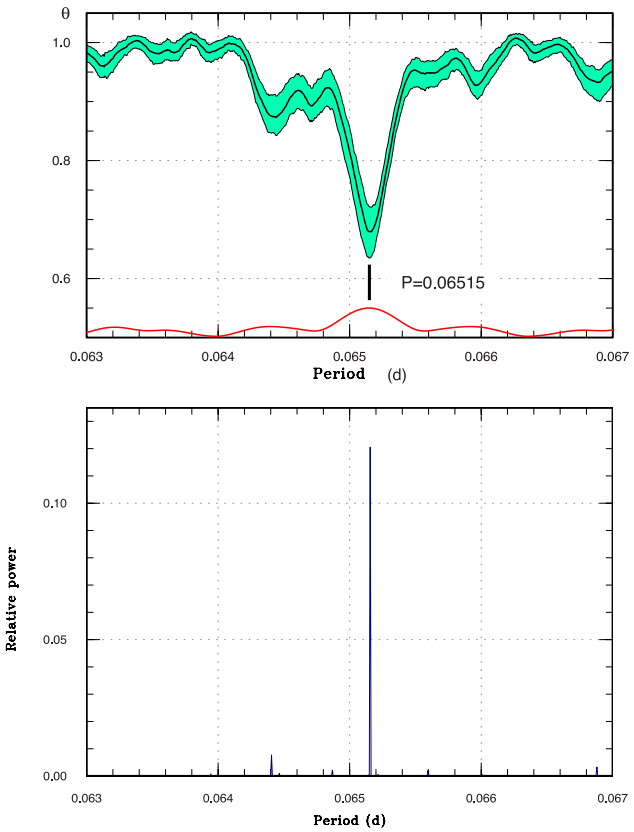

Fig. 11. Period analysis in V1227 Her (2012 September). Upper: PDM analysis. The curve at the bottom refers to the window function. Lower: Lasso analysis ($\log\lambda = -2.07$).

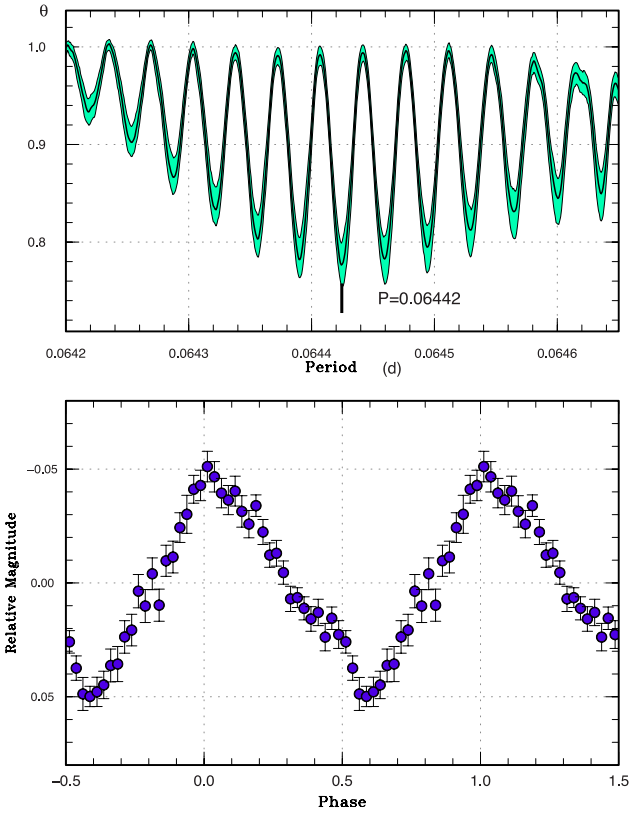

Fig. 12. Possible orbital signal of V1227 Her from the 2012 observation. Upper: PDM analysis. Lower: Phase-averaged profile.

are listed in table 16. These superhumps are stage C superhumps.

3.13 AB Normae

AB Nor was discovered by Swope and Caldwell (1930) during the photographic survey of the southern Milky Way. Only little had been known before 1997, when regular monitoring by R. Stubbings started. During the 2000 outburst, which followed a precursor outburst, superhumps were detected by W.S.G. Walker (vsnet-alert 4589; see Kato et al. 2004a for more history). Kato et al. (2004a) reported on the 2002 superoutburst and established the superhump period—since this work was before the establishment of superhump stages, the updated interpretation was reported in Kato et al. (2009a).

We observed the 2013 superoutburst. The times of superhump maxima are listed in table 17. The final part of stage B and stage C were recorded. A combined $O-C$ diagram (figure 13) suggests that stage B may be relatively long for this $P_{\rm SH}$. Since the middle of stage B was not well observed, observations of this stage are needed.

Table 16. Superhump maxima of MM Hya (2013).

E	Max*	Error	$O-C$†	N‡
0	56364.4629	0.0008	0.0025	61
1	56364.5176	0.0009	−0.0014	56
2	56364.5766	0.0010	−0.0010	45
17	56365.4592	0.0011	0.0021	57
18	56365.5132	0.0011	−0.0026	58
28	56366.0984	0.0119	−0.0037	68
29	56366.1648	0.0015	0.0040	74

*BJD−2400000.
†Against max = 2456364.4604 + 0.058633 E.
‡Number of points used to determine the maximum.

3.14 DT Octantis

DT Oct (= NSV 10934) was originally discovered to be a large-amplitude suspected variable star of unknown classification. Kato et al. (2002a) suggested an X-ray identification and reported the detection of multiple outbursts, leading to a dwarf-nova-type classification. Kato et al. (2004a) reported the first detection of superhumps; this result was updated in Kato et al. (2009a). Two other superoutbursts in 2003 (second one in 2003) and 2008 with poorer coverage were also reported in Kato et al. (2009a).

Table 17. Superhump maxima of AB Nor (2013).

E	Max*	Error	$O-C^{\dagger}$	$N^{\ddagger}$
0	56436.2565	0.0006	−0.0012	184
1	56436.3351	0.0005	−0.0021	182
2	56436.4136	0.0005	−0.0031	183
3	56436.4938	0.0006	−0.0024	184
4	56436.5735	0.0006	−0.0022	183
5	56436.6521	0.0048	−0.0031	61
28	56438.4888	0.0042	0.0052	15
29	56438.5678	0.0016	0.0047	19
30	56438.6469	0.0018	0.0042	13
41	56439.5212	0.0011	0.0041	18
42	56439.6008	0.0009	0.0043	20
55	56440.6307	0.0009	0.0007	17
64	56441.3476	0.0005	0.0021	184
66	56441.5042	0.0013	−0.0003	19
67	56441.5844	0.0013	0.0005	18
68	56441.6628	0.0043	−0.0007	7
78	56442.4555	0.0104	−0.0029	7
79	56442.5325	0.0016	−0.0054	17
80	56442.6142	0.0012	−0.0033	20
91	56443.4941	0.0032	0.0022	17
92	56443.5680	0.0014	−0.0034	17
93	56443.6544	0.0031	0.0035	9
104	56444.5309	0.0035	0.0056	18
105	56444.5979	0.0041	−0.0069	20

*BJD−2400000.
†Against max = 2456436.2577 + 0.079496 E.
‡Number of points used to determine the maximum.

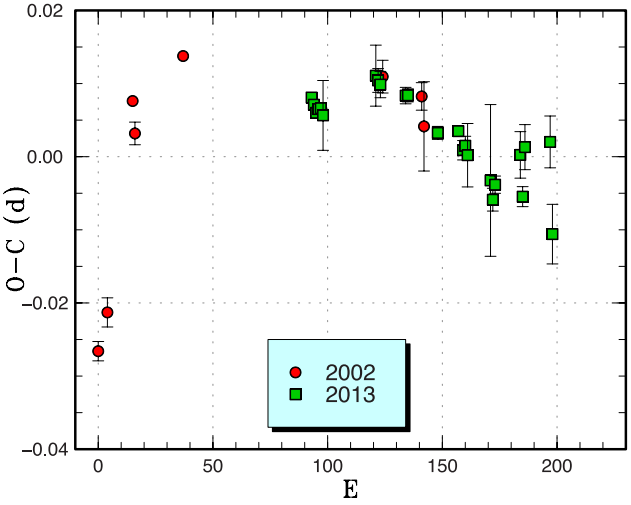

Fig. 13. Comparison of different superoutbursts of AB Nor in the $O-C$ diagrams. A period of 0.07962 d was used to draw this figure. Since the start of the 2013 superoutburst was not well constrained, we shifted the $O-C$ diagram to best fit the better-defined 2002 one.

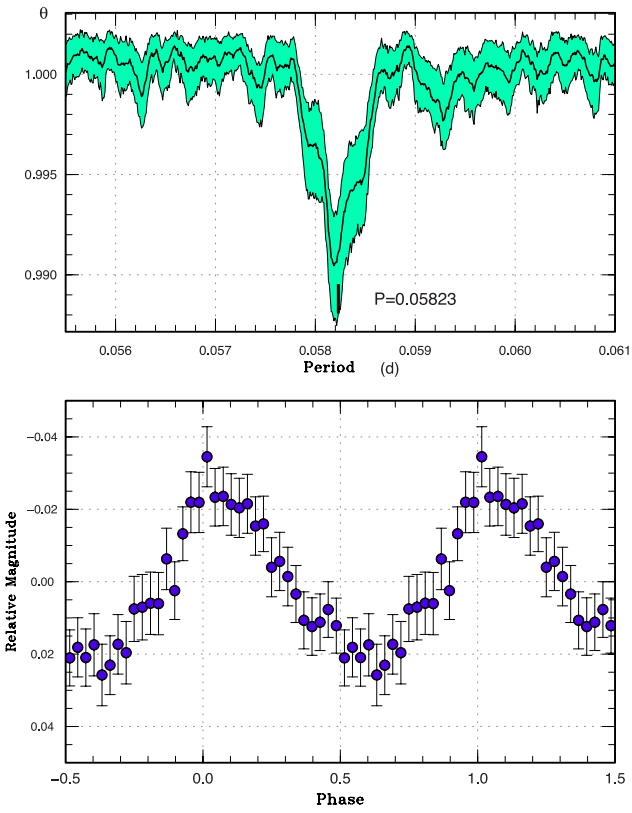

Fig. 14. Superhumps in GR Ori (2013). Upper: PDM analysis. Lower: Phase-averaged profile.

Only the final stage of the 2013 March–April superoutburst was observed. A single superhump maximum BJD 2456376.8560(6) ($N = 74$) was measured.

3.15 GR Orionis

As introduced in Kato, Maehara, and Uemura (2012b),[7] GR Ori was initially recorded as a nova, which was later supposed to be a dwarf nova. The second known outburst was detected on 2013 February 11 at a visual magnitude of 13.0 by R. Stubbings (vsnet-outburst 15096). Astrometric measurement by D. Buczynski during the outburst confirmed the suggested quiescent identification (Robertson et al. 2000; Kato et al. 2012b). Arai and Nogami (2013) confirmed the dwarf-nova-type nature by spectroscopy. Although early observations recorded some variations, no definite period of early superhumps was obtained. The object is likely to have a low orbital inclination.

Ordinary superhumps appeared on February 20–21 (vsnet-alert[8] 15430, 15432, 15434; figure 14). The times of

[7] There was an incorrect citation in Kato, Maehara, and Uemura (2012b). GR Ori had already faded to 13.0 on February 8 (Thiele 1916). Note that the magnitude system in Thiele (1916) was probably 1–2 mag brighter than the present one.

[8] The vsnet-alert archive can be seen at ⟨http://ooruri.kusastro.kyoto-u.ac.jp/pipermail/vsnet-alert/⟩.

Table 18. Superhump maxima of GR Ori (2013).

E	Max*	Error	$O-C^{\dagger}$	$N^{\ddagger}$	E	Max*	Error	$O-C^{\dagger}$	$N^{\ddagger}$
0	56344.9799	0.0009	0.0010	143	62	56348.5917	0.0028	−0.0001	48
1	56345.0365	0.0009	−0.0006	137	63	56348.6512	0.0019	0.0011	40
2	56345.0877	0.0050	−0.0077	118	65	56348.7695	0.0027	0.0030	37
5	56345.2726	0.0012	0.0023	97	68	56348.9342	0.0021	−0.0072	99
6	56345.3295	0.0013	0.0010	129	69	56349.0068	0.0075	0.0071	136
11	56345.6213	0.0002	0.0014	61	75	56349.3563	0.0020	0.0070	98
12	56345.6787	0.0003	0.0005	55	76	56349.4057	0.0012	−0.0019	124
13	56345.7373	0.0005	0.0008	61	78	56349.5250	0.0018	0.0009	16
17	56345.9811	0.0025	0.0116	104	79	56349.5814	0.0032	−0.0009	62
18	56346.0324	0.0016	0.0046	102	80	56349.6408	0.0006	0.0001	70
19	56346.0805	0.0018	−0.0056	83	81	56349.7003	0.0005	0.0013	55
28	56346.6108	0.0015	0.0003	47	85	56349.9319	0.0096	−0.0001	61
29	56346.6703	0.0004	0.0015	62	86	56349.9910	0.0038	0.0007	61
30	56346.7272	0.0005	0.0001	61	91	56350.2800	0.0026	−0.0017	50
35	56347.0186	0.0015	0.0001	44	92	56350.3412	0.0013	0.0013	108
40	56347.3064	0.0029	−0.0034	28	93	56350.3989	0.0017	0.0007	33
41	56347.3685	0.0006	0.0005	69	97	56350.6345	0.0029	0.0032	16
42	56347.4248	0.0008	−0.0015	46	114	56351.6262	0.0010	0.0043	79
44	56347.5432	0.0016	0.0003	22	115	56351.6872	0.0009	0.0070	61
45	56347.6000	0.0007	−0.0011	178	116	56351.7459	0.0031	0.0075	25
46	56347.6553	0.0008	−0.0041	175	132	56352.6812	0.0010	0.0104	56
47	56347.7161	0.0004	−0.0015	117	133	56352.7380	0.0021	0.0089	29
51	56347.9409	0.0021	−0.0099	98	142	56353.2645	0.0007	0.0110	111
52	56348.0160	0.0027	0.0070	88	148	56353.5959	0.0035	−0.0073	141
53	56348.0543	0.0039	−0.0131	97	149	56353.6538	0.0016	−0.0077	118
57	56348.2961	0.0007	−0.0043	139	150	56353.7202	0.0012	0.0005	95
58	56348.3564	0.0007	−0.0022	192	160	56354.2948	0.0062	−0.0076	134
59	56348.4170	0.0008	0.0000	79	161	56354.3533	0.0026	−0.0074	134
61	56348.5281	0.0014	−0.0054	19	167	56354.7034	0.0023	−0.0069	55

*BJD−2400000.

†Against max = 2456344.9789 + 0.058272 E.

‡Number of points used to determine the maximum.

superhump maxima are listed in table 18. Due to the faintness of the object, the errors were relatively large despite fair coverage. During $11 \leq E \leq 142$, we obtained a positive $P_{\rm dot}$ of $+6.4(1.5) \times 10^{-5}$ for stage B (figure 15). Although there was a hint of stage A in the earliest part of the observation, the growing stage of superhumps was unfortunately missed. There was a possible phase jump after $E = 142$, corresponding to the time of the rapid decline.

The object underwent a long-lasting rebrightening (vsnet-alert 15479, 15485, 15508; figure 15) similar to those of WZ Sge (Ishioka et al. 2002; Patterson et al. 2002; Kato et al. 2009a), AL Com (Patterson et al. 1996; Nogami et al. 1997; Ishioka et al. 2002), and OT J012059.6+325545 (Kato et al. 2012a). The overall behavior was not atypical among short $P_{\rm orb}$ WZ Sge-type dwarf novae.

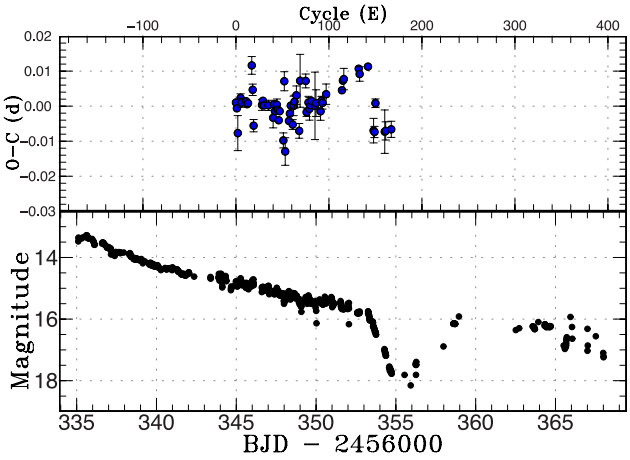

Fig. 15. $O-C$ diagram of superhumps in GR Ori (2013). Upper: $O-C$ diagram. A period of 0.05827 d was used to draw this figure. Lower: Light curve. The observations were binned to 0.012 d.

Table 19. Superhump maxima of V444 Peg (2012).

E	Max*	Error	$O-C$†	N‡
0	56193.6015	0.0005	−0.0001	42
4	56193.9933	0.0008	0.0012	67
5	56194.0911	0.0008	0.0013	68
10	56194.5806	0.0005	0.0026	42
20	56195.5533	0.0007	−0.0010	24
21	56195.6552	0.0014	0.0033	27
26	56196.1394	0.0008	−0.0007	87
30	56196.5254	0.0024	−0.0052	24
31	56196.6237	0.0007	−0.0046	38
34	56196.9240	0.0063	0.0028	120
35	56197.0157	0.0003	−0.0031	279
45	56197.9926	0.0004	−0.0026	268
51	56198.5816	0.0019	0.0007	38
55	56198.9723	0.0006	0.0008	291
60	56199.4610	0.0007	0.0013	80
61	56199.5589	0.0032	0.0016	17
71	56200.5426	0.0021	0.0090	46
72	56200.6239	0.0073	−0.0074	39

*BJD−2400000.
†Against max = 2456193.6016 + 0.097635 E.
‡Number of points used to determine the maximum.

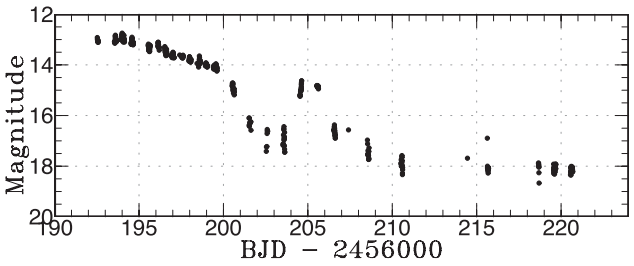

Fig. 16. Light curve of V444 Peg (2013). A post-superoutburst rebrightening occurred immediately after the superoutburst. The data were binned to 0.005 d.

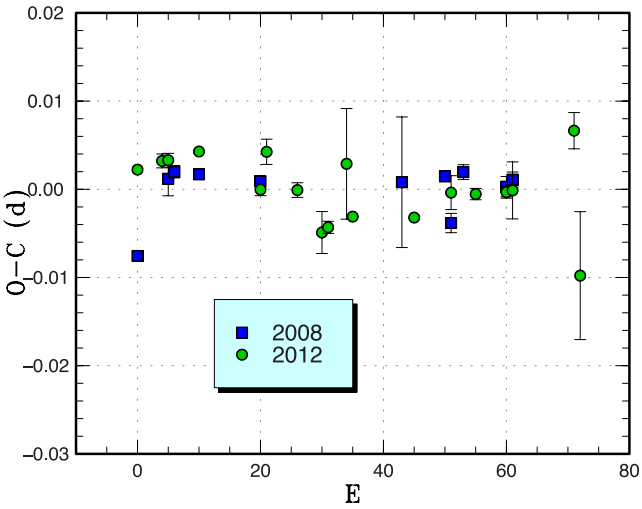

Fig. 17. Comparison of different superoutbursts of V444 Peg in the $O-C$ diagrams. A period of 0.09770 d was used to draw this figure. Since the starts of the outbursts were not well constrained, we used cycle counts (E) after the start of the observation.

3.16 V444 Pegasi

This object (= OT J213701.8+071446) is a dwarf nova discovered by K. Itagaki (cf. Kato et al. 2009a). The analysis of the 2008 superoutburst was reported in Kato et al. (2009a). CRTS detected another bright outburst (12.9 mag on 2012 September 21, communicated by E. Muyllaert, cvnet-outburst 4943). The times of superhump maxima are listed in table 19. Despite the long $P_{\rm SH}$, the period did not decrease with time. Using the likely stage B superhumps, we obtained a significantly positive $P_{\rm dot}$. Similar large positive $P_{\rm dot}$'s in long-period systems were seen in GX Cas (Kato et al. 2012a) and SDSS J170213.26+322954.1 (hereafter SDSS J170213, Kato et al. 2013a). The object is also unusual in the fact that it showed a post-superoutburst rebrightening only 5 d after the rapid fading of the superoutburst (figure 16). Such a phenomenon immediately following the superoutburst is usually seen only in WZ Sge-type dwarf novae—the "dip" phenomenon in WZ Sge (Ishioka et al. 2002; Patterson et al. 2002; Kato et al. 2009a), AL Com (Ishioka et al. 2002; Patterson et al. 1996), and OT J012059.6+325545 (Kato et al. 2012a).

A comparison of different superoutbursts of V444 Peg in the $O-C$ diagrams is given in figure 17. It looks as though the 2008 observation recorded stages A and B, rather than stages B and C, as identified in Kato et al. (2009a).

3.17 V521 Pegasi

This object (= HS 2219+1824) is a dwarf nova reported in Rodríguez-Gil et al. (2005), which reported the detection of superhumps with a period of 0.06184 d and orbital modulations with a period of 0.0599 d. Since then, the object underwent superoutbursts in unfavorable conditions and new period measurements have not been available. The 2012 superoutburst was detected by P. Schmeer visually (vsnet-alert 14926). Only single-night observations were available (vsnet-alert 14959, figure 18). The times of superhump maxima are listed in table 20. The period by the PDM method was 0.0603(2) d. It is not known in which stage this object was observed. The period is too different from that in Rodríguez-Gil et al. (2005) to be considered as a consequence of a stage B–C transition. Since Rodríguez-Gil et al. (2005) observed the very early stage of the outburst, their data may have been contaminated by stage A superhumps. We need better observations to establish the basic periods in this system.

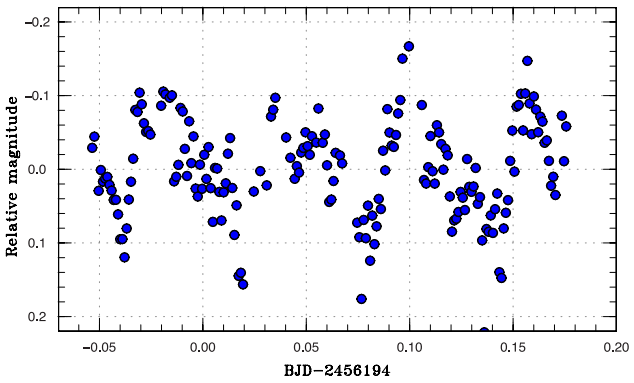

Fig. 18. Superhumps in V521 Peg (2012).

Table 20. Superhump maxima of V521 Peg (2012).

E	Max*	Error	$O-C^{\dagger}$	$N^{\ddagger}$
0	56193.9798	0.0009	−0.0004	42
1	56194.0411	0.0017	0.0008	29
2	56194.1002	0.0007	−0.0002	39
3	56194.1604	0.0009	−0.0001	36

*BJD−2400000.
†Against max = 2456193.9802 + 0.060095 E.
‡Number of points used to determine the maximum.

3.18 V368 Persei

V368 Per was discovered by Richter (1969), who recorded one outburst (JD 2440152.4) lasting ∼2 d. Kurochkin (1973) studied this object on photographic plates and recorded two additional outbursts. The second outburst (JD 2441599.4) lasted 7 d and faded from 15.1 mag to 15.7 mag. Based on these observations, Kurochkin (1973) suggested that the object is a Z Cam-type dwarf nova. This suggestion was probably due to long duration of the second outburst, rather than due to any signature of a standstill. Busch, Häussler, and Splittgerber (1979) further studied this object on Sonneberg plates and found seven more outbursts. One of these (JD 2440151–2440153) was recorded for three consecutive nights, and rapid rise (1 mag in 0.24 d) and fading (1 mag in 1 d) were recorded. No long outburst was recorded. Busch, Häussler, and Splittgerber (1979) classified this object as a dwarf nova.

The object has largely been neglected until S. Brady started systematically monitoring it with a CCD. Although he detected an outburst on 2007 October 13 and found superhumplike modulations, this finding was not broadly communicated. During an outburst in 2012 December, I. Miller reported the detection of superhumps (BAAVSS alert 3113). Follow-up observations confirmed this finding (figure 19). The times of superhump maxima are listed in table 21. Since the object was observed only during the final part of the superoutburst, we identified these superhumps

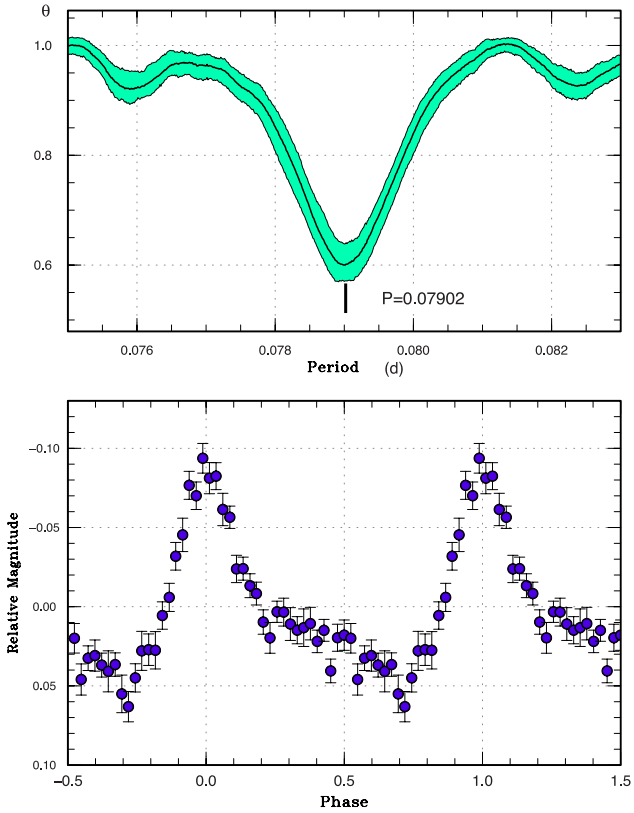

Fig. 19. Superhumps in V368 Per (2012). Upper: PDM analysis. Lower: Phase-averaged profile.

Table 21. Superhump maxima of V368 Per (2012).

E	Max*	Error	$O-C^{\dagger}$	$N^{\ddagger}$
0	56269.4514	0.0008	−0.0007	68
1	56269.5301	0.0009	−0.0010	82
2	56269.6103	0.0010	0.0003	70
11	56270.3214	0.0007	0.0009	174
12	56270.4013	0.0011	0.0018	109
23	56271.2661	0.0090	−0.0018	36
24	56271.3486	0.0014	0.0018	56
25	56271.4269	0.0023	0.0011	69
26	56271.5018	0.0021	−0.0029	67
27	56271.5842	0.0021	0.0006	77

*BJD−2400000.
†Against max = 2456269.4521 + 0.078946 E.
‡Number of points used to determine the maximum.

as stage C superhumps. Although there was an observation 7 d ahead of the first superhump maximum in table 21, only one superhump minimum was recorded. We did not include this observation because no superhump maximum was fully recorded. The superhump amplitude was, however, as large as 0.4 mag.

The rapidly fading outburst in Busch, Häussler, and Splittgerber (1979) was most likely a normal outburst, and

the long-lasting one in Kurochkin (1973) was a superoutburst. This object is yet another example in which a superoutburst was confused as a standstill—see, e.g., AQ Eri (Kato et al. 1989), TT Boo (Meinunger 1966; Kukarkin et al. 1969).

3.19 TY Piscis Austrini

TY PsA has been a well-known SU UMa-type dwarf nova since Barwig et al. (1982). The reported observations since then were, however, rather restricted to high-speed photometry to detect dwarf nova oscillations (Warner et al. 1989) and spectroscopy (O'Donoghue & Soltynski 1992). Until our report on the 2008 superoutburst (Kato et al. 2009a), the superhump period with a limited accuracy by Warner, O'Donoghue, and Wargau (1989) had been long used.

We could obtain a very good coverage of the 2012 superoutburst and its post-superoutburst state by the second normal outburst following this superoutburst. The times of superhump maxima during the superoutburst and the initial part of the post-superoutburst period are listed in table 22. The rapid decline from the superoutburst occurred between $E = 123$ and $E = 133$, and there was no evidence of a phase 0.5 jump as seen in VW Hyi (Kato et al. 2013a). In other words, there was no evidence of traditional late superhumps. As is common to relatively long-$P_{\rm orb}$ systems (e.g., V344 Lyr: Kato et al. 2012a), the stage B–C transition was relatively smooth. The superhumps in the post-superoutburst stage can be interpreted as a smooth extension of stage C superhumps, and this makes a clear contrast with VW Hyi. A comparison of the $O - C$ diagrams between the different superoutbursts is shown in figure 20.

Using the post-superoutburst data, we could determine the orbital period to be 0.08423(1) d.

We applied the two-dimensional Lasso analysis (figure 21). The superhumps were detected to be a

Table 22. Superhump maxima of TY PsA (2012).

E	Max*	Error	$O - C$†	N‡	E	Max*	Error	$O - C$†	N‡
0	56163.0866	0.0004	−0.0110	105	87	56170.7386	0.0012	0.0036	24
1	56163.1751	0.0004	−0.0103	390	88	56170.8274	0.0014	0.0046	25
2	56163.2606	0.0005	−0.0126	268	91	56171.0901	0.0009	0.0040	139
11	56164.0600	0.0004	−0.0033	141	98	56171.7070	0.0035	0.0064	18
12	56164.1469	0.0005	−0.0042	111	99	56171.7907	0.0008	0.0023	33
13	56164.2375	0.0004	−0.0013	121	100	56171.8815	0.0008	0.0053	30
14	56164.3336	0.0015	0.0069	41	102	56172.0481	0.0040	−0.0037	51
19	56164.7679	0.0009	0.0024	28	103	56172.1421	0.0004	0.0026	217
20	56164.8555	0.0005	0.0021	27	104	56172.2288	0.0005	0.0015	231
23	56165.1175	0.0003	0.0008	152	110	56172.7492	0.0019	−0.0049	33
24	56165.2066	0.0002	0.0021	105	111	56172.8469	0.0011	0.0050	35
25	56165.2919	0.0005	−0.0004	101	121	56173.7243	0.0016	0.0046	30
30	56165.7289	0.0013	−0.0024	19	122	56173.8106	0.0022	0.0031	34
31	56165.8206	0.0006	0.0016	29	123	56173.8977	0.0019	0.0024	23
32	56165.9084	0.0015	0.0016	16	133	56174.7777	0.0014	0.0046	44
34	56166.0814	0.0003	−0.0009	285	134	56174.8650	0.0013	0.0041	45
35	56166.1693	0.0003	−0.0009	540	144	56175.7364	0.0019	−0.0023	34
36	56166.2616	0.0004	0.0037	343	145	56175.8249	0.0014	−0.0017	45
43	56166.8745	0.0006	0.0020	30	155	56176.6948	0.0117	−0.0097	44
53	56167.7540	0.0007	0.0037	30	156	56176.7876	0.0024	−0.0046	45
54	56167.8422	0.0006	0.0041	31	157	56176.8768	0.0030	−0.0032	35
64	56168.7193	0.0013	0.0034	15	166	56177.6591	0.0017	−0.0110	47
65	56168.8095	0.0009	0.0058	24	167	56177.7529	0.0035	−0.0049	39
66	56168.8944	0.0006	0.0029	19	168	56177.8452	0.0022	−0.0005	33
76	56169.7704	0.0009	0.0010	25	179	56178.8033	0.0020	−0.0080	30
77	56169.8613	0.0007	0.0042	25	189	56179.6752	0.0041	−0.0139	45
79	56170.0333	0.0009	0.0006	154	190	56179.7816	0.0035	0.0047	30
80	56170.1171	0.0011	−0.0034	118	223	56182.6802	0.0023	0.0063	41
81	56170.2080	0.0007	−0.0003	94	224	56182.7671	0.0015	0.0055	30

*BJD−2400000.

†Against max = 2456163.0977 + 0.087786 E.

‡Number of points used to determine the maximum.

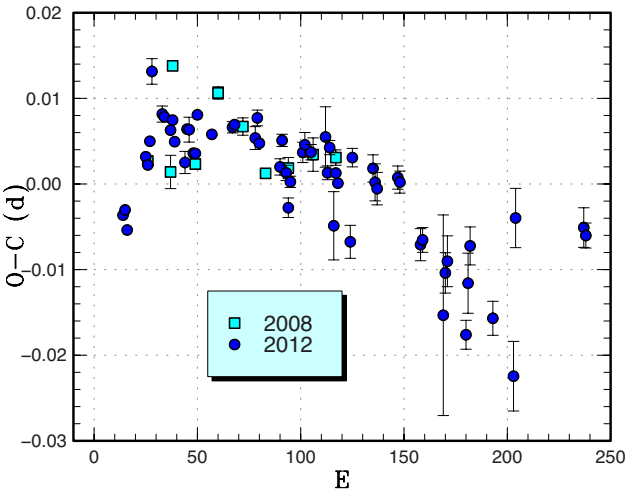

Fig. 20. Comparison of different superoutbursts of TY PsA in the $O-C$ diagrams. A period of 0.08787 d was used to draw this figure. Approximate cycle counts (E) after the start of the superoutburst were used.

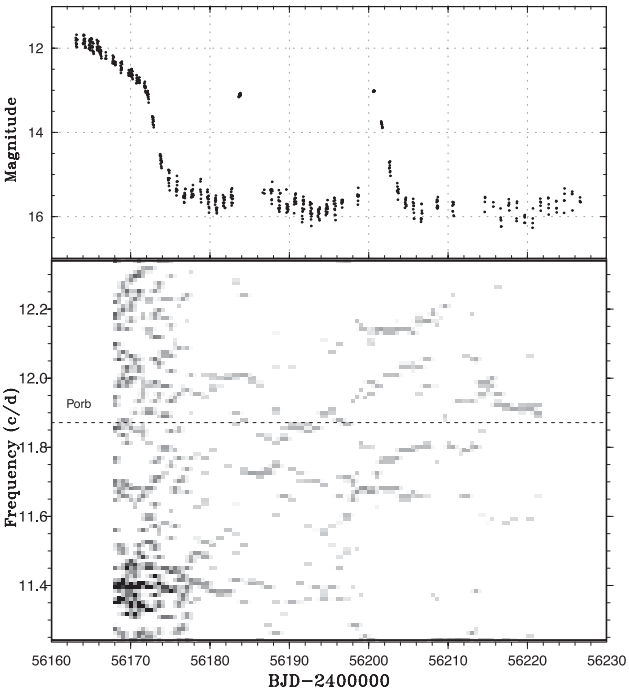

Fig. 21. Two-dimensional Lasso period analysis of TY PsA. Upper: Light curve (binned to 0.01 d). Lower: Two-dimensional Lasso analysis (10 d window, 0.5 d shift, and $\log\lambda = -6.5$).

rather broad band due to the non-sinusoidal profile. The main signal during the quiescent period (BJD 2456186–2456200) following the first normal outburst after the superoutburst was the orbital period. During and after the second normal outburst, a signal at around 12.15 c/d appeared. This signal cannot be explained by a one-day alias of the superhump period, and we consider it to be the signal of negative superhumps. A PDM analysis (range BJD 2456198–2456210) also

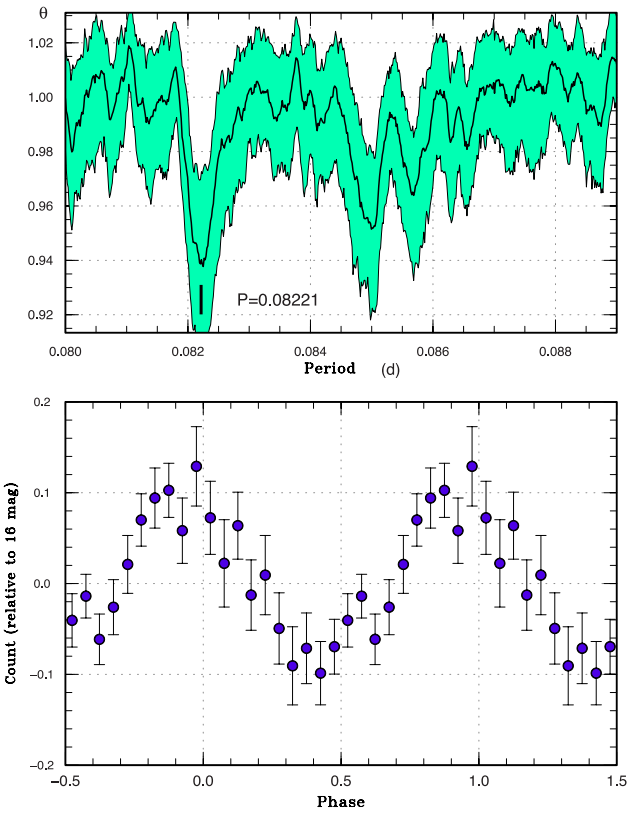

Fig. 22. Negative superhumps in TY PsA around the second normal outburst following the superoutburst. Upper: PDM analysis. Lower: Phase-averaged profile.

supports this identification (figure 22). The ε for this negative superhump was −2.4% (or $\varepsilon^* = -2.5\%$), a value similar to those obtained in the Kepler data of V344 Lyr and V1504 Cyg (cf. Osaki & Kato 2013b). Because of the relatively sparse observation after the second normal outburst, it is not clear whether this signal of negative superhumps persisted or not. It has been shown that a state with negative superhumps (likely arising from a tilted disk) tends to suppress normal outbursts (Osaki & Kato 2013a; Ohshima et al. 2012; Zemko et al. 2013). TY PsA did not show a normal outburst for more than 25 d and this may be a result of such suppression of outbursts.

Stage A superhumps were also observed. The ε^* for stage A superhumps was 4.86(12)%, which corresponds to $q = 0.142(4)$.

3.20 QW Serpentis

This object was originally discovered to be a Mira-type or dwarf nova (TmzV46) (Takamizawa 1988). Kato and Uemura (1999) reported CCD photometry of the brightening in 1999 October, confirming the dwarf nova-type classification. The object was further studied during the 2000 outburst, when superhumps were first detected

Table 23. Superhump maxima of QW Ser (2009).

E	Max*	Error	$O-C^{\dagger}$	$N^{\ddagger}$
0	54983.9862	0.0004	−0.0009	102
1	54984.0639	0.0003	−0.0000	148
2	54984.1413	0.0002	0.0004	226
3	54984.2168	0.0002	−0.0009	260
65	54988.9856	0.0003	0.0027	136
131	54994.0575	0.0005	0.0019	128
132	54994.1291	0.0005	−0.0032	88

*BJD−2400000.
†Against max = 2454983.9871 + 0.076858 E.
‡Number of points used to determine the maximum.

Table 24. Superhump maxima of QW Ser (2013).

E	Max*	Error	$O-C^{\dagger}$	$N^{\ddagger}$
0	56482.9942	0.0061	−0.0059	15
1	56483.0717	0.0006	−0.0051	85
2	56483.1482	0.0006	−0.0054	75
14	56484.0697	0.0020	−0.0048	84
33	56485.5390	0.0008	0.0064	43
34	56485.6145	0.0007	0.0051	48
46	56486.5378	0.0006	0.0075	43
47	56486.6152	0.0006	0.0081	47
59	56487.5331	0.0008	0.0051	23
60	56487.6082	0.0009	0.0035	22
72	56488.5265	0.0008	0.0009	22
73	56488.6037	0.0009	0.0013	22
85	56489.5223	0.0009	−0.0011	19
86	56489.5975	0.0012	−0.0026	19
98	56490.5190	0.0010	−0.0020	20
99	56490.5950	0.0018	−0.0027	19
111	56491.5138	0.0016	−0.0049	20
112	56491.5920	0.0022	−0.0034	19

*BJD−2400000.
†Against max = 2456483.0001 + 0.076744 E.
‡Number of points used to determine the maximum.

(Patterson et al. 2003; Nogami et al. 2004). The 2003 superoutburst was one of the best-observed among SU UMa-type dwarf novae (Olech et al. 2003; Nogami et al. 2004). The object was also selected as a CV in the SDSS (Szkody et al. 2009).

We observed the 2009 and 2013 superoutbursts; the times of superhump maxima are listed in tables 23 and 24, respectively. The latter part of stage B and the stage C were observed in 2013. Around the start of the rapid fading ($E \geq 98$), the period appeared to increase. We consider this as a result of the decrease in the pressure effect as discussed in Nakata et al. (2013), and did not include the data for determining the period of stage C. The period of this phase [0.07661(9) d] corresponds to $q = 0.21$ if we assume a disk radius of 0.30A, and $q = 0.13$ for 0.38A, where A is the binary's separation.

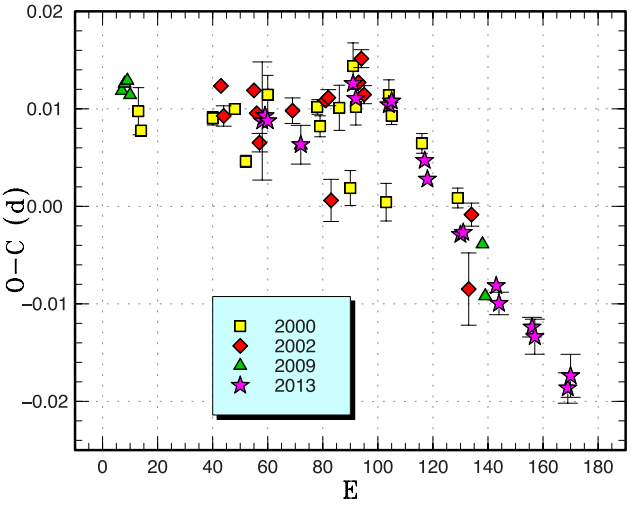

Fig. 23. Comparison of different superoutbursts of QW Ser in the $O-C$ diagrams. A period of 0.07700 d was used to draw this figure. Approximate cycle counts (E) after the start of the superoutburst were used.

A comparison of $O-C$ diagrams between different superoutbursts is shown in figure 23. All superoutbursts followed a similar pattern of stage B–C transition.

We have also updated the orbital period to be 0.074572(1) d using the CRTS data. This value is in agreement with those in Olech et al. (2003) (photometry) and Patterson et al. (2003) (radial-velocity study).

3.21 V493 Serpentis

This object (= SDSS J155644.24−000950.2) was selected as a dwarf nova by SDSS (Szkody et al. 2002). Woudt, Warner, and Pretorius (2004) obtained 0.07408(1) d from quiescent orbital humps. Although H. Maehara detected superhumps during the 2006 superoutburst, it was impossible to determine an accurate period. The 2007 superoutburst was well-observed and was summarized in Kato et al. (2009a).

We observed the 2013 superoutburst. The times of superhump maxima are listed in table 25. Although $P_{\rm dot}$ for stage B superhumps was not measured, there was a clear stage B–C transition. Following the rapid fading, there was a likely phase jump ($E \geq 143$). A PDM analysis of the post-superoutburst part yielded a period of 0.08285(6) d, not very different from that of stage C superhumps. The same as in QW Ser, the disk radii 0.30A and 0.38A correspond to $q = 0.26$ and $q = 0.16$, respectively. A comparison of the $O-C$ diagrams between the 2007 and 2013 superoutbursts is shown in figure 24.

Table 25. Superhump maxima of V493 Ser (2013).

E	Max*	Error	$O-C$†	N‡
0	56478.6582	0.0010	−0.0113	60
1	56478.7454	0.0002	−0.0069	130
2	56478.8271	0.0002	−0.0078	129
12	56479.6620	0.0047	0.0001	17
13	56479.7404	0.0011	−0.0042	46
14	56479.8257	0.0002	−0.0016	136
53	56483.0521	0.0030	−0.0004	50
54	56483.1432	0.0008	0.0080	150
65	56484.0540	0.0008	0.0092	99
66	56484.1380	0.0007	0.0105	153
77	56485.0438	0.0006	0.0066	128
78	56485.1267	0.0009	0.0068	139
82	56485.4510	0.0043	0.0003	13
83	56485.5392	0.0004	0.0058	47
84	56485.6215	0.0003	0.0054	51
95	56486.5293	0.0005	0.0035	46
96	56486.6139	0.0005	0.0055	51
107	56487.5204	0.0009	0.0023	19
119	56488.5110	0.0014	0.0005	25
120	56488.5950	0.0015	0.0019	24
131	56489.5056	0.0014	0.0028	21
132	56489.5845	0.0023	−0.0010	21
143	56490.4863	0.0016	−0.0089	17
144	56490.5614	0.0057	−0.0164	20
145	56490.6533	0.0032	−0.0072	14
157	56491.6494	0.0043	−0.0035	14

*BJD−2400000.
†Against max = 2456478.6695 + 0.082697 E.
‡Number of points used to determine the maximum.

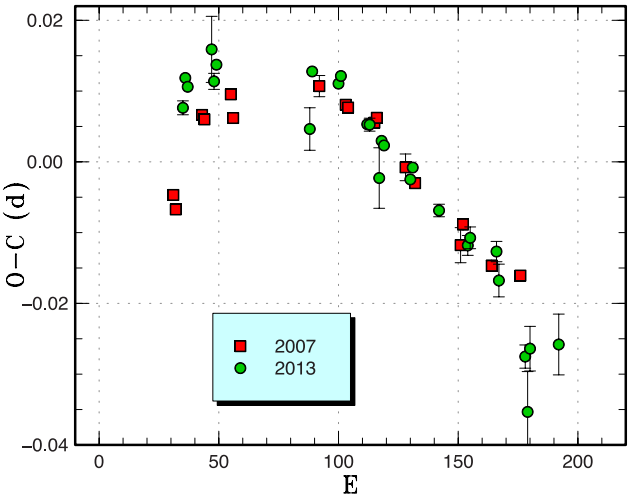

Fig. 24. Comparison of different superoutbursts of V493 Ser in the $O-C$ diagrams. A period of 0.08296 d was used to draw this figure. Approximate cycle counts (E) after the start of the superoutburst were used. Since the start of the 2013 superoutburst was not well constrained, we shifted the $O-C$ diagram to best fit the better-recorded 2007 one.

3.22 AW Sagittae

AW Sge was discovered to be a dwarf nova early in the history of observations (Wolf & Wolf 1906). Although very little was known since then, the SU UMa-type nature was clarified during the 2000 superoutburst. The 2000 and 2006 superoutbursts were reported in Kato et al. (2009a).

The 2012 superoutburst was timely detected by R. Stubbings (vsnet-alert 14768) and subsequent observations showed that we managed to record an evolving stage of superhumps (vsnet-alert 14770, 14776, 14777, 14789). This outburst was the best-observed one for this object.

The times of superhump maxima are listed in table 26. The object showed clear stages A ($E \leq 4$), B, and C. The stage B–C transition occurred at around $E = 57$–59. A comparison of the $O-C$ diagrams between the different superoutbursts is shown in figure 25.

3.23 V1212 Tauri

V1212 Tau was discovered to be an eruptive object near M45 (Parsamyan et al. 1983). Although this object was not named for a long time, possibly due to the confusion that it is a possible Pleiades flare star, members of the Variable Star Observers League in Japan (VSOLJ) suspected the dwarf-nova-type nature of this object and started monitoring it in 1987. The first secure outburst was reported in 2007 by G. Gualdoni (vsnet-alert 9190). During this outburst, J. Patterson reported the detection of superhumps (see Kato et al. 2012a for more history). The well-observed 2011 superoutburst was reported in Kato et al. (2012a), and another in 2011 was also recorded (Kato et al. 2013a).

The 2013 superoutburst was observed on a single night. We obtained a single superhump maximum of BJD 2456330.3366(13) ($N = 56$).

3.24 BZ Ursae Majoris

This object was discovered to be a dwarf nova by Markaryan (1968), and has been relatively well monitored by the AAVSO since 1968. Up to 1984, secure outbursts were recorded at a typical rate of ∼1 per year. Nevertheless, Wenzel (1982) suggested that the object is an intermediate object between a U Gem star and a WZ Sge-type star based on analysis of the photographic plates. Strangely, no secure large-amplitude outbursts were recorded by AAVSO between 1985 and 1990. The object was also identified as a CV by the Palomar–Green (PG) survey (Green et al. 1982). Kaluzny (1986) reported a fading ($B = 17.8$) episode in 1986 December. In the years that followed, the object may have spent a period of decreased mass-transfer rate,

Table 26. Superhump maxima of AW Sge (2012).

E	Max*	Error	$O-C$†	N‡
0	56127.1419	0.0004	−0.0119	155
1	56127.2186	0.0004	−0.0098	142
2	56127.2957	0.0004	−0.0074	53
3	56127.3730	0.0004	−0.0047	126
4	56127.4510	0.0005	−0.0014	73
16	56128.3485	0.0003	0.0007	51
17	56128.4251	0.0002	0.0026	78
18	56128.4997	0.0002	0.0026	74
19	56128.5744	0.0003	0.0027	79
22	56128.7988	0.0004	0.0032	31
35	56129.7722	0.0008	0.0065	35
36	56129.8449	0.0011	0.0045	15
44	56130.4425	0.0005	0.0051	80
45	56130.5182	0.0008	0.0061	87
46	56130.5919	0.0021	0.0052	39
48	56130.7419	0.0013	0.0059	13
49	56130.8131	0.0009	0.0026	19
57	56131.4166	0.0018	0.0090	28
58	56131.4852	0.0013	0.0030	28
59	56131.5656	0.0029	0.0087	46
61	56131.7077	0.0010	0.0016	11
62	56131.7833	0.0012	0.0026	19
63	56131.8545	0.0011	−0.0008	13
70	56132.3785	0.0004	0.0008	168
71	56132.4535	0.0004	0.0011	203
72	56132.5252	0.0007	−0.0018	148
73	56132.6035	0.0024	0.0019	44
74	56132.6750	0.0010	−0.0012	14
75	56132.7483	0.0011	−0.0025	13
76	56132.8212	0.0013	−0.0043	21
84	56133.4190	0.0007	−0.0035	167
85	56133.4918	0.0005	−0.0053	178
86	56133.5676	0.0011	−0.0042	58
87	56133.6340	0.0027	−0.0123	24
89	56133.7926	0.0018	−0.0030	20
97	56134.3905	0.0014	−0.0022	106

*BJD−2400000.
†Against max = 2456127.1538 + 0.074627 E.
‡Number of points used to determine the maximum.

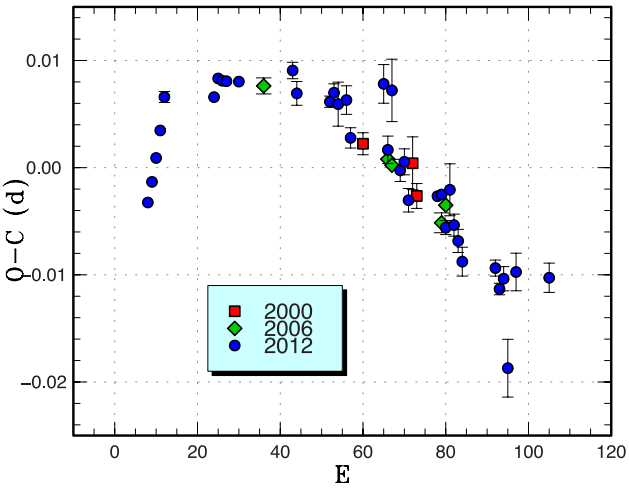

Fig. 25. Comparison of different superoutbursts of AW Sge in the $O-C$ diagrams. A period of 0.07480 d was used to draw this figure. Approximate cycle counts (E) after the start of the superoutburst were used. Since the start of the 2006 superoutburst was not well constrained, we shifted the $O-C$ diagram to best fit the best-recorded 2012 one.

and several detections of (supposedly rare) outbursts were reported in IAU Circulars (e.g., Schmeer et al. 1990). Ringwald and Thorstensen (1990) were the first to report the orbital period of 0.0679 d (see Jurcevic et al. 1994; Ringwald et al. 1994 for more details). Although the orbital period suggested an SU UMa-type dwarf nova, no superoutburst was definitely identified (Jurcevic et al. 1994). Ringwald, Thorstensen, and Hamwey (1994) also reported anomalous low-frequency variations in the radial-velocity data. Kato (1999), Price et al. (2004), and Jiang et al. (2010) reported time-series observations during short (normal) outbursts. Gänsicke et al. (2003) reported UV observations with the HST, and Neustroev, Zharikov, and Michel (2006) reported spectroscopic observations during a normal outburst. Since 1992, bright (10–11 mag) outbursts have been more frequently seen than before. The object was also selected as a CV in the SDSS (Szkody et al. 2003). The long-awaited superoutburst was finally recorded in 2007 (Price et al. 2009; Kato et al. 2009a).

The object again underwent a superoutburst on 2012 November 27 (H. Maehara, vsnet-alert 15148). The outburst was not well observed due to the delay in the announcement of the superoutburst. Only a part of the rapid fading stage was recorded. A PDM analysis yielded a period of 0.06982(4) d, which is consistent with the period of stage C superhumps (Kato et al. 2009a). Due to the large irregularities, we did not attempt to obtain $O-C$ values. According to the AAVSO data, the object was already in full outburst on November 26 at a visual magnitude of 11.3. The object was still in quiescence 2 d before. It was likely that the rise was faster than in 2007, when a slow start of the outburst (likely an inside-out outburst) was recorded (Kato et al. 2009a).

3.25 CI Ursae Majoris

CI UMa was discovered to be a dwarf nova by Goranskij (1972). There was a report of photographic records of outbursts in Kolotovkina (1979). The SU UMa-type nature was established by the detection of superhumps in Nogami and Kato (1997). In Kato et al. (2009a), we reported on superoutbursts in 2001, 2003, and 2006. Parimucha and

Table 27. Superhump maxima of CI UMa (2013).

E	Max*	Error	$O-C^{\dagger}$	$N^{\ddagger}$
0	56385.3116	0.0013	−0.0040	11
1	56385.3778	0.0012	−0.0001	18
2	56385.4414	0.0002	0.0012	195
3	56385.5034	0.0002	0.0007	228
4	56385.5681	0.0003	0.0030	228
5	56385.6270	0.0007	−0.0004	53
32	56387.3113	0.0007	−0.0004	145

*BJD−2400000.
†Against max = 2456385.3155 + 0.062381 E.
‡Number of points used to determine the maximum.

Dubovsky (2006) also reported the detection of superhumps in the 2006 superoutburst. There was another moderately well-observed superoutburst in 2011 (Kato et al. 2012a).

We observed the final part of the 2013 April superoutburst. The times of superhumps are listed in table 27. The observed superhumps are most likely stage C superhumps.

3.26 CY Ursae Majoris

CY UMa was discovered to be a dwarf nova by Goranskij (1977). The VSOLJ members started monitoring this object in 1987, and recorded a long outburst in 1988 January. This outburst turned out to be a superoutburst (Kato et al. 1988; the reported superhump period was incorrect, see Kato 1997). There was a report on its outburst activity (Watanabe et al. 1989). Szkody and Howell (1992) reported a spectrum characteristic of a dwarf nova. Harvey and Patterson (1995) were the first to establish the superhump period during the 1995 superoutburst. Kato (1995a) also reported observations of the two superoutbursts in 1991–1992 and in 1993. The orbital period was determined by Martínez-Pais and Casares (1995) and Thorstensen et al. (1996). Kato and Matsumoto (1999b) reported observations of superhumps during the 1999 superoutburst. A summary of these observations and the 2009 superoutburst were reported in Kato et al. (2009a). The object was also selected as a CV in the SDSS (Szkody et al. 2005).

Only single-night observations were obtained during the 2013 April superoutburst. Only one superhump maximum of BJD 2456397.4024(8) ($N = 106$) was recorded.

3.27 MR Ursae Majoris

MR UMa (= 1RXP J113123+4322.5) is a ROSAT-selected CV (Wei et al. 1997). Its first superoutburst was recorded in 2002 (vsnet-alert 7221). Superhumps during this superoutburst were recorded by different groups, including ours (cf. Holtgrewe & Durig 2002). The results for the 2001 and 2003 superoutbursts were reported in Kato et al. (2009a). The 2007 and 2010 superoutbursts were reported in Kato et al. (2010) and Kato et al. (2013a), respectively. The object was also selected as a CV in the SDSS (Szkody et al. 2006).

Table 28. Superhump maxima of MR UMa (2013).

E	Max*	Error	$O-C^{\dagger}$	$N^{\ddagger}$
0	56354.4000	0.0003	−0.0214	132
1	56354.4652	0.0004	−0.0208	121
2	56354.5301	0.0005	−0.0205	105
3	56354.5972	0.0003	−0.0179	131
4	56354.6669	0.0006	−0.0127	35
29	56356.3040	0.0020	0.0104	80
30	56356.3594	0.0003	0.0012	113
31	56356.4259	0.0007	0.0031	97
32	56356.4904	0.0003	0.0031	128
33	56356.5563	0.0005	0.0044	130
34	56356.6206	0.0003	0.0042	136
47	56357.4626	0.0004	0.0069	65
48	56357.5278	0.0003	0.0075	58
49	56357.5909	0.0003	0.0060	59
94	56360.5028	0.0006	0.0127	72
95	56360.5679	0.0007	0.0134	86
96	56360.6337	0.0008	0.0145	66
106	56361.2748	0.0011	0.0101	84
107	56361.3400	0.0018	0.0107	95
108	56361.4040	0.0011	0.0102	95
109	56361.4694	0.0010	0.0109	95
110	56361.5279	0.0018	0.0049	95
111	56361.5982	0.0012	0.0107	95
216	56368.3566	0.0009	−0.0097	70
217	56368.4301	0.0016	−0.0008	70
230	56369.2532	0.0022	−0.0169	52
231	56369.3230	0.0010	−0.0117	70
232	56369.3972	0.0007	−0.0021	69
233	56369.4536	0.0010	−0.0102	64

*BJD−2400000.
†Against max = 2456354.4214 + 0.064560 E.
‡Number of points used to determine the maximum.

We observed the latter stage of the 2013 superoutburst. The times of superhump maxima are listed in table 28. Both stages B and C can be identified. Although post-superoutburst superhumps were likely recorded ($E \geq 216$), we did not include these maxima for deriving a period of stage C superhumps because these maxima were not on a smooth extension of the times of stage C superhumps during the late plateau phase. The combined $O-C$ curves, however, suggest that they are a part of the persisting stage C superhumps during the post-superoutburst stage (figure 26). The $O-C$ behavior is very similar to that of QZ Vir (figure 160 in Kato et al. 2009a).

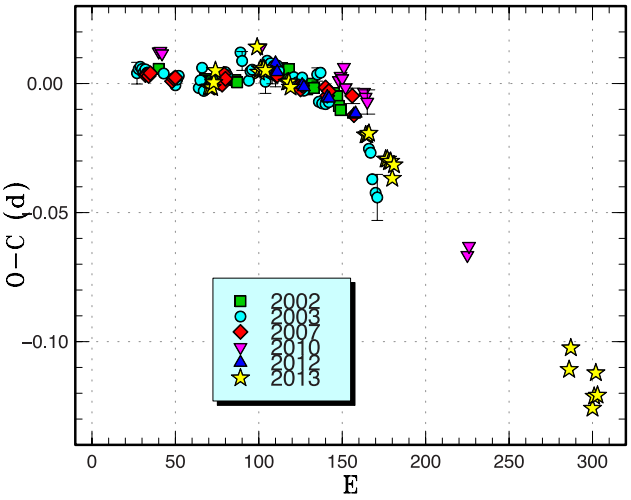

Fig. 26. Comparison of different superoutbursts of MR UMa in the $O - C$ diagrams. A period of 0.06512 d was used to draw this figure. Approximate cycle counts (E) after the start of the superoutburst were used. Since the starts of the superoutbursts were not well constrained other than the 2013 one, we shifted the $O - C$ diagrams to best fit the others. The cycle counts of the last two maxima in the 2010 superoutburst were shifted by one from Kato et al. (2010).

3.28 ASASSN-13ao

This object was discovered by the ASAS-SN survey (Shappee et al. 2013) on 2013 June 8 (Stanek et al. 2013b). The coordinates are $12^{\rm h}43^{\rm m}12\overset{\rm s}{.}05$, $+43^\circ31'59\overset{''}{.}9$.[9] Stanek et al. (2013b) indicated a $g = 21.2$ mag SDSS counterpart and suggested that this outburst has a large outburst amplitude. The SDSS colors also suggested a short orbital period (vsnet-alert 15827). Subsequent observations detected superhumps (vsnet-alert 15837). Only two superhump maxima were recorded: BJD 2456457.0258(8) ($N = 165$) and 2456458.0085(16) ($N = 126$). The object had already faded to 18.6 mag only 3 d later. It was most likely that we only observed the terminal stage of the superoutburst. A PDM analysis favored a period of 0.0895(1) d, although a longer one-day alias is still possible.

3.29 ASASSN-13as

This object was discovered by the ASAS-SN survey on 2013 June 26 (Stanek et al. 2013a). The coordinates are $17^{\rm h}23^{\rm m}06\overset{\rm s}{.}3$, $+17^\circ57'55\overset{''}{.}9$. Follow-up observations detected superhumps (vsnet-alert 15992; figure 27). The times of superhump maxima are listed in table 29. There was a decreasing trend in the superhump period. There may have been a stage A–B or stage B–C transition between BJD 2456475 and 2456476.

[9] All the coordinates in this paper are for the standard equinox of J2000.0.

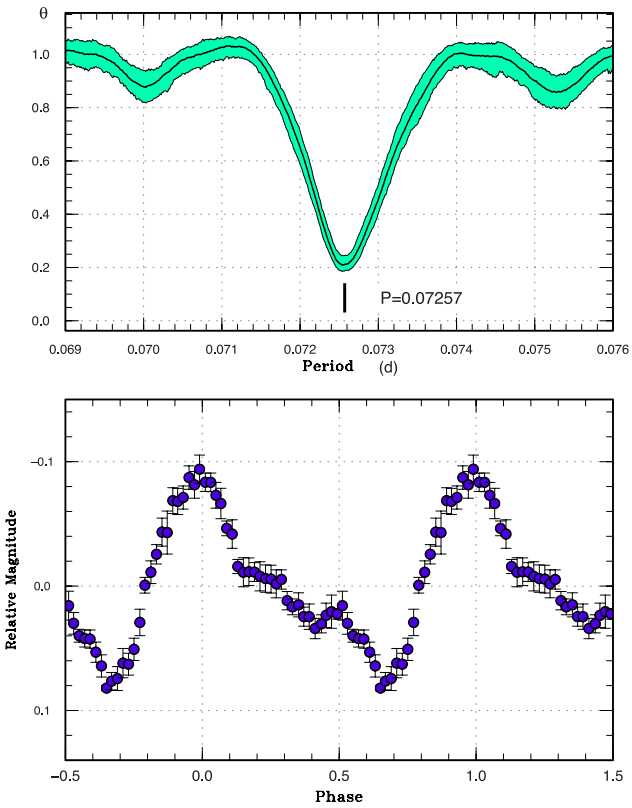

Fig. 27. Superhumps in ASASSN-13as (2013). Upper: PDM analysis. Lower: Phase-averaged profile.

Table 29. Superhump maxima of ASASSN-13as (2013).

E	Max*	Error	$O - C$†	N‡
0	56475.3829	0.0008	−0.0022	40
1	56475.4562	0.0005	−0.0014	36
2	56475.5293	0.0007	−0.0009	28
14	56476.4009	0.0006	0.0006	39
15	56476.4733	0.0006	0.0004	34
27	56477.3523	0.0065	0.0091	15
28	56477.4163	0.0007	0.0006	36
29	56477.4899	0.0009	0.0016	40
41	56478.3502	0.0057	−0.0083	14
42	56478.4315	0.0028	0.0005	16

*BJD−2400000.
†Against max = 2456475.3851 + 0.072522 E.
‡Number of points used to determine the maximum.

3.30 ASASSN-13ax

This object was discovered by the ASAS-SN survey on 2013 June 1 (Copperwheat et al. 2013). The coordinates are $18^{\rm h}00^{\rm m}05\overset{\rm s}{.}8$, $+52^\circ56'33\overset{''}{.}7$. The SDSS quiescent counterpart has a magnitude of $g = 21.2$, making the object a large-amplitude ($\sim$7.7 mag) WZ Sge-type dwarf nova. Subsequent observations detected possible early superhumps (vsnet-alert 15944), whose period was not

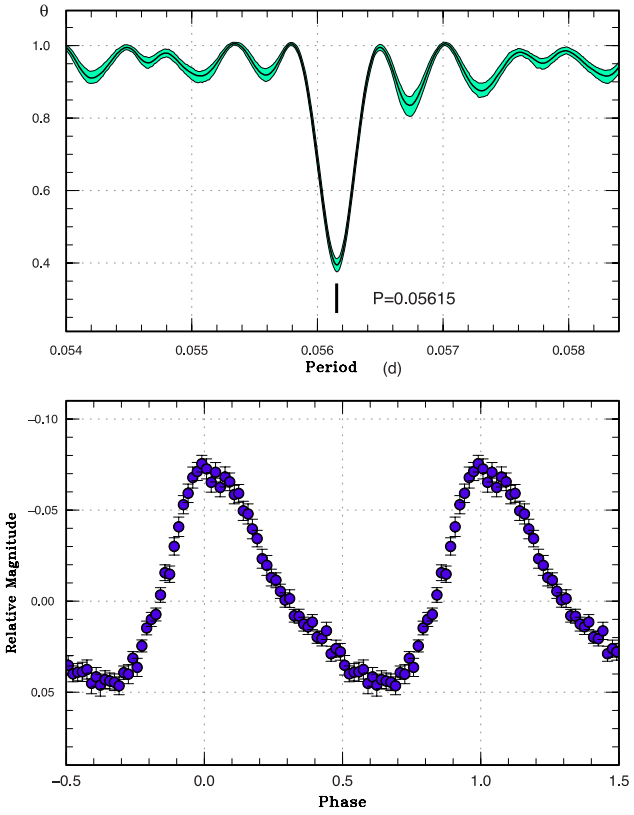

Fig. 28. Ordinary superhumps in ASASSN-13ax (2013). Stage A superhumps were excluded from the analysis. Upper: PDM analysis. Lower: Phase-averaged profile.

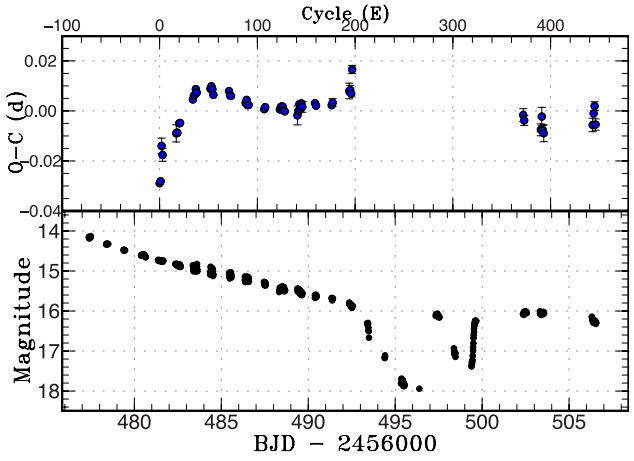

Fig. 29. $O - C$ diagram of superhumps in ASASSN-13ax (2013). Upper: $O - C$ diagram. A period of 0.056212 d was used to draw this figure. Lower: Light curve. The observations were binned to 0.011 d.

convincingly determined due to the low amplitudes and short observing runs. Ordinary superhumps started to grow 7 d after the discovery (vsnet-alert 15951, 15964, 15986, 15995, 16007, 16013, 16032; figure 28). The object then entered a temporary dip 19 d after the discovery (vsnet-alert 16034; figure 29). The dip lasted $\sim$3 d and the object then entered the rebrightening phase. The rebrightening started with a precursor-like outburst (BJD 2456497, July 23, vsnet-alert 16060), which was followed by a shallow dip (BJD 2456499, July 25), then by a plateau-type rebrightening (vsnet-alert 16076, 16082).

The times of (ordinary) superhump maxima are listed in table 30. The times for $E \geq 372$ correspond to the superhumps recorded during the rebrightening phase. The cycle count may not be continuous with the earlier part of this figure. During the dip and the precursor-like outburst, the superhump signal was weak, and we could not measure the times of maxima. In the early part, clear stages A and B can be recognized (figure 29). As in most WZ Sge-type dwarf novae, the object entered the rapid fading stage without a transition to stage C. The $P_{\rm dot}$ for stage B superhumps was determined excluding $E = 88$–91, when an increase of the period was probably due to the reduction of the pressure effect (Nakata et al. 2013). The period of stage A superhumps was determined by the PDM method using the segment of BJD 2456481.40–2456483.63. The mean superhump period during the rebrightening stage was 0.05625(2) d (PDM method), which showed a sharper minimum than maximum, and the amplitude was low (figure 30). Since the amplitudes of the superhumps decreased around the dip and showed a regrowth preceded by a precursor-like outburst, the rebrightening bore some resemblance to an ordinary superoutburst of an SU UMa-type dwarf nova, rather than a long rebrightening consisting of repetitive rebrightenings as shown in WZ Sge (2001) (Ishioka et al. 2002; Patterson et al. 2002; Kato et al. 2009a). A similar rebrightening with a precursor-like outburst was seen in AL Com (1995) (Nogami et al. 1997).

3.31 ASASSN-13bj

This object was discovered by the ASAS-SN survey on 2013 July 10. The coordinates are $16^{\rm h}00^{\rm m}20\overset{\rm s}{.}39$, $+70^\circ50'09\overset{''}{.}4$. The object has a ROSAT counterpart (1RXS J160017.2+705029, vsnet-alert 15960). Only single-night observations were available, which recorded two superhump maxima (figure 31): BJD 2456486.6477(2) ($N = 128$) and 2456486.7212(3) ($N = 128$). The period by the PDM method is 0.0731(3) d.

3.32 ASASSN-13bm

This object was discovered by the ASAS-SN survey on 2013 July 12. The coordinates are $19^{\rm h}25^{\rm m}14\overset{\rm s}{.}46$, $+68^\circ51'22\overset{''}{.}1$. Subsequent observations recorded superhumps (vsnet-alert 16021; figure 32). The times of superhump maxima are listed in table 31. The stage of the superhumps is not known.

Table 30. Superhump maxima of ASASSN-13ax (2013).

E	Max*	Error	$O-C^{\dagger}$	$N^{\ddagger}$	E	Max*	Error	$O-C^{\dagger}$	$N^{\ddagger}$
0	56481.4244	0.0012	−0.0289	91	125	56488.4816	0.0005	0.0019	133
1	56481.4814	0.0012	−0.0281	92	126	56488.5377	0.0004	0.0017	109
2	56481.5518	0.0031	−0.0140	78	127	56488.5925	0.0005	0.0003	80
3	56481.6043	0.0025	−0.0176	63	128	56488.6482	0.0009	−0.0001	47
17	56482.3999	0.0034	−0.0090	77	141	56489.3774	0.0038	−0.0017	27
18	56482.4563	0.0007	−0.0088	149	142	56489.4355	0.0004	0.0001	173
20	56482.5726	0.0006	−0.0049	107	143	56489.4943	0.0005	0.0028	148
21	56482.6289	0.0010	−0.0048	64	144	56489.5483	0.0004	0.0006	136
34	56483.3691	0.0007	0.0046	49	145	56489.6071	0.0007	0.0031	52
35	56483.4268	0.0002	0.0061	117	146	56489.6619	0.0021	0.0017	32
36	56483.4834	0.0002	0.0065	100	159	56490.3941	0.0010	0.0032	47
37	56483.5419	0.0002	0.0088	98	160	56490.4493	0.0006	0.0021	54
38	56483.5967	0.0003	0.0074	70	176	56491.3489	0.0012	0.0023	24
52	56484.3852	0.0002	0.0089	29	177	56491.4061	0.0016	0.0034	19
53	56484.4424	0.0002	0.0099	48	194	56492.3664	0.0031	0.0080	25
54	56484.4974	0.0003	0.0087	30	195	56492.4230	0.0019	0.0084	30
55	56484.5514	0.0012	0.0064	8	196	56492.4777	0.0013	0.0069	28
71	56485.4523	0.0003	0.0080	50	197	56492.5436	0.0016	0.0166	25
72	56485.5068	0.0003	0.0063	60	372	56502.3625	0.0025	−0.0015	29
73	56485.5627	0.0002	0.0060	59	373	56502.4166	0.0020	−0.0037	29
88	56486.4031	0.0003	0.0032	31	390	56503.3684	0.0024	−0.0075	28
89	56486.4606	0.0005	0.0045	71	391	56503.4299	0.0037	−0.0022	30
90	56486.5146	0.0003	0.0023	59	392	56503.4807	0.0020	−0.0076	29
91	56486.5710	0.0003	0.0024	55	393	56503.5357	0.0034	−0.0088	29
107	56487.4687	0.0005	0.0007	39	443	56506.3496	0.0027	−0.0055	28
108	56487.5257	0.0004	0.0016	57	444	56506.4104	0.0013	−0.0009	31
123	56488.3680	0.0007	0.0006	51	445	56506.4696	0.0017	0.0021	25
124	56488.4251	0.0004	0.0016	104	446	56506.5184	0.0023	−0.0053	30

*BJD−2400000.
†Against max = 2456481.4533 + 0.056212 E.
‡Number of points used to determine the maximum.

3.33 ASASSN-13bp

This object was discovered by the ASAS-SN survey on 2013 July 15. The coordinates are $22^{\rm h}53^{\rm m}50^{\rm s}.51$, $+33^{\circ}30'32''.5$. The object showed three outbursts in the CRTS data on BJD 2454299, 2454358, and 2454382. The SDSS colors suggested a short orbital period based on the method of Kato et al. (2012b) (vsnet-alert 15997). Subsequent observations confirmed the presence of superhumps (vsnet-alert 16018, 16019; figure 33). The times of superhump maxima are listed in table 32. The superhump period by the PDM method was 0.06828(16) d.

3.34 ASASSN-13br

This object was discovered by the ASAS-SN survey on 2013 July 19. The coordinates are $17^{\rm h}03^{\rm m}43^{\rm s}.01$, $+66^{\circ}07'45''.5$. Although there is a $g = 17.78$ SDSS star close to this location, a close inspection of the SDSS image and the analysis of the coordinates indicated that the true quiescent counterpart was a much fainter ($\sim$21.5 mag) companion close to this SDSS object. The actual outburst amplitude was estimated to be $\sim$7 mag (vsnet-alert 16026).

Subsequent observations detected superhumps (vsnet-alert 16037, 16045, 16049, 16051, 16055, 16071, 16077, 16083, 16100; figure 34). The object entered the rapid fading stage 12 d after the outburst detection (vsnet-alert 16105). The object is more likely an ordinary SU UMa-type dwarf nova rather than an extreme WZ Sge-type dwarf nova.

The times of superhump maxima are listed in table 33. Stages B and C are clearly seen, and stage B had a clearly positive $P_{\rm dot}$ of $+9.6(1.6) \times 10^{-5}$. The epoch $E = 153$ corresponds to a post-superoutburst superhump, and we disregarded it when estimating the period of stage C superhumps.

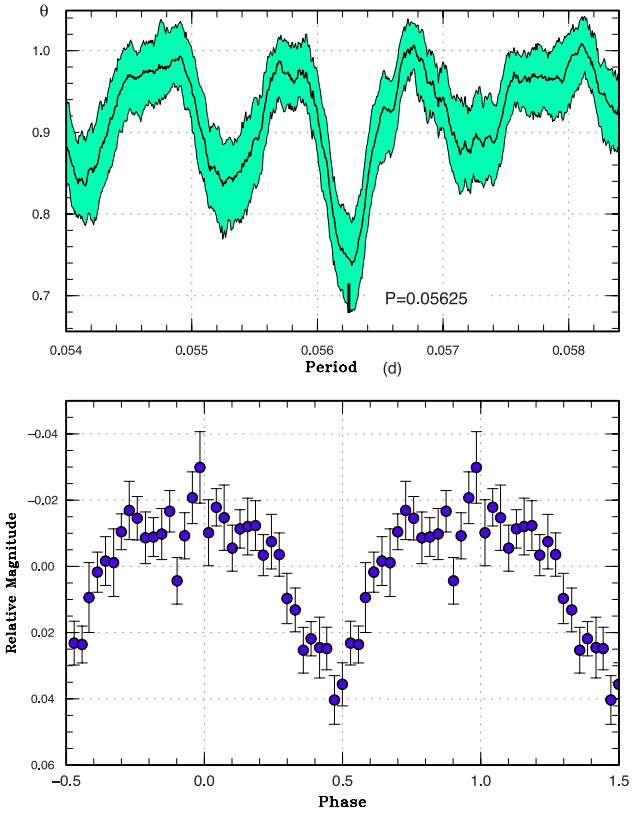

Fig. 30. Superhumps in ASASSN-13ax during the rebrightening phase (2013). Upper: PDM analysis. Lower: Phase-averaged profile.

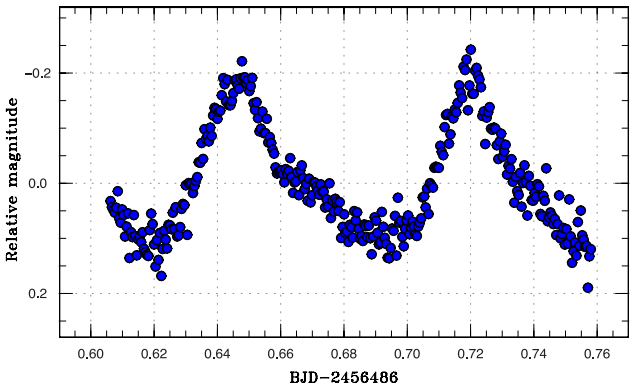

Fig. 31. Superhumps in ASASSN-13bj (2013).

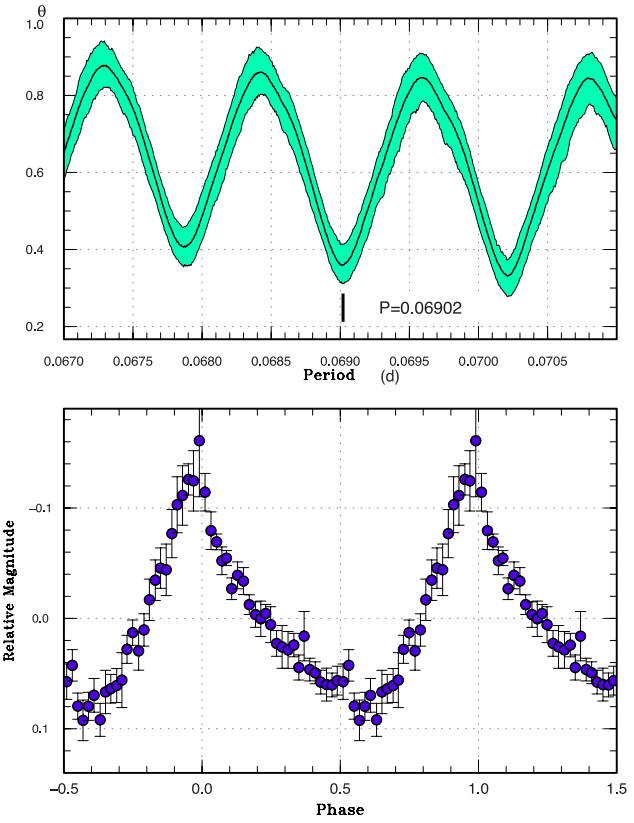

Fig. 32. Superhumps in ASASSN-13bm (2013). Upper: PDM analysis. The alias was selected based on the continuous run on BJD 2456489. Lower: Phase-averaged profile.

Table 31. Superhump maxima of ASASSN-13bm (2013).

E	Max*	Error	$O-C^{\dagger}$	$N^{\ddagger}$
0	56489.3507	0.0031	0.0023	33
1	56489.4160	0.0004	−0.0015	73
2	56489.4864	0.0010	−0.0001	62
3	56489.5547	0.0005	−0.0008	60
4	56489.6246	0.0023	0.0001	34
61	56493.5584	0.0006	0.0001	74

*BJD−2400000.
†Against max = 2456489.3484 + 0.069015 E.
‡Number of points used to determine the maximum.

3.35 CSS J015051.7+332621

This object was detected to be a transient by CRTS (= CSS 111006:015052+332622, hereafter CSS J015051) on 2011 October 6. The quiescent SDSS color suggested an orbital period of 0.069 d (Kato et al. 2012b). Another outburst was detected by the MASTER network (Gorbovskoy et al. 2013) reaching 14.5 mag on 2012 October 10 (Denisenko et al. 2012a; vsnet-alert 14993). Subsequent observations detected superhumps (vsnet-alert 15001, 15011, 15026; figure 35). The times of superhump maxima are listed in table 34. Although the coverage was not sufficient, stages B and C can be recognized (the nature of the $E = 144$ hump is unclear, and was disregarded on analysis).

3.36 CSS J015321.3+340855

This object was discovered by CRTS (= CSS 081026:015321+340857, hereafter CSS J015321) on 2008 October 26. Seven outbursts were recorded in the CRTS data between 2004 November and 2012 January. Another outburst was detected by the MASTER

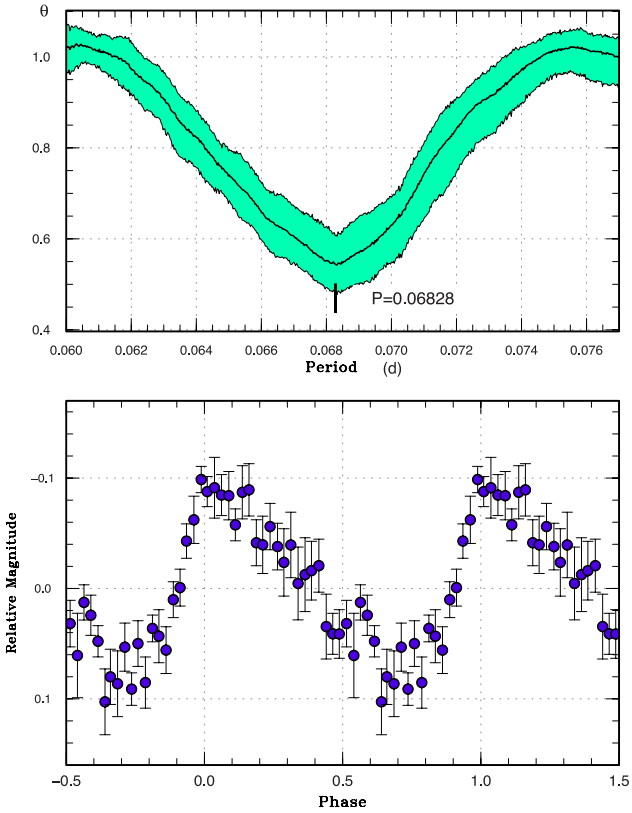

Fig. 33. Superhumps in ASASSN-13bp (2013). Upper: PDM analysis. Lower: Phase-averaged profile.

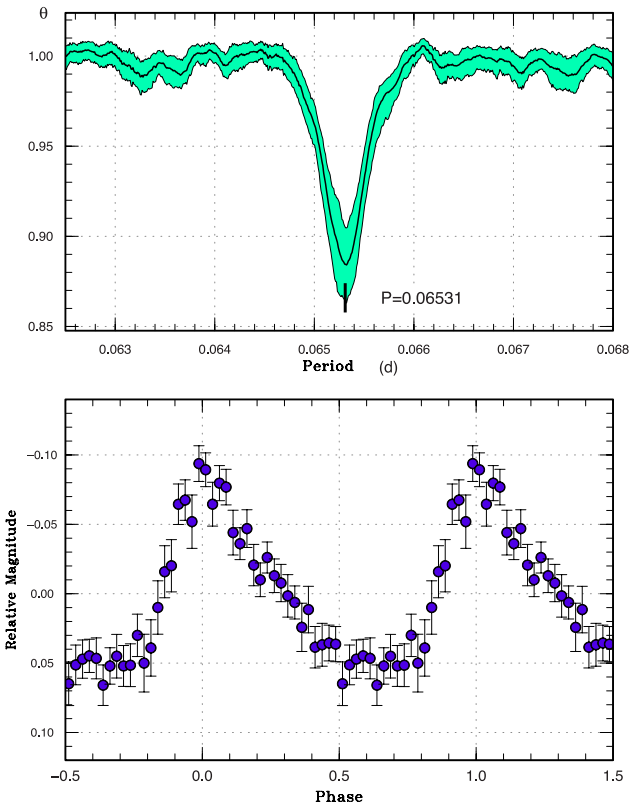

Fig. 34. Superhumps in ASASSN-13br (2013). Upper: PDM analysis. Lower: Phase-averaged profile.

Table 32. Superhump maxima of ASASSN-13bp (2013).

E	Max*	Error	$O-C$†	N‡
0	56492.1678	0.0016	0.0016	61
1	56492.2318	0.0025	−0.0022	29
4	56492.4382	0.0008	0.0008	74
5	56492.5050	0.0007	−0.0002	74

*BJD−2400000.
†Against max = 2456492.1662 + 0.067805 E.
‡Number of points used to determine the maximum.

network (vsnet-alert 15178) on 2012 December 17. This is a bright GALEX UV source, and Erastova (2011) also noted outbursts between 1972 and 1975 (vsnet-alert 15178; the object is also known as SBS 0150+339). Subsequent observations detected superhumps (vsnet-alert 15180, 15182, 15185, 15187; figure 36), qualifying this object as an SU UMa-type dwarf nova in the period gap. The observation recorded the middle-to-late stage of the superoutburst. There was a possible stage B–C transition between $E = 23$ and $E = 31$ (table 35). Although a large positive $P_{\rm dot}$ was obtained, this value is not very reliable due to the short observation segment.

3.37 CSS J102842.8−081930

This object (= OT J102842.9−081927 = CSS 090331: 102843−081927, hereafter CSS J102842), detected by the CRTS, belongs to the small group of hydrogen-rich dwarf novae below the period gap (see subsection 3.3). Kato et al. (2009a) reported superhumps during the 2009 superoutburst. The 2012 superoutburst was also partially observed (Kato et al. 2013a).

3.37.1 Photometry

We observed the 2013 superoutburst. Both stages A and B were recorded (table 36). The periods of stage A and stage B superhumps were similar to those obtained in 2012 (Kato et al. 2013a). A comparison of different superoutbursts in the $O-C$ diagrams is shown in figure 37. The assumption made in drawing this figure is very different from that in Kato et al. (2013a). Since all detections were made by CRTS, there was unavoidable uncertainty as to when the outburst started. The 2013 outburst was, however, apparently caught in an earlier phase than in other outbursts as judged from the brightness and long duration of the observed stage A superhumps. We therefore assumed that the 2013 outburst started ($E = 0$) at the time of the CRTS detection. Since the 2012 $O-C$ diagram recorded a similar stage of the outburst we could match it to the 2013

Table 33. Superhump maxima of ASASSN-13br (2013).

E	Max*	Error	$O-C^{\dagger}$	$N^{\ddagger}$
0	56495.3688	0.0005	−0.0032	78
1	56495.4368	0.0003	−0.0003	106
2	56495.5014	0.0004	−0.0010	103
3	56495.5666	0.0007	−0.0010	71
16	56496.4139	0.0005	−0.0015	48
17	56496.4780	0.0003	−0.0025	63
18	56496.5434	0.0005	−0.0024	58
30	56497.3239	0.0012	−0.0044	19
31	56497.3912	0.0007	−0.0023	35
32	56497.4556	0.0004	−0.0031	34
33	56497.5205	0.0007	−0.0034	113
34	56497.5865	0.0045	−0.0026	24
36	56497.7215	0.0005	0.0020	49
37	56497.7834	0.0005	−0.0013	50
38	56497.8496	0.0004	−0.0003	49
46	56498.3716	0.0017	0.0000	43
47	56498.4345	0.0008	−0.0023	102
48	56498.5011	0.0008	−0.0010	141
49	56498.5662	0.0014	−0.0011	84
62	56499.4166	0.0011	0.0016	105
63	56499.4856	0.0007	0.0054	153
64	56499.5503	0.0011	0.0049	173
65	56499.6187	0.0077	0.0081	29
76	56500.3353	0.0005	0.0074	30
77	56500.4008	0.0006	0.0077	35
78	56500.4654	0.0007	0.0070	34
79	56500.5307	0.0009	0.0071	33
107	56502.3498	0.0011	0.0004	25
108	56502.4168	0.0009	0.0021	34
109	56502.4824	0.0011	0.0025	25
110	56502.5478	0.0018	0.0027	27
122	56503.3224	0.0020	−0.0052	18
123	56503.3908	0.0007	−0.0020	34
124	56503.4598	0.0014	0.0018	32
125	56503.5192	0.0013	−0.0040	33
153	56505.3335	0.0040	−0.0156	11

*BJD−2400000.

†Against max = 2456495.3720 + 0.065210 E.

‡Number of points used to determine the maximum.

one by shifting 80 cycles. The starts of other outbursts were more uncertain, and we assumed a shift of 310 cycles for the 2009 outbursts and 140 for 2010. If this interpretation is correct, we observed late stage B and stage C superhumps in 2009.

Woudt et al. (2012) reported a possible photometric period of 52.1(6) min, which they considered to be the orbital period. If this is the true orbital period, the ε^* values for stage A superhumps for the 2013 and 2012 data are 6.0% and 5.9%, respectively. These values give $q = 0.183$–0.178, and the secondary in CSS J102842

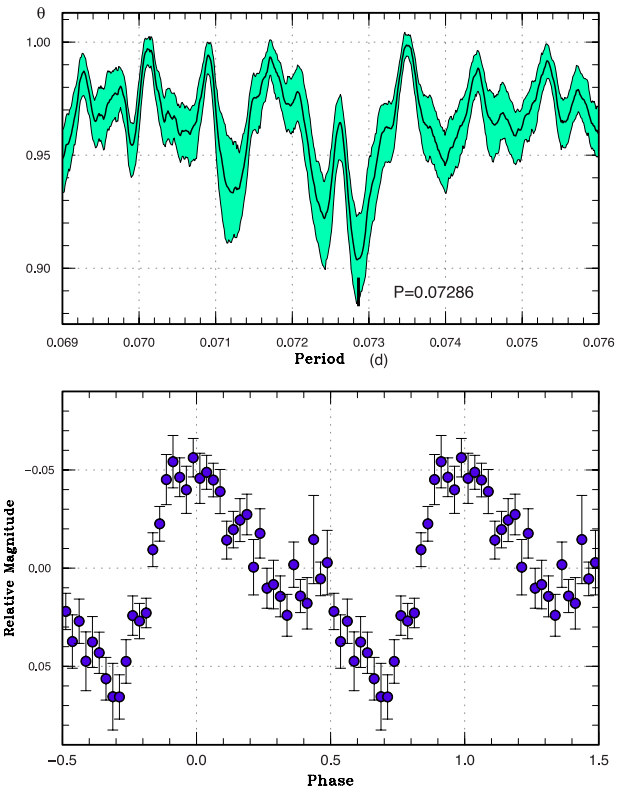

Fig. 35. Superhumps in CSS J015051 (2012). Upper: PDM analysis. Lower: Phase-averaged profile.

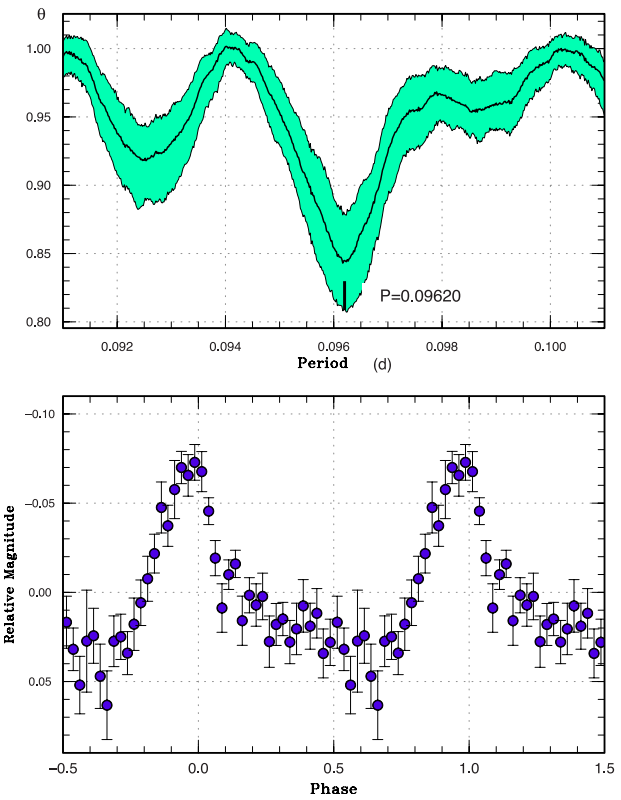

Fig. 36. Superhumps in CSS J015321 (2012). Upper: PDM analysis. Lower: Phase-averaged profile.

Table 34. Superhump maxima of CSS J015051 (2012).

E	Max*	Error	$O-C^{\dagger}$	$N^{\ddagger}$
0	56211.6952	0.0018	−0.0104	58
19	56213.0713	0.0023	−0.0094	52
20	56213.1487	0.0004	−0.0043	118
59	56215.9835	0.0008	0.0078	127
60	56216.0583	0.0006	0.0103	297
61	56216.1284	0.0006	0.0080	275
74	56217.0727	0.0014	0.0114	141
116	56220.1091	0.0041	0.0080	293
144	56222.1062	0.0067	−0.0213	150

*BJD−2400000.
†Against max = 2456211.7056 + 0.072374 E.
‡Number of points used to determine the maximum.

Table 35. Superhump maxima of CSS J015321 (2012).

E	Max*	Error	$O-C^{\dagger}$	$N^{\ddagger}$
0	56279.5922	0.0007	0.0013	85
1	56279.6862	0.0008	−0.0012	101
2	56279.7822	0.0010	−0.0015	101
7	56280.2656	0.0011	−0.0003	56
8	56280.3597	0.0020	−0.0027	76
17	56281.2301	0.0016	−0.0001	89
18	56281.3274	0.0015	0.0007	100
22	56281.7200	0.0021	0.0077	100
23	56281.8125	0.0034	0.0038	75
31	56282.5725	0.0066	−0.0077	97

*BJD−2400000.
†Against max = 2456279.5909 + 0.0964283 E.
‡Number of points used to determine the maximum.

must be very massive for this orbital period. The orbital period should be confirmed by spectroscopy.

3.37.2 Spectroscopy

We reported that "a spectroscopic observation clarified its hydrogen-rich nature (vsnet-alert 11166), suggesting that the object is similar to V485 Cen and EI Psc" in Kato et al. (2009a). Since no spectroscopic observation has been reported yet, we present here our spectrum taken in 2009.

We obtained low-resolution optical spectra of the object with the GLOWS spectrograph attached to the 1.5 m telescope at Gunma Astronomical Observatory on 2009 April 2 (35 frames taken with 180 s exposure, BJD 2454924.040–.166), April 3 (20 frames, BJD 2454925.090–.163), and April 5 (22 frames, BJD 2454927.067–.147). Standard IRAF routines were used for data reduction and a flux calibration was performed by using HR 4963. The optical spectrum of the

Table 36. Superhump maxima of CSS J102842 (2013).

E	Max*	Error	$O-C^{\dagger}$	$N^{\ddagger}$
0	56388.3958	0.0002	−0.0122	30
51	56390.3586	0.0003	0.0006	87
52	56390.3973	0.0004	0.0011	88
53	56390.4355	0.0004	0.0010	86
154	56394.3005	0.0005	0.0042	72
155	56394.3388	0.0003	0.0043	88
156	56394.3773	0.0003	0.0046	88
180	56395.2928	0.0004	0.0024	88
181	56395.3306	0.0004	0.0020	88
182	56395.3682	0.0004	0.0014	88
183	56395.4071	0.0004	0.0021	81
184	56395.4462	0.0022	0.0029	22
205	56396.2459	0.0004	−0.0003	88
206	56396.2855	0.0006	0.0010	88
207	56396.3226	0.0006	−0.0001	95
208	56396.3620	0.0004	0.0010	125
209	56396.3986	0.0005	−0.0006	109
210	56396.4374	0.0007	−0.0001	86
211	56396.4736	0.0009	−0.0020	24
287	56399.3796	0.0010	−0.0020	35
288	56399.4176	0.0012	−0.0022	37
289	56399.4552	0.0017	−0.0029	37
290	56399.4919	0.0014	−0.0044	36
314	56400.4145	0.0036	0.0005	29
315	56400.4497	0.0019	−0.0024	26

*BJD−2400000.
†Against max = 2456388.4080 + 0.038235 E.
‡Number of points used to determine the maximum.

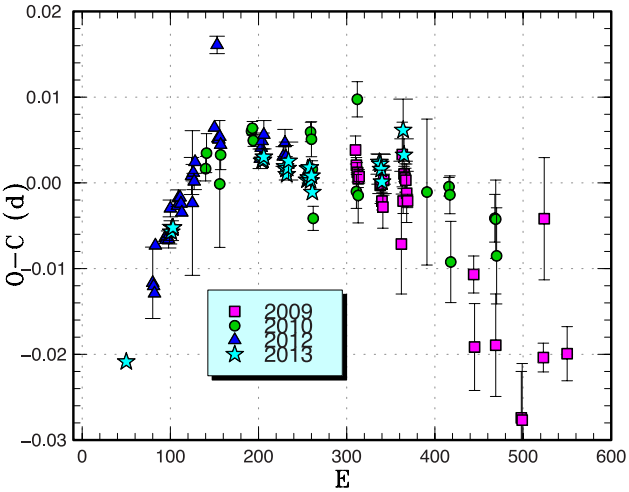

Fig. 37. Comparison of different superoutbursts of CSS J102842 in the $O-C$ diagrams. A period of 0.03819 d was used to draw this figure. Approximate cycle counts (E) after the start of the superoutburst were used. See text for details of the assumption made in drawing this figure.

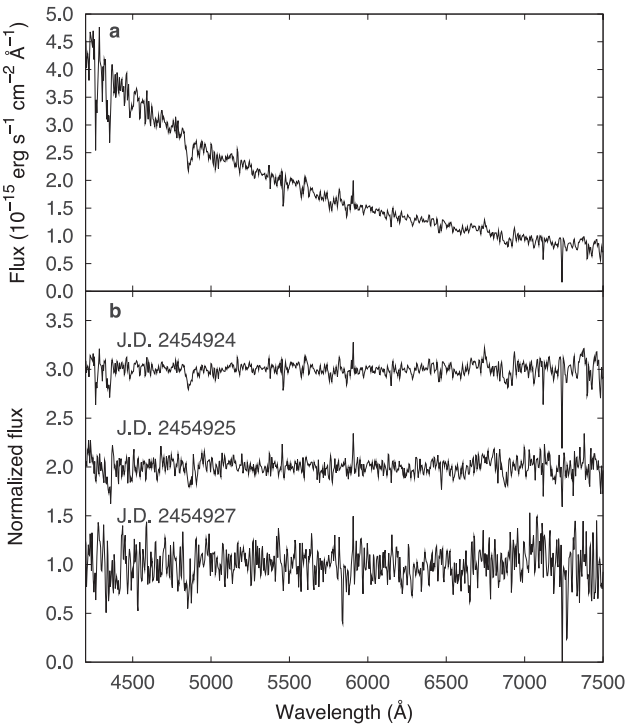

Fig. 38. Upper: Optical spectrum of CSS J102842 obtained on BJD 2454924. Lower: Nightly averaged normalized spectra of CSS J102842.

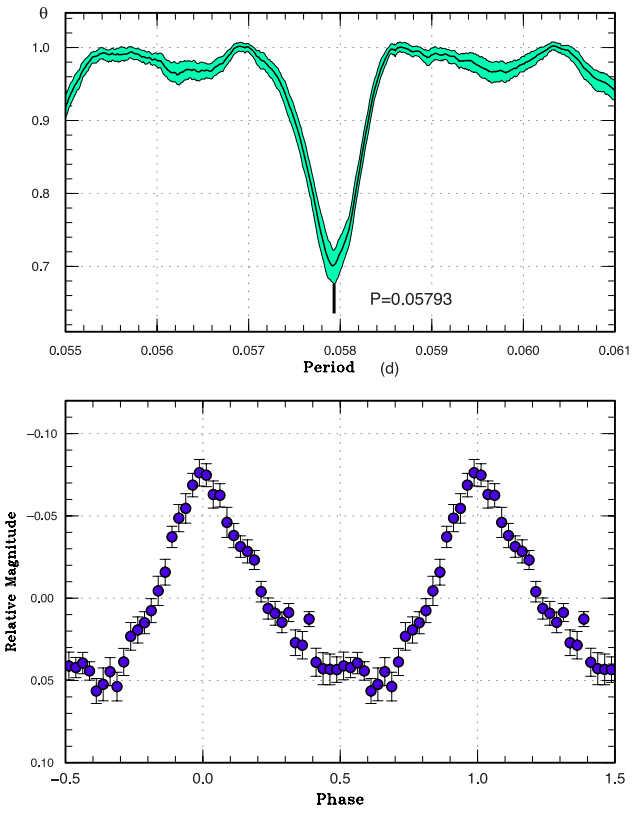

Fig. 39. Superhumps in CSS J105835 (2012). Upper: PDM analysis. Lower: Phase-averaged profile.

object on BJD 2454924 is displayed in the upper panel of figure 38, and the nightly spectra, normalized by the continuum, are presented in the lower panel of figure 38. These spectra show a smooth blue continuum and the Hβ line in absorption. The equivalent width (EW) of the Hβ absorption line is 12 Å (measured from the summed spectrum). The Hα absorption is much weaker (4 Å), suggesting that the line has an emission core. The He I absorption lines are weak in the spectra (He I 5876 has an EW of 3 Å). These features indicate that the object is a hydrogen-rich dwarf nova in outburst, and the weakness of the helium lines makes a clear contrast with SBS 1108+574 (Carter et al. 2013; Littlefield et al. 2013) and CSS J174033.5+414756 (Prieto et al. 2013; T. Ohshima et al. in preparation), which are dwarf novae having an orbital period below the period gap. The He I 5876/Hβ ratio is 0.2–0.3, which places the object in a range of hydrogen-rich CVs within the observational error (see figure 4 of Littlefield et al. 2013).

3.38 CSS J105835.1+054703

This object was discovered by CRTS (= CSS 081025:105835+054706, hereafter CSS J105835) on 2008 October 25. There were three known outbursts in 2007 December (15.0 mag), 2008 October (15.8 mag), and 2012 November–December (14.6 mag). The 2012 outburst was detected by CRTS MLS. Using SDSS colors, Kato et al. (2012b) estimated an orbital period of 0.07 d. The 2012 outburst soon turned out to be a superoutburst by the detection of superhumps (vsnet-alert 15155, 15166; figure 39). The times of superhump maxima are listed in table 37. Although a stage A–B transition was recorded, the data were insufficient to determine the period of stage A.

3.39 CSS J150904.0+465057

This object was detected to be a transient by CRTS (= CSS 130324:150904+465057, hereafter CSS J150904) on 2013 March 24. Two past outbursts (2007 April, 17.8 mag, and 2009 March, 16.8 mag) were recorded in the CRTS data. A relatively large intra-night variation was suggestive of eclipses (vsnet-alert 15543). Subsequent observations detected superhumps and shallow eclipses (vsnet-alert 15545, 15548; figures 40 and 41). The times of superhump maxima are listed in table 38. The superhump period given in table 2 was obtained by the PDM analysis. The MCMC analysis introduced in Kato et al. (2013a) yielded the eclipse ephemeris of BJD 2456376.9751(6) + 0.068440(8)E; a large systematic error is, however, expected due to the presence of superhumps.

Table 37. Superhump maxima of CSS J105835 (2012).

E	Max*	Error	$O-C^{\dagger}$	$N^{\ddagger}$
0	56268.2217	0.0052	−0.0112	104
1	56268.2872	0.0016	−0.0037	102
33	56270.1551	0.0031	0.0089	60
34	56270.2089	0.0006	0.0048	104
35	56270.2660	0.0004	0.0040	103
51	56271.1940	0.0006	0.0042	100
52	56271.2487	0.0005	0.0010	84
68	56272.1834	0.0011	0.0081	103
69	56272.2331	0.0003	−0.0001	206
70	56272.2893	0.0002	−0.0020	239
81	56272.9270	0.0004	−0.0020	54
82	56272.9847	0.0003	−0.0023	55
83	56273.0451	0.0007	0.0001	31
86	56273.2179	0.0008	−0.0010	91
87	56273.2765	0.0011	−0.0003	89
88	56273.3324	0.0007	−0.0024	47
98	56273.9107	0.0020	−0.0039	24
99	56273.9706	0.0003	−0.0020	55
100	56274.0294	0.0004	−0.0012	49
116	56274.9581	0.0006	−0.0001	55
117	56275.0171	0.0005	0.0009	55

*BJD−2400000.
†Against max = 2456268.2329 + 0.057977 E.
‡Number of points used to determine the maximum.

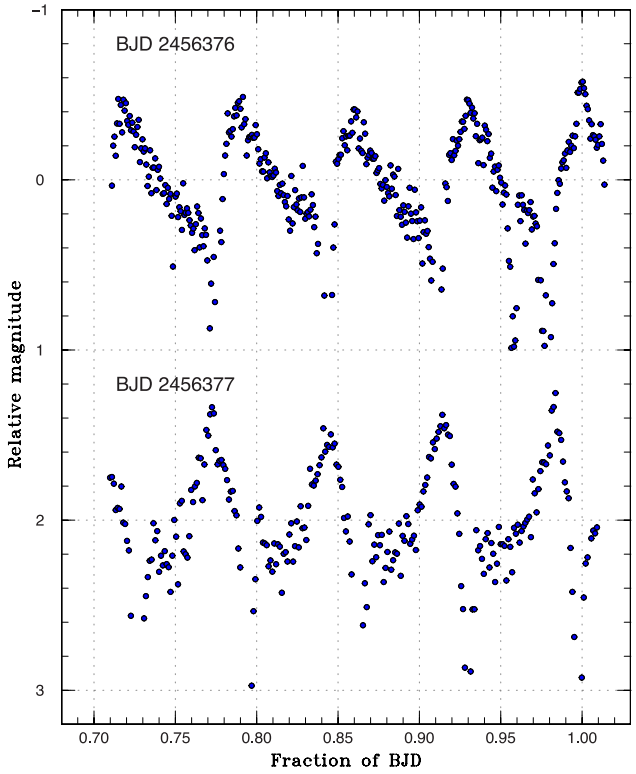

Fig. 40. Light curves of CSS J150904 (2013). Large-amplitude superhumps and shallow eclipses are seen.

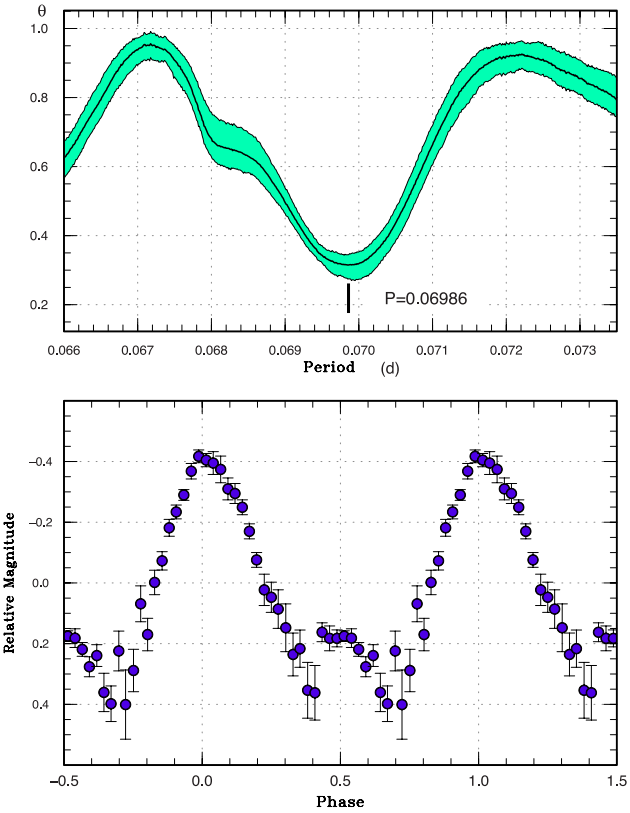

Fig. 41. Superhumps in CSS J150904 (2013). Upper: PDM analysis. Lower: Phase-averaged profile.

Table 38. Superhump maxima of CSS J150904 (2013).

E	Max*	Error	$O-C^{\dagger}$	$N^{\ddagger}$
0	56376.7211	0.0008	−0.0016	48
1	56376.7941	0.0006	0.0014	67
2	56376.8634	0.0007	0.0008	63
3	56376.9318	0.0007	−0.0008	64
4	56377.0011	0.0004	−0.0014	49
14	56377.7088	0.0083	0.0065	21
15	56377.7717	0.0010	−0.0006	43
16	56377.8422	0.0010	−0.0000	43
17	56377.9104	0.0013	−0.0018	46
18	56377.9797	0.0014	−0.0025	44

*BJD−2400000.
†Against max = 2456376.7226 + 0.069977 E.
‡Number of points used to determine the maximum.

3.40 CSS J203937.7−042907

This object was detected to be a transient by CRTS (= CSS 120813:203938−042908, hereafter CSS J203937) on 2012 August 13. Subsequent observations indicated that the object showed superhumps (figure 42) and is a dwarf nova in the period gap (vsnet-alert 14858, 14859). The times of superhump maxima are listed in table 39. The $O-C$ values indicate that the period was increasing during

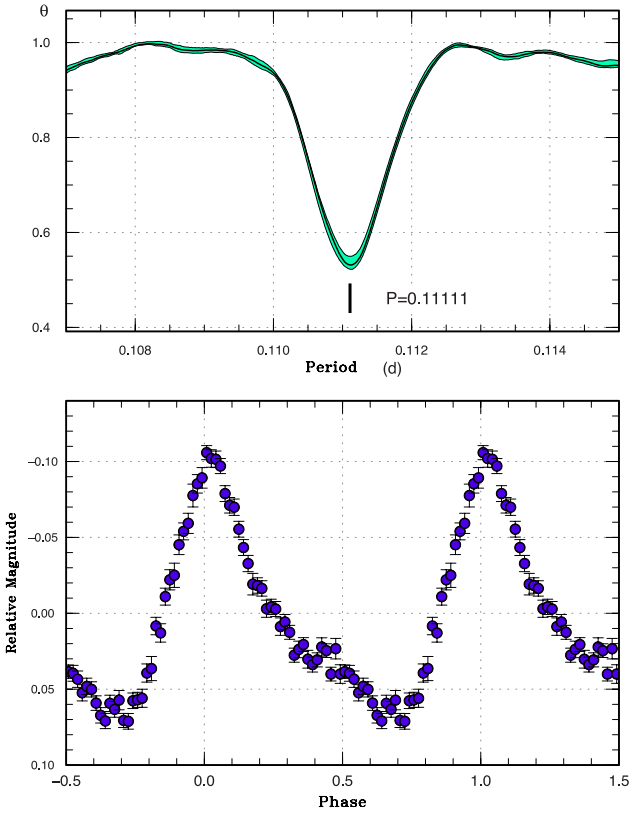

Fig. 42. Superhumps in CSS J203937 (2012). Upper: PDM analysis. Lower: Phase-averaged profile.

the entire observation. Since the cycle count was somewhat ambiguous in the initial part, $E = 0$ was not used for determining the $P_{\rm dot}$ listed in table 2. If we use this point, $P_{\rm dot}$ becomes $+10.2(2.5) \times 10^{-5}$.

There have been at least two long-$P_{\rm orb}$ objects with large positive $P_{\rm dot}$ (GX Cas: Kato et al. 2012a; SDSS J170213: Kato et al. 2009a, 2013a). CSS J203937 appears to be similar to SDSS J170213, another SU UMa-type dwarf nova in the period gap. CRTS data recorded only one past outburst in 2005 October, and the frequency of outbursts seems to be as low as that of SDSS J170213 (Kato et al. 2013a).

Using CRTS data in quiescence, we obtained a period of 0.1057216(1) d (figure 43), which we consider to be the orbital period. The light curve has double humps, which likely reflect a combination of the ellipsoidal variation of the secondary and the orbital hump. The value of ε (for mean $P_{\rm SH}$) amounts to 5.1(1)%, which is also similar to that of SDSS J170213 (Kato et al. 2013a).

3.41 CSS J214934.6-121909

This object was detected as a transient by CRTS (= CSS 120922:214934−121908, hereafter CSS J214934) on 2012 September 22. Subsequent observations confirmed the presence of superhumps (vsnet-alert 14944, 14947; figure 44). The times of two superhump maxima are BJD 2456194.3570(4) ($N = 66$) and 2456194.4272(4) ($N = 69$). The period by the PDM method was 0.0702(5) d.

Table 39. Superhump maxima of CSS J203937 (2012).

E	Max*	Error	$O - C^{\dagger}$	$N^{\ddagger}$
0	56155.6569	0.0005	0.0152	110
18	56157.6427	0.0006	−0.0001	105
19	56157.7531	0.0013	−0.0009	99
23	56158.2058	0.0096	0.0072	74
24	56158.3106	0.0004	0.0008	254
25	56158.4229	0.0003	0.0020	367
26	56158.5327	0.0005	0.0006	159
27	56158.6416	0.0012	−0.0017	38
28	56158.7568	0.0038	0.0023	13
34	56159.4314	0.0066	0.0099	37
35	56159.5265	0.0007	−0.0062	108
36	56159.6397	0.0007	−0.0042	170
37	56159.7562	0.0025	0.0012	75
42	56160.3037	0.0130	−0.0072	29
43	56160.4189	0.0007	−0.0031	129
44	56160.5292	0.0008	−0.0040	108
45	56160.6433	0.0013	−0.0011	39
51	56161.3025	0.0010	−0.0089	167
52	56161.4138	0.0005	−0.0088	299
53	56161.5260	0.0005	−0.0077	342
54	56161.6389	0.0009	−0.0060	106
55	56161.7511	0.0014	−0.0050	63
62	56162.5309	0.0015	−0.0033	76
63	56162.6517	0.0031	0.0062	44
69	56163.3101	0.0007	−0.0023	255
70	56163.4182	0.0006	−0.0055	305
71	56163.5296	0.0013	−0.0052	214
72	56163.6441	0.0012	−0.0019	102
73	56163.7669	0.0073	0.0097	16
79	56164.4243	0.0041	0.0002	57
80	56164.5360	0.0020	0.0007	79
81	56164.6540	0.0027	0.0075	105
82	56164.7604	0.0053	0.0027	87
88	56165.4249	0.0011	0.0003	64
89	56165.5266	0.0038	−0.0093	93
90	56165.6650	0.0049	0.0180	105
97	56166.4328	0.0036	0.0076	59
98	56166.5365	0.0031	0.0001	77

*BJD−2400000.
†Against max = 2456155.6417 + 0.111170 E.
‡Number of points used to determine the maximum.

3.42 DDE 26

DDE 26 is a dwarf nova discovered by Denisenko (2012) and is located at $22^{\rm h}03^{\rm m}28^{\rm s}.2$, $+30^{\circ}56'37''$. D. Denisenko detected a bright outburst on 2012 July 25 (vsnet-alert

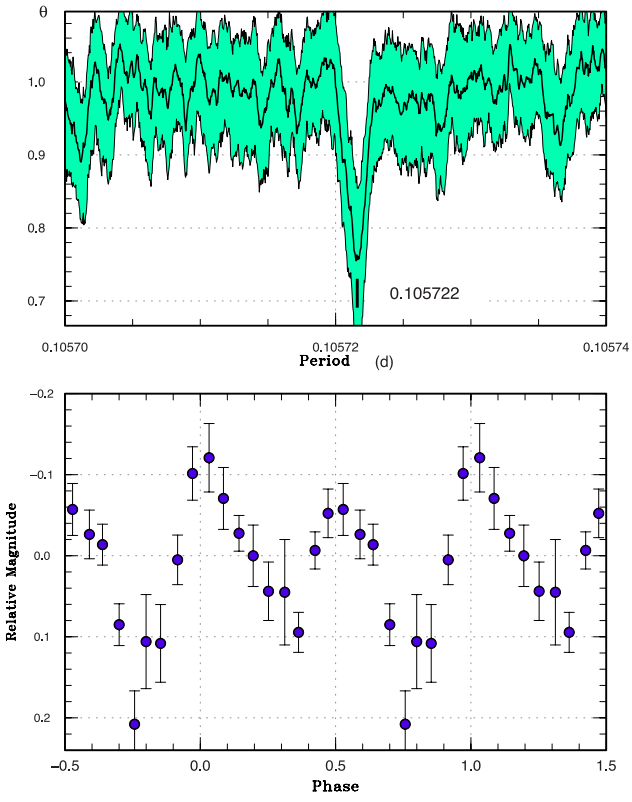

Fig. 43. Orbital variation in CSS J203937 in quiescence. Upper: PDM analysis. Lower: Phase-averaged profile.

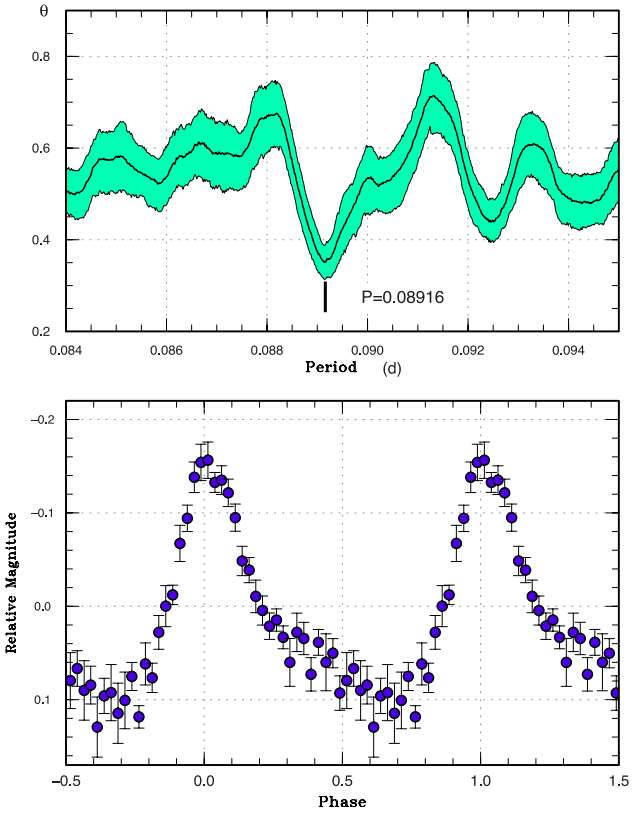

Fig. 45. Superhumps in DDE 26 (2012). Upper: PDM analysis. Lower: Phase-averaged profile.

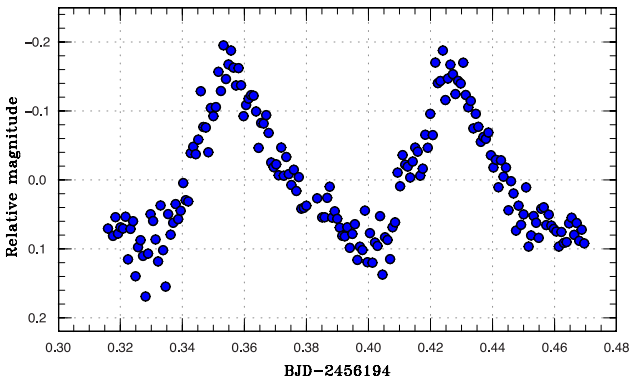

Fig. 44. Superhumps in CSS J214934 (2012).

Table 40. Superhump maxima of DDE 26 (2012).

E	Max*	Error	$O-C^{\dagger}$	$N^{\ddagger}$
0	56134.6787	0.0005	−0.0011	129
1	56134.7696	0.0006	0.0005	152
20	56136.4679	0.0004	0.0017	31
31	56137.4476	0.0011	−0.0011	33

*BJD−2400000.
†Against max = 2456134.6798 + 0.089320 E.
‡Number of points used to determine the maximum.

14792). Subsequent observations detected superhumps (vsnet-alert 14799; figure 45).

The times of superhump maxima are listed in table 40. The $P_{\rm dot}$ was determined globally. The large negative $P_{\rm dot}$ indicates that the object belongs to a group of long-$P_{\rm orb}$ SU UMa-type dwarf novae with large $P_{\rm SH}$ variations, whose best-known member is UV Gem (Kato et al. 2009a).

3.43 MASTER OT J000820.50+773119.1

This object was detected to be a transient by the MASTER network (Denisenko et al. 2012d, hereafter MASTER J000820). Subsequent observations detected superhumps (vsnet-alert 14967; figure 46). The times of superhump maxima are listed in table 41. The period listed in table 2 was obtained by the PDM method.

3.44 MASTER OT J001952.31+464933.0

This object (hereafter MASTER J001952) was discovered by the MASTER network (Denisenko et al. 2012e) on

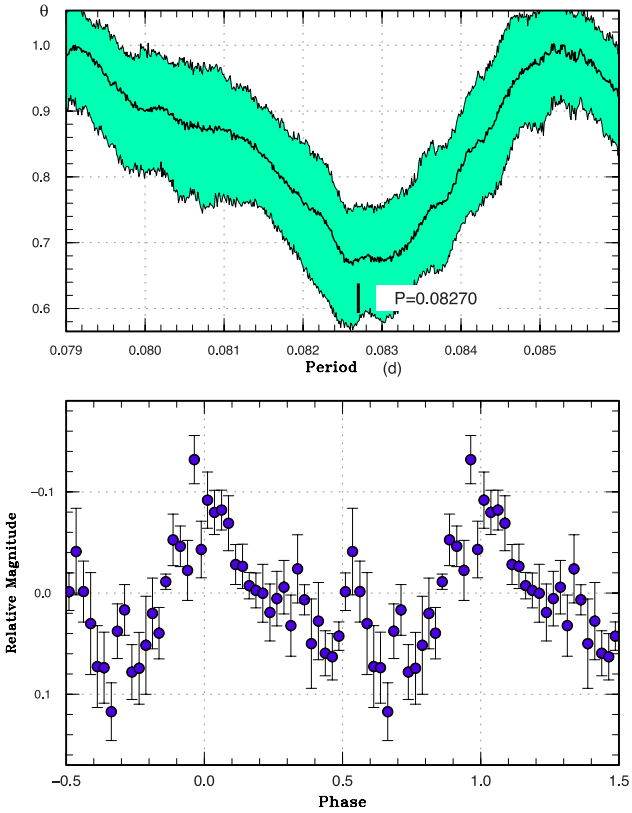

Fig. 46. Superhumps in MASTER J000820 (2012). Upper: PDM analysis. Lower: Phase-averaged profile.

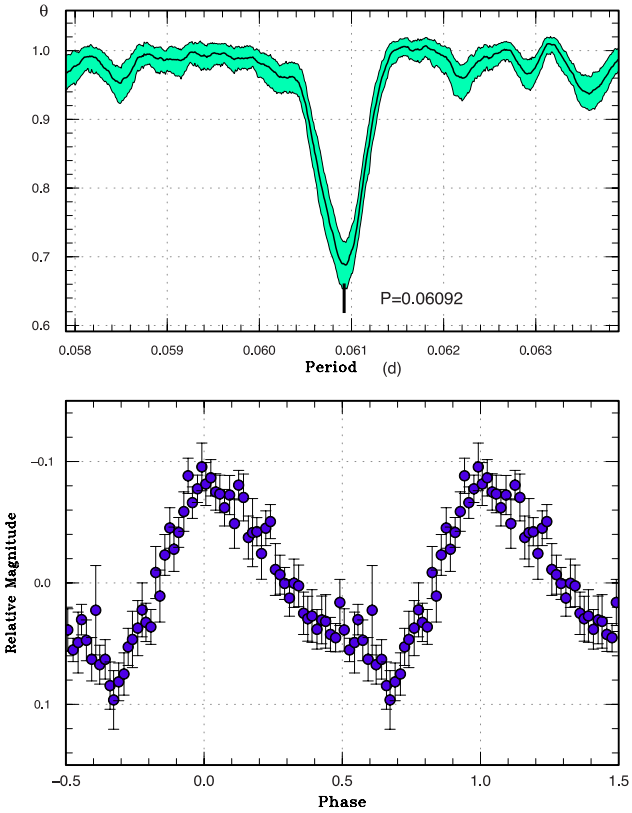

Fig. 47. Superhumps in MASTER J001952 (2012). Upper: PDM analysis. Lower: Phase-averaged profile.

Table 41. Superhump maxima of MASTER J000820 (2012).

E	Max*	Error	$O-C^{\dagger}$	$N^{\ddagger}$
0	56203.3346	0.0014	−0.0005	46
1	56203.4187	0.0013	0.0007	41
12	56204.3276	0.0027	−0.0016	45
13	56204.4135	0.0027	0.0014	46

*BJD−2400000.
†Against max = 2456203.3351 + 0.082841 E.
‡Number of points used to determine the maximum.

2012 October 15. Follow-up observations detected superhumps (vsnet-alert 15012, 15014, 15015, 15017, 15065; figure 47). The times of superhump maxima are listed in table 42. The epoch $E = 0$ corresponds to a stage A superhump. A positive $P_{\rm dot}$ of $+10.4(2.7) \times 10^{-5}$ was observed in stage B superhumps. This value is typical of this $P_{\rm SH}$.

3.45 MASTER OT J030128.77+401104.9

This object (hereafter MASTER J030128) was discovered by the MASTER network (Balanutsa et al. 2012b) on 2012 December 27. The outburst amplitude was ∼ 6 mag. Subsequent observations possibly detected variations (vsnet-alert 15224), but superhumps clearly appeared only 8 d later

Table 42. Superhump maxima of MASTER J001952 (2012).

E	Max*	Error	$O-C^{\dagger}$	$N^{\ddagger}$
0	56217.3383	0.0029	−0.0094	34
15	56218.2674	0.0004	0.0050	33
16	56218.3297	0.0005	0.0063	34
17	56218.3889	0.0004	0.0045	34
32	56219.3020	0.0005	0.0028	33
33	56219.3613	0.0005	0.0011	34
34	56219.4268	0.0010	0.0056	12
44	56220.0309	0.0010	−0.0002	84
45	56220.0882	0.0010	−0.0039	82
60	56220.9998	0.0014	−0.0071	47
61	56221.0678	0.0009	−0.0001	82
62	56221.1225	0.0015	−0.0064	82
63	56221.1897	0.0052	−0.0001	18
77	56222.0462	0.0015	0.0026	51
78	56222.0965	0.0017	−0.0081	55
79	56222.1638	0.0050	−0.0018	23
111	56224.1216	0.0022	0.0044	44
112	56224.1840	0.0056	0.0058	39
113	56224.2382	0.0012	−0.0010	44

*BJD−2400000.
†Against max = 2456217.3477 + 0.060987 E.
‡Number of points used to determine the maximum.

(vsnet-alert 15247; figure 48). Although initial observations possibly recorded the precursor phase (vsnet-alert 15247), it is difficult to determine the outburst phase due to the gaps in the observation. The object entered into the rapid fading phase on 2013 January 11. The times of superhump maxima are listed in table 43; the times were well measured only after $E = 96$, and the cycle numbers for $E \leq 34$ may not be correct. It was not certain whether we observed stage B or stage C.

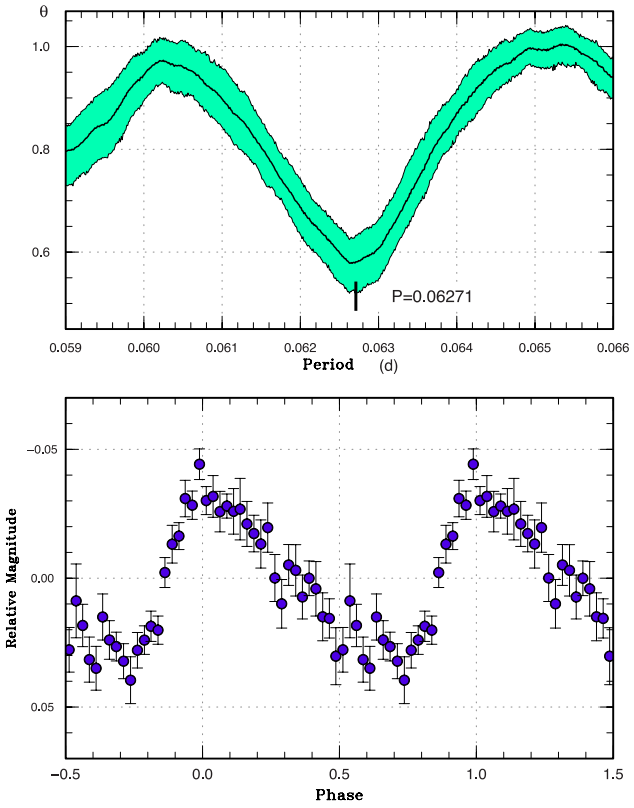

Fig. 48. Superhumps in MASTER J030128 (2012). The data for BJD 2456298–2456300 were used. Upper: PDM analysis. Lower: Phase-averaged profile.

Table 43. Superhump maxima of MASTER J030128 (2012).

E	Max*	Error	$O-C^{\dagger}$	$N^{\ddagger}$
0	56292.2948	0.0213	0.0062	35
1	56292.3560	0.0023	0.0047	35
2	56292.4184	0.0028	0.0044	35
34	56294.3985	0.0018	−0.0217	60
96	56298.3035	0.0015	−0.0035	51
97	56298.3752	0.0010	0.0056	65
100	56298.5580	0.0011	0.0003	49
101	56298.6191	0.0007	−0.0014	62
102	56298.6822	0.0009	−0.0009	46
112	56299.3089	0.0016	−0.0012	42
113	56299.3770	0.0008	0.0043	42
114	56299.4387	0.0030	0.0033	22

*BJD−2400000.
†Against max = 2456292.2886 + 0.062691 E.
‡Number of points used to determine the maximum.

3.46 MASTER OT J042609.34+354144.8

This object (hereafter MASTER J042609) was discovered by the MASTER network (Denisenko et al. 2012d). The object has a ROSAT counterpart (1RXS J042608.9+354151) and a GALEX UV source. There were at least three past outburst detections in the CRTS data: 2008 November 1 (13.4 mag), 2010 February 19 (14.7 mag), and 2011 November 18 (14.4 mag), and its frequency of outbursts is not particularly low. Subsequent observations confirmed superhumps (vsnet-alert 14970, 14979, 14989, 14992; figure 49). The times of superhump maxima are listed in table 44. Since these superhumps were observed in the latter phase of the superoutburst and in the early post-outburst phase, the period decrease likely corresponds to a stage B–C transition. Since only the latter part of stage B was observed, we did not attempt to determine $P_{\rm dot}$.

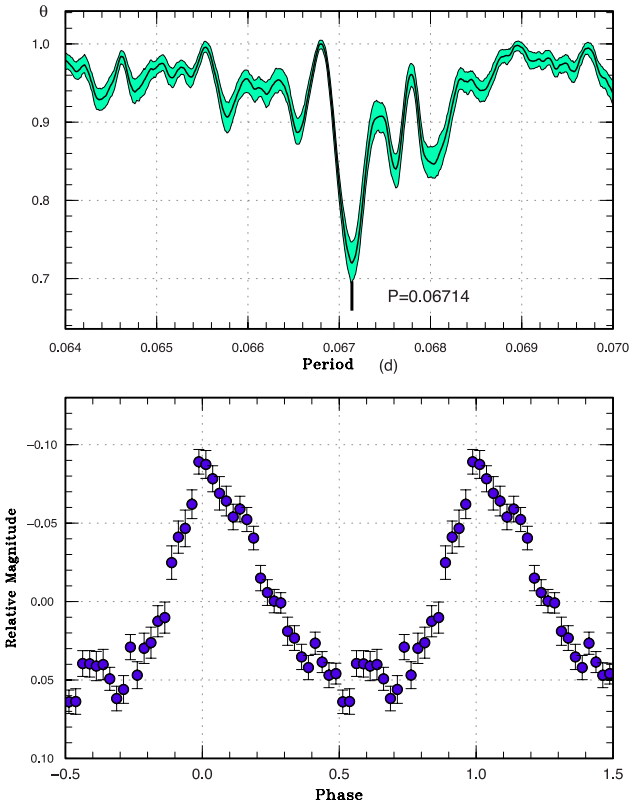

Fig. 49. Superhumps in MASTER J042609 (2012). Upper: PDM analysis. Lower: Phase-averaged profile.

Table 44. Superhump maxima of MASTER J042609 (2012).

E	Max*	Error	$O-C^{\dagger}$	$N^{\ddagger}$
0	56202.6263	0.0007	−0.0087	67
1	56202.6949	0.0005	−0.0072	65
12	56203.4360	0.0007	−0.0049	93
13	56203.5040	0.0004	−0.0040	124
14	56203.5718	0.0003	−0.0034	191
15	56203.6388	0.0004	−0.0035	162
16	56203.7086	0.0008	−0.0009	63
29	56204.5867	0.0005	0.0040	65
31	56204.7228	0.0007	0.0058	52
38	56205.1918	0.0005	0.0047	119
40	56205.3286	0.0006	0.0071	121
81	56208.0835	0.0004	0.0084	182
87	56208.4849	0.0012	0.0068	39
88	56208.5549	0.0005	0.0096	69
89	56208.6201	0.0004	0.0077	69
90	56208.6899	0.0006	0.0102	63
103	56209.5470	0.0016	−0.0058	46
104	56209.6195	0.0015	−0.0004	45
105	56209.6875	0.0008	0.0004	94
106	56209.7514	0.0009	−0.0028	60
107	56209.8211	0.0011	−0.0003	54
120	56210.6878	0.0016	−0.0067	35
148	56212.5722	0.0004	−0.0029	51
158	56213.2336	0.0018	−0.0131	136

*BJD−2400000.
†Against max = 2456202.6349 + 0.0671633 E.
‡Number of points used to determine the maximum.

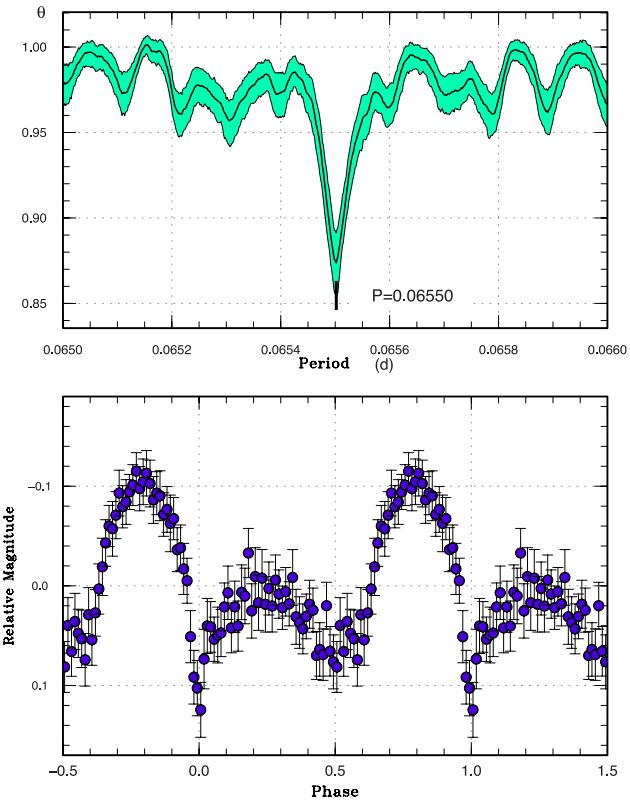

Fig. 50. Orbital modulation in MASTER J042609 in quiescence. Upper: PDM analysis. Lower: Phase-averaged profile.

Between 2012 November 20 and 2013 January 5, the object was observed in quiescence. A period analysis yielded a light curve characteristic of a grazing eclipsing system with a prominent orbital hump (figure 50). The orbital period determined from this analysis was 0.0655015(17) d. By combining the period with the CRTS data in quiescence, we have obtained a refined period of 0.0655022(1) d. The eclipse minimum in figure 50 corresponds to BJD 2456276.6430. The quiescent orbital profile bears some similarity to WZ Sge-type dwarf nova, particularly with a very low q, in the double-wave modulations.[10] Zharikov et al. (2013) suggested that these double-wave modulations can be interpreted as a result of the spiral structure caused by the 2:1 resonance. Most recently, however, SDSS J152419.33+220920.0, which appears to have a higher q and less likely achieves the 2:1 resonance, was reported to show double-wave modulations (Michel et al. 2013). MASTER J042609 would provide an additional example for a rather ordinary SU UMa-type dwarf nova showing double-wave modulations. It may be that there are different mechanisms to produce double-wave modulations in quiescence. A classical interpretation assuming a semitransparent accretion disk allowing the light from the hot spot to escape in two directions (Skidmore et al. 2000) may be an alternative mechanism.

The high orbital inclination would explain the relatively small outburst amplitude for a short-$P_{\rm orb}$ SU UMa-type dwarf nova.

[10] See, e.g., WZ Sge and AL Com (Patterson et al. 1996), V455 And (Araujo-Betancor et al. 2005; Kato et al. 2009a), V386 Ser (Mukadam et al. 2010), EZ Lyn (Kato et al. 2009b; Zharikov et al. 2013), BW Scl (Augusteijn & Wisotzki 1997; Kato et al. 2013a).

3.47 MASTER OT J054317.95+093114.8

This object (hereafter MASTER J054317) was discovered by the MASTER network (Balanutsa et al. 2012a). There was no visible quiescent counterpart in the DSS plates to 21 mag (Balanutsa et al. 2012a). The large outburst amplitude (≥ 7 mag) attracted attention. For the initial four days, the object did not show clear superhumps (vsnet-alert 14986). The object then started to show superhumps (vsnet-alert 14998, 15016, 15018, 15020; figure 51). The times of superhump maxima are listed in table 45. Although stages A–C are recognized, the period of stage A was not determined due to the lack of observations. The coverage of stage B was also somewhat insufficient.

Despite the large outburst amplitude, the behavior of superhumps resembles that of ordinary SU UMa-type dwarf

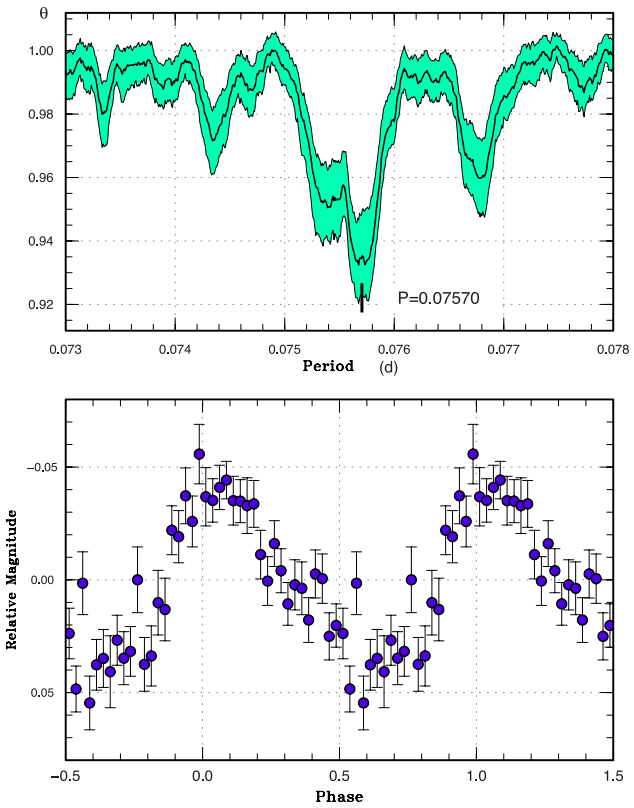

Fig. 51. Superhumps in MASTER J054317 (2012). Upper: PDM analysis. Lower: Phase-averaged profile.

novae rather than WZ Sge-type dwarf novae. There are several long-$P_{\rm orb}$ SU UMa-type dwarf novae with a large outburst amplitude—V1251 Cyg (Kato 1995b; Kato et al. 2009a), EF Peg (Howell et al. 1993; Kato 2002b; Kato et al. 2009a, 2010)—and MASTER J054317 may resemble these objects.

3.48 MASTER OT J064725.70+491543.9

This object (hereafter MASTER J064725) was detected as a dwarf nova by the MASTER network on 2013 March 7 (Tiurina et al. 2013). Superhumps were immediately detected (vsnet-alert 15476, 15477, 15495; figure 52). The times of superhump maxima are listed in table 46. Stages B and C can be identified. When deriving the period of stage C superhumps, we did not include post-superoutburst maxima ($E \geq 243$) and $E = 156$, which was measured on the rapid declining phase and at a small amplitude.

3.49 MASTER OT J073418.66+271310.5

This object (hereafter MASTER J073418) was detected as a dwarf nova by the MASTER network on 2013 February 25 (Denisenko et al. 2012b). The 2MASS color using neural network analysis (Kato et al. 2012b) suggested an orbital period of 0.060 d (vsnet-alert 15445). Superhumps were indeed detected (vsnet-alert 15453, 15461; figure 53). The times of superhump maxima are listed in table 47. Since the object faded soon after these observations, we most likely observed only stage C superhumps.

Table 45. Superhump maxima of MASTER J054317 (2012).

E	Max*	Error	$O-C^{\dagger}$	$N^{\ddagger}$
0	56205.8134	0.0015	−0.0095	20
6	56206.2708	0.0061	−0.0069	33
39	56208.7789	0.0007	−0.0008	24
40	56208.8534	0.0016	−0.0022	17
53	56209.8383	0.0009	−0.0028	32
65	56210.7509	0.0014	−0.0001	23
66	56210.8239	0.0018	−0.0029	24
118	56214.7718	0.0034	0.0026	21
123	56215.1595	0.0007	0.0111	54
131	56215.7654	0.0023	0.0105	24
136	56216.1429	0.0005	0.0090	62
137	56216.2187	0.0010	0.0089	217
138	56216.2931	0.0014	0.0075	154
144	56216.7536	0.0023	0.0131	24
145	56216.8212	0.0052	0.0048	13
157	56217.7311	0.0026	0.0050	23
158	56217.8009	0.0034	−0.0011	24
171	56218.7856	0.0051	−0.0020	24
172	56218.8676	0.0027	0.0042	13
182	56219.6201	0.0006	−0.0014	72
183	56219.7065	0.0199	0.0091	16
184	56219.7751	0.0034	0.0019	24
185	56219.8426	0.0040	−0.0064	22
190	56220.2226	0.0062	−0.0055	147
191	56220.2932	0.0039	−0.0107	101
197	56220.7554	0.0024	−0.0034	24
198	56220.8191	0.0022	−0.0155	24
199	56220.9071	0.0009	−0.0033	70
200	56220.9832	0.0017	−0.0030	70
203	56221.2068	0.0047	−0.0069	145
204	56221.2897	0.0163	0.0001	72
210	56221.7523	0.0195	0.0078	23
211	56221.8091	0.0030	−0.0112	22

*BJD−2400000.
†Against max = 2456205.8229 + 0.075817 E.
‡Number of points used to determine the maximum.

3.50 MASTER OT J081110.46+660008.5

This object (hereafter MASTER J081110) was detected as a large-amplitude transient by the MASTER network (Denisenko et al. 2012b). The outburst amplitude of ~8 mag and the SDSS color (vsnet-alert 15037) were suggestive of a WZ Sge-type dwarf nova. There were modulations resembling early superhumps in the early

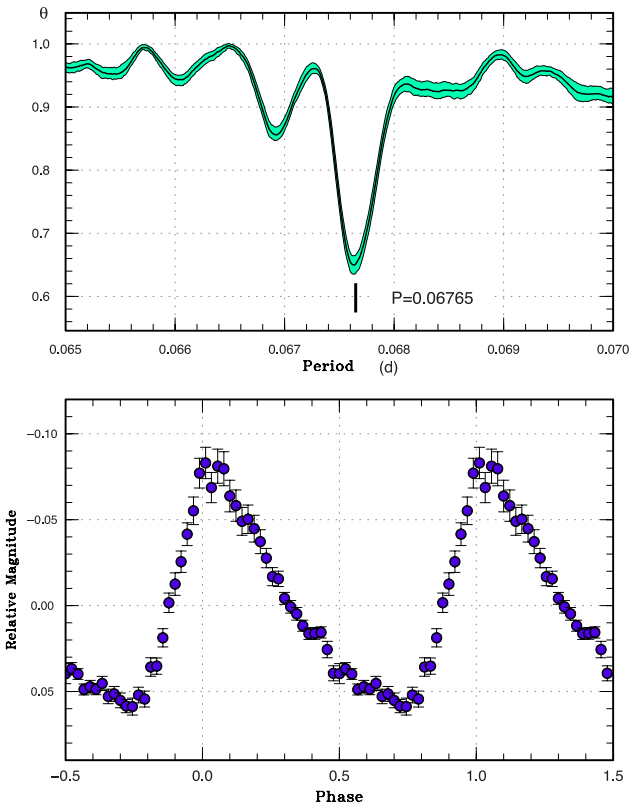

Fig. 52. Superhumps in MASTER J064725 (2013). Upper: PDM analysis. Lower: Phase-averaged profile.

follow-up observations (vsnet-alert 15041, 15045, 15049). Ordinary superhumps grew soon after them (vsnet-alert 15055, 15063, 15066, 15075; figure 54). It was likely that most of the early superhump phase was missed. The times of superhump maxima are listed in table 48. Stages A and B are clearly seen. The $P_{\rm dot}$ was small [$+4.5(0.3) \times 10^{-5}$] and there was no hint as to a transition to stage C, both of which are usual for a WZ Sge-type dwarf nova. Although early superhumps were not unambiguously detected, we consider this object to be a WZ Sge-type dwarf nova.

3.51 MASTER OT J094759.83+061044.4

This object (hereafter MASTER J094759) was discovered by the MASTER network (Denisenko et al. 2013b) on 2013 May 4. There is a $g = 20.4$ mag SDSS counterpart. There were two previous fainter outbursts in the CRTS data. Subsequent observations detected possible early superhumps (vsnet-alert 15679, 15692). After ~ 5 d, ordinary superhumps started to develop (vsnet-alert 15706; figure 55). The times of superhump maxima are listed in table 49.

The amplitudes of early superhumps were very small and it was extremely difficult to determine the period. It was likely that the signal was detected on only the first two nights of observation (before BJD 2456419.2; figure 56). We should bear in mind that this period [0.05588(9) d] has a large uncertainty due to the short observational baseline.

The $O - C$ values of ordinary superhumps were, however, well defined and showed clear stages A and B. The period of stage A superhumps was 0.05717(21) d and, even if we assume a conservative error of 0.004 d in the period of early superhumps, ε^* for stage A corresponds to 2.3(3)%,

Table 46. Superhump maxima of MASTER J064725 (2013).

E	Max*	Error	$O - C^\dagger$	$N^\ddagger$
0	56360.0846	0.0015	−0.0122	37
7	56360.5579	0.0015	−0.0117	126
8	56360.6326	0.0004	−0.0045	182
9	56360.6994	0.0003	−0.0053	190
10	56360.7669	0.0003	−0.0054	174
15	56361.1069	0.0004	−0.0031	30
18	56361.3103	0.0002	−0.0023	101
19	56361.3787	0.0002	−0.0014	137
37	56362.6057	0.0028	0.0097	48
38	56362.6627	0.0002	−0.0008	132
39	56362.7296	0.0002	−0.0015	132
42	56362.9303	0.0007	−0.0034	39
43	56363.0008	0.0005	−0.0005	55
57	56363.9522	0.0008	0.0053	71
58	56364.0180	0.0006	0.0036	63
82	56365.6457	0.0003	0.0101	132
83	56365.7130	0.0005	0.0099	132
84	56365.7793	0.0003	0.0087	132
87	56365.9801	0.0006	0.0068	40
88	56366.0497	0.0008	0.0089	45
97	56366.6535	0.0003	0.0048	132
98	56366.7206	0.0004	0.0044	132
99	56366.7869	0.0003	0.0031	122
108	56367.3919	0.0006	0.0002	75
109	56367.4595	0.0007	0.0002	76
110	56367.5266	0.0010	−0.0003	76
111	56367.5933	0.0010	−0.0011	76
123	56368.4043	0.0011	−0.0006	83
124	56368.4717	0.0010	−0.0008	84
125	56368.5472	0.0020	0.0072	83
126	56368.6069	0.0016	−0.0006	83
136	56369.2885	0.0014	0.0055	38
137	56369.3465	0.0008	−0.0041	80
138	56369.4139	0.0007	−0.0042	118
139	56369.4805	0.0016	−0.0051	45
140	56369.5458	0.0011	−0.0074	40
156	56370.6496	0.0025	0.0157	131
157	56370.6940	0.0017	−0.0075	131
243	56376.5035	0.0016	−0.0069	47
244	56376.5647	0.0018	−0.0132	46

*BJD−2400000.
†Against max = 2456360.0968 + 0.067546 E.
‡Number of points used to determine the maximum.

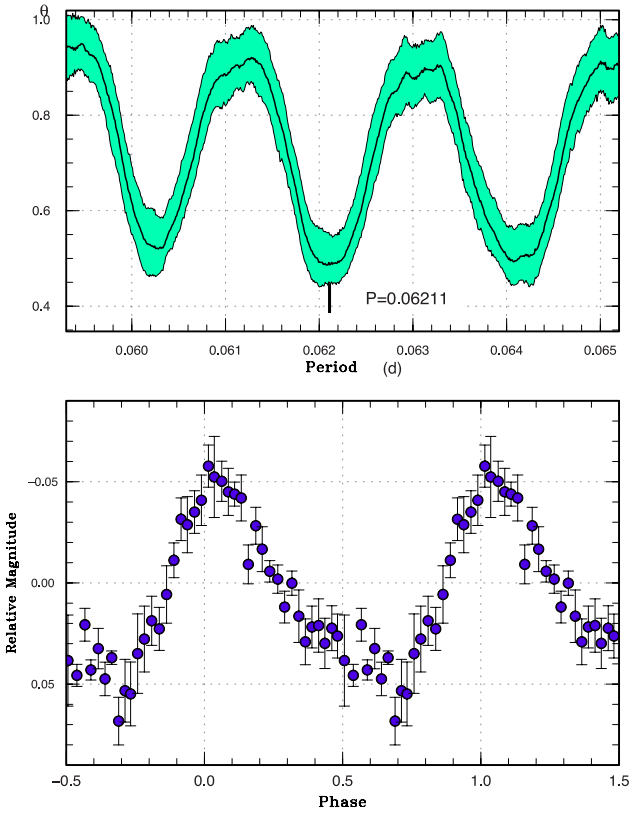

Fig. 53. Superhumps in MASTER J073418 (2013). Upper: PDM analysis. Lower: Phase-averaged profile.

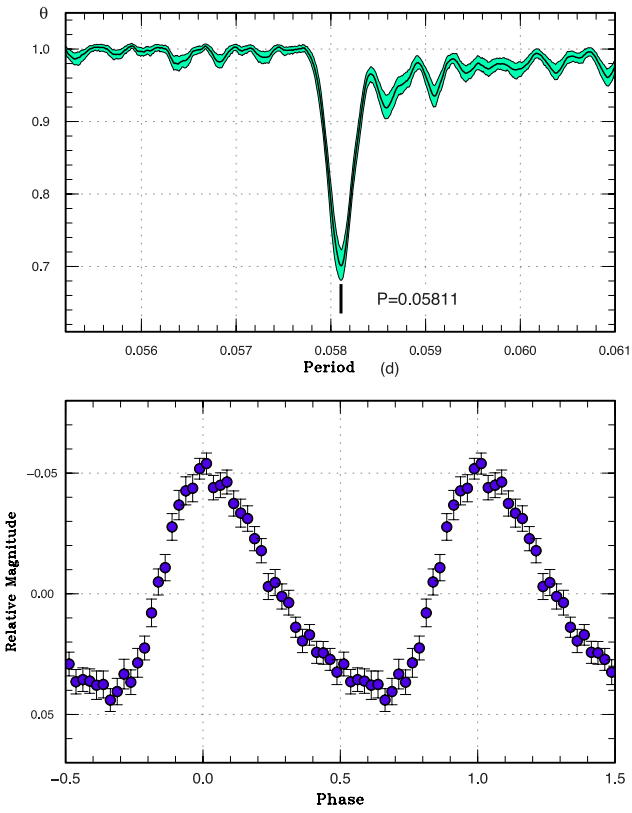

Fig. 54. Superhumps in MASTER J081110 (2012). Upper: PDM analysis. Lower: Phase-averaged profile.

Table 47. Superhump maxima of MASTER J073418 (2013).

E	Max*	Error	$O-C^{\dagger}$	$N^{\ddagger}$
0	56352.4162	0.0009	−0.0018	44
1	56352.4803	0.0006	0.0002	61
2	56352.5433	0.0011	0.0013	30
32	56354.4047	0.0009	0.0027	44
33	56354.4662	0.0012	0.0022	45
34	56354.5240	0.0060	−0.0020	24
36	56354.6474	0.0009	−0.0026	27

*BJD−2400000.
†Against max = 2456352.4180 + 0.061999 E.
‡Number of points used to determine the maximum.

and q is estimated to be 0.060(8). The low value appears to be consistent with the short $P_{\rm orb}$.

3.52 MASTER OT J105025.99+332811.4

This object (hereafter MASTER J105025) was discovered by the MASTER network (Balanutsa et al. 2012b) on 2012 December 25. The object was already in outburst on December 19. The quiescent SDSS colors suggest an orbital period of 0.07 d by using the method in Kato

Table 48. Superhump maxima of MASTER J081110 (2012).

E	Max*	Error	$O-C^{\dagger}$	$N^{\ddagger}$
0	56224.4837	0.0015	−0.0161	61
16	56225.4249	0.0015	−0.0056	57
17	56225.4763	0.0012	−0.0124	61
23	56225.8338	0.0008	−0.0039	55
24	56225.8911	0.0004	−0.0047	55
25	56225.9512	0.0004	−0.0027	55
26	56226.0105	0.0005	−0.0016	41
29	56226.1872	0.0009	0.0005	96
30	56226.2453	0.0007	0.0004	123
31	56226.3051	0.0008	0.0021	123
40	56226.8354	0.0003	0.0089	55
41	56226.8922	0.0002	0.0075	55
42	56226.9517	0.0002	0.0088	55
43	56227.0103	0.0003	0.0092	43
57	56227.8235	0.0003	0.0081	55
58	56227.8808	0.0003	0.0072	55
59	56227.9395	0.0004	0.0077	54
60	56227.9969	0.0002	0.0070	55
74	56228.8092	0.0004	0.0049	50
75	56228.8670	0.0004	0.0046	55
76	56228.9263	0.0003	0.0056	55
77	56228.9829	0.0003	0.0042	55
91	56229.7963	0.0006	0.0032	39

Table 48. (Continued)

E	Max*	Error	$O-C^{\dagger}$	$N^{\ddagger}$
92	56229.8529	0.0004	0.0015	55
93	56229.9101	0.0004	0.0006	55
94	56229.9674	0.0004	−0.0003	55
108	56230.7794	0.0079	−0.0027	20
109	56230.8396	0.0006	−0.0006	43
110	56230.8972	0.0004	−0.0012	43
111	56230.9548	0.0004	−0.0017	43
112	56231.0125	0.0005	−0.0022	33
125	56231.7705	0.0047	−0.0004	16
126	56231.8253	0.0006	−0.0037	43
127	56231.8824	0.0005	−0.0048	43
128	56231.9405	0.0005	−0.0049	43
129	56231.9987	0.0005	−0.0049	44
143	56232.8146	0.0006	−0.0033	43
144	56232.8731	0.0005	−0.0030	43
145	56232.9296	0.0006	−0.0047	43
146	56232.9889	0.0004	−0.0035	43
160	56233.8046	0.0005	−0.0022	72
161	56233.8604	0.0004	−0.0046	70
162	56233.9171	0.0004	−0.0061	70
163	56233.9759	0.0004	−0.0054	70
211	56236.7737	0.0085	0.0003	24
212	56236.8307	0.0016	−0.0009	36
213	56236.8860	0.0012	−0.0037	35
214	56236.9437	0.0012	−0.0042	35
215	56237.0055	0.0032	−0.0006	35
229	56237.8236	0.0014	0.0031	35
230	56237.8804	0.0010	0.0018	35
231	56237.9414	0.0015	0.0046	35
232	56237.9984	0.0013	0.0035	36
246	56238.8205	0.0044	0.0111	36

*BJD−2400000.
†Against max = 2456224.4998 + 0.058168 E.
‡Number of points used to determine the maximum.

et al. (2012b) (vsnet-alert 15216). Although possible superhumps were reported (vsnet-alert 15228), the duration of the observation was not sufficient to determine the period. Another observation 6 d later detected a clearer superhump at BJD 2456299.0108(15) ($N = 67$). The period was not determined.

3.53 MASTER OT J111759.87+765131.6

This object (hereafter MASTER J111759) was discovered by the MASTER network (Balanutsa et al. 2013) on 2013 April 4. Subsequent observations confirmed the presence of superhumps (vsnet-alert 15598, 15610; figure 57). The times of superhump maxima are listed in table 50. Most of our observations were obtained between April 12 and 18, the late stage of the superoutburst. Thus the superhumps for $E \geq 100$ are likely to be stage C superhumps. Although

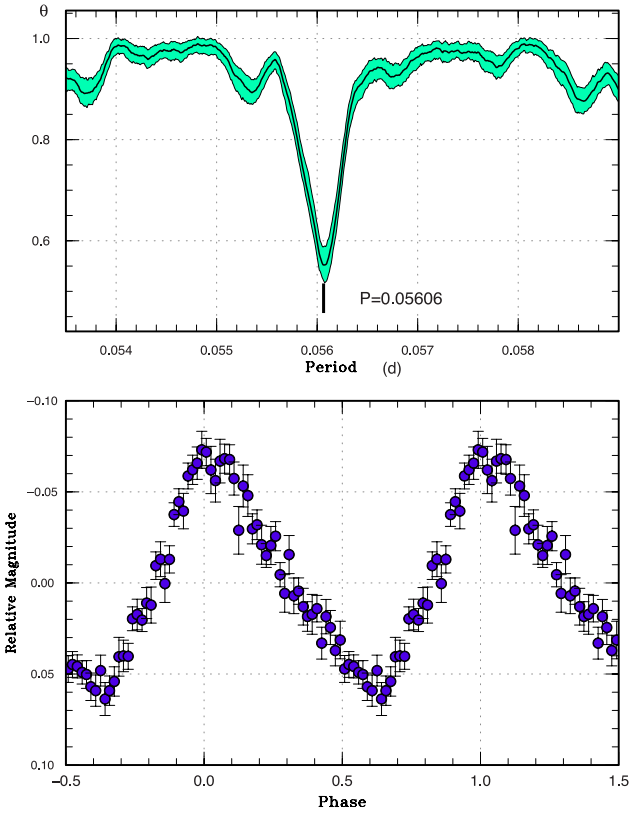

Fig. 55. Superhumps in MASTER J094759 (2013). Upper: PDM analysis. Lower: Phase-averaged profile.

$0 \leq E \leq 2$ may be stage B superhumps, it was impossible to determine the period.

3.54 MASTER OT J165236.22+460513.2

This object (hereafter MASTER J165236) was discovered by the MASTER network (Denisenko et al. 2013c) on 2013 March 12. The object was suggested to be a WZ Sge-type dwarf nova due to the large (larger than 7 mag) outburst amplitude (vsnet-alert 15493). The quiescent SDSS counterpart ($g = 22.1$) has a red color ($g - z = +1.3$), unlike a WZ Sge-type object (vsnet-alert 15496). The evolution of superhumps was soon detected (vsnet-alert 15506, 15519, 15535). The period of superhumps (~ 0.084 d) was also unusually long for a WZ Sge-type dwarf nova. The times of superhump maxima are listed in table 51. Although the growing stage of the superhumps was detected, the period of stage A superhumps could not be determined due to lack of observation. The mean profile of stage B superhumps is shown in figure 58. After BJD 2456368, the amplitudes of superhumps became smaller and the times of maxima were not meaningfully determined. Although the initial evolution of the superhumps resembled those of ordinary long-$P_{\rm orb}$ SU UMa-type dwarf novae, the rapid decay of the superhump amplitude was unusual. Although the object might be

Table 49. Superhump maxima of MASTER J094759 (2013).

E	Max*	Error	$O-C^{\dagger}$	$N^{\ddagger}$
0	56421.9647	0.0010	−0.0154	72
1	56422.0147	0.0009	−0.0218	85
6	56422.2959	0.0012	−0.0218	61
10	56422.5408	0.0020	−0.0018	10
11	56422.5913	0.0057	−0.0076	11
27	56423.5055	0.0007	0.0066	13
28	56423.5595	0.0010	0.0044	13
45	56424.5242	0.0005	0.0128	12
46	56424.5817	0.0005	0.0141	11
53	56424.9734	0.0002	0.0121	104
54	56425.0295	0.0002	0.0119	105
55	56425.0821	0.0011	0.0083	48
71	56425.9817	0.0006	0.0079	144
72	56426.0367	0.0007	0.0065	158
73	56426.0904	0.0019	0.0041	48
89	56426.9959	0.0032	0.0095	47
90	56427.0412	0.0044	−0.0014	28
98	56427.4921	0.0012	−0.0005	12
99	56427.5486	0.0015	−0.0003	13
107	56427.9974	0.0005	−0.0014	66
113	56428.3409	0.0007	0.0045	37
124	56428.9567	0.0026	0.0016	32
125	56429.0049	0.0013	−0.0064	32
142	56429.9634	0.0004	−0.0042	69
143	56430.0169	0.0012	−0.0070	69
213	56433.9599	0.0088	−0.0014	28
214	56434.0042	0.0048	−0.0134	55

*BJD−2400000.
†Against max = 2456421.9802 + 0.056249 E.
‡Number of points used to determine the maximum.

a period bouncer, we do not have additional data to check this possibility. Detailed observations are desired.

3.55 MASTER OT J174902.10+191331.2

This object (hereafter MASTER J174902) was originally discovered by the MASTER network (Denisenko et al. 2012c) on 2012 August 20. Nesci (2012) reported a prediscovery spectrum on the Digitized First Byurakan Survey and suggested that there was a past outburst in 1974. The 2012 outburst was a brief one and it faded rapidly (R. Pickard, see vsnet-alert 16001). The object was again detected in outburst on 2013 July 14 by the ASAS-SN survey. The outburst had been detected by C. Chiselbrook (AAVSO) two days before. Subsequent observations detected superhumps (vsnet-alert 16044, 16061, 16072; figure 59) and it immediately became apparent that this object is located in the period gap. The times of superhump maxima are listed in table 52.

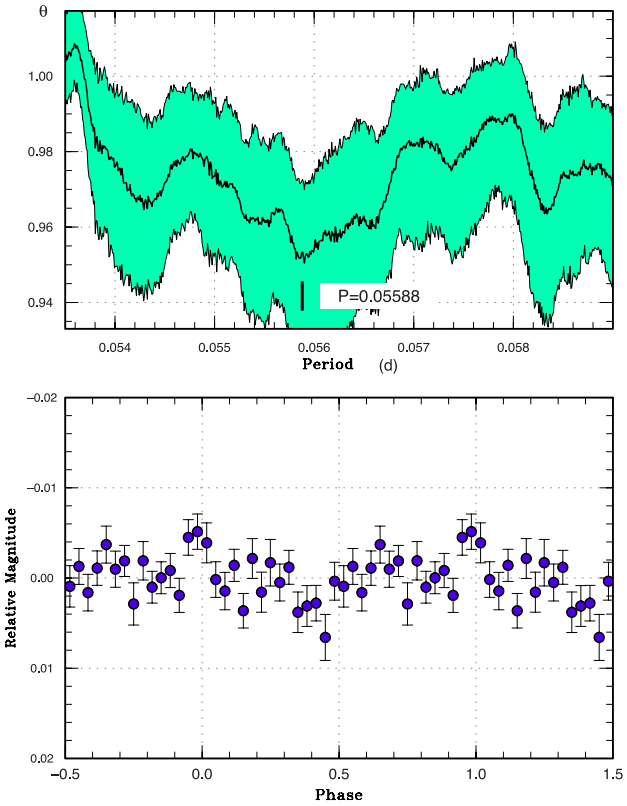

Fig. 56. Possible early superhumps in MASTER J094759 (2013). Upper: PDM analysis. Lower: Phase-averaged profile.

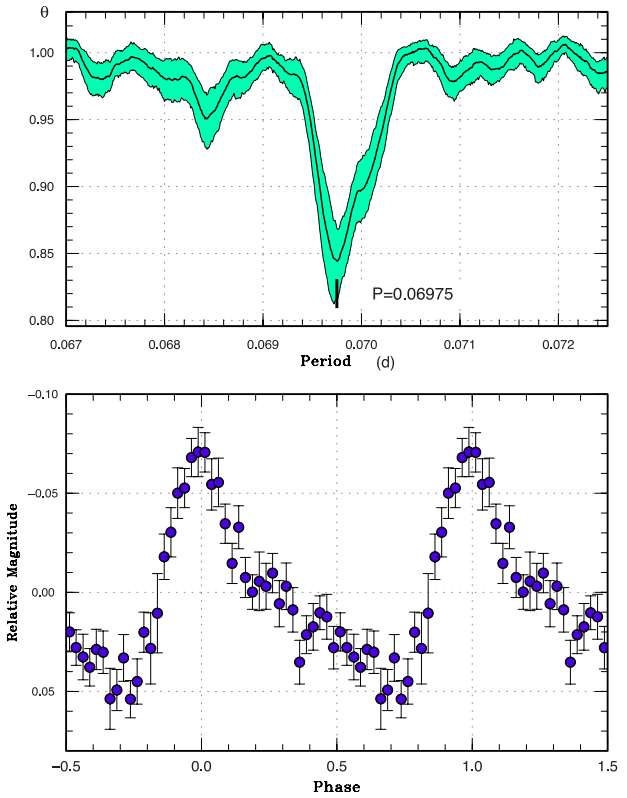

Fig. 57. Superhumps in MASTER J111759 (2013). Upper: PDM analysis. Lower: Phase-averaged profile.

Table 50. Superhump maxima of MASTER J111759 (2013).

E	Max*	Error	$O-C^{\dagger}$	$N^{\ddagger}$
0	56388.5388	0.0026	−0.0004	54
1	56388.6119	0.0011	0.0031	84
2	56388.6826	0.0008	0.0041	83
100	56395.5017	0.0007	−0.0016	56
101	56395.5703	0.0006	−0.0027	63
102	56395.6397	0.0005	−0.0030	68
115	56396.5466	0.0006	−0.0014	73
116	56396.6142	0.0007	−0.0034	72
117	56396.6868	0.0013	−0.0005	40
127	56397.3774	0.0012	−0.0062	73
128	56397.4530	0.0009	−0.0003	53
129	56397.5179	0.0024	−0.0051	67
130	56397.5924	0.0008	−0.0002	67
131	56397.6608	0.0013	−0.0014	32
155	56399.3368	0.0013	0.0032	69
156	56399.4032	0.0017	−0.0001	53
158	56399.5456	0.0010	0.0030	140
159	56399.6214	0.0019	0.0092	67
169	56400.3131	0.0020	0.0045	47
170	56400.3793	0.0024	0.0011	69
171	56400.4440	0.0045	−0.0039	71
172	56400.5196	0.0042	0.0020	64

*BJD−2400000.
†Against max = 2456388.5392 + 0.069642 E.
‡Number of points used to determine the maximum.

Table 51. Superhump maxima of MASTER J165236 (2013).

E	Max*	Error	$O-C^{\dagger}$	$N^{\ddagger}$
0	56365.8839	0.0009	−0.0124	64
1	56365.9593	0.0009	−0.0228	77
11	56366.8532	0.0006	0.0134	75
12	56366.9379	0.0007	0.0124	79
13	56367.0282	0.0014	0.0169	32
15	56367.1933	0.0033	0.0105	69
16	56367.2763	0.0005	0.0077	176
28	56368.2952	0.0004	−0.0026	178
29	56368.3774	0.0005	−0.0062	71
30	56368.4646	0.0004	−0.0048	87
31	56368.5473	0.0005	−0.0078	85
32	56368.6367	0.0009	−0.0042	41

*BJD−2400000.
†Against max = 2456365.8963 + 0.085767 E.
‡Number of points used to determine the maximum.

3.56 MASTER OT J181953.76+361356.5

This object (hereafter MASTER J181953) was discovered by the MASTER network (Shurpakov et al. 2013) on 2013 July 5 at an unfiltered CCD magnitude of 13.9. The quiescent counterpart has a magnitude of 21.6.

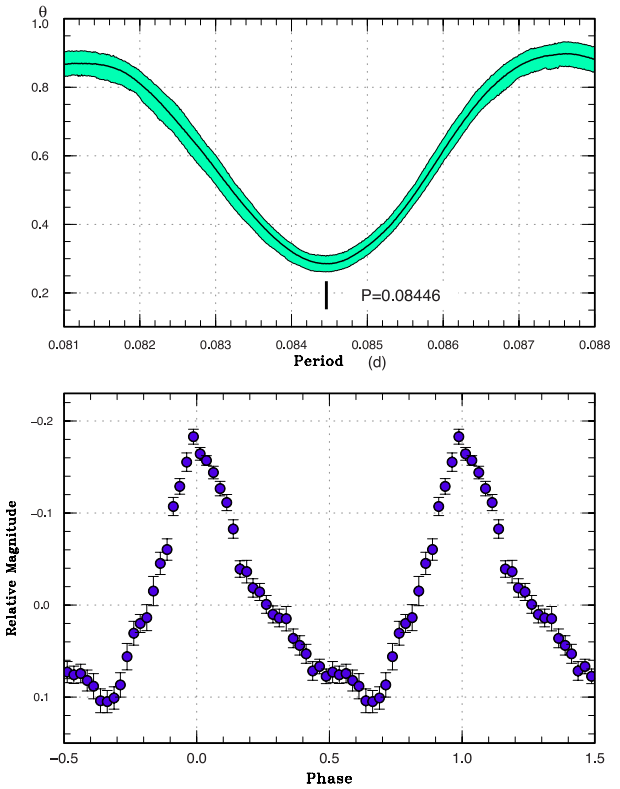

Fig. 58. Superhumps in MASTER J165236 (2013). The data were limited to the range of BJD 2456367.2–2456368.7, when stage B superhumps were clearly detected. Upper: PDM analysis. Lower: Phase-averaged profile.

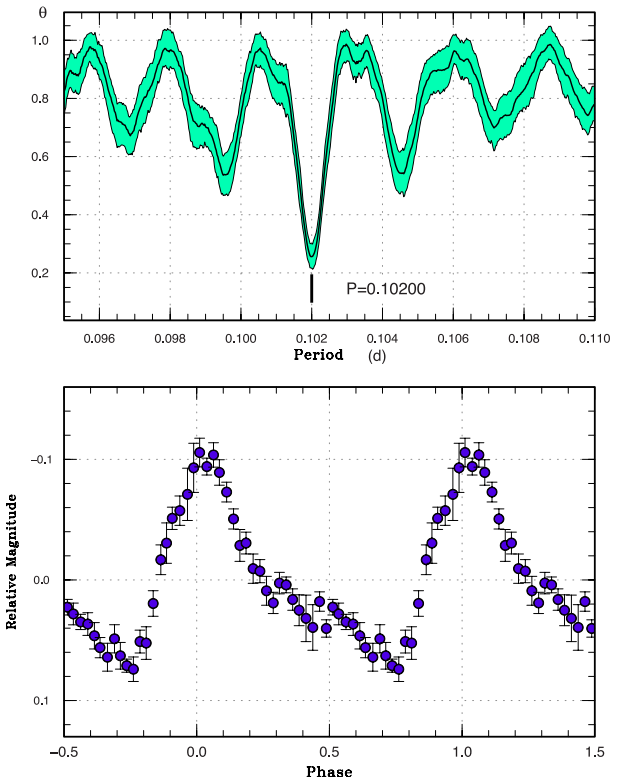

Fig. 59. Ordinary superhumps in MASTER J174902 (2013). Upper: PDM analysis. Lower: Phase-averaged profile.

The large outburst amplitude reminded us of a WZ Sge-type dwarf nova. Subsequent observations detected likely early superhumps (vsnet-alert 15929, 15940; figure 60). Ordinary superhumps then appeared (vsnet-alert 15950, 15956, 15971, 15977, 15987, 15994, 16014, 16023; figure 61). The object started to fade rapidly 14 d after the initial detection (vsnet-alert 16052).

The period of the early superhumps was determined to be 0.05684(2) d (figure 60). The times of superhump maxima are listed in table 53. There were clear stage A and stage B superhumps (figure 62). When determining $P_{\rm dot}$ of the stage B superhumps, we excluded the part with the rapid decline ($E \geq 173$), as in ASASSN-13ax. The last epoch $E = 209$ appeared to show a phase reversal, whose origin in WZ Sge-type dwarf novae is still unclear. Using the period of the stage A superhumps ($E \leq 21$), we could obtain $\epsilon^* = 0.0259(3)$. This value corresponds to $q = 0.069(1)$.

The object showed an oscillating-type long rebrightening (figure 62) similar to WZ Sge (2001) and OT J012059.6+325545 (Kato et al. 2012a).

Table 52. Superhump maxima of MASTER J174902 (2013).

E	Max*	Error	$O-C^{\dagger}$	$N^{\ddagger}$
0	56496.4480	0.0008	−0.0001	49
1	56496.5502	0.0012	0.0002	33
30	56499.5048	0.0017	−0.0005	35
38	56500.3182	0.0042	−0.0023	22
39	56500.4249	0.0006	0.0025	50
40	56500.5244	0.0010	0.0001	48

*BJD−2400000.
†Against max = 2456496.4480 + 0.101908 E.
‡Number of points used to determine the maximum.

3.57 MASTER OT J212624.16+253827.2

This object (hereafter MASTER J212624) was discovered by the MASTER network (Denisenko et al. 2013a) on 2013 June 6 at an unfiltered CCD magnitude of 14.1. The object underwent an even brighter (13.8 mag) outburst in 2012 December. The SU UMa-type nature was suggested by the large outburst amplitude. Subsequent observations confirmed the presence of superhumps (vsnet-alert 15813, 15821, 15829, 15842; figure 63). The times of superhump maxima are listed in table 54. The observation recorded mostly stage B superhumps with a large positive $P_{\rm dot}$ of $+29(4) \times 10^{-5}$. It was likely that only the latter part of the superoutburst was recorded; this is

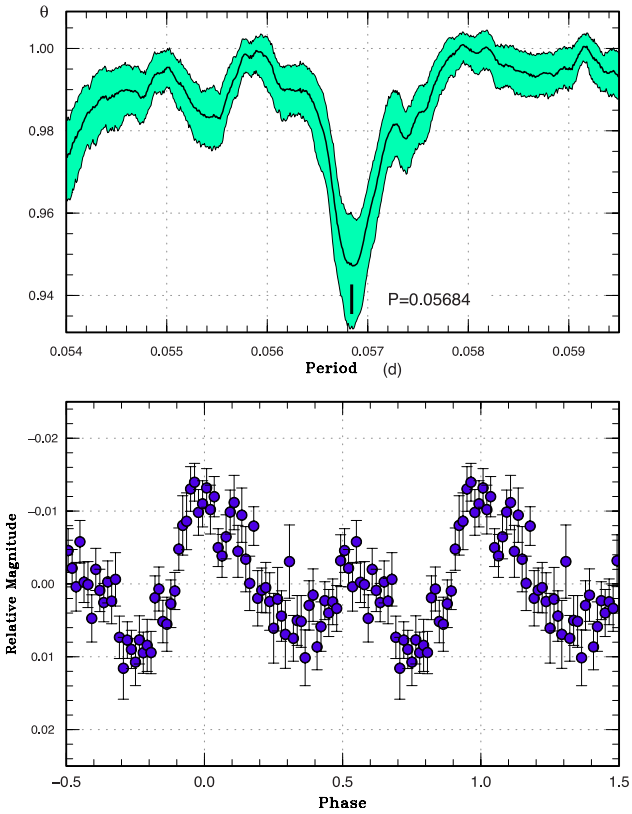

Fig. 60. Early superhumps in MASTER J181953 (2013). Upper: PDM analysis. Lower: Phase-averaged profile.

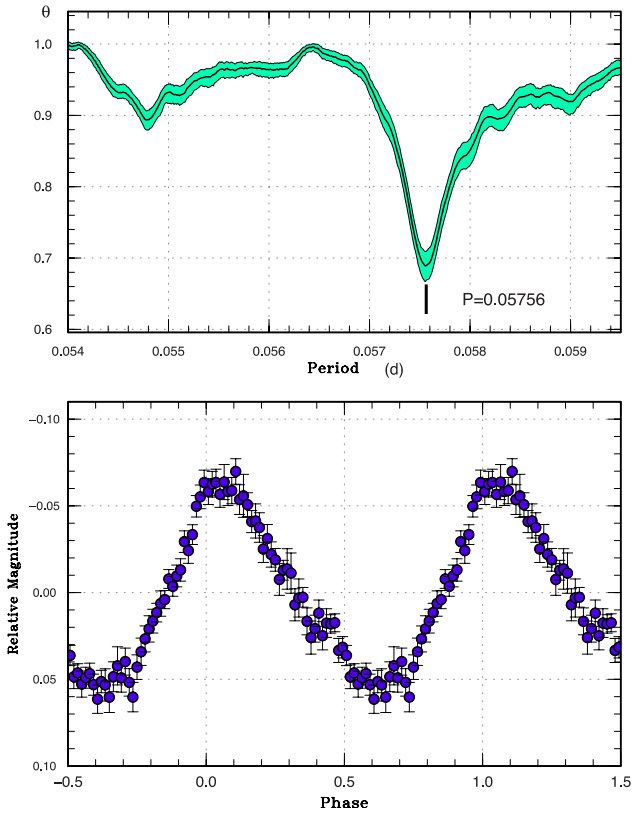

Fig. 61. Ordinary superhumps in MASTER J181953 (2013). Upper: PDM analysis. Lower: Phase-averaged profile.

Table 53. Superhump maxima of MASTER J181953 (2013).

E	Max*	Error	$O-C^{\dagger}$	$N^{\ddagger}$
0	56484.0826	0.0008	−0.0127	167
1	56484.1405	0.0012	−0.0123	199
2	56484.1979	0.0014	−0.0125	86
16	56485.0141	0.0005	−0.0019	115
17	56485.0735	0.0004	−0.0001	165
18	56485.1317	0.0003	0.0006	275
19	56485.1919	0.0004	0.0032	183
20	56485.2482	0.0011	0.0020	92
21	56485.3084	0.0012	0.0046	49
23	56485.4234	0.0006	0.0045	64
24	56485.4811	0.0005	0.0047	64
25	56485.5381	0.0004	0.0041	64
26	56485.5942	0.0011	0.0027	38
35	56486.1156	0.0005	0.0062	122
39	56486.3429	0.0006	0.0032	61
40	56486.4000	0.0005	0.0027	62
41	56486.4566	0.0005	0.0019	58
42	56486.5137	0.0005	0.0014	61
43	56486.5723	0.0012	0.0024	55
54	56487.2013	0.0004	−0.0016	81
55	56487.2606	0.0008	0.0001	65
56	56487.3202	0.0008	0.0022	63
57	56487.3761	0.0012	0.0005	50
58	56487.4334	0.0006	0.0003	50
59	56487.4920	0.0005	0.0013	61
60	56487.5459	0.0009	−0.0023	54
61	56487.6081	0.0022	0.0024	30
73	56488.2968	0.0007	0.0005	54
74	56488.3532	0.0009	−0.0007	67
91	56489.3331	0.0013	0.0009	63
104	56490.0774	0.0008	−0.0029	64
105	56490.1351	0.0005	−0.0028	65
106	56490.1954	0.0008	−0.0001	26
139	56492.0963	0.0007	0.0017	58
140	56492.1492	0.0010	−0.0029	53
141	56492.2098	0.0017	0.0001	28
156	56493.0742	0.0012	0.0013	53
157	56493.1267	0.0019	−0.0037	55
173	56494.0552	0.0011	0.0039	60
174	56494.1142	0.0015	0.0054	35
191	56495.0978	0.0023	0.0107	42
209	56496.1039	0.0047	−0.0191	38

*BJD−2400000.
†Against max = 2456484.0953 + 0.057549 E.
‡Number of points used to determine the maximum.

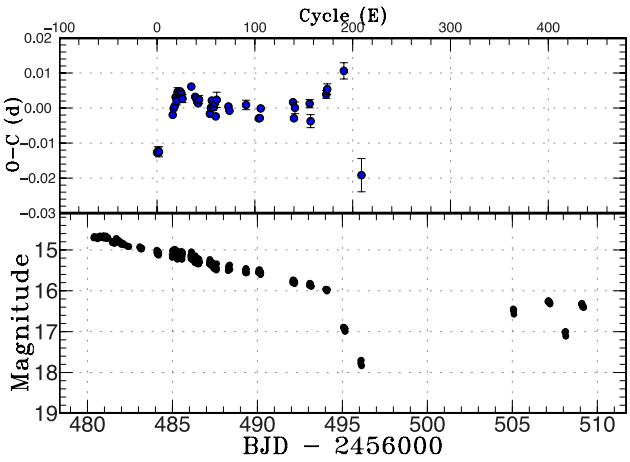

Fig. 62. $O-C$ diagram of superhumps in MASTER J181953 (2013). Upper: $O-C$ diagram. A period of 0.057549 d was used to draw this figure. Lower: Light curve. The observations were binned to 0.012 d.

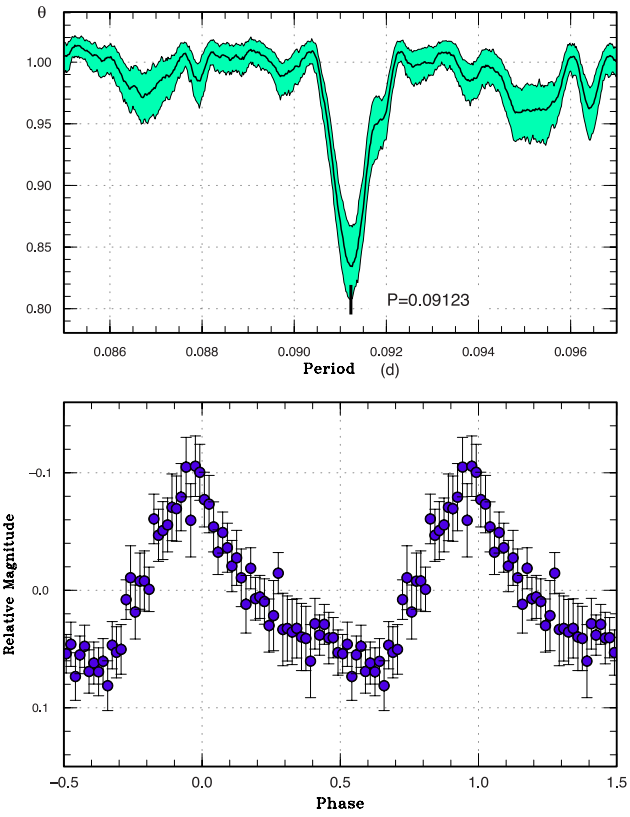

Fig. 63. Superhumps in MASTER J212624 (2013). Upper: PDM analysis. Lower: Phase-averaged profile.

consistent with the fainter recorded maximum than that in 2012 December. Such a large positive $P_{\rm dot}$ is rather unusual for such a long-$P_{\rm SH}$ object. There have been a small number of similar objects (GX Cas: Kato et al. 2012a; OT J145921.8+354806: Kato et al. 2013a) showing a large positive $P_{\rm dot}$.

3.58 OT J112619.4+084651

This is a dwarf nova discovered by CRTS (= CSS 130106:112619+084651, hereafter OT J112619) on 2013 January 6 at a magnitude of 14.8. There was no past outburst in the CRTS data. The quiescent counterpart is very faint ($g = 21.8$), and the outburst amplitude immediately suggested a WZ Sge-type dwarf nova (vsnet-alert

Table 54. Superhump maxima of MASTER J212624 (2013).

E	Max*	Error	$O-C^{\dagger}$	$N^{\ddagger}$
0	56451.5930	0.0008	0.0018	75
9	56452.4186	0.0004	0.0054	64
10	56452.5092	0.0006	0.0047	65
20	56453.4195	0.0006	0.0016	64
21	56453.5100	0.0005	0.0008	54
31	56454.4169	0.0076	−0.0056	24
32	56454.5099	0.0007	−0.0040	55
42	56455.4222	0.0005	−0.0051	65
43	56455.5109	0.0006	−0.0077	48
53	56456.4268	0.0007	−0.0051	95
54	56456.5232	0.0010	−0.0001	108
64	56457.4418	0.0011	0.0052	134
65	56457.5297	0.0012	0.0018	45
75	56458.4332	0.0017	−0.0081	90
76	56458.5422	0.0020	0.0095	51
86	56459.4508	0.0019	0.0048	44

*BJD−2400000.
†Against max = 2456451.5911 + 0.091335 E.
‡Number of points used to determine the maximum.

15246). Early observations detected double-wave early superhumps (vsnet-alert 15249, 15252, 15264; figure 64). The object started to show ordinary superhumps on January 12 (figure 65). The times of superhump maxima are listed in table 55. The $O-C$ diagram very clearly shows stage A ($E \leq 43$) and stage B ($55 \leq E \leq 260$) superhumps (figure 66). The value of ε^* for stage A superhumps was 0.0317(6), which corresponds to $q = 0.086(2)$.

3.59 OT J191443.6+605214

The 2008 superoutburst of this object, which was discovered by K. Itagaki (Yamaoka et al. 2008), was studied by Kato et al. (2009a). The 2012 outburst was detected by E. Muyllaert (baavss-alert 2989). Subsequent observations detected superhumps (vsnet-alert 14864, 14873). The times of superhump maxima are listed in table 56. In table 2, we listed a period obtained by the PDM method.

3.60 OT J205146.3−035828

This is a dwarf nova discovered by CRTS (= CSS 121004:205146−035827, hereafter OT J205146) on 2012 October 4 at a magnitude of 14.1. There was no past outburst in the CRTS data. Subsequent observations recorded superhumps (vsnet-alert 14987, 14996; figure 67).

The times of superhump maxima are listed in table 57. Although the scatters were large, especially during the latter stage, stages B and C can be recognized. The pattern of period variation suggests that the object

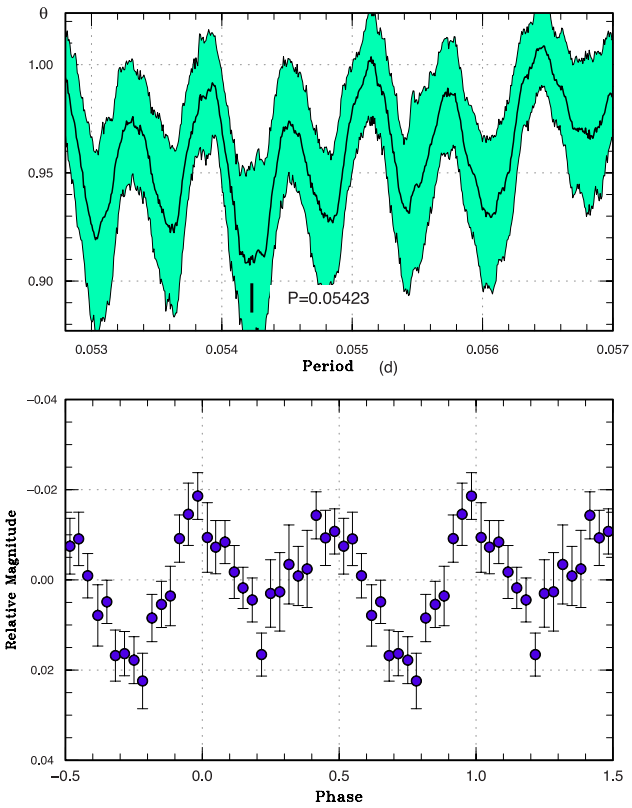

Fig. 64. Early superhumps in OT J112619 (2013). Upper: PDM analysis. Lower: Phase-averaged profile.

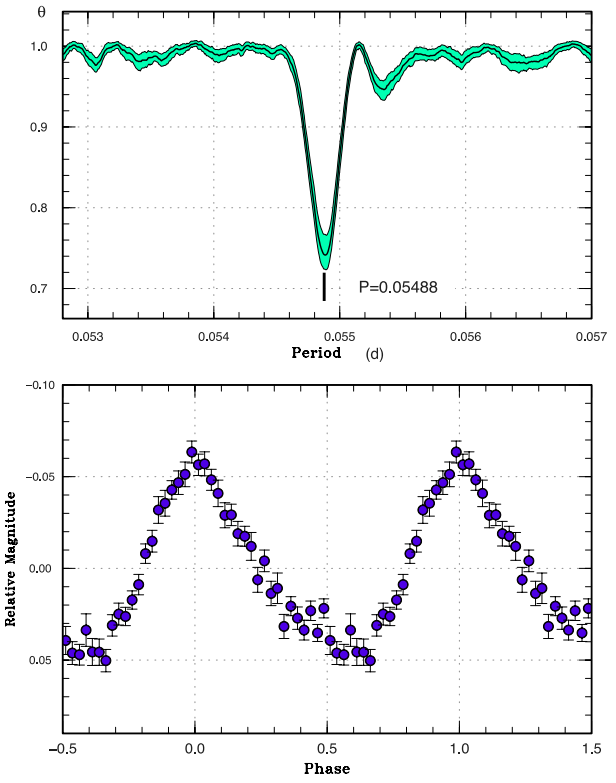

Fig. 65. Superhumps in OT J112619 (2013). Upper: PDM analysis. Lower: Phase-averaged profile.

Table 55. Superhump maxima of OT J112619 (2013).

E	Max*	Error	$O-C^{\dagger}$	$N^{\ddagger}$	E	Max*	Error	$O-C^{\dagger}$	$N^{\ddagger}$
0	56304.5700	0.0015	−0.0402	39	115	56310.9314	0.0004	0.0007	67
1	56304.6261	0.0015	−0.0391	26	116	56310.9873	0.0005	0.0017	75
19	56305.6396	0.0011	−0.0149	59	130	56311.7569	0.0025	0.0019	22
37	56306.6410	0.0016	−0.0028	36	131	56311.8084	0.0011	−0.0016	23
38	56306.7003	0.0007	0.0016	50	132	56311.8631	0.0033	−0.0018	17
39	56306.7566	0.0009	0.0029	59	135	56312.0255	0.0011	−0.0044	40
40	56306.8117	0.0009	0.0030	24	148	56312.7482	0.0031	0.0039	12
41	56306.8682	0.0009	0.0046	25	149	56312.7970	0.0012	−0.0023	43
42	56306.9240	0.0007	0.0054	23	150	56312.8516	0.0008	−0.0026	97
43	56306.9770	0.0007	0.0035	28	151	56312.9041	0.0005	−0.0051	92
55	56307.6463	0.0009	0.0132	35	152	56312.9602	0.0006	−0.0040	103
56	56307.6985	0.0006	0.0105	51	153	56313.0128	0.0018	−0.0063	52
57	56307.7557	0.0006	0.0127	59	168	56313.8380	0.0016	−0.0055	49
58	56307.8083	0.0008	0.0103	25	169	56313.8951	0.0010	−0.0034	57
59	56307.8640	0.0010	0.0111	24	170	56313.9489	0.0008	−0.0045	67
60	56307.9182	0.0009	0.0103	22	171	56314.0050	0.0027	−0.0034	41
61	56307.9720	0.0009	0.0091	25	185	56314.7788	0.0033	0.0009	32
62	56308.0231	0.0037	0.0053	12	186	56314.8319	0.0015	−0.0009	38
76	56308.7949	0.0010	0.0077	71	187	56314.8844	0.0021	−0.0034	30
77	56308.8478	0.0014	0.0056	79	188	56314.9383	0.0019	−0.0044	40
78	56308.9065	0.0010	0.0094	68	189	56314.9958	0.0043	−0.0019	41
79	56308.9577	0.0018	0.0056	30	190	56315.0487	0.0013	−0.0039	11
80	56309.0122	0.0015	0.0052	20	204	56315.8188	0.0009	−0.0033	116
95	56309.8365	0.0005	0.0050	57	205	56315.8731	0.0009	−0.0040	80
96	56309.8900	0.0007	0.0036	38	206	56315.9289	0.0012	−0.0031	86
97	56309.9458	0.0018	0.0045	26	207	56315.9817	0.0006	−0.0052	114
98	56309.9994	0.0014	0.0031	25	259	56318.8525	0.0150	0.0076	25
113	56310.8227	0.0007	0.0019	77	260	56318.9001	0.0119	0.0002	24

*BJD−2400000.
†Against max = 2456304.6103 + 0.054960 E.
‡Number of points used to determine the maximum.

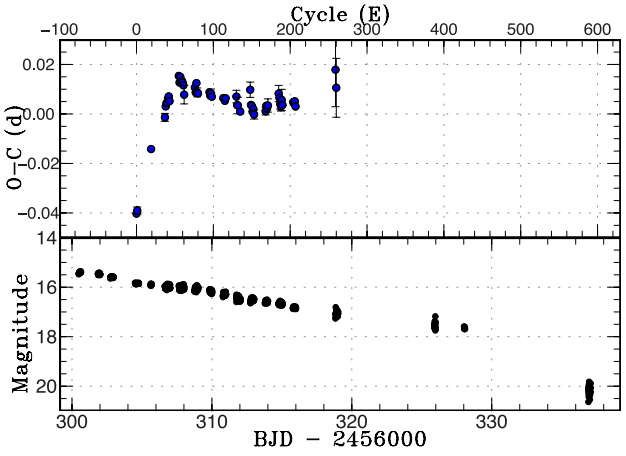

Fig. 66. $O-C$ diagram of superhumps in OT J112619 (2013). Upper: $O-C$ diagram. A period of 0.05492 d was used to draw this figure. Lower: Light curve. The observations were binned to 0.0055 d.

resembles ordinary SU UMa-type dwarf novae rather than extreme WZ Sge-type dwarf novae. The data at $E = 250$ were excluded when we determined the period of stage C superhumps in table 2.

3.61 OT J220641.1+301436

This object was detected by CRTS (= CSS 110921:220641+301436, hereafter OT J220641) on 2011 September 21. A new outburst was detected by the MASTER network (vsnet-alert 15029). The object has a faint ($g = 23.2$) SDSS counterpart and the amplitude suggested a superoutburst (vsnet-alert 15033). Subsequent observations detected superhumps (vsnet-alert 15036, 15038; figure 68). The times of superhump maxima are listed in table 58. The superhump period in table 2 was determined by the PDM method.

3.62 OT J232727.2+085539

This object (= PNV J23272715+0855391, hereafter OT J232727) was discovered by K. Itagaki at a magnitude of 13.9 on 2012 September 13.568 UT (Itagaki et al. 2012).[11] Although the object was initially reported as a

[11] See also ⟨http://www.cbat.eps.harvard.edu/unconf/followups/J23272715+0855391.html⟩.

Table 56. Superhump maxima of OT J191443 (2012).

E	Max*	Error	$O-C^{\dagger}$	$N^{\ddagger}$
0	56159.3779	0.0003	−0.0003	44
1	56159.4498	0.0002	0.0003	75
13	56160.3042	0.0004	−0.0000	70

*BJD−2400000.
†Against max = 2456159.3782 + 0.071234 E.
‡Number of points used to determine the maximum.

possible nova, the presence of a blue quiescent counterpart in SDSS and a UV object in the GALEX catalog already suggested a WZ Sge-type dwarf nova (vsnet-alert 14921). Shortly after the discovery announcement, some indication of short-period variation was reported (vsnet-alert 14925). Although the period was difficult of determination due to the small amplitude and large airmass degrading the quality of photometry, a very short $P_{\rm orb}$ was already inferred (vsnet-alert 14931, 14937). The object started to show ordinary superhumps (vsnet-alert 14938, 14939, 14948, 14952; figure 69). Since the comparison star was much redder than the variable and some observations were done at high airmasses, we corrected observations by using a second-order atmospheric extinction whose coefficients were experimentally determined. The period of

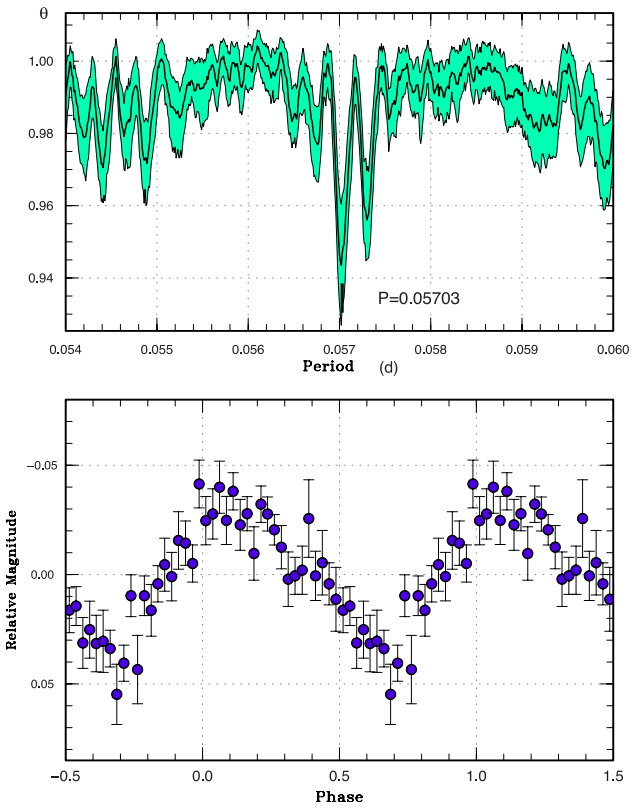

Fig. 67. Superhumps in OT J205146 (2012). Upper: PDM analysis. Lower: Phase-averaged profile.

Table 57. Superhump maxima of OT J205146.

E	Max*	Error	$O-C^{\dagger}$	$N^{\ddagger}$
0	56207.9950	0.0005	−0.0048	116
1	56208.0512	0.0006	−0.0057	88
22	56209.2503	0.0003	−0.0041	92
23	56209.3068	0.0003	−0.0046	95
24	56209.3661	0.0009	−0.0024	61
57	56211.2476	0.0028	−0.0028	16
58	56211.3102	0.0009	0.0028	27
59	56211.3636	0.0022	−0.0009	28
88	56213.0293	0.0025	0.0110	117
92	56213.2612	0.0008	0.0149	61
93	56213.3205	0.0011	0.0171	38
126	56215.1870	0.0035	0.0017	36
127	56215.2440	0.0029	0.0017	51
139	56215.9418	0.0038	0.0151	114
162	56217.2272	0.0014	−0.0112	28
163	56217.2814	0.0020	−0.0140	28
180	56218.2549	0.0013	−0.0099	43
215	56220.2514	0.0020	−0.0094	43
216	56220.3066	0.0022	−0.0112	44
250	56222.2734	0.0030	0.0166	10

*BJD−2400000.
†Against max = 2456207.9998 + 0.057028 E.
‡Number of points used to determine the maximum.

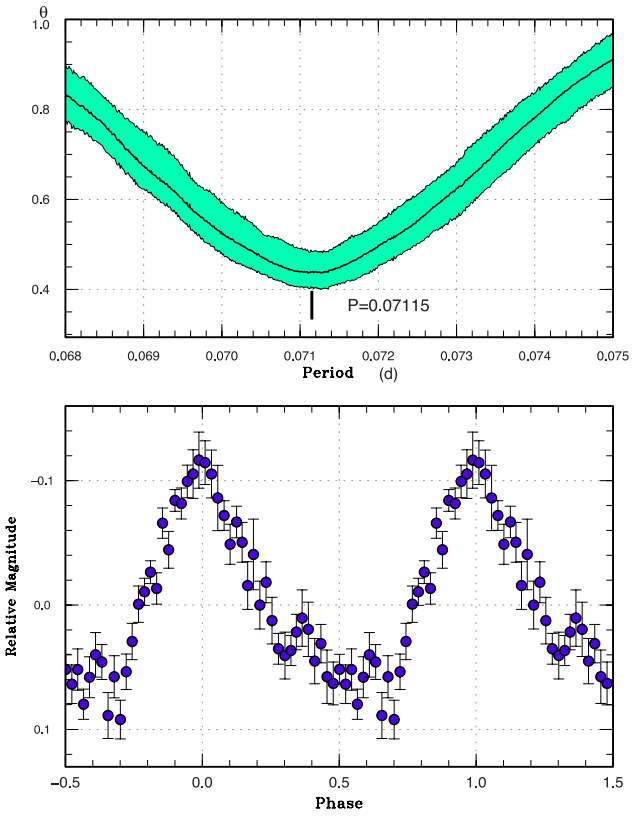

Fig. 68. Superhumps in OT J220641 (2012). Upper: PDM analysis. Lower: Phase-averaged profile.

early superhumps up to BJD 2456188.5 was 0.05277(2) d (figure 70), which is almost the same value as the expected $P_{\rm orb}$ of V1265 Tau (Shafter et al. 2007), a record holder in the shortest $P_{\rm orb}$ of (hydrogen-rich, ordinary) SU UMa-type dwarf novae.

The times of superhump maxima are listed in table 59. Stages A and B were very clearly detected. The $P_{\rm dot}$ for stage B superhumps was small [$+4.0(1.1) \times 10^{-5}$], which is usual for a very short-$P_{\rm orb}$ object. The period of stage A superhumps was measured when the superhump was growing ($E \leq 29$). The resultant value of $\varepsilon^* = 0.0303(5)$ corresponds to $q = 0.082(2)$. For an averaged white dwarf mass of $0.75\,M_\odot$ (Littlefair et al. 2008; Savoury et al. 2011), the secondary has a mass of $0.06\,M_\odot$. The object is located at the exact position of the period minimum expected by the experimentally modified model of Knigge (2006).

No post-superoutburst rebrightening was reported, although it may have been missed since the object became more difficult to observe in the latter season of this year.

Table 58. Superhump maxima of OT J220641 (2012).

E	Max*	Error	$O-C$†	N‡
0	56223.2038	0.0007	0.0003	47
1	56223.2730	0.0009	−0.0015	45
6	56223.6321	0.0005	0.0028	69
7	56223.7020	0.0007	0.0017	68
8	56223.7686	0.0009	−0.0026	68
9	56223.8415	0.0028	−0.0007	35

*BJD−2400000.
†Against max = 2456223.2035 + 0.070966 E.
‡Number of points used to determine the maximum.

3.63 PNV J06270375+3952504

This object (hereafter PNV J062703) is a transient initially reported as a possible nova by S. Kaneko.[12] This object was detected in outburst on 2013 April 3.445 UT at an unfiltered CCD magnitude of 12.0. According to the observation of the MASTER network, the object was not in outburst on March 31 (figure 71). There is a 20 mag star in the USNO catalog, and the object was likely thought to be a WZ Sge-type dwarf nova. Subsequent observations detected double-wave early superhumps [vsnet-alert 15581, 15592, 15594, 15607; figure 72, period 0.05787(2) d], qualifying the WZ Sge-type classification. On April 8, the object started to show ordinary superhumps (vsnet-alert 15599)

[12] (http://www.cbat.eps.harvard.edu/unconf/followups/J06270375+3952504.html).

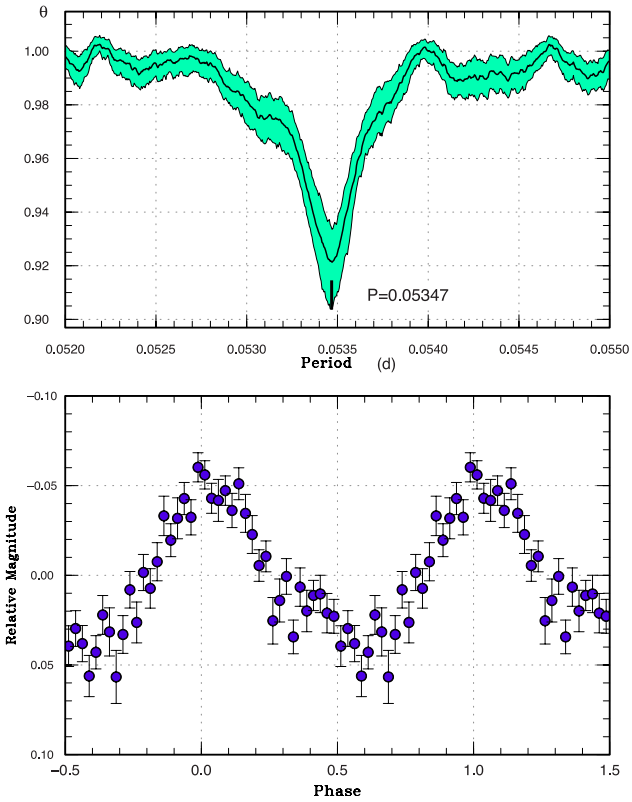

Fig. 69. Superhumps in OT J232727 (2012). Upper: PDM analysis. Lower: Phase-averaged profile.

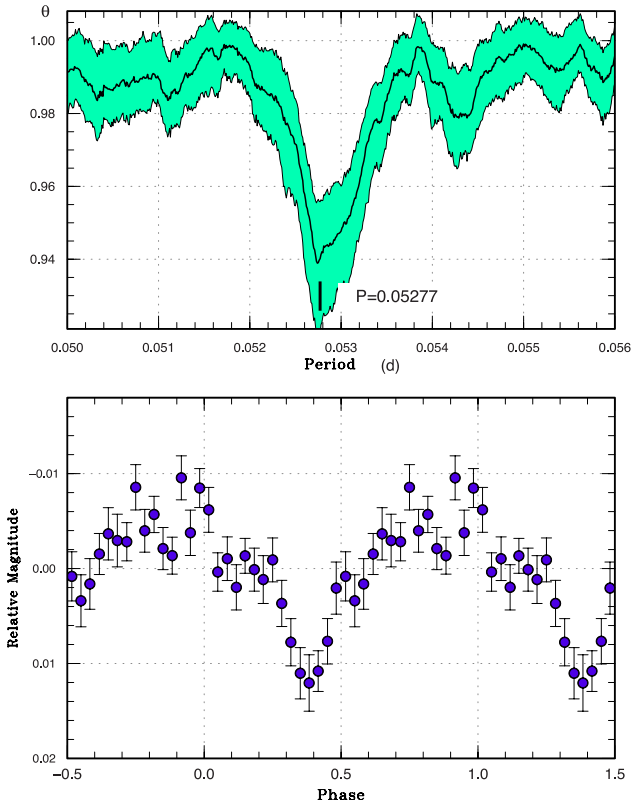

Fig. 70. Early superhumps in OT J232727 (2012). Upper: PDM analysis. Lower: Phase-averaged profile.

Table 59. Superhump maxima of OT J232727 (2012).

E	Max*	Error	$O-C^{\dagger}$	$N^{\ddagger}$
0	56192.5540	0.0013	−0.0263	20
15	56193.3710	0.0007	−0.0114	104
16	56193.4258	0.0006	−0.0101	103
28	56194.0773	0.0003	−0.0002	57
29	56194.1329	0.0003	0.0019	48
32	56194.2960	0.0006	0.0045	49
33	56194.3484	0.0003	0.0035	54
34	56194.4023	0.0003	0.0039	54
35	56194.4537	0.0016	0.0018	23
37	56194.5644	0.0009	0.0055	29
40	56194.7256	0.0004	0.0063	92
41	56194.7794	0.0008	0.0066	89
65	56196.0635	0.0027	0.0075	68
66	56196.1137	0.0012	0.0042	109
67	56196.1649	0.0014	0.0019	106
68	56196.2208	0.0020	0.0043	83
72	56196.4341	0.0011	0.0037	26
73	56196.4917	0.0024	0.0079	27
74	56196.5408	0.0019	0.0035	29
85	56197.1257	0.0011	0.0001	110
87	56197.2339	0.0028	0.0014	19
88	56197.2833	0.0008	−0.0026	41
89	56197.3410	0.0005	0.0015	111
90	56197.3943	0.0005	0.0014	89
91	56197.4454	0.0005	−0.0009	84
92	56197.4990	0.0003	−0.0009	60
103	56198.0931	0.0023	0.0050	90
104	56198.1377	0.0036	−0.0038	111
105	56198.1929	0.0018	−0.0021	101
108	56198.3532	0.0042	−0.0023	30
182	56202.3055	0.0137	−0.0069	21
183	56202.3641	0.0007	−0.0018	48
184	56202.4190	0.0012	−0.0004	44
185	56202.4756	0.0014	0.0028	46
186	56202.5192	0.0017	−0.0071	46
187	56202.5740	0.0010	−0.0058	46
201	56203.3306	0.0013	0.0023	40
202	56203.3806	0.0018	−0.0013	42
216	56204.1326	0.0046	0.0021	93
217	56204.1842	0.0040	0.0003	51

*BJD−2400000.

†Against max = 2456192.5803 + 0.053473 E.

‡Number of points used to determine the maximum.

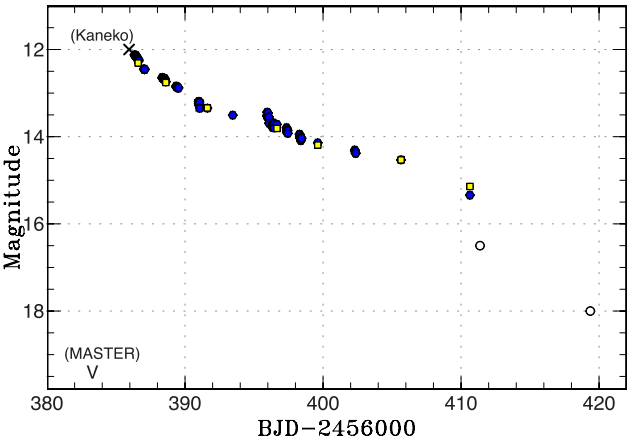

Fig. 71. Light curve of PNV J062703 (2013). Filled circles, filled squares, and open circles represent our CCD observations (binned to 0.02 d), AAVSO *R*-band observations, and unfiltered snapshot photometry by E. Morillon, respectively. The cross represents the discovery observation and the "V" sign represents the upper limit of MASTER.

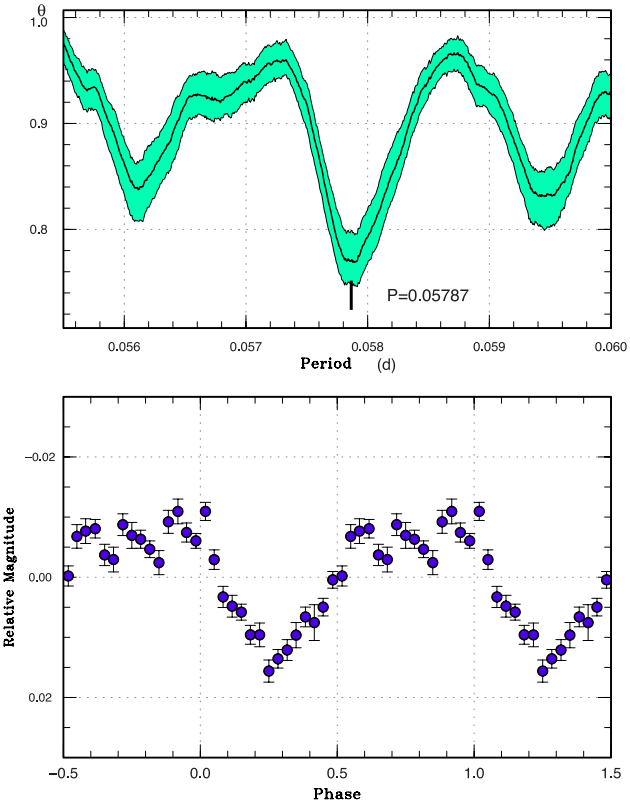

Fig. 72. Early superhumps in PNV J062703 (2013). Upper: PDM analysis. Lower: Phase-averaged profile.

and they later evolved (vsnet-alert 15609, 15616; figure 73). The times of superhump maxima are listed in table 60. Although the observations on April 8 likely detected stage A superhumps, we could not convincingly measure the times of maxima, and they are not listed in the table.

Considering the nondetection by MASTER, the duration of early superhumps was less than 8 d, which is shorter than those in well-observed WZ Sge-type dwarf novae. The object apparently started to rapidly fade 25 d after the discovery (figure 71). The late phase of the outburst was not well observed due to the proximity to the Sun.

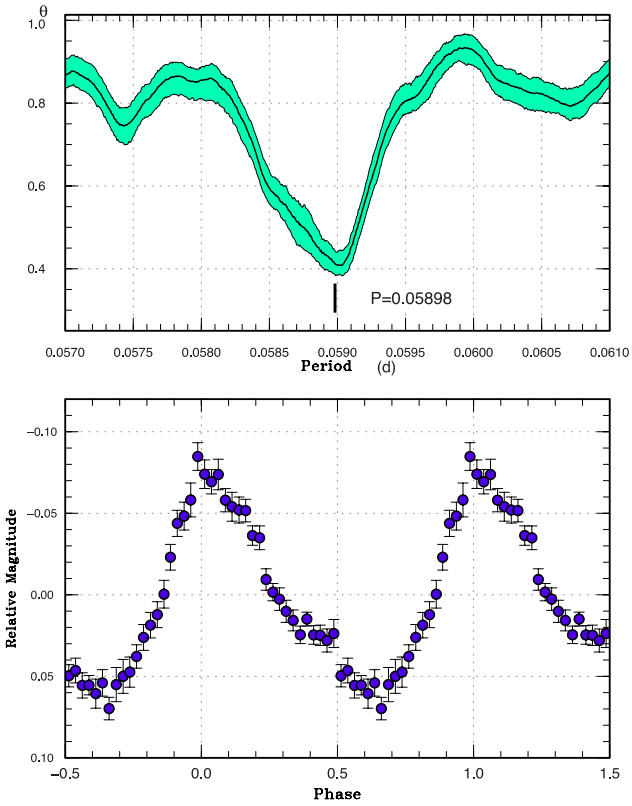

Fig. 73. Ordinary superhumps in PNV J062703 (2013). The data after BJD 2456394 were used in the analysis. Upper: PDM analysis. Lower: Phase-averaged profile.

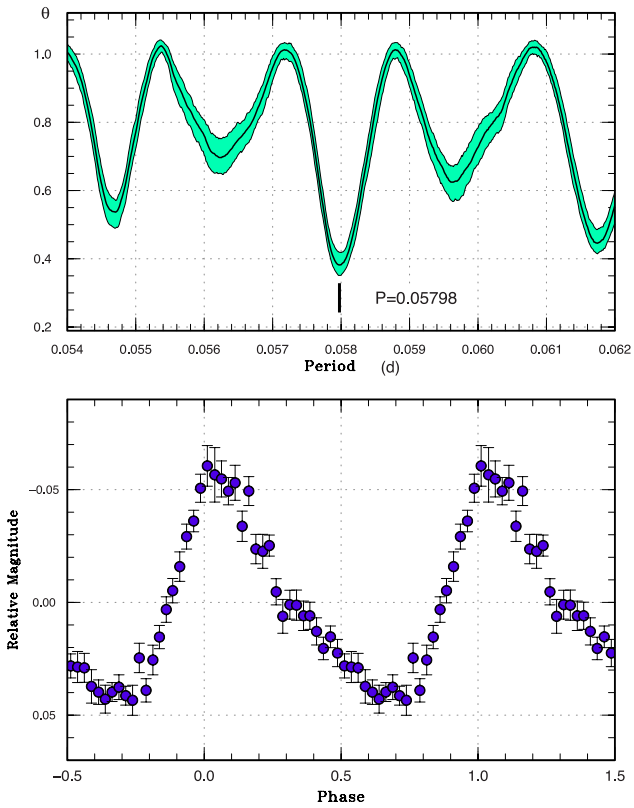

Fig. 74. Superhumps in SDSS J075107 (2013). Upper: PDM analysis. Lower: Phase-averaged profile.

Table 60. Superhump maxima of PNV J062703 (2013).

E	Max*	Error	$O-C^{\dagger}$	$N^{\ddagger}$
0	56395.9469	0.0003	0.0030	97
1	56396.0050	0.0003	0.0021	97
2	56396.0630	0.0004	0.0010	98
7	56396.3582	0.0004	0.0012	67
8	56396.4165	0.0003	0.0004	73
24	56397.3561	0.0009	−0.0045	48
25	56397.4190	0.0007	−0.0006	73
40	56398.3043	0.0005	−0.0007	49
41	56398.3611	0.0003	−0.0028	59
42	56398.4205	0.0010	−0.0025	38
108	56402.3220	0.0016	0.0033	56

*BJD−2400000.
†Against max = 2456395.9439 + 0.059026 E.
‡Number of points used to determine the maximum.

Table 61. Superhump maxima of SDSS J075107 (2013).

E	Max*	Error	$O-C^{\dagger}$	$N^{\ddagger}$
0	56338.4881	0.0035	−0.0009	29
1	56338.5471	0.0005	0.0001	63
2	56338.6055	0.0005	0.0005	58
32	56340.3460	0.0069	0.0016	27
33	56340.4017	0.0008	−0.0006	60
34	56340.4606	0.0005	0.0003	50
35	56340.5174	0.0007	−0.0008	53
36	56340.5765	0.0008	0.0002	56
50	56341.3887	0.0008	0.0007	59
51	56341.4448	0.0014	−0.0011	33

*BJD−2400000.
†Against max = 2456338.4890 + 0.057980 E.
‡Number of points used to determine the maximum.

3.64 SDSS J075107.50+300628.4

This object (hereafter SDSS J075107) was selected as a dwarf nova by Wils et al. (2010). The SDSS colors suggested an orbital period of 0.067 d (Kato et al. 2012b). E. Muyllaert detected an outburst on 2013 February 12 (cvnet-outburst 5248). Subsequent observations detected superhumps (vsnet-alert 15395, 15408; figure 74). The times of superhump maxima are listed in table 61. It is not known whether stage B or stage C was recorded.

3.65 SDSS J080033.86+192416.5

This object (hereafter SDSS J080033) is a dwarf nova identified by Wils et al. (2010). The SDSS color suggested an

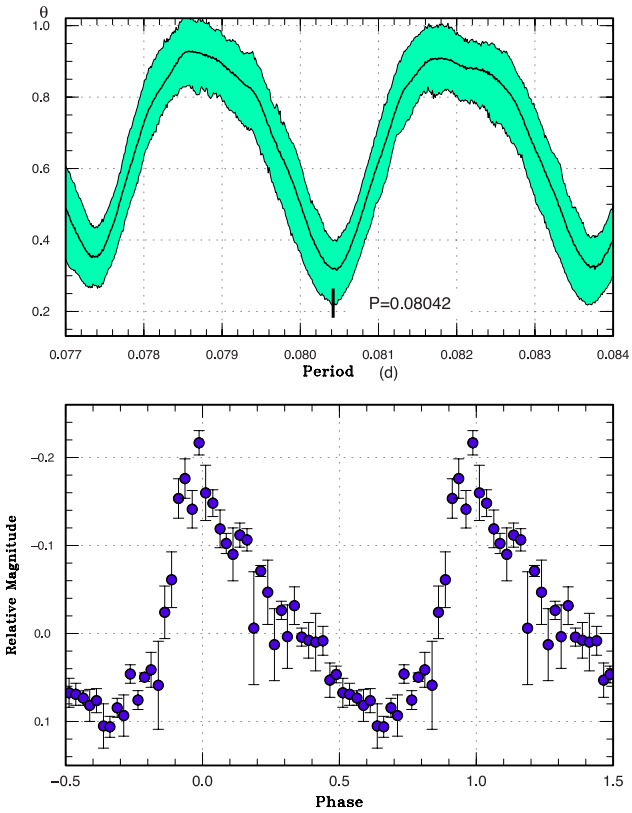

Fig. 75. Superhumps in SDSS J080033 (2012). Upper: PDM analysis. Lower: Phase-averaged profile.

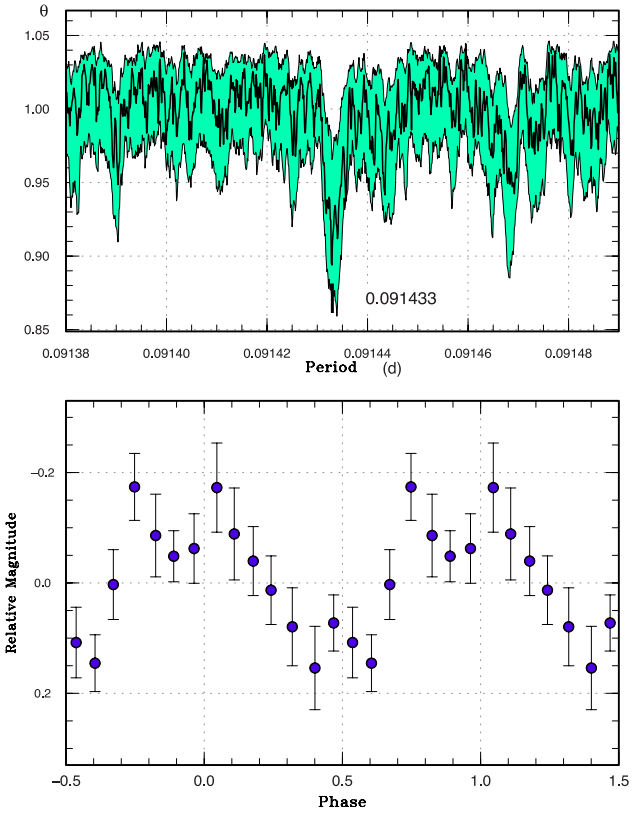

Fig. 76. Orbital modulation in SDSS J162520 in quiescence. Upper: PDM analysis. Lower: Phase-averaged profile.

Table 62. Superhump maxima of SDSS J080033 (2012).

E	Max*	Error	$O-C^{\dagger}$	$N^{\ddagger}$
0	56221.5897	0.0004	−0.0026	84
1	56221.6756	0.0018	0.0028	21
25	56223.6045	0.0019	−0.0005	43
26	56223.6858	0.0044	0.0004	17

*BJD−2400000.
†Against max = 2456221.5923 + 0.080507 E.
‡Number of points used to determine the maximum.

orbital period of 0.065–0.074 d (Kato et al. 2012b). The MASTER network detected a bright outburst on 2012 October 19 (vsnet-alert 15021). Subsequent observations detected superhumps (vsnet-alert 15028, 15040; figure 75). SDSS J080033 is a long-$P_{\rm SH}$ object with a large superhump amplitude. The times of superhump maxima are listed in table 62. The superhump period in table 2 was determined by the PDM method.

According to the CRTS data, the object showed very frequent outbursts and the duty cycle of the outburst (magnitude brighter than 17.5) was 0.23. The object must be a long-$P_{\rm orb}$, active SU UMa-type dwarf nova like YZ Cnc.

3.66 SDSS J162520.29+120308.7

This object (hereafter SDSS J162520) in the period gap was studied in Kato et al. (2009a) and Olech et al. (2011). Although we do not have new data, we discuss this object again since we have been able to identify the orbital period in the CRTS data. The resultant orbital period was 0.091433(1) d (figure 76). This value is slightly (by 2σ) longer than the 0.09111(15) d obtained by radial velocity study (Olech et al. 2011). We consider that this period is highly plausible because any candidate period within the error of Olech et al. (2011) did not yield a smooth orbital light curve (in figure 76, only a small segment of the period search is shown because the signal is very narrow due to the long baseline of the CRTS data). The ε^* for stage A superhumps (Kato et al. 2010) amounts to 7.2(2)%. The q estimated by using the relation in Kato and Osaki (2013b) is 0.23(1). This object showed a post-superoutburst rebrightening (Kato et al. 2010; Olech et al. 2011), rather unusual for a long-$P_{\rm orb}$ object. We could detect superhumps in the faint state between the main superoutburst and the rebrightening. The period was 0.09579(5) d, corresponding to $\varepsilon^* = 4.54(5)\%$. Using the relation in Kato and Osaki (2013b) and Kato et al. (2013b), this precession rate can be translated to a disk radius of 0.36(1)A, since the pressure

Table 63. Superhump maxima of SSS J122221 (2013).

E	Max*	Error	$O-C^{\dagger}$	$N^{\ddagger}$	E	Max*	Error	$O-C^{\dagger}$	$N^{\ddagger}$
0	56304.7444	0.0026	−0.0639	17	270	56325.5272	0.0005	0.0153	329
1	56304.8131	0.0019	−0.0718	26	271	56325.6027	0.0004	0.0141	286
7	56305.2810	0.0006	−0.0641	124	272	56325.6836	0.0014	0.0184	15
13	56305.7377	0.0020	−0.0674	19	273	56325.7548	0.0014	0.0129	69
27	56306.8266	0.0018	−0.0521	28	274	56325.8328	0.0007	0.0142	76
33	56307.2834	0.0007	−0.0553	136	278	56326.1472	0.0040	0.0218	54
39	56307.7508	0.0019	−0.0480	23	279	56326.2158	0.0017	0.0138	96
40	56307.8341	0.0015	−0.0414	33	286	56326.7450	0.0010	0.0062	29
53	56308.8362	0.0012	−0.0362	38	287	56326.8277	0.0015	0.0123	32
58	56309.2329	0.0019	−0.0228	133	288	56326.9011	0.0046	0.0089	9
59	56309.2946	0.0023	−0.0378	110	298	56327.6675	0.0030	0.0085	10
79	56310.8469	0.0013	−0.0191	42	299	56327.7395	0.0010	0.0038	23
136	56315.2502	0.0010	0.0134	107	300	56327.8174	0.0008	0.0051	30
152	56316.4853	0.0005	0.0216	207	306	56328.2771	0.0024	0.0047	63
156	56316.7909	0.0018	0.0205	30	321	56329.4335	0.0005	0.0109	224
157	56316.8619	0.0006	0.0149	31	322	56329.5036	0.0006	0.0044	329
161	56317.1689	0.0095	0.0151	94	323	56329.5744	0.0004	−0.0016	329
162	56317.2512	0.0016	0.0207	136	333	56330.3544	0.0011	0.0116	219
165	56317.4788	0.0003	0.0183	269	334	56330.4201	0.0004	0.0006	325
166	56317.5448	0.0006	0.0076	108	335	56330.4974	0.0003	0.0013	329
168	56317.7064	0.0015	0.0159	21	336	56330.5701	0.0004	−0.0027	293
169	56317.7778	0.0010	0.0105	44	347	56331.4130	0.0004	−0.0032	329
170	56317.8654	0.0011	0.0215	34	348	56331.4921	0.0003	−0.0009	329
174	56318.1698	0.0036	0.0192	101	349	56331.5633	0.0003	−0.0063	329
175	56318.2541	0.0029	0.0268	132	360	56332.4074	0.0007	−0.0057	328
181	56318.7087	0.0021	0.0214	20	361	56332.4874	0.0004	−0.0024	328
182	56318.7815	0.0020	0.0175	45	362	56332.5593	0.0004	−0.0072	324
183	56318.8606	0.0010	0.0199	37	416	56336.6777	0.0014	−0.0295	28
187	56319.1724	0.0013	0.0250	116	417	56336.7533	0.0015	−0.0305	28
188	56319.2395	0.0013	0.0154	132	418	56336.8308	0.0015	−0.0298	26
190	56319.4006	0.0037	0.0231	92	442	56338.6806	0.0031	−0.0203	26
191	56319.4762	0.0004	0.0220	329	443	56338.7549	0.0011	−0.0226	26
192	56319.5529	0.0005	0.0220	329	455	56339.6873	0.0016	−0.0104	25
194	56319.7122	0.0058	0.0280	19	456	56339.7563	0.0022	−0.0181	25
195	56319.7794	0.0018	0.0184	17	457	56339.8489	0.0009	−0.0022	27
203	56320.4049	0.0004	0.0306	232	468	56340.6872	0.0012	−0.0074	26
204	56320.4761	0.0004	0.0251	330	469	56340.7597	0.0021	−0.0115	25
205	56320.5504	0.0004	0.0227	329	470	56340.8351	0.0008	−0.0128	27
213	56321.1655	0.0013	0.0243	89	483	56341.8333	0.0020	−0.0114	26
214	56321.2345	0.0011	0.0167	137	484	56341.9082	0.0019	−0.0133	7
216	56321.3938	0.0062	0.0226	112	494	56342.6694	0.0010	−0.0188	23
217	56321.4715	0.0004	0.0237	328	496	56342.8266	0.0015	−0.0150	28
218	56321.5476	0.0003	0.0231	329	507	56343.6651	0.0022	−0.0200	26
219	56321.6261	0.0007	0.0249	204	508	56343.7494	0.0043	−0.0123	25
240	56323.2273	0.0006	0.0158	126	509	56343.8154	0.0012	−0.0230	27
246	56323.6925	0.0011	0.0209	16	510	56343.9100	0.0140	−0.0051	11
247	56323.7681	0.0026	0.0198	40	520	56344.6745	0.0018	−0.0075	25
248	56323.8379	0.0011	0.0129	36	521	56344.7422	0.0030	−0.0164	25
252	56324.1601	0.0025	0.0284	81	522	56344.8264	0.0085	−0.0089	14
253	56324.2285	0.0008	0.0201	136	523	56344.9001	0.0058	−0.0119	18
256	56324.4544	0.0004	0.0160	328	535	56345.8158	0.0027	−0.0164	28
257	56324.5283	0.0003	0.0132	329	536	56345.8957	0.0043	−0.0131	21
258	56324.6079	0.0012	0.0161	252	549	56346.8933	0.0017	−0.0123	24
269	56325.4505	0.0003	0.0153	319	562	56347.8933	0.0035	−0.0092	23

*BJD−2400000.

†Against max = 2456304.8083 + 0.076680 E.

‡Number of points used to determine the maximum.

effect can be ignored in a cold disk (Osaki & Kato 2013b; Kato & Osaki 2013b). This value is a usual one for the post-superoutburst disk (Kato & Osaki 2013b).

Although Olech et al. (2011) considered the double-wave hump signal during the early stage of the outburst as early superhumps, we consider this unlikely because ordinary superhumps in the growing stage are known to sometimes appear doubly humped, and the object was quickly fading (0.37 mag d^{-1}), which is apparently characteristic of precursor outbursts and not of the early superhump stage. A growing superhump signal during the fading branch of precursor is also very commonly seen (Osaki & Kato 2013a, 2013b). The short period detected by Olech et al. (2011) was probably due to a large error in period analysis for a very short (0.22 d) segment. We therefore see no reason why early superhumps should be present in this object, and the claim by Olech et al. (2011) regarding the origin of the early superhumps is not justified.

3.67 SSS J122221.7−311523

The times of superhump maxima of SSS J122221.7−311523 (hereafter SSS J122221) used in Kato et al. (2013b) are listed in table 63. The mean profile of stage A superhumps is also given in figure 77.

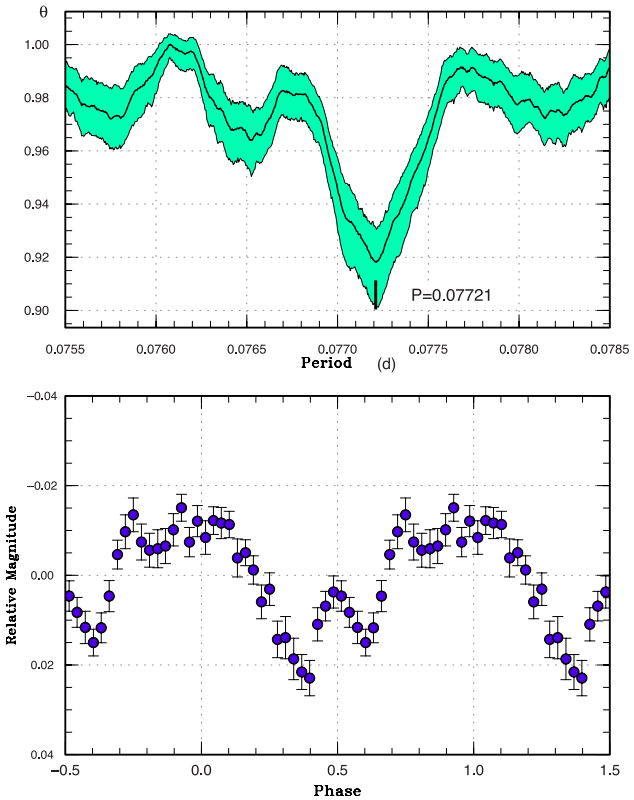

Fig. 77. Stage A superhumps in SSS J122221. Upper: PDM analysis. Lower: Phase-averaged profile.

3.68 SSS J224739.7−362253

SSS J224739.7−362253 is a dwarf nova discovered by CRTS SSS (= SSS 120724:224740−362254, hereafter SSS J224739) on 2012 July 24 at a magnitude of 14.2. The CRTS data indicated that the object underwent a brighter (11.0 mag) outburst in 2006 July (vsnet-alert 14791; figure 78). Subsequent observations recorded large-amplitude variations with a scale of days, and short-term (∼0.06 d) variations resembling superhumps (vsnet-alert 14797, 14804, 14805, 14808). Later it became apparent that these variations were the post-superoutburst repetitive rebrightening phase of a WZ Sge-type dwarf nova (vsnet-alert 14821; figure 79). The case is similar to EL UMa (Kato et al. 2010), for which only the multiple rebrightening phase was recorded. The amplitudes of these rebrightenings were rather small (∼1 mag), suggesting that the outburst was an intermediate between WZ Sge-type (type-A rebrightening) and discrete multiple rebrightenings (type-B). The mean superhump period during the post-superoutburst stage was

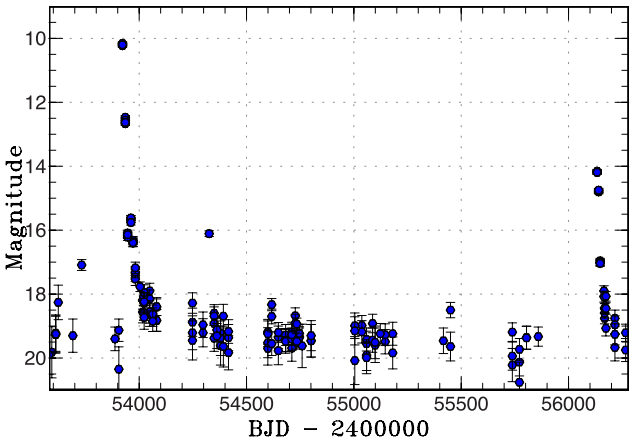

Fig. 78. Long-term curve of SSS J224739. The data are from CRTS SSS observations.

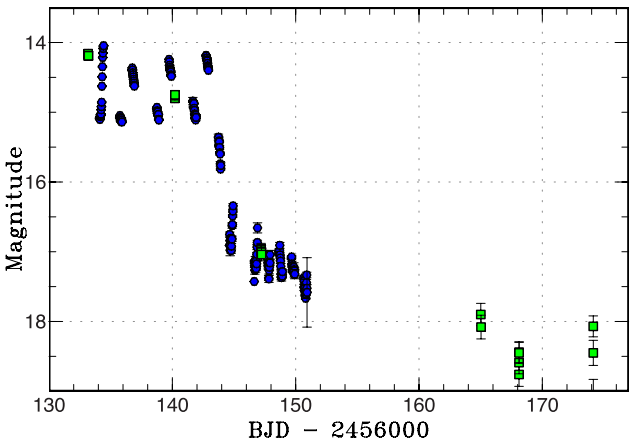

Fig. 79. Overall light curve of SSS J224739 (2012). The time-series data (filled circles) were binned to 0.02 d. The filled squares are CRTS SSS observations.

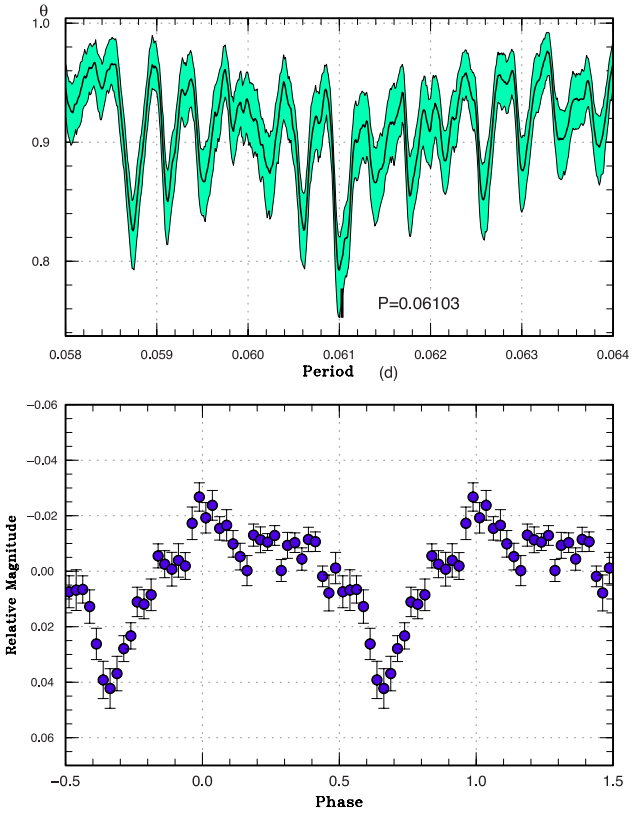

Fig. 80. Superhumps in SSS J224739 (2012). Upper: PDM analysis. Lower: Phase-averaged profile.

0.06103(1) d (PDM method; figure 80). The times of superhump maxima are listed in table 64. A PDM analysis of the observations after the rebrightenings yielded a period of 0.06101(3) d, which is almost identical to the superhump period during the rebrightening phase. No signal of the orbital modulation was detected in either our time-series data or the CRTS data.

The relatively short interval between two superoutbursts (2006 and 2012) suggests that superoutbursts are more frequent in this object than in other WZ Sge-type dwarf novae. The case is similar to EZ Lyn (Shears et al. 2007; Pavlenko et al. 2007; Kato et al. 2009b, 2012a) which underwent superoutbursts in 2006 and 2010 and also showed multiple post-superoutburst rebrightenings. Since the object is one of the brightest (10 mag) WZ Sge-type dwarf novae, further detailed observations are encouraged. The object was also detected as a GALEX source [near-UV magnitude of 19.67(9)].

3.69 TCP J15375685−2440136

This is a transient object (hereafter TCP J153756)[13] discovered by K. Itagaki at a magnitude of 13.6 on 2013 February 8.779 UT. There was a 21.7 mag quiescent counterpart and the large outburst amplitude suggested a WZ Sge-type dwarf nova (vsnet-alert 15366). Double-wave early superhumps were immediately observed (vsnet-alert 15368, 15382, 15390, 15416; figure 81). After this, possible signals of ordinary superhumps were detected (vsnet-alert 15443; figure 82). Individual times of superhump maxima could not be determined. The detected signal [0.06190(2) d] was longer than the period of early superhumps [0.061007(14) d] by 1.5%. This fractional superhump excess is too small for stage A superhumps, and it was likely that stage A evolution was missed during the 2 d gap in the observation. The period is longer than those of typical WZ Sge-type dwarf novae, and is rather typical of WZ Sge-type dwarf novae with multiple rebrightenings (Nakata et al. 2013). Observations for the post-superoutburst stage were not available and it was not known whether this object underwent rebrightenings.

Table 64. Superhump maxima of SSS J224739 (2012).

E	Max*	Error	$O-C^{\dagger}$	$N^{\ddagger}$
0	56134.1020	0.0063	−0.0013	84
1	56134.1628	0.0009	−0.0016	109
2	56134.2225	0.0016	−0.0028	125
3	56134.2891	0.0008	0.0028	125
4	56134.3427	0.0005	−0.0047	125
5	56134.4004	0.0009	−0.0081	124
27	56135.7549	0.0016	0.0039	15
28	56135.8173	0.0020	0.0052	16
29	56135.8775	0.0010	0.0045	22
46	56136.9167	0.0116	0.0061	17
78	56138.8692	0.0018	0.0057	22
79	56138.9152	0.0042	−0.0092	14
125	56141.7416	0.0038	0.0100	22
126	56141.7870	0.0051	−0.0057	26
127	56141.8580	0.0023	0.0042	26
128	56141.9145	0.0031	−0.0003	21
143	56142.8272	0.0045	−0.0029	26
159	56143.8033	0.0016	−0.0033	27
160	56143.8654	0.0023	−0.0022	27
161	56143.9284	0.0064	−0.0003	13

*BJD−2400000.
†Against max = 2456134.1033 + 0.061027 E.
‡Number of points used to determine the maximum.

3.70 TCP J17521907+5001155

This is a transient object (hereafter TCP J175219)[14] discovered by H. Mikuz on 2012 August 17. Subsequent observations confirmed the presence of superhumps (vsnet-alert 14888, 14893; figure 83). The times of superhump maxima are listed in table 65. The period adopted in table 2 was obtained by PDM analysis.

[13] ⟨http://www.cbat.eps.harvard.edu/unconf/followups/J15375685-2440136.html⟩.

[14] ⟨http://www.cbat.eps.harvard.edu/unconf/followups/J17521907+5001155.html⟩.

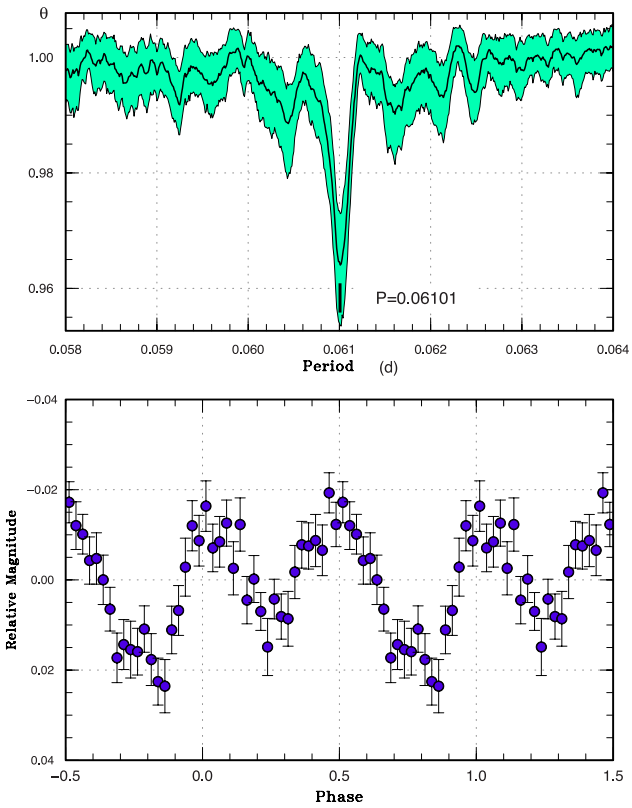

Fig. 81. Early superhumps in TCP J153756 (2013). Upper: PDM analysis. Lower: Phase-averaged profile.

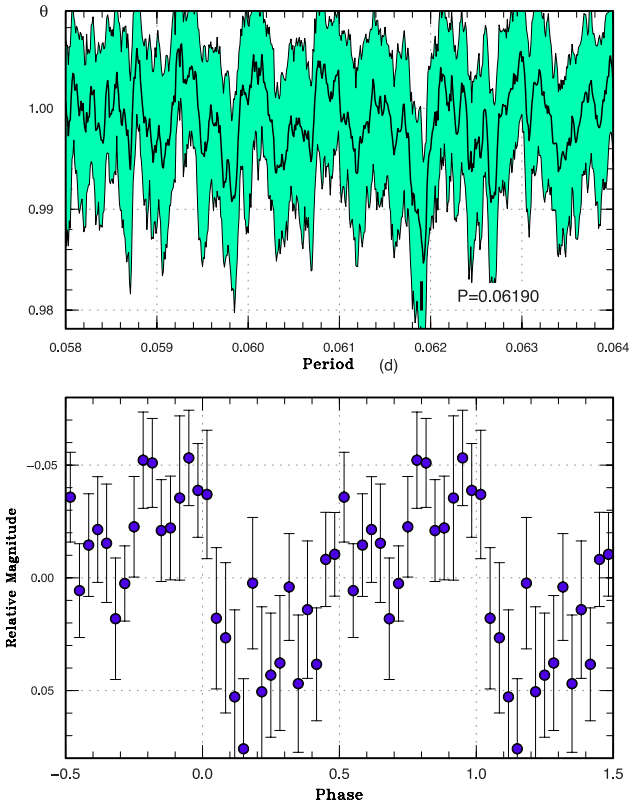

Fig. 82. Possible superhumps in TCP J153756 (2013). Upper: PDM analysis. Lower: Phase-averaged profile.

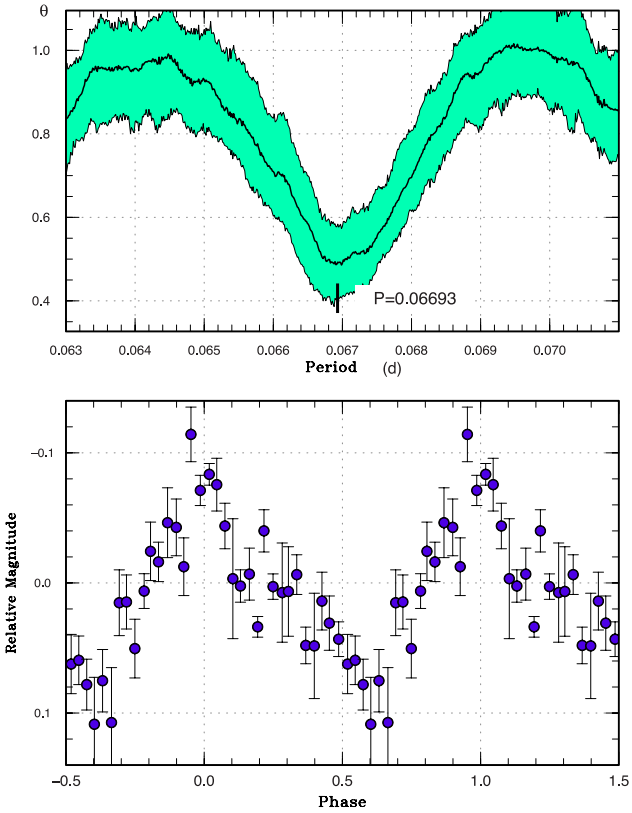

Fig. 83. Superhumps in TCP J175219 (2012). Upper: PDM analysis. Lower: Phase-averaged profile.

Table 65. Superhump maxima of TCP J175219 (2012).

E	Max*	Error	$O-C^{\dagger}$	$N^{\ddagger}$
0	56162.5043	0.0020	−0.0001	39
12	56163.3113	0.0011	0.0007	33
13	56163.3772	0.0013	−0.0006	37

*BJD−2400000.
†Against max = 2456162.5044 + 0.067186 E.
‡Number of points used to determine the maximum.

4 General discussion

In this section we report on general statistical properties of the sample together with the earlier sample, the same as in Kato et al. (2013a).

4.1 Period derivatives during stage B

The same as in Kato et al. (2013a), we have determined period derivatives of new superoutbursts during stage B (figure 84). All the objects with $P_{\rm orb} < 0.086$ d followed the trend reported in Kato et al. (2013a). Although AQ Eri (2012) showed a large $P_{\rm dot}$, this was due to the limited coverage, and the resultant error was large. We found three additional objects with a large positive $P_{\rm dot}$ despite the long $P_{\rm orb}$: V444 Peg, CSS J203937, and MASTER J212624.

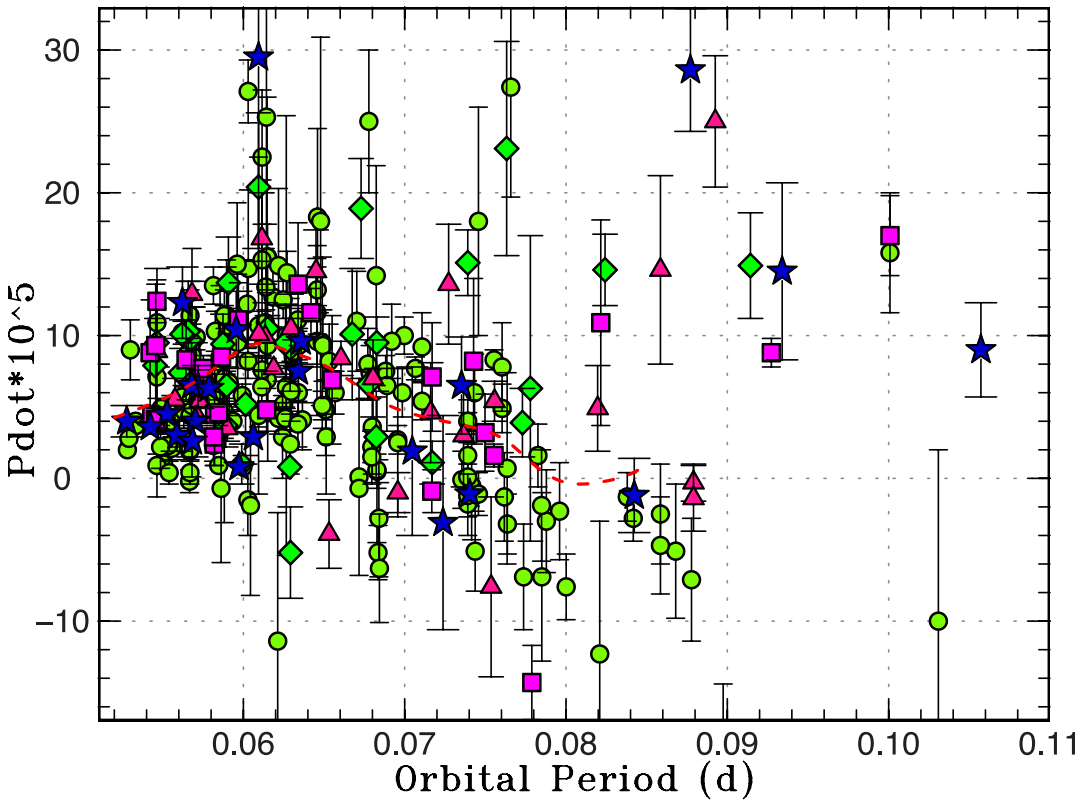

Fig. 84. $P_{\rm dot}$ for stage B versus $P_{\rm orb}$. Filled circles, filled diamonds, filled triangles, filled squares, and filled stars represent samples in Kato et al. (2009a, 2010, 2012a, 2013a) and this paper, respectively. The curve represents the spline-smoothed global trend.

Table 66. New estimates for the binary mass ratio from stage A superhumps.

Object	ε^* (stage A)	q from stage A
YZ Cnc	0.0559(12)	0.168(5)
V503 Cyg	0.0688(12)	0.218(5)
TY PsA	0.0486(12)	0.142(4)
MASTER J094759	0.023(3)	0.060(8)
MASTER J181953	0.0259(3)	0.069(1)
OT J112619	0.0317(6)	0.086(2)
OT J232727	0.0303(5)	0.082(2)
SDSS J162520	0.072(2)	0.23(1)

Table 67. Superhump periods during stage A.

Object	Year	Period (d)	Error
YZ Cnc	2011	0.09194	0.00044
V503 Cyg	2012	0.08350	0.00011
V660 Her	2012	0.07826	—
V660 Her	2013	0.07826	—
V1227 Her	2012a	0.06442	—
V1227 Her	2012b	0.06442	—
V1227 Her	2013	0.06442	—
TY PsA	2012	0.08854	0.00011
AW Sge	2012	0.07743	0.00014
ASAS SN-13ax	2013	0.05712	0.00002
CSS J102842	2013	0.03849	0.00000
CSS J174033	2013	0.04640	0.00006
MASTER J081110	2012	0.05876	0.00008
MASTER J094759	2013	0.05717	0.00020
MASTER J181953	2013	0.05835	0.00004
MASTER J203749	2012	0.06271	—
MASTER J211258	2012	0.06158	0.00005
OT J112619	2013	0.05601	0.00004
OT J232727	2012	0.05442	0.00003
SSS J122221	2013	0.07721	0.00011

It has become evident that large positive-$P_{\rm dot}$ objects are relatively more common among long-$P_{\rm orb}$ systems than expected.

Poleski et al. (2011) reported a large negative (-2×10^{-3}) period variation of superhumps in OGLE-BLG-DN-001, an SU UMa-type dwarf nova in the period gap. Their data, however, covered the growing stage of superhumps and this large negative $P_{\rm dot}$ is most likely a result of stage A–B transition. Since only the initial part of stage B was observed, more data are needed to determine the true $P_{\rm dot}$. The frequency of the outbursts in this object looks much lower than that in MN Dra and NY Ser—the objects Poleski et al. (2011) compared—and it would be interesting to see how $P_{\rm dot}$ depends on the outburst frequency in long-$P_{\rm orb}$ systems. The object, however, very much resembles

Table 68. Parameters of WZ Sge-type superoutbursts.

Object	Year	P_{SH}	P_{orb}	P_{dot}*	Error*	ε	Type†	N_{reb}‡	Delay§	Max	Min
GR Ori	2013	0.058333	—	6.4	1.5	—	D	0	9	13.0	22.4
ASAS SN-13ax	2013	0.056155	—	4.5	0.6	—	A	1(2)	≥7	]13.5	21.2
CSS J174033	2013	0.045548	0.045048	1.6	0.1	0.011	A	1	≥7	]14.0	20.1
MASTER J081110	2012	0.058147	—	4.5	0.3	—	—	—	—	]14.1	22.1
MASTER J094759	2013	0.056121	0.05588	3.0	1.1	0.004	—	—	≥2	]13.6	20.4
MASTER J165236	2013	0.084732	—	—	—	—	—	—	—	]14.8	21.9
MASTER J181953	2013	0.057519	0.05684	2.6	1.1	0.012	A	1(≥3)	≥3	]13.9	21.6
MASTER J203749	2012	0.061307	0.06051	2.9	1.0	0.013	B	≥4	≥3	]14.1	21.3
MASTER J211258	2012	0.060227	0.059732	0.8	1.0	0.008	B	8	12	14.1	21.3
OT J112619	2013	0.054886	0.05423	3.6	0.4	0.012	—	—	≥6	]14.8	21.8
OT J232727	2012	0.053438	0.05277	4.0	1.1	0.013	—	—	≥11	]13.9	21.8
PNV J062703	2013	0.059026	0.05787	6.3	1.3	0.020	—	—	≥4	]12.0	21.0
SSS J122221	2013	0.076486	—	− 1.1	0.7	—	E	0	—	]11.8	18.7
TCP J153756	2013	0.061899	0.06101	—	—	0.015	—	—	≥4	]13.6	21.7

*In units of 10^{-5}.
†A: long-lasting rebrightening, B: multiple rebrightenings, C: single rebrightening, D: no rebrightening.
‡Number of rebrightenings.
§Days before ordinary superhumps appeared.

SDSS J162520 (subsection 3.66), which showed a post-superoutburst rebrightening and only two outbursts in the CRTS data.

4.2 Periods of stage A superhumps

It has recently been shown that stage A superhumps can be directly used for estimating the binary's q (Osaki & Kato 2013b; Kato & Osaki 2013b). Stage A superhumps recorded in the present study are listed in table 67. The q values can be determined if the orbital period is known. The q values for such objects are discussed individually in section 3. A summary of newly determined q values is shown in table 66. The best examples are MASTER J211258 and MASTER J203749, WZ Sge-type dwarf novae with multiple rebrightenings, whose q values were estimated by using stage A superhumps (Nakata et al. 2013). Nakata et al. (2013) suggested that WZ Sge-type dwarf novae with multiple rebrightenings do not have strikingly smaller q than other SU UMa-type dwarf novae with a similar orbital period, and that these objects are not good candidates for period bouncers. This suggestion needs to be

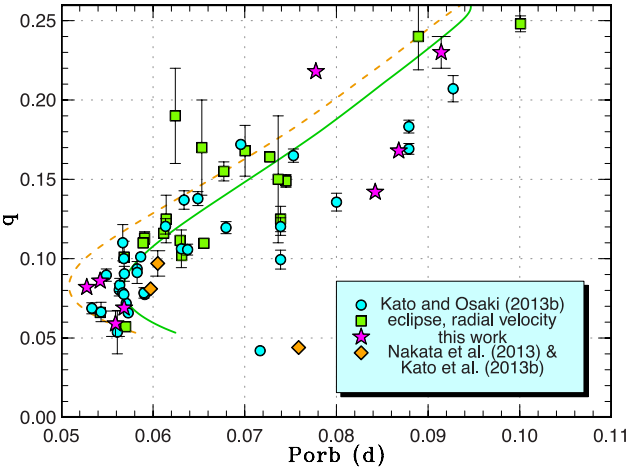

Fig. 85. Mass ratio versus orbital period. The dashed and solid curves represent the standard and optimal evolutionary tracks in Knigge, Baraffe, and Patterson (2011), respectively. The filled circles, filled squares, filled stars, and filled diamonds represent q values from Kato and Osaki (2013b) [the improved q for V1504 Cyg in subsection 4.2 of Kato & Osaki (2013b) is adopted here], known q values from quiescent eclipses or radial velocity study (see Kato & Osaki 2013b for the data source), q estimated in this work, and the two publications of Nakata et al. (2013) and Kato et al. (2013b), respectively.

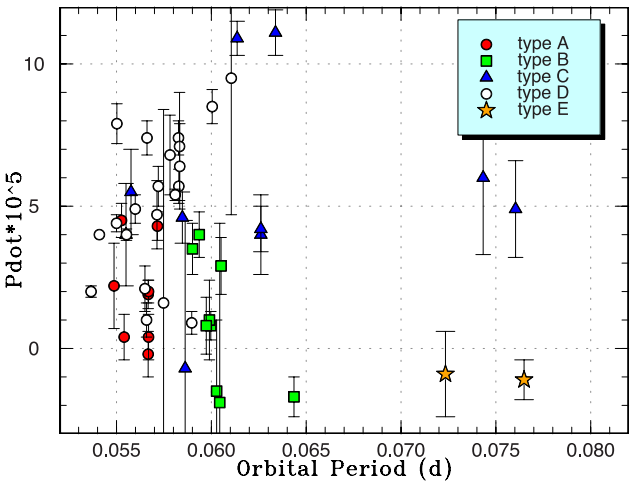

Fig. 86. P_{dot} versus P_{orb} for WZ Sge-type dwarf novae. The symbols represent the type (cf. Kato et al. 2009a) of outburst: type-A (filled circles), type-B (filled squares), type-C (filled triangles), type-D (open circles), and the newly introduced type-E (filled stars) which shows double superoutbursts as shown in Kato et al. (2013b).

Table 69. Rate of slow decline in SU UMa-type dwarf novae.

Object	Year	Rate*	Error*	Start†	End†	Mean P_{SH} (stage B)‡	Source§
FO And	2010	0.106	0.001	55487.3	55494.7	0.07451	3
KV And	1994	0.135	0.003	49578.2	49583.3	0.07460	1
KV And	2002	0.079	0.001	52584.1	52591.2	0.07450	1
V402 And	2005	0.182	0.007	53671.1	53673.7	0.06323	1
V402 And	2008	0.130	0.002	54755.0	54761.2	0.06353	1
DH Aql	2002	0.099	0.001	52483.1	52493.2	0.08002	1
V1141 Aql	2003	0.131	0.007	52824.1	52827.5	0.06296	1
VY Aqr	2008	0.113	0.001	54648.1	54656.3	0.06466	1
EG Aqr	2006	0.140	0.001	54050.2	54057.0	0.07896	1
EG Aqr	2008	0.143	0.001	54802.9	54808.0	0.07876	1
QV Aqr	2011	0.173	0.004	55834.4	55836.5	0.07531	4
QZ Aqr	2008	0.127	0.005	54819.8	54821.9	0.06463	1
BF Ara	2002	0.101	0.001	52505.0	52510.4	0.08789	1
V663 Ara	2004	0.110	0.002	53195.4	53199.5	0.07642	1
V877 Ara	2002	0.117	0.001	52435.0	52443.3	0.08393	1
BG Ari	2009	0.076	0.001	55086.5	55099.6	0.08510	2
TT Boo	2004	0.073	0.001	53161.0	53174.8	0.07809	1
TT Boo	2010	0.104	0.001	55311.1	55318.3	0.07812	3
TT Boo	2012	0.066	0.001	56016.4	56021.3	0.07808	4
NN Cam	2007	0.077	0.001	54364.5	54367.6	0.07429	1
NN Cam	2009	0.073	0.001	55142.3	55147.8	0.07426	2
NN Cam	2011	0.108	0.001	55905.0	55913.1	0.07420	4
V342 Cam	2008	0.149	0.001	54532.2	54538.8	0.07840	1
V342 Cam	2010	0.142	0.001	55444.1	55451.3	0.07846	2
V391 Cam	2005	0.156	0.001	53450.0	53455.4	0.05716	1
V391 Cam	2008	0.161	0.001	54477.9	54481.0	0.05713	1
SY Cap	2011	0.085	0.003	55803.1	55805.1	0.06375	4
GX Cas	1999	0.080	0.001	51472.1	51477.3	0.09352	1
GX Cas	2010	0.116	0.001	55502.0	55505.3	0.09300	3
KP Cas	2008	0.131	0.001	54767.0	54771.0	0.08553	1
V359 Cen	2002	0.146	0.002	52425.8	52430.8	0.08121	1
V1040 Cen	2002	0.171	0.001	52366.2	52372.7	0.06218	1
WX Cet	1989	0.120	0.001	47683.6	47695.7	0.05962	1
WX Cet	1998	0.120	0.001	51128.9	51138.2	0.05962	1
WX Cet	2001	0.162	0.002	52092.3	52097.9	0.05955	1
WX Cet	2004	0.102	0.001	53347.9	53358.0	0.05953	1
RX Cha	2009	0.091	0.005	54858.0	54860.1	0.08492	1
BZ Cir	2004	0.111	0.001	53184.2	53193.5	0.07661	1
PU CMa	2005	0.152	0.001	53401.9	53407.1	0.05801	1
PU CMa	2009	0.221	0.001	55159.1	55162.4	0.05809	2
AQ CMi	2010	0.117	0.001	55296.0	55303.0	0.06618	2
YZ Cnc	2007	0.105	0.001	54144.0	54152.0	0.09031	1
AK Cnc	1992	0.092	0.002	48639.1	48644.3	0.06751	1
CC Cnc	2001	0.117	0.001	52226.3	52233.4	0.07589	1
GZ Cnc	2010	0.096	0.001	55269.1	55273.2	0.09277	1
GZ Cnc	2013	0.151	0.002	56331.9	56335.1	0.09284	5
KK Cnc	2007	0.118	0.001	54424.9	54430.3	0.06105	1
GO Com	2003	0.145	0.001	52795.1	52801.4	0.06308	1
GO Com	2005	0.188	0.001	53484.0	53488.3	0.06305	1
GO Com	2010	0.170	0.002	55287.6	55291.1	0.06307	2
GO Com	2012	0.139	0.002	55984.3	55987.7	0.06302	4
V728 CrA	2003	0.141	0.001	52821.3	52825.6	0.08238	1
VW CrB	2003	0.109	0.001	52849.4	52855.5	0.07292	1
VW CrB	2006	0.085	0.004	53842.7	53846.7	0.07268	1
TU Crt	2001	0.121	0.002	52010.0	52020.0	0.08518	1

Table 69. (Continued)

Object	Year	Rate*	Error*	Start†	End†	Mean P_{SH} (stage B)‡	Source§
TV Crv	2001	0.123	0.001	51961.1	51968.2	0.06500	1
TV Crv	2004	0.136	0.002	53162.5	53168.7	0.06509	1
TV Crv	2009	0.138	0.002	55183.2	55189.4	0.06506	2
V337 Cyg	2006	0.167	0.002	53886.4	53888.6	0.07000	1
V337 Cyg	2010	0.152	0.001	55421.4	55425.2	0.07033	2
V503 Cyg	2002	0.153	0.002	52478.2	52483.3	0.08139	1
V503 Cyg	2008	0.090	0.001	54822.9	54828.9	0.08177	1
V503 Cyg	2011	0.097	0.001	55744.4	55751.6	0.08131	4
V503 Cyg	2011b	0.113	0.001	55831.2	55840.5	0.08124	4
V503 Cyg	2012	0.069	0.001	56093.7	56099.0	0.08123	5
V630 Cyg	2008	0.122	0.002	54692.0	54698.2	0.07918	1
V632 Cyg	2008	0.112	0.001	54782.9	54791.0	0.06583	1
V1028 Cyg	1995	0.124	0.001	49928.1	49938.3	0.06175	1
V1028 Cyg	1999	0.129	0.002	51430.1	51435.3	0.06170	1
V1028 Cyg	2002	0.142	0.002	52618.9	52624.0	0.06177	1
V1113 Cyg	1994	0.120	0.004	49600.0	49603.1	0.07906	1
V1113 Cyg	2008	0.135	0.002	54757.3	54760.0	0.07905	1
V1454 Cyg	2006	0.099	0.001	54068.9	54080.9	0.06102	1
V1454 Cyg	2009	0.129	0.002	55058.1	55063.6	0.05765	2
V1504 Cyg	2007	0.129	0.002	54326.4	54333.6	0.07232	3
HO Del	1994	0.124	0.002	49591.0	49595.2	0.06456	1
HO Del	2008	0.127	0.001	54684.4	54690.8	0.06436	1
BC Dor	2003	0.025	0.001	52958.0	52968.1	0.06847	1
CP Dra	2003	0.130	0.002	52648.1	52653.2	0.08370	1
CP Dra	2009	0.199	0.001	54917.4	54922.5	0.08382	1
DM Dra	2003	0.152	0.002	52706.2	52710.4	0.07571	1
KV Dra	2002	0.169	0.003	52519.5	52523.4	0.06030	1
KV Dra	2004	0.155	0.001	53120.0	53127.2	0.06045	1
KV Dra	2005	0.171	0.002	53465.2	53468.3	0.06034	1
AQ Eri	2006	0.083	0.002	54070.1	54076.2	0.06168	1
AQ Eri	2008	0.101	0.001	54830.0	54836.1	0.06236	1
AQ Eri	2010	0.160	0.001	55202.0	55206.2	0.06237	2
AQ Eri	2012	0.087	0.001	56213.3	56217.2	0.06240	5
KY Eri	2004	0.172	0.003	53198.5	53204.9	0.06864	1
AX For	2005	0.116	0.001	53555.6	53563.7	0.08120	1
UV Gem	2003	0.087	0.001	52647.9	52653.6	0.09355	1
AW Gem	1995	0.076	0.002	50001.2	50005.4	0.07983	1
AW Gem	2008	0.111	0.001	54565.0	54572.1	0.07899	1
AW Gem	2010	0.122	0.002	55257.3	55261.6	0.07906	2
AW Gem	2011	0.136	0.001	55572.1	55579.3	0.07938	3
CI Gem	2005	0.094	0.003	53476.3	53485.7	0.11931	1
V660 Her	2012	0.119	0.003	56177.4	56179.5	0.08089	5
V844 Her	1997	0.091	0.001	50592.4	50602.5	0.05601	1
V844 Her	1999	0.107	0.002	51451.9	51457.0	0.05591	1
V844 Her	2006	0.151	0.001	53854.0	53860.3	0.05587	1
V844 Her	2008	0.134	0.001	54577.1	54584.5	0.05593	1
V844 Her	2009	0.136	0.001	54887.5	54892.7	0.05592	2
V844 Her	2010b	0.085	0.002	55496.3	55499.3	0.05611	3
V844 Her	2012	0.155	0.001	56052.0	56057.3	0.05590	4
V1227 Her	2012b	0.131	0.002	56183.6	56187.8	0.06508	5
RU Hor	2003	0.104	0.001	52912.4	52917.4	0.07095	1
RU Hor	2008	0.128	0.001	54686.5	54688.7	0.07103	1
CT Hya	1999	0.127	0.002	51224.9	51231.2	0.06642	1
CT Hya	2000	0.169	0.002	51880.1	51887.4	0.06639	1
CT Hya	2002a	0.099	0.003	52317.1	52321.3	0.06638	1

Table 69. (Continued)

Object	Year	Rate*	Error*	Start†	End†	Mean P_{SH} (stage B)‡	Source§
CT Hya	2002b	0.107	0.002	52592.1	52601.4	0.06641	1
CT Hya	2009	0.161	0.003	54848.0	54852.0	0.06663	1
MM Hya	1998	0.073	0.005	50882.3	50886.3	0.05896	1
MM Hya	2011	0.145	0.001	55661.0	55665.2	0.05885	3
MM Hya	2012	0.117	0.001	55993.6	56000.8	0.05887	4
V498 Hya	2008	0.156	0.001	54491.0	54497.2	0.06047	1
VW Hyi	2011	0.095	0.001	55895.5	55901.8	0.07691	4
RZ LMi	2012	0.084	0.002	55985.5	55989.7	0.05944	4
RZ LMi	2012b	0.064	0.001	56013.4	56017.8	0.05947	4
RZ LMi	2012c	0.076	0.001	56031.6	56036.8	0.05941	4
SX LMi	1994	0.160	0.004	49702.2	49705.3	0.06948	1
SX LMi	2001	0.121	0.002	51938.3	51944.3	0.06914	1
SX LMi	2002	0.144	0.003	52300.3	52307.3	0.06934	1
BK Lyn	2012b	0.059	0.001	56023.3	56030.7	0.07851	4
FV Lyn	2007	0.076	0.001	54161.0	54172.2	0.06977	1
AY Lyr	2008	0.076	0.002	54754.9	54758.1	0.07623	1
AY Lyr	2009	0.085	0.001	54963.0	54970.3	0.07616	1
DM Lyr	1996	0.147	0.003	50280.0	50282.2	0.06709	1
DM Lyr	1997	0.095	0.003	50509.3	50513.4	0.06721	1
DM Lyr	2002	0.188	0.013	52583.9	52587.0	0.06723	1
V344 Lyr	1993	0.099	0.002	49133.1	49140.3	0.09135	1
V419 Lyr	1999	0.065	0.002	51415.1	51422.2	0.09015	1
V419 Lyr	2006	0.109	0.001	53935.4	53941.5	0.09006	1
V585 Lyr	2003	0.152	0.001	52900.3	52906.9	0.06036	1
FQ Mon	2004	0.090	0.001	53068.9	53081.1	0.07335	1
FQ Mon	2006	0.105	0.002	53759.0	53764.2	0.07392	1
FQ Mon	2007	0.083	0.001	54466.1	54472.2	0.07335	1
AB Nor	2002	0.066	0.003	52519.2	52522.0	0.07962	1
AB Nor	2013	0.107	0.001	56436.2	56441.7	0.07976	5
DT Oct	2003	0.137	0.001	52645.9	52652.2	0.07476	1
V699 Oph	2003	0.086	0.001	52824.2	52829.1	0.07033	1
V699 Oph	2008	0.070	0.001	54618.1	54624.2	0.07013	1
V2527 Oph	2004	0.093	0.001	53211.9	53219.1	0.07205	1
V2527 Oph	2008	0.103	0.001	54711.0	54720.0	0.07194	1
V1159 Ori	2002	0.076	0.001	52605.2	52610.3	0.06414	1
EF Peg	1991	0.079	0.001	48547.9	48555.1	0.08693	1
EF Peg	1997	0.058	0.001	50758.0	50764.1	0.08704	1
EF Peg	2009	0.045	0.001	55187.9	55195.0	0.08735	2
V364 Peg	2004	0.173	0.004	53329.2	53331.7	0.08534	1
V368 Peg	2000	0.105	0.001	51786.0	51792.3	0.07038	1
V368 Peg	2005	0.135	0.001	53621.0	53628.1	0.07038	1
V368 Peg	2009	0.144	0.001	55101.5	55112.9	0.07036	2
V444 Peg	2008	0.132	0.001	54778.0	54783.3	0.09945	1
V444 Peg	2012	0.212	0.001	56193.9	56199.6	0.09764	5
UV Per	2000	0.124	0.001	51904.5	51913.1	0.06663	1
UV Per	2003	0.110	0.001	52949.3	52957.4	0.06667	1
UV Per	2010	0.122	0.003	55203.4	55205.6	0.06671	2
PV Per	2008	0.019	0.002	54745.4	54753.2	0.08080	1
QY Per	1999	0.123	0.001	51545.1	51552.3	0.07861	1
QY Per	2005	0.124	0.001	53667.0	53676.3	0.07861	1
TY PsA	2008	0.135	0.001	54798.9	54805.0	0.08799	1
TY PsA	2012	0.118	0.001	56163.1	56171.1	0.08781	5
TY Psc	2005	0.067	0.002	53614.2	53616.3	0.07034	1
TY Psc	2008	0.097	0.001	54754.9	54759.5	0.07066	1
GV Psc	2011	0.109	0.002	55852.3	55854.9	0.09431	4

Table 69. (Continued)

Object	Year	Rate*	Error*	Start†	End†	Mean P_{SH} (stage B)‡	Source§
VZ Pyx	2008	0.084	0.001	54790.2	54796.4	0.07605	1
DT Pyx	2005	0.082	0.002	53448.0	53450.1	0.06289	1
DV Sco	2004	0.135	0.002	53272.2	53277.3	0.09978	1
QW Ser	2002	0.060	0.001	52427.2	52435.2	0.07703	1
V493 Ser	2007	0.114	0.001	54312.0	54324.1	0.08296	1
RZ Sge	1994	0.094	0.002	49576.0	49580.1	0.07057	1
RZ Sge	1996	0.139	0.002	50305.1	50308.3	0.07064	1
RZ Sge	2002	0.096	0.001	52549.0	52558.1	0.07044	1
AW Sge	2012	0.108	0.001	56127.1	56132.9	0.07473	5
V551 Sgr	2003	0.143	0.001	52903.9	52910.4	0.06760	1
V4140 Sgr	2004	0.083	0.001	53269.2	53286.7	0.06351	1
V701 Tau	1995	0.088	0.001	50078.0	50090.1	0.06908	1
V1208 Tau	2000	0.106	0.004	51580.7	51586.2	0.07050	1
V1208 Tau	2002	0.120	0.001	52635.1	52642.1	0.07054	1
V1212 Tau	2011	0.101	0.001	55589.6	55601.4	0.07011	3
V1265 Tau	2006	0.085	0.001	54035.4	54043.5	0.05341	1
EK TrA	2009	0.124	0.001	55028.9	55036.1	0.06483	2
FL TrA	2005	0.136	0.001	53581.2	53585.4	0.05985	1
SU UMa	1999	0.113	0.001	51189.9	51197.1	0.07909	1
SU UMa	2010	0.128	0.002	55220.5	55223.6	0.07907	2
SW UMa	1996	0.134	0.001	50191.3	50198.0	0.05819	1
SW UMa	1997	0.119	0.001	50744.5	50752.7	0.05828	1
SW UMa	2000	0.133	0.001	51589.9	51601.4	0.05826	1
SW UMa	2002	0.103	0.001	52572.2	52581.3	0.05832	1
SW UMa	2006	0.113	0.001	53997.2	54009.3	0.05821	1
SW UMa	2010	0.155	0.001	55538.2	55545.4	0.05821	3
BC UMa	2000	0.131	0.001	51638.3	51647.1	0.06456	1
BC UMa	2003	0.125	0.001	52674.0	52682.4	0.06457	1
BC UMa	2009	0.129	0.001	55108.9	55118.7	0.06455	2
BZ UMa	2007	0.119	0.001	54205.3	54213.6	0.07018	1
CI UMa	2003	0.100	0.001	52739.3	52747.5	0.06269	1
CI UMa	2011	0.211	0.002	55660.4	55663.6	0.06269	3
CI UMa	2013	0.222	0.001	56385.3	56396.3	0.06238	5
CY UMa	1998	0.110	0.001	50882.4	50891.6	0.07246	1
CY UMa	1999	0.142	0.001	51222.9	51230.0	0.07222	1
CY UMa	2009	0.146	0.001	54917.9	54924.6	0.07222	1
DI UMa	2007	0.077	0.002	54206.3	54211.5	0.05531	4
KS UMa	2003	0.125	0.001	52691.0	52696.7	0.07018	1
KS UMa	2007	0.129	0.001	54150.1	54155.3	0.07026	1
MR UMa	2002	0.102	0.001	52342.0	52347.4	0.06516	1
MR UMa	2003	0.123	0.001	52712.0	52717.5	0.06514	1
SS UMi	2012	0.159	0.002	56008.4	56012.0	0.07036	4
CU Vel	2002	0.107	0.001	52620.2	52630.2	0.08094	1
HS Vir	1996	0.119	0.001	50155.2	50161.3	0.08006	1
HS Vir	2008	0.119	0.001	54619.0	54624.0	0.08003	1
QZ Vir	1993	0.134	0.001	48993.2	49000.3	0.06035	1
QZ Vir	2007	0.135	0.001	54111.1	54113.4	0.06048	1
QZ Vir	2008	0.159	0.001	54470.2	54473.4	0.06044	1
QZ Vir	2009	0.133	0.001	54857.1	54860.4	0.06038	1
RX Vol	2003	0.135	0.001	52764.0	52770.3	0.06136	1
TY Vul	2010	0.122	0.001	55371.4	55375.9	0.08046	2
DO Vul	2008	0.073	0.003	54671.0	54674.1	0.05820	1
NSV 04838	2007	0.098	0.001	54143.1	54151.2	0.06992	1
NSV 14652	2004	0.111	0.002	53251.4	53256.4	0.08151	1
1RXS J231935.0+364705	2011	0.158	0.001	55835.4	55843.3	0.06599	4

Table 69. (Continued)

Object	Year	Rate*	Error*	Start†	End†	Mean P_{SH} (stage B)‡	Source§
ASAS J224349+0809.5	2009	0.097	0.001	55113.0	55121.8	0.06981	2
CSS J015051.7+332621	2012	0.156	0.001	56211.6	56217.1	0.07271	5
CSS J105835.1+054703	2012	0.104	0.001	56268.2	56275.0	0.05788	5
CSS J203937.7−042907	2012	0.087	0.001	56155.6	56163.7	0.11121	5
Lanning 420	2010	0.119	0.001	55438.6	55444.7	0.06159	2
MASTER OT J042609.34+354144.8	2012	0.188	0.003	56202.6	56205.3	0.06756	5
MASTER OT J054317.95+093114.8	2012	0.101	0.001	56205.8	56218.9	0.07595	5
MASTER OT J064725.70+491543.9	2013	0.134	0.001	56362.6	56366.1	0.06777	5
MASTER OT J081110.46+660008.5	2012	0.081	0.001	56225.3	56234.0	0.05815	5
MisV 1446	2012	0.171	0.002	55936.5	55940.1	0.07807	4
SDSS J033449.86−071047.8	2009	0.122	0.001	54856.0	54860.1	0.07477	1
SDSS J073208.11+413008.7	2010	0.082	0.001	55199.6	55210.0	0.07995	2
SDSS J074640.62+173412.8	2009	0.127	0.002	54874.9	54884.2	0.06679	1
SDSS J075107.50+300628.4	2013	0.108	0.002	56338.5	56340.7	0.05798	5
SDSS J080303.90+251627.0	2011	0.096	0.004	55654.3	55657.1	0.09195	4
SDSS J080306.99+284855.8	2011	0.096	0.004	55654.3	55657.1	0.07510	3
SDSS J081207.63+131824.4	2008	0.142	0.002	54754.2	54759.3	0.07756	3
SDSS J081207.63+131824.4	2011	0.133	0.001	55645.5	55653.0	0.07789	3
SDSS J083931.35+282824.0	2010	0.139	0.002	55295.3	55298.5	0.07852	2
SDSS J125023.85+665525.5	2008	0.169	0.004	54491.9	54496.9	0.06033	2
SDSS J125023.85+665525.5	2011	0.174	0.003	55665.0	55668.7	0.06026	3
SDSS J161027.61+090738.4	2009	0.113	0.001	55040.4	55050.5	0.05782	2
SDSS J162520.29+120308.7	2010	0.154	0.001	55386.4	55389.8	0.09605	2
SDSS J162718.39+120435.0	2008	0.103	0.001	54620.6	54627.6	0.10974	1
SDSSp J173008.38+624754.7	2001	0.134	0.003	52205.9	52209.1	0.07941	1
OT J014150.4+090822	2010	0.124	0.002	55527.9	55532.2	0.06249	3
OT J040659.8+005244	2008	0.074	0.002	54687.3	54690.3	0.07995	1
OT J041350.0+094515	2011	0.090	0.001	55587.6	55591.8	0.05483	3
OT J043112.5−031452	2011	0.129	0.002	55575.2	55580.9	0.06758	3
OT J050617.4+354738	2009	0.121	0.002	55162.1	55171.6	0.06932	2
OT J055718+683226	2006	0.082	0.001	54087.1	54097.3	0.05351	1
OT J055721.8−363055	2011	0.142	0.003	55926.5	55932.2	0.05976	4
OT J064608.2+403305	2011	0.126	0.004	55923.4	55925.0	0.06110	4
OT J064804.5+414702	2011	0.148	0.003	55590.6	55593.5	0.06632	3
OT J075414.5+313216	2011	0.130	0.003	55666.3	55668.5	0.06308	3
OT J081418.9−005022	2008	0.051	0.002	54765.6	54770.3	0.07652	1
OT J094854.0+014911	2012	0.139	0.001	56002.3	56007.9	0.05750	4
OT J102616.0+192045	2010	0.117	0.001	55534.5	55541.4	0.08283	3
OT J102637.0+475426	2010	0.144	0.001	55270.5	55274.6	0.06873	2
OT J130030.3+115101	2008	0.142	0.002	54653.0	54660.1	0.06439	1
OT J132900.9−365859	2011	0.109	0.002	55656.4	55660.7	0.07100	3
OT J144011.0+494734	2009	0.046	0.001	54985.4	54991.9	0.06462	2
OT J144252.0−225040	2012	0.120	0.001	56035.7	56043.7	0.06513	4
OT J144341.9−175550	2009	0.119	0.001	54942.1	54953.3	0.07218	1
OT J145921.8+354806	2011	0.107	0.005	55728.4	55731.5	0.08511	4
OT J163120.9+103134	2008	0.174	0.001	54592.3	54597.6	0.06413	1
OT J191443.6+605214	2008	0.086	0.001	54743.1	54753.1	0.07135	1
OT J210950.5+134840	2011	0.129	0.001	55707.8	55718.3	0.06005	4
OT J214738.4+244553	2011	0.099	0.001	55839.2	55845.8	0.09715	4
OT J215818.5+241925	2011	0.180	0.001	55863.2	55866.0	0.06740	4
OT J221232.0+160140	2011	0.110	0.001	55922.2	55931.3	0.09032	4

*In units of mag d^{-1}.
†BJD−2400000.
‡In units of d.
§1: Kato et al. (2009a), 2: Kato et al. (2010), 3: Kato et al. (2012a), 4: Kato et al. (2013a), 5: this work.

tested by further data and observations. An updated summary of q estimates is shown in figure 85. The objects in table 67 but without a known orbital period will be prime targets for measuring their orbital periods, which will lead to an increase in the number of new q estimates from stage A superhumps.

4.3 WZ Sge-type stars

New WZ Sge-type dwarf novae and candidates are listed in table 68. It is noteworthy that both the MASTER network and amateur astronomers (Itagaki and Kaneko) were very productive of the detection of WZ Sge-type dwarf novae.

Figure 86 shows the updated relation between $P_{\rm dot}$ and $P_{\rm orb}$ and its relation to the type of post-superoutburst rebrightening phenomenon. We used an updated $P_{\rm dot}$ of $+3.5(0.9) \times 10^{-5}$ ($31 \leq E \leq 143$) for stage B superhumps in EZ Lyn (2010) since the original identification of stage B in Kato et al. (2012a) included the rapid fading stage when the period sharply increased due to the decrease of the pressure effect (Nakata et al. 2013).

We use here the types of the superoutburst in terms of rebrightenings as introduced in Imada et al. (2006) and Kato et al. (2009a): type-A outburst (long-duration rebrightening), type-B outburst (multiple discrete rebrightenings), type-C outburst (single rebrightening), and type-D outburst (no rebrightening) (see, e.g., figure 37 in Kato et al. 2009a). In this figure, we newly introduce type-E which shows double superoutbursts (a superoutburst with early superhumps and another superoutburst with ordinary superhumps) the same as in Kato et al. (2013b). OT J184228.1+483742 was reclassified to type-E following the discussion in Kato et al. (2013b). These objects showing type-E superoutbursts are good candidates for period bouncers (Kato et al. 2013a, 2013b).

5 Fading rate during superoutbursts

5.1 Background

During the superoutburst of an SU UMa-type dwarf nova, there exists an almost exponential slow decline phase. Osaki (1989) was the first to derive the time scale of this slow fading:

$$t_{\rm d} \simeq 8.14 \ {\rm d} \ R_{\rm d,10}^{0.4} \ \alpha_{0.3}^{-0.7}, \tag{2}$$

where $R_{\rm d,10}$ is the disk radius in units of 10^{10} cm and $\alpha_{0.3} = \alpha_{\rm hot}/0.3$.[15] Warner (1995a, 1995b) discussed the dependence of this relation on system parameters, and obtained the following relation:

$$t_{\rm d} \sim t_{\nu} = 17 \ {\rm d} \ \alpha_{\rm hot,-1}^{-4/5} P_{\rm h}^{1/4} m_1^{1/6}, \tag{3}$$

where $P_{\rm h}$ is the orbital period in hr, $\alpha_{\rm hot,-1} = \alpha_{\rm hot}/0.1$, and $m_1 = M_1/M_{\odot}$ (Cannizzo et al. 2010).

Cannizzo et al. (2010) studied the Kepler light curves of V344 Lyr and V1504 Cyg and compared the slow fading rate during the superoutburst with other SU UMa-type dwarf novae. Cannizzo et al. (2010) suggested from Kepler observations that the fading rate has a much stronger dependence on the orbital period than equations (2) and (3).

Cannizzo et al. (2010) postulated that this difference could arise from the strong dependence of the viscosity in quiescence ($\alpha_{\rm cold}$); that is, a smaller $\alpha_{\rm cold}$ gives rise to a larger surface density at the start of the superoutburst and hence a steeper viscous decay.

5.2 Our sample

We undertook in this study a more homogeneous survey of fading rates during the superoutbursts of SU UMa-type dwarf novae; indeed, there was only a limited number of (not necessarily homogeneous) samples listed in Cannizzo et al. (2010). We used the superoutburst data in Kato et al. (2009a, 2010, 2012a, 2013a) and this paper. We did not attempt a complete survey, but chose observations with high quality. We also did not attempt to survey the data in the literature which may be potentially useful. We also excluded deeply eclipsing systems since it is difficult to remove the effect of the eclipses and since these objects usually show a beat phenomenon. Note that the data "with high quality" do not necessarily correspond to the data giving high-quality times of superhump maxima, and the qualification of the data does not agree with the data classification in the tables of outburst observations (such as table 2).

We examined each light curve of a superoutburst (after correction of the difference between different observers) visually and identified the linear part to obtain the fading rate. Some objects tend to brighten when stage C superhumps appear (see also Kato et al. 2003b), and we neglected this part.

We conveniently divided the objects into two categories: ordinary SU UMa-type dwarf novae and WZ Sge-type dwarf novae including candidate period bouncers. Since there is no clear dividing line between ordinary SU UMa-type dwarf novae and WZ Sge-type, we adopted the category in Kato et al. (2009a): the objects that show early superhumps, a manifestation of the 2:1 resonance, and/or the objects with large ($\sim$8 mag) outburst amplitudes and long (several to tens of years) supercycles. The objects with

[15] Note that there are two different definitions of α (cf. subsection 4.3 in Osaki 1996), and α here corresponds to $\alpha = 0.2$ in Smak (1984) or Warner (1995b).

frequent normal outbursts are not included in WZ Sge-type dwarf novae even if the amplitude satisfies this condition.

The results are listed in tables 69 and 70. Unless new variable star designations were given, we used the names of the objects given in the references for the reader's convenience. Note that the errors given in the tables only refer to random errors, and the real errors should be larger due to systematic errors arising from a number of factors, such as poor zero-point calibration, difference between observers, variable weather conditions, poor flat-fielding, atmospheric extinction, and selection of the segment used for calculation. A comparison between different superoutbursts of the same object suggests an order of 0.01–0.02 mag d^{-1} as a typical systematic error.

5.3 Comparison with the previous study

Although Cannizzo et al. (2010) suggested a much steeper dependence of $P_{\rm h}$, our data on SU UMa-type dwarf novae do not show a significant deviation from equations (2) and (3)—see figure 87. The $P_{\rm orb}$-dependence in $t_{\rm d} \propto P_{\rm orb}^{\psi}$ was estimated to be $\psi = 0.38(0.13)$, consistent with the predicted value $\psi = 0.25$ by a 1σ level. For at least ordinary SU UMa-type dwarf novae, we do not need a special explanation for the deviation from this relation.

The case of the difference between V344 Lyr and V1504 Cyg in Cannizzo et al. (2010) appears to reflect the intrinsic difference between different objects, since there appears to be a sufficient scatter among SU UMa-type dwarf novae in our sample. It is possibly related to the condition that V1504 Cyg ($P_{\rm orb} = 1.67$ hr) has an anomalously high outburst frequency, and hence has a higher mass-transfer rate than in other SU UMa-type dwarf nova with similar $P_{\rm orb}$.

It is not clear whether the long outburst of U Gem (Cannizzo et al. 2010) can be compared to these results, partly because the magnitudes of the comparison stars for U Gem used in the 1980s were different from the modern V magnitude (e.g., 9.0 mag for the modern $V = 9.51$ star HD 64813), and the variation in the brighter part of the outburst was systematically underestimated. Furthermore, the VSOLJ record suggests that there were two peaks in the light curve with an intervening temporary fading (to 10 mag around 1985 October 18–19) between them. This fading was recorded by a very skillful observer (H. Narumi).[16] While two AAVSO observers recorded the same fading (10.5 mag on 1985 October 18), other observers tended to give brighter magnitudes as before, which was likely a psychological bias. We thus regard this outburst of U Gem as composed of two different parts and it is inadequate to estimate the linear fading rate.

Although there was also a suggestion that this outburst was a superoutburst with superhumps (Smak & Waagen 2004), Schreiber (2007) questioned the statistical significance of the superhump detection. We also doubt the detection because the resultant period was 0.20 d, which was one fifth of the sampling interval of the same longitude and it could easily be produced by systematic errors. The poor quality of the comparison star sequence at that time and the lack of suitable comparison stars between 9.3 and 10.2 (magnitudes used at the time of the 1985 observation) made the detection of subtle variations such as superhumps by human eyes particularly difficult. There was likely a psychological bias as stated above, and visual observations under such adverse conditions should not be weighed too much.[17]

5.4 WZ Sge-type objects

The other problem in Cannizzo et al. (2010) is that they used the rapidly fading (not linearly fading) part of the WZ Sge-type outbursts. This part of the outburst is different from those of ordinary SU UMa-type dwarf novae in that it reflects the viscous depletion process of the high-mass disk (Osaki 1995b), and also this phase corresponds to early superhumps, which are different from ordinary superhumps. Therefore this part of WZ Sge-type outbursts cannot be directly compared to the linear decline rate in SU UMa-type dwarf novae. Our results in the linear part of the outbursts in WZ Sge-type dwarf novae are in agreement with the $P_{\rm orb}^{1/4}$ dependence for objects with longer $P_{\rm orb}$ (≥ 0.07 d), and these objects (notably RZ Leo and V1251 Cyg) appear to have the same properties as the ordinary SU UMa-type dwarf novae. The fading rates for the systems with shorter $P_{\rm orb}$ appear to be smaller than those expected for the $P_{\rm orb}^{1/4}$ dependence. We interpret that this is an effect of a smaller degree of removal of the angular momentum caused by the tidal instability as explained in the following subsection. Our conclusion is that the linear fading part of WZ Sge-type dwarf novae is essentially the same as for ordinary SU UMa-type dwarf novae and there is no special need for a steep dependence of the quiescent viscosity on the orbital period (nor can the linear fading rate reflect the quiescent viscosity), though a subtle deviation exists in WZ Sge-type dwarf novae with small q.

5.5 Candidate period bouncers and objects with multiple rebrightenings

Among the studied objects, OT J184228.1+483742 (Kato et al. 2013a; Katysheva et al. 2013) and SSS J122221.7−311523 (Kato et al. 2013b) have remarkably

[16] H. Narumi is one of the world's top observers in the history of visual variable star observation (Kiyota 2012), and is renowned for his very accurate observation.

[17] One of the authors (TK) actually visually observed U Gem during this outburst, and realized the difficulty in estimating this object without suitable comparison stars.

Table 70. Rate of slow decline in WZ Sge-type dwarf novae.

Object	Year	Rate*	Error*	Start†	End†	Mean P_{SH} (stage B)‡	Type§	Source‖
LL And	1993	0.035	0.001	49330.9	49334.1	0.05690	1	1
LL And	2004	0.071	0.002	53151.2	53161.3	0.05658	1	1
V455 And	2007	0.133	0.001	54355.3	54366.3	0.05713	1	1
V466 And	2008	0.092	0.001	54722.2	54734.6	0.05720	1	1
V500 And	2008	0.085	0.001	54810.9	54821.0	0.05689	1	1
V572 And	2005	0.123	0.001	53695.0	53704.2	0.05559	1	1
SV Ari	2011	0.074	0.001	55776.6	55796.9	0.05552	1	4
UZ Boo	2003	0.087	0.001	52981.3	52989.4	0.06192	2	1
DY CMi	2008	0.104	0.001	54486.6	54494.6	0.06074	2	1
EG Cnc	1996	0.090	0.001	50425.2	50429.4	0.06034	2	1
AL Com	1995	0.090	0.001	49824.9	49836.2	0.05723	1	1
V1251 Cyg	2008	0.121	0.001	54764.2	54772.1	0.07597	1	1
V2176 Cyg	1997	0.031	0.002	50704.5	50710.7	0.05624	1	1
VX For	2009	0.121	0.001	55092.0	55097.3	0.06133	2	1
PR Her	2011	0.102	0.002	55900.2	55905.6	0.05502	1	4
V592 Her	2010	0.108	0.001	55413.7	55424.1	0.05661	1	2
RZ Leo	2000	0.126	0.001	51903.0	51913.4	0.07866	1	1
RZ Leo	2006	0.123	0.001	53886.0	53896.0	0.07843	1	1
IK Leo	2006	0.048	0.001	54060.8	54065.7	0.05631	1	1
GW Lib	2007	0.088	0.001	54212.3	54223.2	0.05409	1	1
QZ Lib	2004	0.135	0.001	53043.2	53048.9	0.06460	1	1
EZ Lyn	2010	0.135	0.001	55464.9	55471.0	0.05963	2	3
V358 Lyr	2008	0.049	0.001	54793.4	54815.0	0.05563	1	1
V453 Nor	2005	0.122	0.001	53533.9	53543.2	0.06497	1	1
GR Ori	2013	0.110	0.001	56343.4	56352.0	0.05833	1	5
FL Psc	2004	0.139	0.001	53263.8	53271.0	0.05709	1	1
BW Scl	2011	0.100	0.001	55865.0	55877.0	0.05500	1	4
WZ Sge	2001	0.102	0.001	52131.2	52138.2	0.05720	1	1
CT Tri	2008	0.066	0.001	54773.4	54793.0	0.05366	1	1
V355 UMa	2011	0.094	0.001	55604.4	55615.8	0.05809	1	3
HV Vir	1992	0.114	0.002	48744.0	48749.2	0.05828	1	1
HV Vir	2002	0.130	0.001	52281.0	52290.0	0.05827	1	1
HV Vir	2008	0.133	0.001	54517.1	54526.3	0.05832	1	1
V498 Vul	2005	0.106	0.003	53606.4	53612.1	0.05992	1	1
ASAS J102522−1542.4	2006	0.139	0.001	53762.9	53773.0	0.06337	1	1
1RXS J023238.8−371812	2007	0.141	0.001	54379.1	54383.1	0.06617	2	1
MASTER OT J203749.39+552210.3	2012	0.052	0.001	56228.3	56233.7	0.06131	2	6
MASTER OT J211258.65+242145.4	2012	0.127	0.001	56119.2	56124.9	0.06023	2	6
MisV 1443	2011	0.115	0.001	55571.4	55581.5	0.05672	1	3
SDSS J220553.98+115553.7	2011	0.178	0.002	55702.2	55708.0	0.05815	1	4
OT J111217.4−353829	2007	0.050	0.001	54469.2	54493.3	0.05896	1	1
OT J112619.4+084651	2013	0.104	0.001	56308.7	56319.0	0.05489	1	5
OT J213806.6+261957	2010	0.128	0.001	55332.8	55339.9	0.05502	1	2
OT J012059.6+325545	2010	0.089	0.001	55545.0	55553.4	0.05783	1	3
OT J184228.1+483742	2011	0.045	0.001	55841.2	55851.5	0.07234	3	4
OT J232727.2+085539	2012	0.092	0.001	56192.3	56205.1	0.05344	1	5
PNV J06270375+3952504	2013	0.102	0.002	56391.0	56402.4	0.05892	1	5
PNV J19150199+0719471	2013	0.069	0.001	56455.5	56464.9	0.05821	1	8
SSS J122221.7−311523	2013	0.020	0.001	56312.3	56328.3	0.07649	3	7

*In units of mag d^{-1}.
†BJD−2400000.
‡In units of d.
§1: no or one rebrightening, 2: multiple rebrightenings, 3: double superoutburst.
‖1: Kato et al. (2009a), 2: Kato et al. (2010), 3: Kato et al. (2012a), 4: Kato et al. (2013a), 5: this work, 6: Nakata et al. (2013), 7: Kato et al. (2013b), 8. C. Nakata et al. in preparation.

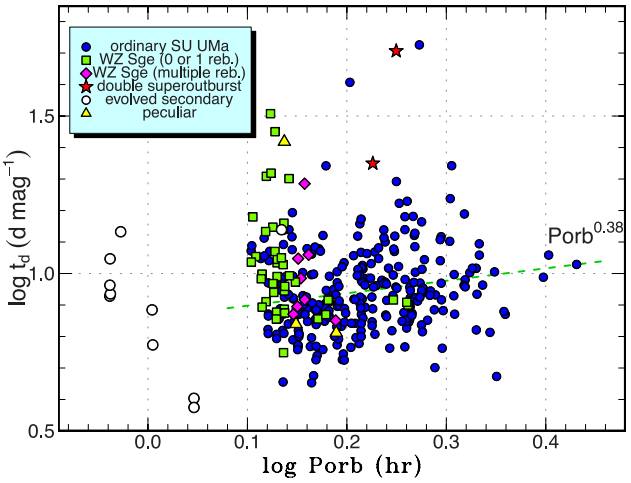

Fig. 87. Dependence of slow fading rate of superoutbursts on the orbital period. The orbital period was estimated from the period of stage B superhumps by using the relation in Kato et al. (2012b). Filled circles, filled squares, filled diamonds, filled stars, open circles, and filled triangles represent ordinary SU UMa-type dwarf novae, WZ Sge-type dwarf novae with zero or one rebrightening, WZ Sge-type dwarf novae with multiple rebrightenings, objects with double superoutbursts (candidate period bouncers), systems with an evolved secondary, and objects with unusually low-amplitude superhumps, respectively.

small slow fading rates compared to the objects with a similar orbital period. These objects are suggested to be candidate period bouncers, whose very low q was inferred from the dynamical precession rates of stage A superhumps (Kato & Osaki 2013b; Kato et al. 2013b).

We first consider the effect of the disk radius on the fading rate. Since there is a relation $t_{\rm d} \propto R_{\rm d}^{0.4}$ [equation (2)], a larger disk would produce a slower fading. The binary's separation A is proportional to $M_1^{1/3}(1+q)^{1/3}P_{\rm orb}^{2/3}$ [cf. equation (2.1b) in Warner 1995a]. The radius of the 3:1 resonance also depends on q as in the equation:

$$r_{3:1} = 3^{(-2/3)}(1+q)^{-1/3}. \quad (4)$$

Combining these effects, the fading rate is 3.6% smaller in the $q = 0.05$ case than in the $q = 0.2$ case. This value is clearly insufficient to explain the observation.

Although the mass of the primary also matters with a dependence of $m_1^{0.13}$, the known primary mass of short-period systems is confined to a relatively narrow region ($M_1 = 0.83\,M_\odot$ with an intrinsic scatter of $0.07\,M_\odot$ for systems with $P_{\rm orb} \leq 0.066$ d; Savoury et al. 2011), and it is unlikely to be the main reason.

We then consider the effect of the disk viscosity in the hot state. Since the theoretical fading rate [equations (2) and (3)] is correlated with $\alpha_{\rm hot}$, we consider that $\alpha_{\rm hot}$ is smaller in these candidate period bouncers. As shown in Kato et al. (2013a, 2013b), the amplitudes of ordinary superhumps in these systems were small compared to those in ordinary SU UMa-type dwarf novae. This likely reflects the very small tidal effect on the disk resulting from low q. The small tidal effect produces a smaller degree of removal of the angular momentum (such as enhanced viscous dissipation in the compressed region; cf. Wood et al. 2011) due to the development of the tidal instability, and the net $\alpha_{\rm hot}$ is expected to be smaller than in higher-q systems. The unusually slow fading rates may become a discriminative signature for candidate period bouncers. A recently discovered WZ Sge-type dwarf nova OT J075418.7+381225 (= CSS 130131:075419+381225), which has an 8 mag amplitude despite the long (0.0716 d) superhump period (C. Nakata et al. in preparation), showed a very slow fading rate [0.0189(3) mag d^{-1}], and is also a likely candidate for a period bouncer. OT J230425.8+062546 (Kato et al. 2012a) also showed a slow fading rate [0.0340(4) mag d^{-1} for the entire plateau, 0.061(1) mag d^{-1} if we restrict ourselves to the portion (after BJD 24455573.5) after the change in the superhump period] despite its relatively long (0.0663–0.0672 d) superhump period. This object also may be a candidate period bouncer.

Most of the objects with multiple rebrightenings (UZ Boo, EG Cnc, DY CMi, VX For, EZ Lyn, MASTER OT J211258.65+242145.4, 1RXS J023238.8−371812) showed fading rates similar to those of ordinary SU UMa-type dwarf novae with a corresponding superhump period. We should, however, note that we selected the linear part of the light curve the same as in ordinary SU UMa-type dwarf novae. At least one of the objects with multiple rebrightenings (VX For) appeared to show a slower fading part before this linear part, and the inclusion of the slower part would produce a smaller fading rate like those of candidate period bouncers. We did not include this slower fading part because this object was observed in high airmass and the mean magnitude was not very well calibrated, which may have produced an artificial trend. The only two WZ Sge-type objects, OT J111217.4−353829 and MASTER OT J203749.39+552210.3, showed smaller fading rates. The former is a WZ Sge-type dwarf nova without a detected rebrightening (Kato et al. 2009a) and the latter showed multiple rebrightenings. The present result seems to favor the recent suggestion that objects showing multiple rebrightenings are not considered to be likely candidates for period bouncers (Nakata et al. 2013).

5.6 Systems with an evolved secondary

The results for the systems with secondary having an evolved core are summarized in table 71. Since equation (2) only weakly depends on q, the decline rate for these ultrashort-$P_{\rm orb}$ objects are generally expected to follow the relation of a smooth extension of ordinary

Table 71. Rate of slow decline in systems with an evolved secondary.

Object	Year	Rate*	Error*	Start†	End†	Mean P_{SH} (stage B)‡	Source§
V485 Cen	2001	0.130	0.003	51999.8	52005.2	0.04207	1
V485 Cen	2013	0.169	0.003	56399.8	56402.9	0.04214	3
GZ Cet	2003	0.073	0.001	52996.9	53007.1	0.05677	1
EI Psc	2001	0.249	0.001	52218.0	52221.1	0.04635	1
EI Psc	2009	0.266	0.015	54993.6	54995.7	0.04635	1
CSS J102842.8−081930	2009	0.118	0.002	54923.0	54925.3	0.03814	1
CSS J102842.8−081930	2010	0.109	0.002	55544.7	55551.3	0.03815	3
CSS J102842.8−081930	2012	0.090	0.001	55958.6	55963.9	0.03817	2
CSS J102842.8−081930	2013	0.116	0.001	56394.3	56400.5	0.03820	3
SBS 1108+574	2012	0.074	0.001	56040.6	56050.7	0.03912	2

*In units of mag d^{-1}.
†BJD−2400000.
‡In units of d.
§1: Kato et al. (2009a), 2: Kato et al. (2013a), 3: this work.

Table 72. Rate of slow decline in peculiar systems.

Object	Year	Rate*	Error*	Start†	End†	Mean P_{SH} (stage B)‡
CC Scl	2011	0.145	0.004	55870.5	55873.8	0.06001
MASTER OT J072948.66+593824.4	2012	0.154	0.002	55976.3	55978.7	0.06625
OT J173516.9+154708	2011	0.038	0.001	55739.4	55742.2	0.05827

*In units of mag d^{-1}.
†BJD−2400000.
‡In units of d.

SU UMa-type dwarf novae. Figure 87 appears to confirm this expectation. Several objects need more explanation. Although EI Psc showed larger decline rates than expected, both superoutbursts (2001, 2009) were observed in their late stage (cf. Uemura et al. 2002; Skillman et al. 2002; Kato et al. 2009a), and these measurements may not reflect the slowly fading part proper. Future observation of the full superoutburst is awaited. SBS 1108+574 has a light secondary and shows infrequent outbursts (Kato et al. 2013a; Carter et al. 2013; Littlefield et al. 2013), resembling a WZ Sge-type dwarf nova. The relatively slow decline rate of this object may be explained in the same way as for WZ Sge-type dwarf novae.

5.7 Systems with unusually low-amplitude superhumps

In Kato et al. (2013a), we reported on three systems with unusually low-amplitude superhumps. These systems apparently showed two closely separated periods, one of which is likely the superhump period. The results for these systems are listed in table 72 (we tentatively chose the longer period as the superhump period). Both CC Scl and OT J072948.66+593824.4 showed usual decline rates comparable to the systems with similar P_{SH}. OT J173516.9+154708, however, showed a very slow decline rate. Although only a limited segment of the light curve was recorded, this decline rate might suggest a candidate period bouncer.

6 Comment on dwarf novae in the OGLE data

Quite recently, Mroz et al. (2013) reported on detection of a number of dwarf novae in the OGLE-III data. They reported a number of "SU UMa-type dwarf novae" having supercycles in the range of 20–90 d, and claimed that there is no gap in the distribution of supercycles between (ordinary) SU UMa-type dwarf novae and ER UMa stars. Since this conclusion is against the knowledge based on which we compiled the present series of papers starting from Kato et al. (2009a), we examine here the validity of their claim. We also checked superhump periods reported in Mroz et al. (2013) and tried to interpret the data referring to the superhump stages by our definition. The results are not included in table 2. We used the publicly available electronic data for these objects.

6.1 OGLE-GD-DN-001

As stated in Mroz et al. (2013), this object showed four post-superoutburst rebrightenings. In the light curve, there was

a jump around BJD 2454177–2454178. This jump most likely corresponds to the growth of ordinary superhumps (cf. Nakata et al. 2013). After this we detected superhumps with a mean period of 0.06067(2) d by profile-fitting, using the MCMC method (Kato et al. 2010). Although early superhumps were expected before this jump, we could not detect a convincing signal. The duration of this phase was only 6 d, which is much shorter than those of ordinary WZ Sge-type dwarf novae (see a discussion of the implications in Nakata et al. 2013).

6.2 OGLE-GD-DN-007

We obtained a mean superhump period of 0.08083(2) d using the 2007 and 2008 superoutbursts, assuming a common period and independent phases between them. An interesting point is that there was a precursor 10 d prior to the 2008 superoutburst. We analyzed the data between this precursor and the main superoutburst, and obtained a possible period of 0.08201(6) d. This long period is consistent with the expected period of stage A superhumps, and the growing stage of the superhump took place during the quiescence state between the precursor and the main superoutburst. This finding strengthens the TTI model in which the superhumps play a central role in triggering a superoutburst (cf. Osaki & Kato 2014). We detected a possible signal of the orbital period at 0.0782183(4) d, which needs future verification.

6.3 OGLE-GD-DN-008

We obtained a mean superhump period of 0.08400(1) d during the 2007 superoutburst. This outburst had a precursor which was followed by a small dip. During this dip, the superhump was not yet evident. This phenomenon exactly reproduces the Kepler observations of V344 Lyr and V1504 Cyg (Osaki & Kato 2013a, 2013b) and again strengthens the TTI model. In quiescence, this object showed fairly strong orbital humps with a mean amplitude of 0.23 mag. The orbital period is 0.080919(1) d. The resultant $\varepsilon = 3.7\%$ is typical of this orbital period.

6.4 OGLE-GD-DN-014

This object showed two post-superoutburst rebrightenings. During the plateau phase, we obtained superhumps with a mean period of 0.08921(2) d. This period is much longer than those of most WZ Sge-type dwarf novae with multiple rebrightenings (cf. Nakata et al. 2013). The object may be similar to QZ Ser (T. Ohshima et al. in preparation), which has an orbital period of 0.083161 d with an undermassive, evolved secondary, and showed two post-superoutburst rebrightenings. OGLE-GD-DN-014 may also have an unusual secondary, and would be worth further study.

6.5 OGLE-GD-DN-039

We obtained a mean superhump period of 0.08347(1) d using three recorded superoutbursts. The duration of the superoutburst (13.0 d) comprises 16% of the supercycle (81.3 d), which is much smaller than that in ER UMa (46%) in 1995 (Kato & Kunjaya 1995). OGLE-GD-DN-039 resembles BF Ara which has a supercycle of 83.4 d (Kato et al. 2001c, 2003a) and a superoutburst duration of (11–17 d). Kato et al. (2003a) suggested that BF Ara and SS UMi (Kato et al. 1998, 2000a) are ordinary SU UMa-type dwarf novae with the shortest supercycle, which are on a smooth extension of the already known objects. OGLE-GD-DN-039 apparently fits this category.

6.6 Objects with short supercycles

Mroz et al. (2013) reported four objects with a very short (24.5–86.8 d) supercycle (OGLE-GD-DN-003, OGLE-GD-DN-004, OGLE-GD-DN-009, and OGLE-GD-DN-036) and claimed that they fill the gap in the distribution of supercycles between ordinary SU UMa-type dwarf novae and ER UMa stars. We examined the OGLE light curves of these objects, and could not find any evidence of superhumps during the long outbursts of these objects. Furthermore, often the light curves of these long outbursts did not have the linear segment which is present in superoutbursts (cf. section 5). The duration of the long outbursts is shorter (10–14 d) than that in typical superoutbursts. Mroz et al. (2013) detected a period of 0.1310(3) d in OGLE-GD-DN-009, which is a typical value for an SS Cyg-type dwarf nova. Although we cannot completely exclude the possibility that some of these objects resemble the unusual object RZ LMi (Robertson et al. 1995; Nogami et al. 1995; Olech et al. 2008), which shows low superhump amplitudes and has a superoutburst of short duration, we conclude that these OGLE objects are SS Cyg-type dwarf novae. If this is the case, the discussion on the distribution of the supercycle in Mroz et al. (2013) is pointless. In figure 88, one can see how well an SS Cyg-type dwarf nova (CY Lyr, $P_{\rm orb} = 0.207584(7)$ d; Thorstensen et al. 1998) imitates a quasi-supercycle of 50–60 d. Another dwarf nova VW Vul [$P_{\rm orb} = 0.16870(7)$ d] has also been long thought likely to be an SU UMa-type dwarf nova based on its "superoutburst"-like behavior (e.g., Shafter 1985; Robinson et al. 1987).

Patterson et al. (2013) recently proposed an evolutionary scenario where ER UMa stars are transitional objects during the cooling phase of post-eruption classical novae (the idea

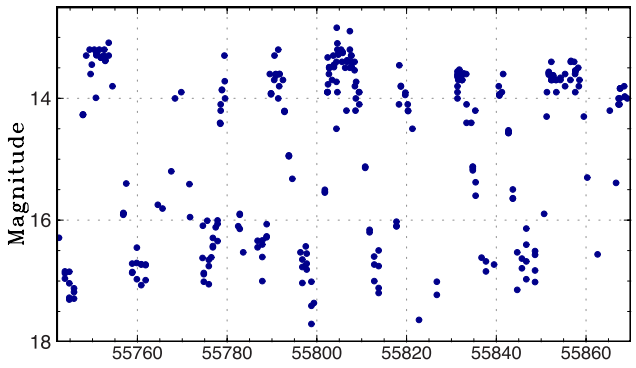

Fig. 88. Light curve of CY Lyr from AAVSO observations. Long outbursts sometimes appear quasi-cyclically.

was not new and had already been proposed in Kato & Kunjaya 1995). Following Patterson et al. (2013), post-eruption classical novae below the period gap spend $\sim 10^3$ yr in a state like BK Lyn (borderline novalike and ER UMa-type object), $\sim 10^4$ yr in a state like ER UMa, and a longer time with a further reduced mass-transfer rate. This picture predicts that ER UMa stars are ten times more numerous than BK Lyn-like stars, and intermediate objects between ER UMa stars and ordinary SU UMa-type dwarf novae are 10–100 times more numerous than ER UMa stars. Apparently, this is not what is actually observed (see figure 14 in Mroz et al. (2013) after omitting the four objects discussed here). This tendency is even clearer on the mass-transfer rate versus $P_{\rm orb}$ plane (figure 9 in Patterson et al. 2013). While in the longer-$P_{\rm orb}$ region ($P_{\rm orb} \geq 0.06$–0.07 d) ER UMa stars and ordinary SU UMa-type dwarf novae look like to form a continuum,[18] the gap between ER UMa stars and ordinary SU UMa-type dwarf novae still remains in the short-$P_{\rm orb}$ ($P_{\rm orb} \leq 0.06$ d) region. These two problems (number density and lack of intermediate objects in the short-$P_{\rm orb}$ region) have not yet been solved even with the OGLE data, and the picture may not be as simple as that in Patterson et al. (2013).

7 Notes on certain objects

In this section, we provide new phenomena and findings for the objects we treated in the earlier works in this series. These subsections provide supplementary information to earlier studies, mainly reporting on new phenomena occurring in the objects we reported earlier. Subsection 7.4 is provided to illustrate the result of two-dimensional Lasso power spectral analysis in order to help readers interpret the two-dimensional Lasso power spectral analysis by comparing our familiar objects, WZ Sge and HT Cas, since this method is first introduced for the ground-based data in this paper. Subsection 7.5 is a new application of the method in Kato and Osaki (2013b). Since the sources of the data were shown (with some additional data for BK Lyn) in earlier papers or the collective data (such as data from the AAVSO) were used, these objects are not included in tables 1 and 2.

[18] Note that Patterson et al. (2013) changed the original classification of ER UMa stars and included SU UMa-type dwarf novae with short supercycles.

7.1 BK Lyncis returned to novalike state

Since we have developed a new technique of two-dimensional power spectrum using Lasso after the publication of Kato et al. (2013a), we present a power spectrum of the corresponding data. The data include those obtained by E. de Miguel in addition to the ones in Kato et al. (2013a). Osaki and Kato (2014) also represent the result of period analysis using PDM to the question raised by Smak (2013). The continuous presence of negative superhumps in the 2012 data can be very clearly seen (figure 89). Positive superhumps were only present during the early phase of the superoutbursts the same as in ER UMa (Ohshima et al. 2012, 2014). The frequency of the negative superhumps varied systematically; the frequency reaches the minimum just after the superoutburst and increases toward

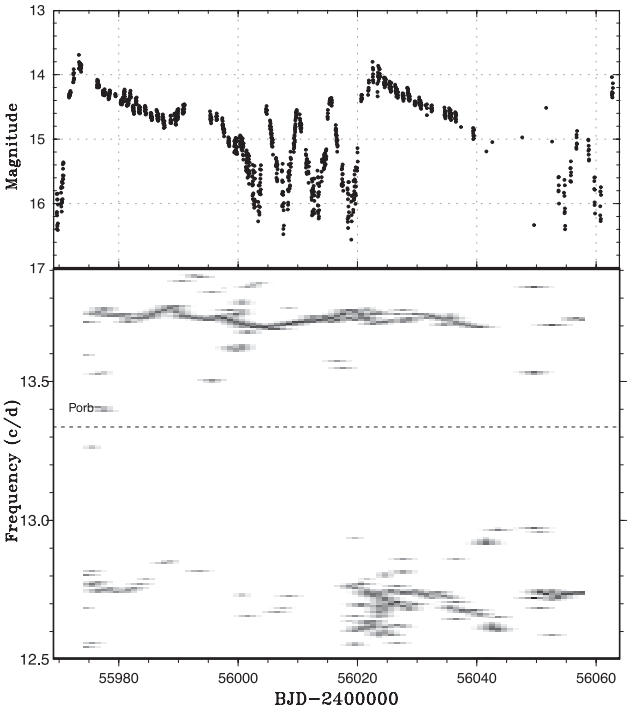

Fig. 89. Two-dimensional Lasso period analysis of BK Lyn (2012). Upper: Light curve (binned to 0.02 d). Lower: Two-dimensional Lasso analysis (10 d window, 1 d shift, and $\log\lambda = -7.8$). The signal of negative superhumps was continuously present with a systematic variation of the frequency in relation to the supercycle phase. Positive superhumps only appeared during the early phase of the superoutbursts. Note that the density of the spectrum varies according to the density of observations. No spectrum was detected when sufficiently long observation runs were not obtained.

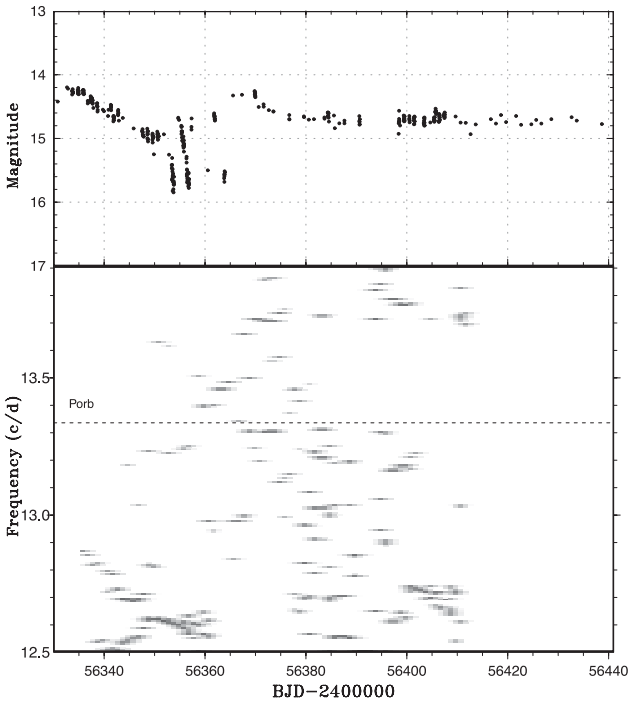

Fig. 90. Two-dimensional Lasso period analysis of BK Lyn (2013). Upper: Light curve (binned to 0.02 d). Lower: Two-dimensional Lasso analysis (10 d window, 1 d shift, and $\log\lambda = -7.8$). The signal of negative superhumps was not detected and positive superhumps were the prevalent signal. The object reached a standstill (novalike state) after the second superoutburst.

the end of the supercycle. Since the bin used for drawing this figure (10 d) is longer than the interval of normal outbursts, in contrast to V1504 Cyg or V344 Lyr (Osaki & Kato 2013b), the frequency variation associated with the ignition of normal outbursts was not resolved in this figure. This short-term variation can be better recognized with the PDM analysis, and is presented in Osaki and Kato (2014).

On the other hand, the object did not show a strong signal of negative superhumps in 2013 February–March (including a superoutburst in BJD 2456333–2456352; figure 90). Following the next outburst (this outburst appears to be a superoutburst, but its maximum was much fainter than the maxima of other superoutbursts; no time-resolved photometry is available other than that on BJD 2456369, when unidentified 0.04 d semiperiodic variations with an amplitude of 0.1 mag were recorded) on BJD 2456365, the object entered into a standstill or a novalike state. This transition was quite similar to that of a Z Cam-type dwarf nova as well as that in the model calculation of a higher mass-transfer rate with system parameters of ER UMa (Osaki 1995a). The interval between the superoutbursts, however, did not increase so much as in Osaki (1995a) just before the object entered into the novalike state. This transition to a novalike state has confirmed that the object can undergo a state transition between dwarf nova state and novalike state (the same as in Z Cam-type dwarf novae) and the transition from the novalike state to the dwarf nova-type state in 2004–2012 cannot be directly attributed to secular evolution in a cooling post-nova state as proposed in Patterson et al. (2013). As suggested in Kato et al. (2013a), the time-scale (several years) of this transition appears to be too short compared to the proposed duration (∼1900 yr) of the post-nova state. This transition may be driven either by a varying mass-transfer rate or by the disappearance of the disk tilt. Since the interval between the superoutbursts did not show variations as expected from the increased mass transfer, the latter possibility might deserve consideration. In the presence of disk tilt, the accretion stream hits the inner part of the disk, and it is expected to provide less material in the outer part of the disk compared to a condition without a tilt. Under this condition, the mass-transfer rate in the outer part of the disk may be insufficient to maintain the hot (novalike) state. It would be very interesting to know how the disk tilt might govern the disk dynamics, and this needs to be investigated in more detail.

7.2 Variation in supercycles in CR Bootis

In Kato et al. (2013a), we reported that CR Boo in 2012 showed a period variation of superhumps very similar to those of hydrogen-rich SU UMa-type dwarf novae. In the meantime, Honeycutt et al. (2013) quite recently published the RoboScope light curve of CR Boo in 1990–2012. It has become apparent that this object has at least two distinct states: (a) fainter quiescence and regular superoutbursts (1990 December–1991 July, 1994 May–1995 January, 1997 May–1999 March, likely 1999 July, and 2007 November–2012 August), which corresponds to the "ER UMa-like" state reported by Kato et al. (2000b); (b) brighter quiescence with frequent outbursts (1992 December–1994 April, 1995 February–1997 April, 1999 March–2007 June). The behavior in the latter state was somewhat variable and varied from regular outbursts, regular short superoutbursts to almost standstill (in 1996 May–July and 1997 April). If short superoutbursts were present in the latter state, the intervals of these outbursts tended to be 10–20 d (Kato et al. 2001a). Note that Honeycutt et al. (2013) used a criterion of superoutbursts different from ours; we distinguished superoutbursts by using the behavior rather than the magnitude, i.e., based on the presence of a slowly fading segment (cf. section 5). We must also note that there is no guarantee that superhumps were excited in these short superoutbursts, but we regard it likely, considering the presence of superhumps in similar states (Patterson et al. 1997b).

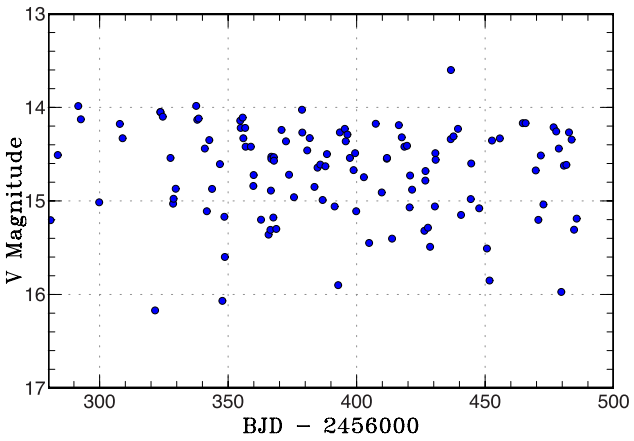

Fig. 91. AAVSO light curve of CR Boo (2013). The ∼46 d supercycle seen in the 2012 data disappeared. Instead, the object showed frequent outbursts with a typical interval of 10–20 d.

Our 2012 observation in Kato et al. (2013a) happened to record the most typical "ER UMa-like" state of this object. Ramsay et al. (2012a) also recorded this state in 2009–2011. The situation was very different in the season of 2012 December–2013 July. In this season, the object showed bright quiescence and frequent outbursts (the second state of those described above). The cycle lengths of superoutbursts were ∼ 15 d with some variation (figure 91). It looks like this object switches between these two states and the maximum duration of each state is several years. The reason why the object shows these distinct states is not yet known.

7.3 Unusual superoutbursts in NY Serpentis

In the late 1990s, NY Ser was known to show superoutbursts separated by 85–100 d and normal outbursts with recurrence times of 6–9 d (Nogami et al. 1998; Iida et al. 1995; figure 92). We have, however, noticed that this pattern disappeared recently (this tendency may be even traced back to 2009–2010) in the AAVSO data (figure 93).

In 2011, there was a distinct superoutburst around BJD 2455714–2455730. This outburst has been confirmed to be a genuine superoutburst by the presence of superhumps on BJD 2455719–2455720. The outburst immediately preceding this superoutburst (BJD 2455700) was unusual in that it showed slower decline than in normal outbursts. Although there may have been superhumps, the limited data hindered secure detection. Around BJD 2455779–2455783, there was an outburst of an intermediate duration (∼ 4 d), 65 d after the superoutburst.

In 2012, long superoutbursts were not apparent (we cannot exclude a long superoutburst around BJD 2456116–2456126), and only normal outbursts and outbursts with intermediate duration (around BJD 2456000, 2456024,

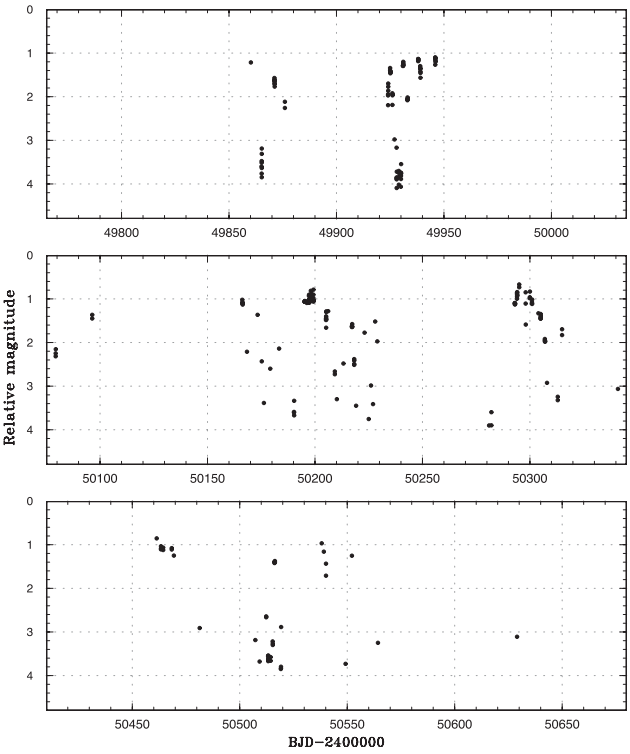

Fig. 92. Light curve of NY Ser in the 1990s. The data were taken from Nogami et al. (1998) and were binned to 0.02 d. The magnitude was relative to the comparison star in Nogami et al. (1998).

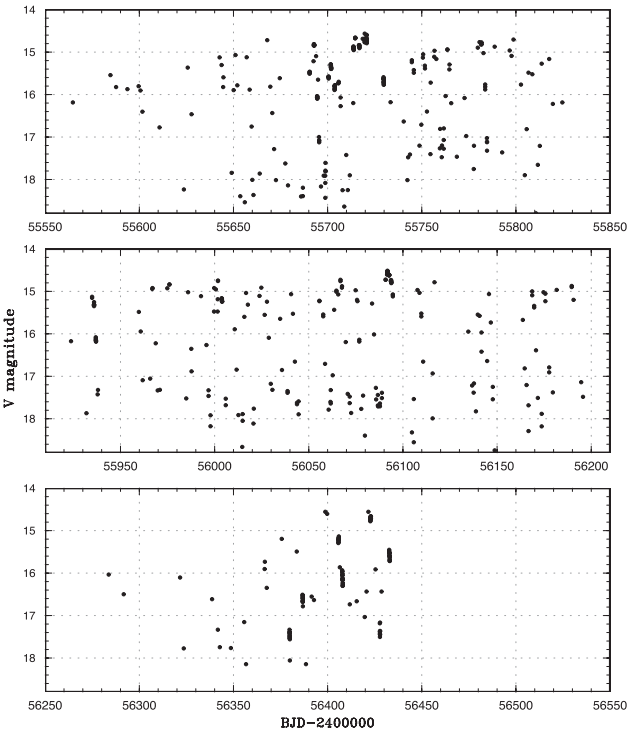

Fig. 93. Light curve of NY Ser in 2011–2013. The data were taken from the AAVSO database and were binned to 0.02 d.

2456064, 2456091, 2456108) were frequently recorded. The tendency appears to be the same as in 2013.

The interval of these outbursts with intermediate duration was 17–40 d, which is much shorter than the supercycles recorded in Nogami et al. (1998). There appear to be at least two different states in NY Ser, the same as in CR Boo (subsection 7.2). The quiescent brightness or the outburst amplitudes were, however, not so different in these states, unlike CR Boo. Observations of superhumps during such states might shed light on the mechanism of the change in the outburst behavior.

7.4 Two-dimensional Lasso period analysis of WZ Sagittae and HT Cassiopeiae

Since we have successfully obtained a two-dimensional Lasso spectrum for the long cadence Kepler data of V585 Lyr (Kato & Osaki 2013a) using two spectral windows, we applied the same technique to the 2001 superoutburst of WZ Sge using the data in Kato et al. (2009a). This application was motivated by the report of the possible detection of transient negative superhumps in Patterson et al. (2002) and by the possible detection of negative superhumps in FL Psc during the post-superoutburst stage (Kato et al. 2012a). The result is shown in figure 94. Unlike Kepler data, ground-based observations have uneven coverage with occasional gaps. One should remember that the detected frequencies may not be real signals. We used a long window size of 10 d for resolving different signals, rather than trying to follow the rapid frequency variation (note that the initial part has a dirty spectrum because this part contained the segments of early superhumps and ordinary superhumps together). The orbital signal was present both in the fundamental and in the first overtone. The signal of positive superhumps with variable frequency was recorded during the superoutburst plateau, rebrightening phase, and post-superoutburst stage. Possible signals of negative superhumps were present during the dip phase and rebrightening phases near the frequencies 17.85 c/d and 35.4 c/d, as suggested by Patterson et al. (2002). There was also a possible signal at around 35.9 c/d. We consider the detection of 17.85 c/d likely, because this frequency did not match any side lobe of the frequencies of the orbital signal and (positive) superhumps, although there might remain a

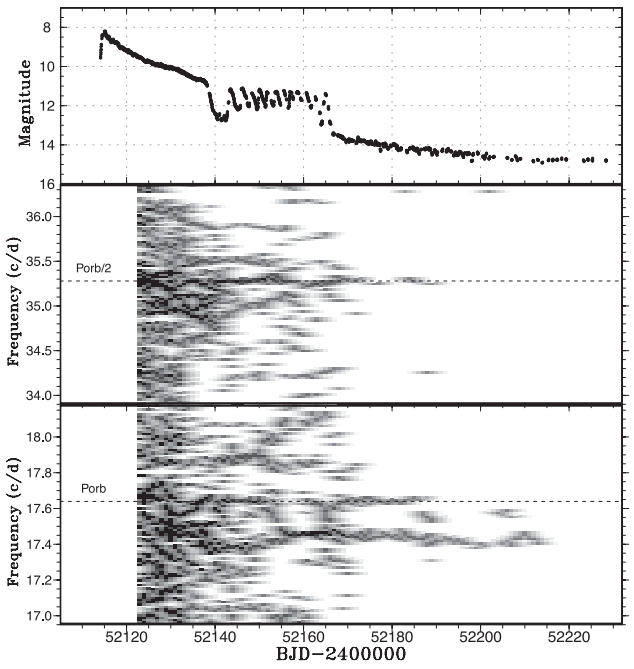

Fig. 94. Lasso analysis of WZ Sge (2001). Above: Light curve. The data were taken from Kato et al. (2009a) and were binned to 0.02 d. Center: First overtone of the superhump and orbital signals. Below: Fundamental of the superhump and orbital signal. The orbital signal was present both in the fundamental and in the first overtone. The signal of positive superhumps with variable frequency was recorded during the superoutburst plateau, rebrightening phase, and post-superoutburst stage. Possible signals of negative superhumps were present during the dip phase and rebrightening phases near the frequencies 17.85 c/d and 35.4 c/d, as suggested by Patterson et al. (2002). There was also possibly a signal around 35.9 c/d. The parameter $\log\lambda = -3.8$ was used. The width of the sliding window and the time step used are 10 d and 1 d, respectively.

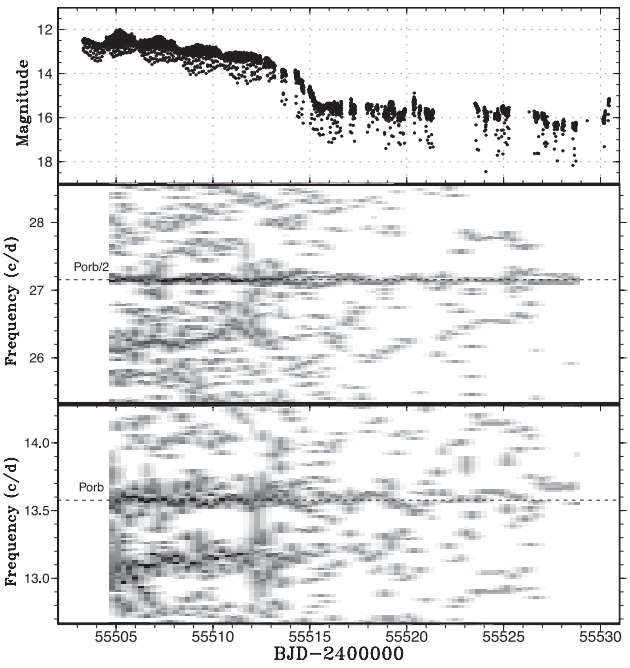

Fig. 95. Lasso analysis of HT Cas (2010). Above: Light curve. The data were taken from Kato et al. (2009a) and were binned to 0.003 d. Center: First overtone of the superhump and orbital signals. Below: Fundamental of the superhump and orbital signal. The orbital signal was present both in the fundamental and in the first overtone. The signal of positive superhumps with variable frequency was recorded during the superoutburst plateau and the post-superoutburst stage. The decay of the superhump signal was quicker than in WZ Sge. The parameter $\log\lambda = -5.3$ was used. The width of the sliding window and the time step used are 3 d and 0.3 d, respectively.

possibility that strong variation of the orbital signal could produce such a signal as described in Patterson et al. (2002). Our result seems to strengthen the detection of these signals in Patterson et al. (2002). If these signals are indeed negative superhumps and arise from the disk tilt, such a tilt could affect the behavior of the disk (Ohshima et al. 2012; Osaki & Kato 2013a). It is interesting that the signal of possible negative superhumps only appeared after the dip and during the rebrightenings. Although we have no concrete explanation, the repeated small-amplitude rebrightenings in WZ Sge may be somehow related to the disk tilt.

Figure 95 presents a two-dimensional Lasso analysis of the 2010 superoutburst of HT Cas (Kato et al. 2012a). No strong negative superhumps were detected. There was possibly an increase of the superhump frequency when the system started to fade more quickly (BJD 2455513). This increase in the superhump frequency was probably a result of the decrease in the pressure effect. At other times, the superhump frequency rather monotonously decreased, reflecting the decreasing disk radius.

7.5 Late-stage superhumps in KV Ursae Majoris

We may apply the analysis of precession frequency to low-mass X-ray binaries (LMXBs). As shown in Pearson (2006), the disk in LMXBs appears to have pressure effects different from CVs, possibly due to the higher temperature. We may avoid the problem of the unknown pressure effect by using superhumps after the outburst. There is such an observation in KV UMa = XTE J1118+480 (Zurita et al. 2002), reporting superhumps near quiescence having $\varepsilon^* = 0.0033$. If we assume that the disk radius in KV UMa after the outburst is similar to those of SU UMa-type dwarf novae (Kato & Osaki 2013b), we can expect a radius in a range of 0.30–0.38A. The mass ratio is estimated to be $q = 0.023$ for 0.30A and $q = 0.014$ for 0.38A. Although these values are slightly smaller than spectroscopically determined mass ratios, e.g., 0.037(7) (Orosz 2001), 0.027(9) (González Hernández et al. 2008), 0.024(9) or 0.0435(100) (Calvelo et al. 2009), the value for the radius 0.30A is marginally in agreement with the spectroscopic value considering the intrinsic uncertainty in analysis of the spectroscopic data. If a disk radius typical of post-outburst LMXBs is established, the superhump period would become a promising tool for determining the mass ratio, and hence the mass of the black hole or neutron star in LMXBs.

8 Summary

Continuing the project described by Kato et al. (2009a), we collected times of superhump maxima for SU UMa-type dwarf novae mainly observed during the 2012–2013 season. Most of the short-$P_{\rm orb}$ objects showed period variations consistent with the trend reported up to Kato et al. (2013a). We found three objects (V444 Peg, CSS J203937, and MASTER J212624) having strongly positive $P_{\rm dot}$ despite the long $P_{\rm orb}$. It appears that such $P_{\rm dot}$-objects are more numerous in the long-$P_{\rm orb}$ region than expected. V444 Peg also showed a post-superoutburst rebrightening.

We studied ten new WZ Sge-type dwarf novae and updated the relation between $P_{\rm orb}$ and the rebrightening type. Although many of them were neither discovered early nor sufficiently observed to determine the duration of the early superhump stage and the presence of rebrightenings, a greatly increased number of WZ Sge-type dwarf novae illustrates the ability of modern transient surveys, especially the MASTER survey.

By using the period of growing stage (stage A) superhumps, we obtained mass ratios for seven objects and updated the $P_{\rm orb}$–q relation. This result strengthened the two conclusions in Kato and Osaki (2013b) that most WZ Sge-type dwarf novae have secondaries close to the border of the lower main sequence and brown dwarfs, and that most of the objects have not yet reached the evolutionary stage of period bouncers. Combined with the $P_{\rm orb}$–q diagram, our result seems to support the minimum period at around 0.054–0.055 d in ordinary hydrogen-rich CVs.

We made a pilot survey of the decline rate of the slowly fading part of SU UMa-type and WZ Sge-type outbursts. The decline time-scale was found to generally follow the expected $P_{\rm orb}^{1/4}$, and WZ Sge-type outbursts also generally follow this trend. There is no need to introduce a steep dependence of the quiescent viscosity parameter $\alpha_{\rm cold}$ on $P_{\rm orb}$ as suggested by Cannizzo et al. (2010). There are, however, some objects which show a significantly slower decline rate, and we consider these objects likely candidates for period bouncers. MASTER OT J165236.22+460513.2 showed an outburst with a large amplitude and with long-period ($\sim$0.084 d) superhumps. This object might be a period bouncer. We also suggested OT J173516.9+154708 as a candidate period bouncer.

In addition to these main results:

- We reexamined dwarf novae discovered in Mroz et al. (2013) and indicated that their claim of detections of a number of SU UMa-type dwarf novae with a short supercycle is unfounded.
- BK Lyn, which was recently found to show a transition from a novalike object to an ER UMa-type dwarf nova, again returned to the novalike state in 2013. This observation indicates that the transition to the ER UMa-type state does not immediately reflect the secular decrease of the mass-transfer rate as proposed by Patterson et al.

(2013). Instead, the supercycle length did not significantly vary before the transition to the novalike state, indicating that the mass-transfer rate did not change greatly. The signal of negative superhumps showed a dramatic disappearance in 2013, and this may be related to the transition to the novalike state.

- CR Boo stopped showing "ER UMa-like" state with $\sim$46 d supercycle in the 2012–2013 season. The object instead showed outbursts with intermediate duration and smaller outburst amplitudes.
- NY Ser showed frequent occurrence of outbursts with intermediate duration (likely faint superoutbursts) in 2012–2013. The shortest interval was 17 d.
- We applied a least absolute shrinkage and selection operator (Lasso) power spectral analysis, which has been proven to be very effective in analyzing the Kepler data, to the ground-based photometry. We detected possible negative superhumps in TY PsA and confirmed the result of possible detection of negative superhumps in WZ Sge (2001) by Patterson et al. (2002). The frequency variation of positive superhumps was also well visualized in WZ Sge and HT Cas (2010).
- We studied whether our interpretation of the precession rate of positive superhumps can be applied to black-hole binaries. An application to KV UMa resulted in $q = 0.023$, assuming a disk radius of $0.30A$ after the outburst. This method could become a promising tool in determining the mass ratios if a disk radius typical of post-outburst black-hole binaries is established.

Acknowledgments

This work was supported by a Grant-in-Aid "Initiative for High-Dimensional Data-Driven Science through Deepening of Sparse Modeling" from the Ministry of Education, Culture, Sports, Science and Technology (MEXT) of Japan. The authors are grateful to the observers of the VSNET Collaboration and to VSOLJ observers who supplied vital data. We acknowledge with thanks the variable star observations from the AAVSO International Database contributed by observers worldwide and used in this research. This work is deeply indebted to outburst detection and announcement by a number of variable star observers worldwide, including participants of CVNET and BAA VSS alert. We thank Professor Yoji Osaki for his comments on the discussion on the decay rate of superoutbursts and the interpretation of BK Lyn. The CCD operation of the Bronberg Observatory is partly sponsored by the Center for Backyard Astrophysics. The CCD operation by Peter Nelson is on loan from AAVSO, funded by the Curry Foundation. We are grateful to the Catalina Real-time Transient Survey team for making their real-time detection of transient objects available to the public.

References

Arai, A., & Nogami, D. 2013, Astronomer's Telegram, 4811
Araujo-Betancor, S., et al. 2005, A&A, 430, 629
Augusteijn, T., van der Hooft, F., de Jong, J. A., & van Paradijs, J. 1996, A&A, 311, 889
Augusteijn, T., van Kerkwijk, M. H., & van Paradijs, J. 1993, A&A, 267, L55
Augusteijn, T., & Wisotzki, L. 1997, A&A, 324, L57
Bailey, J. 1979, MNRAS, 189, 41P
Balanutsa, P., et al. 2012a, Astronomer's Telegram, 4446
Balanutsa, P., et al. 2012b, Astronomer's Telegram, 4682
Balanutsa, P., et al. 2013, Astronomer's Telegram, 4956
Barclay, T., Still, M., Jenkins, J. M., Howell, S. B., & Roettenbacher, R. M. 2012, MNRAS, 422, 1219
Barwig, H., Kudritzki, R. P., Vogt, N., & Hunger, K. 1982, A&A, 114, L11
Busch, H., Häussler, K., & Splittgerber, E. 1979, Veröff. Sternw. Sonneberg, 9, 125
Calvelo, D. E., Vrtilek, S. D., Steeghs, D., Torres, M. A. P., Neilsen, J., Filippenko, A. V., & González Hernández, J. I. 2009, MNRAS, 399, 539
Cannizzo, J. K. 2012, ApJ, 757, 174
Cannizzo, J. K., Smale, A. P., Wood, M. A., Still, M. D., & Howell, S. B. 2012, ApJ, 747, 117
Cannizzo, J. K., Still, M. D., Howell, S. B., Wood, M. A., & Smale, A. P. 2010, ApJ, 725, 1393
Carter, P. J., et al. 2013, MNRAS, 431, 372
Copperwheat, C. M., et al. 2013, Astronomer's Telegram, 5195
Denisenko, D., et al. 2012a, Astronomer's Telegram, 4475
Denisenko, D., et al. 2012b, Astronomer's Telegram, 4506
Denisenko, D., et al. 2012c, Astronomer's Telegram, 4324
Denisenko, D., et al. 2012d, Astronomer's Telegram, 4441
Denisenko, D., et al. 2012e, Astronomer's Telegram, 4488
Denisenko, D., et al. 2013a, Astronomer's Telegram, 5111
Denisenko, D., et al. 2013b, Astronomer's Telegram, 5049
Denisenko, D., et al. 2013c, Astronomer's Telegram, 4881
Denisenko, D. V. 2012, Astron. Lett., 38, 249
Dillon, M., et al. 2008, MNRAS, 386, 1568
Downes, R. A. 1990, AJ, 99, 339
Drake, A. J., et al. 2009, ApJ, 696, 870
Erastova, L. K. 2011, Astrophysics, 54, 143
Fernie, J. D. 1989, PASP, 101, 225
Gänsicke, B. T., et al. 2003, ApJ, 594, 443
Garbusov, G. A. 1979, Perem. Zvezdy, Prilozh., 3, 639
González Hernández, J. I., Rebolo, R., Israelian, G., Filippenko, A. V., Chornock, R., Tominaga, N., Umeda, H., & Nomoto, K. 2008, ApJ, 679, 732
Goranskij, V. P. 1972, Astron. Tsirk., 696
Goranskij, V. P. 1977, Astron. Tsirk., 955, 8
Gorbovskoy, E. S., et al. 2013, Astron. Rep., 57, 233
Green, R. F., Ferguson, D. H., Liebert, J., & Schmidt, M. 1982, PASP, 94, 560
Harvey, D., Skillman, D. R., Patterson, J., & Ringwald, F. A. 1995, PASP, 107, 551
Harvey, D. A., & Patterson, J. 1995, PASP, 107, 1055
Hirose, M., & Osaki, Y. 1993, PASJ, 45, 595
Holtgrewe, K. S., & Durig, D. T. 2002, J. Am. Assoc. Variable Star Obs., 31, 69
Honeycutt, R. K., Adams, B. R., Turner, G. W., Robertson, J. W., Ost, E. M., & Maxwell, J. E. 2013, PASP, 125, 126

Howell, S. B., Schmidt, R., DeYoung, J. A., Fried, R., Schmeer, P., & Gritz, L. 1993, PASP, 105, 579
Iida, M., Nogami, D., & Kato, T. 1995, IBVS, 4208
Imada, A., Kubota, K., Kato, T., Nogami, D., Maehara, H., Nakajima, K., Uemura, M., & Ishioka, R. 2006, PASJ, 58, L23
Ishioka, R., et al. 2002, A&A, 381, L41
Itagaki, K., et al. 2012, Cent. Bur. Electron. Telegrams, 3228
Jiang, L.-L., Jiang, F.-Z., Li, Z.-Y., Zhao, Y.-H., & Gu, Q.-S. 2010, Chin. J. Astron. Astrophys., 34, 265
Jurcevic, J. S., Honeycutt, R. K., Schlegel, E. M., & Webbink, R. F. 1994, PASP, 106, 481
Kaluzny, J. 1986, IAU Circ., 4287
Kato, T. 1991, IBVS, 3671
Kato, T. 1995a, IBVS, 4236
Kato, T. 1995b, IBVS, 4152
Kato, T. 1997, VSOLJ Variable Star Bull., 25, 2
Kato, T. 1999, IBVS, 4768
Kato, T. 2001, IBVS, 5107
Kato, T. 2002a, PASJ, 54, L11
Kato, T. 2002b, PASJ, 54, 87
Kato, T., et al. 2001a, IBVS, 5120
Kato, T., et al. 2002a, A&A, 396, 929
Kato, T., et al. 2004a, MNRAS, 347, 861
Kato, T., et al. 2009a, PASJ, 61, S395
Kato, T., et al. 2009b, PASJ, 61, 601
Kato, T., et al. 2010, PASJ, 62, 1525
Kato, T., et al. 2012a, PASJ, 64, 21
Kato, T., et al. 2013a, PASJ, 65, 23
Kato, T., Bolt, G., Nelson, P., Monard, B., Stubbings, R., Pearce, A., Yamaoka, H., & Richards, T. 2003a, MNRAS, 341, 901
Kato, T., Fujino, S., & Iida, M. 1989, VSOLJ Variable Star Bull., 9, 33
Kato, T., Fujino, S., Iida, M., Makiguchi, N., & Koshiro, S. 1988, VSOLJ Variable Star Bull., 5, 18
Kato, T., Hanson, G., Poyner, G., Muyllaert, E., Reszelski, M., & Dubovsky, P. A. 2000a, IBVS, 4932
Kato, T., Ishioka, R., & Uemura, M. 2002b, PASJ, 54, 1029
Kato, T., & Kunjaya, C. 1995, PASJ, 47, 163
Kato, T., Lipkin, Y., Retter, A., & Leibowitz, E. 1998, IBVS, 4602
Kato, T., & Maehara, H. 2013, PASJ, 65, 76
Kato, T., Maehara, H., & Uemura, M. 2012b, PASJ, 64, 63
Kato, T., & Matsumoto, K. 1999a, IBVS, 4767
Kato, T., & Matsumoto, K. 1999b, IBVS, 4763
Kato, T., Monard, B., Hambsch, F.-J., Kiyota, S., & Maehara, H. 2013b, PASJ, 65, L11
Kato, T., Nogami, D., Baba, H., Hanson, G., & Poyner, G. 2000b, MNRAS, 315, 140
Kato, T., Nogami, D., Baba, H., Matsumoto, K., Arimoto, J., Tanabe, K., & Ishikawa, K. 1996, PASJ, 48, L21
Kato, T., Nogami, D., Moilanen, M., & Yamaoka, H. 2003b, PASJ, 55, 989
Kato, T., & Osaki, Y. 2013a, PASJ, 65, 97
Kato, T., & Osaki, Y. 2013b, PASJ, 65, 115
Kato, T., Sekine, Y., & Hirata, R. 2001b, PASJ, 53, 1191
Kato, T., Stubbings, R., Pearce, A., Nelson, P., & Monard, B. 2001c, IBVS, 5119
Kato, T., & Uemura, M. 1999, IBVS, 4802
Kato, T., & Uemura, M. 2012, PASJ, 64, 122
Kato, T., Uemura, M., Buczynski, D., & Schmeer, P. 2001d, IBVS, 5123
Kato, T., Uemura, M., Ishioka, R., Nogami, D., Kunjaya, C., Baba, H., & Yamaoka, H. 2004b, PASJ, 56, S1
Katysheva, N., et al. 2013, Cent. Eur. Astrophys. Bull., 37, 335
Khruslov, A. V. 2005, Perem. Zvezdy, Prilozh., 5, 4
Kiyota, S. 2012, J. Am. Assoc. Variable Star Obs., 40, 178
Knigge, C. 2006, MNRAS, 373, 484
Knigge, C., Baraffe, I., & Patterson, J. 2011, ApJS, 194, 28
Kolotovkina, S. A. 1979, Perem. Zvezdy, Prilozh., 3, 665
Kukarkin, B. V., et al. 1969, General Catalogue of Variable Stars, 3rd edition (Moscow: Astronomical Council of the Academy of Sciences in the USSR)
Kurochkin, N. E. 1973, Perem. Zvezdy, Prilozh., 1, 439
Littlefair, S. P., Dhillon, V. S., Marsh, T. R., Gänsicke, B. T., Southworth, J., Baraffe, I., Watson, C. A., & Copperwheat, C. 2008, MNRAS, 388, 1582
Littlefield, C., et al. 2013, AJ, 145, 145
Liu, Wu., Hu, J. Y., Zhu, X. H., & Li, Z. Y. 1999, ApJS, 122, 243
Livio, M., & Shara, M. M. 1987, ApJ, 319, 819
Lubow, S. H. 1992, ApJ, 401, 317
Markaryan, B. E. 1968, Astrophysics, 4, 46
Martínez-Pais, I. G., & Casares, J. 1995, MNRAS, 275, 699
Meinunger, L. 1966, Mitt. Veränderl. Sterne, 3, 113
Mennicken, R., & Vogt, N. 1993, Rev. Mex. Astron. Astrofis., 26, 111
Michel, R., Echevarria, J., & Hernandez-Santisteban, J. V. 2013, A&A, 554, A25
Misselt, K. A., & Shafter, A. W. 1995, AJ, 109, 1757
Montgomery, M. M. 2001, MNRAS, 325, 761
Montgomery, M. M. 2012a, ApJ, 745, L25
Montgomery, M. M. 2012b, ApJ, 753, L27
Montgomery, M. M., & Bisikalo, D. V. 2010, MNRAS, 405, 1397
Montgomery, M. M., & Martin, E. L. 2010, ApJ, 722, 989
Mroz, P., et al. 2013, Acta Astron., 63, 135
Mukadam, A. S., et al. 2010, ApJ, 714, 1702
Murray, J. R. 1998, MNRAS, 297, 323
Nakata, C., et al. 2013, PASJ, 65, 117
Nesci, R. 2012, Astronomer's Telegram, 4330
Neustroev, V. V., Zharikov, S., & Michel, R. 2006, MNRAS, 369, 369
Nogami, D., et al. 2004, PASJ, 56, S99
Nogami, D., & Kato, T. 1997, PASJ, 49, 109
Nogami, D., Kato, T., Baba, H., & Masuda, S. 1998, PASJ, 50, L1
Nogami, D., Kato, T., Baba, H., Matsumoto, K., Arimoto, J., Tanabe, K., & Ishikawa, K. 1997, ApJ, 490, 840
Nogami, D., Kato, T., Masuda, S., Hirata, R., Matsumoto, K., Tanabe, K., & Yokoo, T. 1995, PASJ, 47, 897
O'Donoghue, D., & Soltynski, M. G. 1992, MNRAS, 254, 9
Ohshima, T., et al. 2012, PASJ, 64, L3
Ohshima, T., et al. 2011, PASJ submitted
Ohshima, T., et al. 2014, PASJ, 66 in press (arXiv:1402.5747)
Olech, A. 1997, Acta Astron., 47, 281
Olech, A., et al. 2011, A&A, 532, A64
Olech, A., Kędzierski, P., Złoczewski, K., Mularczyk, K., & Wiśniewski, M. 2003, A&A, 411, 483
Olech, A., Wisniewski, M., Zloczewski, K., Cook, L. M., Mularczyk, K., & Kedzierski, P. 2008, Acta Astron., 58, 131

Olech, A., Zloczewski, K., Cook, L. M., Mularczyk, K., Kedzierski, P., & Wisniewski, M. 2005, Acta Astron., 55, 237
Orosz, J. A. 2001, Astronomer's Telegram, 67
Osaki, Y. 1989, PASJ, 41, 1005
Osaki, Y. 1995a, PASJ, 47, L11
Osaki, Y. 1995b, PASJ, 47, 47
Osaki, Y. 1996, PASP, 108, 39
Osaki, Y., & Kato, T. 2013a, PASJ, 65, 50
Osaki, Y., & Kato, T. 2013b, PASJ, 65, 95
Osaki, Y., & Kato, T. 2014, PASJ, 66, 15
Osaki, Y., & Meyer, F. 2002, A&A, 383, 574
Parimucha, S., & Dubovsky, P. 2006, Open Eur. J. on Variable Stars, 50
Parsamyan, E. S., Oganyan, G. B., Kazaryan, E. S., & Yankovich, I. I. 1983, Astron. Tsirk., 1269, 7
Patterson, J. 1979, AJ, 84, 804
Patterson, J., et al. 1997b, PASP, 109, 1100
Patterson, J., et al. 2002, PASP, 114, 721
Patterson, J., et al. 2003, PASP, 115, 1308
Patterson, J., et al. 2013, MNRAS, 434, 1902
Patterson, J., Augusteijn, T., Harvey, D. A., Skillman, D. R., Abbott, T. M. C., & Thorstensen, J. 1996, PASP, 108, 748
Patterson, J., Kemp, J., Saad, J., Skillman, D. R., Harvey, D., Fried, R., Thorstensen, J. R., & Ashley, R. 1997a, PASP, 109, 468
Pavlenko, E., et al. 2007, in ASP Conf. Ser. 372, 15th European Workshop on White Dwarfs, ed. R. Napiwotzki & M. R. Burleigh (San Francisco: ASP), 511
Pavlenko, E. P., Samsonov, D. A., Antonyuk, O. I., Andreev, M. V., Baklanov, A. V., & Sosnovskij, A. A. 2012, Astrophysics, 55, 494
Pearson, K. J. 2006, MNRAS, 371, 235
Poleski, R., et al. 2011, Acta Astron., 61, 123
Price, A., et al. 2009, PASP, 121, 1205
Price, A., et al. 2004, IBVS, 5526
Prieto, J. L., et al. 2013, Astronomer's Telegram, 4999
Ramsay, G., Barclay, T., Steeghs, D., Wheatley, P. J., Hakala, P., Kotko, I., & Rosen, S. 2012a, MNRAS, 419, 2836
Ramsay, G., Cannizzo, J. K., Howell, S. B., Wood, M. A., Still, M., Barclay, T., & Smale, A. 2012b, MNRAS, 425, 1479
Richter, G. A. 1969, Mitt. Veränderl. Sterne, 5, 88
Ringwald, F. A., & Thorstensen, J. R. 1990, BAAS, 22, 1291
Ringwald, F. A., Thorstensen, J. R., & Hamwey, R. M. 1994, MNRAS, 271, 323
Robertson, J. W., Honeycutt, R. K., Hillwig, T., Jurcevic, J. S., & Henden, A. A. 2000, AJ, 119, 1365
Robertson, J. W., Honeycutt, R. K., & Turner, G. W. 1995, PASP, 107, 443
Robinson, E. L., Shafter, A. W., Hill, J. A., Wood, M. A., & Mattei, J. A. 1987, ApJ, 313, 772
Rodríguez-Gil, P., Gänsicke, B. T., Hagen, H.-J., Marsh, T. R., Harlaftis, E. T., Kitsionas, S., & Engels, D. 2005, A&A, 431, 269
Savoury, C. D. J., et al. 2011, MNRAS, 415, 2025
Schmeer, P., Poyner, G., & Wenzel, W. 1990, IAU Circ., 5051
Schreiber, M. R. 2007, A&A, 466, 1025
Shafter, A. W. 1985, AJ, 90, 643
Shafter, A. W., Coelho, E. A., & Reed, J. K. 2007, PASP, 119, 388
Shafter, A. W., & Hessman, F. V. 1988, AJ, 95, 178
Shappee, B. J., et al. 2013, ApJ submitted (arXiv:1310.2241)
Shears, J., Klingenberg, G., & de Ponthiere, P. 2007, J. Br. Astron. Assoc., 117, 331
Shears, J., Miller, I., Pickard, R., & Sabo, R. 2013, J. Br. Astron. Assoc. in press (arXiv:1303.7088)
Sheets, H. A., Thorstensen, J. R., Peters, C. J., Kapusta, A. B., & Taylor, C. J. 2007, PASP, 119, 494
Shugarov, S. Yu. 1975, Astron. Tsirk., 862, 8
Shurpakov, S., et al. 2013, Astronomer's Telegram, 5196
Skidmore, W., Mason, E., Howell, S. B., Ciardi, D. R., Littlefair, S., & Dhillon, V. S. 2000, MNRAS, 318, 429
Skillman, D. R., et al. 2002, PASP, 114, 630
Smak, J. 1984, Acta Astron., 34, 161
Smak, J. 2013, Acta Astron., 63, 369
Smak, J., & Waagen, E. O. 2004, Acta Astron., 54, 433
Spogli, C., Fiorucci, M., & Tosti, G. 1998, A&AS, 130, 485
Stanek, K. Z., et al. 2013a, Astronomer's Telegram, 5168
Stanek, K. Z., et al. 2013b, Astronomer's Telegram, 5118
Stellingwerf, R. F. 1978, ApJ, 224, 953
Still, M., Howell, S. B., Wood, M. A., Cannizzo, J. K., & Smale, A. P. 2010, ApJ, 717, L113
Swope, H. H., & Caldwell, I. W. 1930, Harvard Coll. Obs. Bull., 879
Szkody, P., et al. 2002, AJ, 123, 430
Szkody, P., et al. 2003, AJ, 126, 1499
Szkody, P., et al. 2006, AJ, 131, 973
Szkody, P., et al. 2005, AJ, 129, 2386
Szkody, P., et al. 2009, AJ, 137, 4011
Szkody, P., & Howell, S. B. 1992, ApJS, 78, 537
Szkody, P., & Mattei, J. A. 1984, PASP, 96, 988
Takamizawa, K. 1988, VSOLJ Variable Star Bull., 30–31, 3
Tappert, C., & Bianchini, A. 2003, A&A, 401, 1101
Tappert, C., & Mennickent, R. E. 2001, IBVS, 5101, 1
Thiele, H. 1916, Astron. Nachr., 202, 213
Thorstensen, J. R., & Fenton, W. H. 2003, PASP, 115, 37
Thorstensen, J. R., Patterson, J. O., Shambrook, A., & Thomas, G. 1996, PASP, 108, 73
Thorstensen, J. R., Taylor, C. J., & Kemp, J. 1998, PASP, 110, 1405
Tibshirani, R. 1996, J. R. Statistical Soc. Ser. B, 58, 267
Tiurina, N., et al. 2013, Astronomer's Telegram, 4871
Uemura, M., et al. 2002, PASJ, 54, L15
Uemura, M., et al. 2005, A&A, 432, 261
Warner, B. 1995a, Cataclysmic Variable Stars (Cambridge: Cambridge University Press)
Warner, B. 1995b, Ap&SS, 226, 187
Warner, B., O'Donoghue, D., & Wargau, W. 1989, MNRAS, 238, 73
Watanabe, M., Hirosawa, K., Kato, T., & Narumi, H. 1989, VSOLJ Variable Star Bull., 10, 40
Wei, J., Li, C., Xu, D., Hu, J., & Li, Q. 1997, Acta Astrophs. Sin., 17, 107
Wenzel, W. 1982, IBVS, 2256
Whitehurst, R. 1988, MNRAS, 232, 35
Wils, P., Gänsicke, B. T., Drake, A. J., & Southworth, J. 2010, MNRAS, 402, 436
Wolf, M., & Wolf, G. 1906, Astron. Nachr., 170, 361
Wood, M. A., & Burke, C. J. 2007, ApJ, 661, 1042
Wood, M. A., Still, M. D., Howell, S. B., Cannizzo, J. K., & Smale, A. P. 2011, ApJ, 741, 105

Woudt, P. A., Warner, B., de Budé, D., Macfarlane, S., Schurch, M. P. E., & Zietsman, E. 2012, MNRAS, 421, 2414
Woudt, P. A., Warner, B., & Pretorius, M. L. 2004, MNRAS, 351, 1015
Yamaoka, H., Itagaki, K., Maehara, H., & Nakano, S. 2008, Cent. Bur. Electron. Telegrams, 1535
Zemko, P., Kato, T., & Shugarov, S. 2013, PASJ, 65, 54
Zharikov, S., Tovmassian, G., Aviles, A., Michel, R., Gonzalez-Buitrago, D., & Garcia-Diaz, M. T. 2013, A&A, 549, A77
Zurita, C., et al. 2002, MNRAS, 333, 791